Recognition of anionic guests with benzimidazole and benzothiazole functionalized acyclic hosts: solution phase and solid state studies

A Dissertation

Submitted in partial fulfillment for the degree of

Doctor of Philosophy

Nilotpal Borah

(Roll No. 136122013)

Thesis Supervisor: Prof. Gopal Das

Department of Chemistry

Indian Institute of Technology Guwahati

Assam -781039, India

Recognition of anionic guests with benzimidazole and benzothiazole functionalized acyclic hosts: solution phase and solid state studies

A Dissertation

Submitted in partial fulfillment for the degree of

Doctor of Philosophy

Nilotpal Borah

(Roll No. 136122013)

Thesis Supervisor: Prof. Gopal Das

Department of Chemistry

Indian Institute of Technology Guwahati

Assam-781039, India

Dedicated

to

my parents,

the reason of what I am today.

INDIAN INSTITUTE OF TECHNOLOGY GUWAHATI

Department of Chemistry

STATEMENT

I do hereby declare that the matter embodied in this thesis is the result of investigations carried out by me in the Department of Chemistry, Indian Institute of Technology Guwahati, India, under the guidance of Prof. Gopal Das, Department of Chemistry, Indian Institute of Technology Guwahati, India.

In keeping with the general practice of reporting scientific observations, due acknowledgements have been made wherever this work is based on the findings of other investigators.

Nilotpal Borah

1st September, 2020 **Nilotpal Borah**

IIT Guwahati

INDIAN INSTITUTE OF TECHNOLOGY GUWAHATI

Department of Chemistry

CERTIFICATE

This is to certify that Mr. Nilotpal Borah has been working under my supervision since July, 2013 as a regular registered Ph. D. student. His thesis entitled **"Recognition of anionic guests with benzimidazole and benzothiazole functionalized acyclic hosts: solution phase and solid state studies"** is authentic record of the results obtained from the research work carried out under my supervision in the Department of Chemistry, Indian Institute of Technology Guwahati, Assam, India. I am forwarding his thesis to submit for the award of degree of Doctor of Philosophy, from this institute. I hereby certify that he has fulfilled all the requirements, according to the rules of this institute regarding the investigations embodied in his thesis and this work has not been submitted elsewhere for a degree.

Prof. Gopal Das
(Thesis Supervisor)
Professor
Department of Chemistry
IIT Guwahati
Assam - 781039, India

Acknowledgement

If each of my words were a drop of water, you would see through them and glimpse what I feel: gratitude, acknowledgement. —— **Octavio Paz** in his Nobel Lecture

Standing at the final stage of a truly unforgettable journey towards my intellectual destination, it is very difficult to mention all the people who have genuinely helped me and I would like to thank all those who have made this thesis a reality. At the very outset, I would like to express my deepest gratitude towards my parents for having irrational and unbreakable belief in me. Their unconditional love, support and timely morale boost have made me reach this stage of my life. I am highly indebted to my thesis supervisor Prof. Gopal Das for his kind support, insightful advice and encouragement. I earnestly thank him for his nice guidance, freedom to work, encouragement and inspiration which helped me to explore the domain of my work assembled in this thesis.

Besides my supervisor, I would also like to give sincere gratitude to my doctoral committee members, Dr. Lal Mohan Kundu, Dr. Debasis Manna and Dr. A. S. Achalkumar for their advice and valuable suggestions. I would also like to thank Head of the Department, Scientific officer Dr. Babulal Das and other technical and non-technical staff members of the Department of Chemistry, IIT Guwahati for providing me with the necessary facilities whenever required. I sincerely appreciate the staffs of central instrument facility, for their help and guidance in handling several analytical instruments, required during my research work.

I take this opportunity to thank my extraordinary lab seniors like Sandeep da, Arghya Da, Jiban Da, Chirantan da, Najbul Da, Romen Da, Barun Da, Soham and talented juniors like Rupinder, Utsab, Santanu, Senjuti, Asesh, Debojit, Megha, Sagnik, Arnab, Jaikrishna, Deepa, Sikhamoni and Subhashree for their cooperation and inspiration in my research work which eases the hurdles during the PhD work. From sharing the morning tea to evening snacks, I have lived my life to the fullest in these few years with these fellow warriors. From sharing jokes to dancing to the tunes of "*Jai Jai Shivshankar*", making funny Snapchat videos to partying in the city on smallest of occasions, it was always great to work and spend times with these interesting human beings and I will always cherish these memories throughout my life. I wish them great success in every aspect of their life. Special mention of two special people is mandatory whom I have met during my PhD life. My lab senior yet mentor cum friend Abhijit da, whom I shall always be obliged for his constant guidance; from basics of lab techniques to every aspect of research work. Without his unconditional support, I would have given this up a long time ago. The other person whom I have to mention is my lab junior Bishu (Biswajit) who has become my brother from another mother. Words cannot suffice his never-ending help and support during this tenure.

I also owe my obligations to my other seniors, batch mates and juniors of PhD fraternity of the chemistry department for their help and support.

I take this opportunity to thank my friend Amlan, Shyamal, Hiranya, Jugal, Sourav, Pingal, Anupal Da, Tridip Da, Naba Da, Manash Da, Subrat (Vigi) Da, Debu, Dip, Tushar, Chiranjib, Puneet for being the source of my encouragement and love throughout this time. Though my schoolmates were far apart during this tenure, the names of Ladu, Bap, Apu, Mantu and Chinmoy are also worth mentioning.

Besides, words fall short to express my feelings for my beloved wife Rimlee, whose love and care have been the constant source of inspiration throughout the phase including the frustrating times. All this is meaningless without you. I would like to offer my thanks to my sister Nilakshi for her untiring smile and love for me throughout my life. Words of wisdom and support from my in-laws in every stage of my PhD life is worth mentioning.

It would be an injustice if I have not mentioned my badminton buddies as we used to spend daily 3 hours in the court playing our hearts out. Kishor, Swapnali Baideu, Bhaskar Da, Shyam, Mukul, Puneet, Subrat, Basant, Subhasish, Dhanesh, Jagadish, Panda Sir, Saikia Sir, Kadulkar Sir, Arindam Sir are the gems of the game.

No words would suffice to express my feelings for my teachers from my school, college and university to whom I owe a debt for their teachings and benevolence.

Finally, I would like to thank the Microsoft Corporation for presenting the MS word for documentation and equation to symbols, Grammarly for the grammar check, Adobe Corporation for AI, LR and PS software.

Still, many names are missing whose contribution and help is worth mentioning.

Nilotpal

The thesis entitled "**Recognition of anionic guests with benzimidazole and benzothiazole functionalised acyclic hosts: solution phase and solid state studies"** is divided into five chapters based on the results of experimental work performed during the research period.

Chapter 1: Introduction

As the anion coordination chemistry continues to develop apace in the recent past, selective anion recognition has emerged to be an active area of the research owing to the diverse roles that anions play in biology, medicine, catalysis, and the environment. Apart from its encouraging presence in biological systems, anions can have damaging effects on the environment too, which can scarcely be underestimated. This comprehension urges the research fraternity to drive towards the development of systems capable of functioning under real-world conditions, which includes the development of new catalysts, receptors, and anion transporters. The design of abiotic receptors with enriched anion recognition properties is often a challenging task primarily because of the charge to radius ratio of the target anion, in addition to its geometry and protonation state. Either of neutral or positively charged receptors are conventionally composed of organic frameworks that contain apposite functionalities with suitable hydrogen bond donors that guide the molecular recognition. In a chemosensor, the concurrent recognition event is supported by the presence of fluorophore/chromophore as interaction with the guest analyte changes the electron distribution of the chemosensor. The response of which is perceived through differential colorimetric and fluorescence signals. With the added advantages of ease of handling, rapid response times, their ability to function in a more relaxed condition and low detection limits, optical (chromogenic and fluorogenic) sensors are becoming increasingly popular. The astute design input in the receptors possesses the prospective to deduce valuable information about biological, environmental, and chemical issues through differential light signaling. Most neutral artificial receptors establish hydrogen-bonding interactions that expend the hydrogen bonds offered by specific binding sites from different functionalities to recognize and selectively bind the anions within an appropriate framework. On account of its amphoteric nature and sheer existence inside the human body as active sites in different histidine and histamine containing metalloproteins, the imidazole core has been involved in binding both anions and cations as well as neutral organic molecules. Benzimidazole moiety is a better fluorophore over the imidazole unit. The significance of benzothiazole functionalities in medicinal chemistry lies in their potential application as anticancer, antimicrobial, anticonvulsant, antiviral, antitubercular, antimalarial, anthelmintic, analgesic, anti-inflammatory, antidiabetic, antifungal, antibacterial, antioxidant etc. The benzothiazole unit increases the conjugation in the system, as well as the presence of both

hard/borderline N and soft S atoms in the core, was expected to respond to multiple ions. In our works in this thesis, we have incorporated both benzimidazole and benzothiazole moieties in novel non-symmetric tripodal platform and benzothiazole in simple Schiff base dipodal for anion recognition. In the synthesized receptors, the aforementioned groups are assisted by other acidic hydrogen bond donors viz. amide –NH and hydrazinyl –NH keeping in mind the probability of anion selectivity both in the solution phase and solid state.

Chapter 2: Experimental methods and characterization

This chapter encompasses the comprehensive information about the various materials used in the synthesis of the receptors/probes along with specifics of the synthetic procedures, binding studies, minutes of crystallization, specifications of the analytical instruments used for the characterization of the synthesized compounds.

Chapter 3: Anion binding aptitude of a benzimidazole and amide functionalized non-symmetrical tripodal receptor

In this chapter, we report a novel non-symmetric tripodal receptor (**L_1**) decorated with two symmetric arms containing benzimidazole moiety along with an amide linked π acidic nitrophenyl moiety and its anion binding studies in solid as well as solution phase. Three units of protonated receptors (**L_1**) involves in creating a pseudo-cavity around the hexafluorosilicate anion with its symmetric arms. In contrast, the oxygen atom of the π acidic nitrophenyl moiety of the non-symmetric arm plays a pivotal role in forming the three-dimensional array. In another instance, binding of one sulfate and two bisulfates in unison by two protonated units of the receptor (**L_1**) arises. The benzimidazole –NHs are found to be the the strongest hydrogen bond donors in both the crystal complexes controlling dominance over amide –NHs. In UV-Vis absorption studies, upon addition of 10 equivalents fluoride anions, the neutral receptor imparted a naked eye visible colorimetric change from colorless to orange-red type, which was accompanied by a redshift of 138 nm.

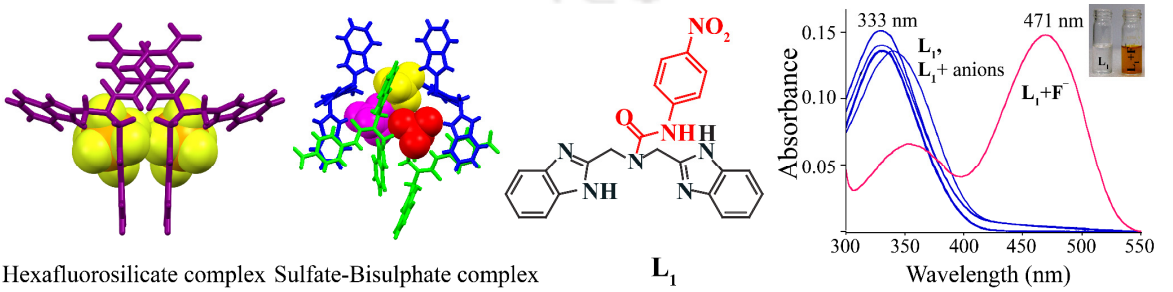

Scheme 1. A comprehensive representation of the research work included in **chapter 3**.

^{1}H NMR studies establish the fluoride-induced deprotonation of the seldom observed amide protons as the addition of fluoride solution rendered disappearance of the amide –NH peak. Comparative ^{1}H NMR studies of the neutral receptor and its protonated form in the complexes suggested the strong involvement of aromatic and aliphatic –CH in anion binding in the solution phase.

Chapter 4: A case study of ratiometric fluorescent sensing of fluoride ions and solid state recognition of sulfate ions by a benzimidazole based non-symmetrical tripodal receptor

This chapter deals with another rationally designed non-symmetric tripodal receptor **L_2**, which has been reported as a fluorescent chemosensor for the fluoride ions as well as sulfate anion binding receptor. The probe **L_2** was designed with two similar benzimidazole arms and amide linked naphthyl group as the non-symmetric arm that assists the fluorescence signals during anion sensing. The recognition of fluoride ions by the probe was accompanied by ratiometric change as well as a visual change in color from violet to cyan under UV light. The remarkable redshift of 100 nm in acetonitrile medium could be attributed to the Intramolecular Charge Transfer (ICT) mechanism. Emission spectroscopy-based titration study confirmed 1:3 (receptor: fluoride) binding stoichiometry and a limit of detection as low as 0.875 ppb. ^{1}H NMR studies revealed the selective formation of hydrogen-bonded host-guest complex and subsequent deprotonation of acidic benzimidazole and amide protons on the addition of fluoride ions. As acidic hydrogens were involved, the INHIBIT type logic gate at the molecular level was fabricated using the reversibility and reusability of the probe towards F^- and H^+ ions. Detection of the fluoride ions under UV light by the receptor coated TLC plates, and paper strips indicated the practicality of probe in solid state. Single crystal X-ray studies reveal that the asymmetric unit in sulfate crystal of **L_2** comprises of one pair of non-symmetric protonated receptors that exhibit conformational isomorphism and two units of sulfate anion. The two bound sulfates experience two different binding environments wherein each case, the benzimidazole –NH moiety, offers the strongest hydrogen bonds. In the protonated complex, seven numbers of protonated receptors aggregate to form a pseudocapsular cavity where encapsulation of two pairs of sulfate anions takes place.

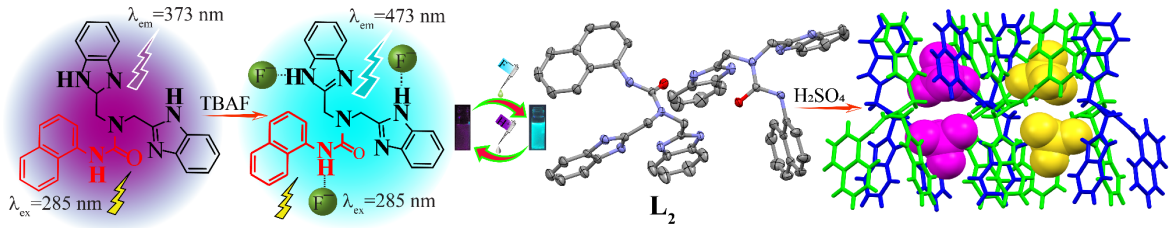

Scheme 2. A schematic representation of the research work included in **chapter 4**.

Chapter 5: Colorimetric detection of fluoride and acetate ions by benzothiazole based receptors: Fluorescence based selective acetate sensing

This chapter describes the comparative anion sensing abilities of three analogous benzothiazole based Schiff bases. In the core of each Schiff base design, the imine bonds join the specific chromophore and the 2-hydrazineylbenzothiazole unit for extending conjugation. The Schiff base probe **L_3**, containing imine linked 1-hydroxy naphthyl group and benzothiazole moiety, impelled excellent colorimetric response in the presence of both F^- and OAc^- anions. The 72 nm red shift in each case was accompanied by a change in color from colorless to yellowish type. The Job's plot from the UV titration data suggests 1:2 and 1:1 binding stoichiometry for fluoride and acetate anions, respectively. The probe **L_4** was deliberately modified with the coumarin chromophore to enhance the chromogenic properties. The Chloro group present in the **L_4** was supposed to increase the acidity of the –NH protons and would help in charge-transfer interactions. A bathochromic shift of 147 nm was observed in the presence of both F^- and OAc^- ions in acetonitrile solution. Naked eye detection of the aforementioned anions was more feasible as the addition of the anions rendered beautiful purple coloration from the original light yellowish solution. The free probe, **L_4** coordinates in a 1:1 stoichiometric manner to both F^- and OAc^- ions in solution. **L_5** has been modified by introducing another similar imine linked benzothiazole arm to **L_3**, thereby forming a dimeric cage-like structure with –OH and –NH functionalities. The probe**,** **L_5** is also exhibiting colorimetric response towards both fluoride and acetate ions. The Job's plots from the UV-Vis titration spectra suggest the formation 1:3 host-guest complex in case of F^- anions and 1:1 host-guest complex in case of OAc^- anions. In all these cases, an intramolecular charge transfer (ICT) interaction plays a pivotal role in the colorimetric detection of the anions. Interestingly, **L_5** displayed rapid 'turn-on' fluorescence emission signals with respect to acetate ions in acetonitrile, thereby distinguishing it from other anions. In the presence of acetate ions, the colorless

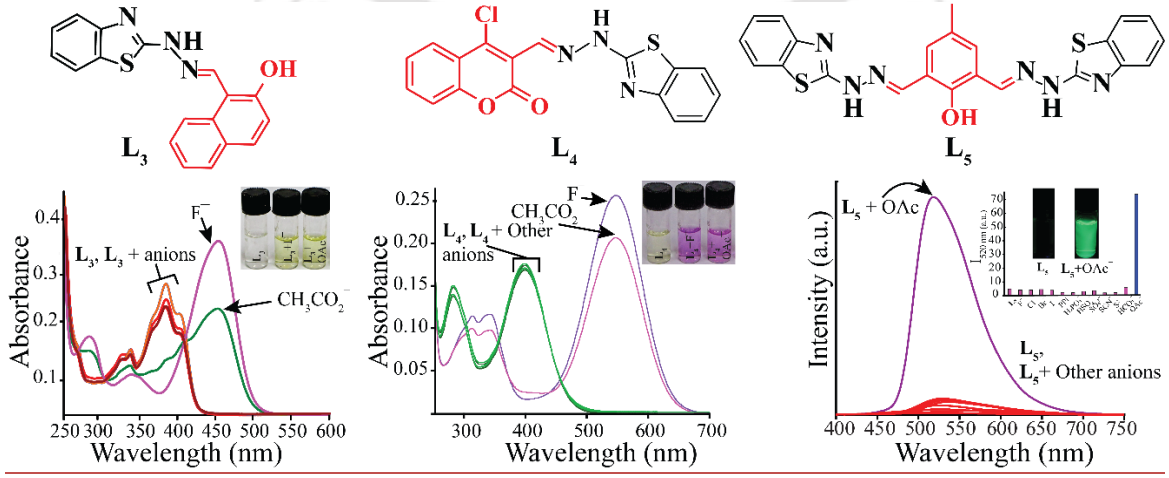

Scheme 3. A comprehensive illustration of the research work included in **chapter 5**.

chemosensor solution exhibited a strong greenish fluorescence and thus enabled naked-eye detection of the anion. The Job's plot from the titration data suggested a 1:1 host-guest complex with the acetate anions. ^{1}H NMR titration studies confirmed the initial formation –NH···F$^-$ hydrogen bond by each of the three probes with the incoming fluoride and acetate anions and subsequent deprotonation of acidic protons in the probe on excess addition of the anions above.

Conclusion and future perspective

This thesis illustrates the constant efforts in improvisations of certain benzimidazole/benzothiazole based receptors and their binding propensity towards biologically and environmentally relevant anions. Novel non-symmetrical tripodal, **L$_1$** has been synthesized, and its anion binding aptitude has been explored both in solid and solution phases. In solid state, protonated **L$_1$** encapsulates hexafluorosilicate anion, and in another case, it binds one sulfate and two bisulfates in unison. Moreover, **L$_1$** can selectively detect fluoride ions in the solution phase and exhibit a sharp colorimetric response. **L$_2$**, another novel non-symmetric tripodal, acts as a ratiometric fluorescent sensor for fluoride ion in the solution phase and binds sulfate ions in solid state. The series of dipodal Schiff bases **L$_3$**, **L$_4$**, and **L$_5$** can selectively sense fluoride and acetate ions in acetonitrile solution via absorption spectroscopy.

Interestingly, only **L$_5$** can distinguish the acetate and fluoride anions by differential fluorescence response in acetonitrile solution. In a nutshell, this thesis portrays a sequential plethora of systematic development in the field of chemosensing as well as solid state study. Starting with the synthesis of a novel non-symmetric tripodal and its solid state anion binding studies and absorption spectroscopy based solution study (Chapter 3), we continued our study with another non-symmetric tripodal analogue in fluorescence spectroscopy based solution study assisted by its solid state anion recognition (Chapter 4) to conclude with series of three simple Schiff base dipodals as anion sensors in solution phase only (Chapter 5). By tuning the functionalities of the third arm, our design of non- symmetrical tripodal has successfully bind anions in both the solution phase as well solid state, which is otherwise a stimulating task to endeavor. Keeping in mind added benefits of non-symmetrical tripodals, recognition, and binding of anions could be employed in specific applications such as removal and extraction toxic anions and salts from water, drug delivery, transmembrane anion transport, salt solubilization, extraction, catalysis, stabilizing the anionic reactive intermediates inside the molecular assembly, etc. Our works on distinctions of anions with analogous chemical properties viz. F$^-$ in presence of OAc$^-$ or vice versa were achieved by tuning smart designs of receptors, which in turn, would help in distinguishing such anions in a physiological medium as well. In essence, we believe that designing novel anion

receptors and its binding study would contribute to both analytical chemistry and solid state chemistry community for enhancing cognizance and development in the particular field of research.

Contents

Chapter 3

Anion binding aptitude of a benzimidazole and amide functionalized non-symmetrical tripodal receptor

Chapter 4

A case study of ratiometric fluorescent sensing of fluoride ions and solid state recognition of sulfate ions by a benzimidazole based non-symmetrical tripodal receptor

Chapter 1

Introduction

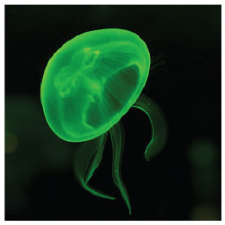

Chapter 1

1. Supramolecular anion recognition in solution phase and solid state

1.1 Supramolecular Chemistry: *Chemistry beyond the molecules*

The wise aphorism by erudite Aristotle *'The whole is greater than the sum of its parts',* aptly outlines the modern concept of synergy, which can be applied to supramolecules. Nobel laureate Jean-Marie Lehn suggested supramolecule to be an organised, complex entity that is resulted from the association of two or more chemical species held together by intermolecular forces.[1.1] Initially, the non-covalent interaction between a 'host' and a 'guest' molecule was used to define the supramolecular chemistry which with time, included other definitive phrases like 'the chemistry involving non-covalent bond' and 'non-molecular chemistry'. The swift development in supramolecular chemistry over the recent past has encompassed not merely host-guest systems but also molecular recognition, molecular devices and machines, self-assembly as well as self-organisation and even shared its boundaries with the development of complex matter and nanochemistry.[1.2] Another fascinating description of supramolecular chemistry is as 'lego™ chemistry' wherein an individual lego™ brick characterises a molecular building block and there exists a reversible intermolecular interaction that holds them together to constitute a supramolecular aggregate.[1.3] The intermolecular interactions present in the realms of supramolecular chemistry comprise mostly electrostatic interactions, hydrogen bonding, π–π interactions, dispersion interactions and hydrophobic or solvophobic effects. In a supramolecular system, it is essential to consider all these interactions and their interplay during binding or complexation event and their outcomes relating to both the host and the guest as well as their surroundings.[1.1] In an elementary sense, if one molecule is considerably larger than another so that it can encompass the smaller one, then the larger one is characterized as 'host' while the smaller enveloped one is its 'guest'. Another verbatim definition refers the host to be a molecular entity that possesses converging binding sites (e.g. hydrogen bond donors, Lewis basic donor atoms etc.) while the guest molecules contain binding sites that diverge in the complex (e.g. a spherical, Lewis acidic metal cation or hydrogen bond acceptor halide anion).[1.4] In turn, binding sites are the regions of a molecule that have the pertinent size, appropriate geometry and distinct functionalities to accept and bind a second molecule via non-covalent interactions.[1.3] Thus proper assignment of binding sites in a host molecule leads to the successful recognition of guest molecule forming a supramolecular host-guest entity.

1.2 Molecular recognition

Molecular recognition is the prototypical supramolecular processes where a molecular receptor selectively binds a substrate to form a supramolecule. In fact, the molecular recognition process depends profoundly upon the molecular information stored in the interacting species. For an efficacious recognition, the design of receptors should possess steric as well as electronic features that complement those of the substrate to be captured and a balance between rigidity and flexibility makes the process facile and effortless.[1.5] The proclivity towards particular guest molecule by a host is accompanied by a degree of selectivity towards the species which is reliant upon several factors such as complementarity in binding sites of the host and guest molecule, preorganisation of the host conformation as well as co-operativity of the binding groups.[1.3] The more the extent of complementarity of the binding sites offered by the host, the greater the binding energy between the host and the guest. Besides referring to individual non-covalent bonds, this also alludes to entire shape and the complete electrostatic surface of the two molecules associated in binding. For a fruitful selective binding, the combined contribution of impeccable steric fit, as well as decent match of the charge distributions of guest surface and host's cavity, plays the pivotal role. In addition, the spatial arrangement of supramolecular interactions like hydrogen bond donors and acceptors should be appropriate to maximise the attractive forces between the host and the guest while diminishing the repulsive forces.[1.6]

1.3 Overview of Anion recognition chemistry

1.3.1 *Why anions are targeted*

Because of its omnipresence throughout biological systems, anions have an innumerable impact upon our lives. Looking inside our bodies, DNA, the prime carrier of our genetic information is basically anionic as is the RNA. Roughly, 70% of enzyme substrates and cofactors (e.g. ATP) are composed of anions. In case of the halides, chloride which is present extensively in extracellular fluid, regulates blood pressure, blood pH while its misregulation leads to diseases such as cystic fibrosis,[1.7] iodide is essential for the biosynthesis of hormones by the thyroid gland.[1.8] The smallest halide, fluoride was used for artificial fluoridation of water supplies[1.9] and during the treatment of osteoporosis.[1.10] Bicarbonate finds its vital use in maintaining the pH levels in the body. Cyanide is proven to be extremely toxic as it inhibits cellular respiration by binding strongly with a heme unit of cytochrome c oxidase. The adverse effects of certain anions on the environment around us can scarcely be overlooked. Nitrate and sulfate lead the deposition of acidic species during acid rain[1.11] while uncontrolled use of phosphates and nitrates in fertilisers has led to eutrophication in waterways.[1.12] Though perchlorate is used extensively as oxidisers in rocket propellant and

explosives, it also acts as anthropogenic pollutant along with pertechnetate which is a by-product of nuclear fuel reprocessing.[1.13-1.14] Arsenate, a naturally occurring pollutant, is associated with alterations in the peripheral circulation of blood as well as vascular disease.[1.15] Thus, selective recognition of anionic guests has risen to be a frontline area of supramolecular research in the recent past because of the crucial functions it plays in biological, clinical, catalysis, and environmental processes. With all these positive and negative effects of anions, there has been a keen motivation that has persistently persuaded investigations of binding and sensing of anionic species.

1.3.2 *Anion receptor chemistry*

The field of anion complexation chemistry can be traced back to the exhibition of halide complexation properties by a series of macrobicyclic hosts, katapinands by Simmons and Park in 1968. Although anion binding was concurrent with the discovery of crown ethers for cation binding, its growth curve was far flatter. The design of hosts towards both cation and anion utilises the similar specificity principle developed from a preorganised position of complementary binding sites. The initial slower growth in the field of anion recognition may be addressed based on a number of intrinsic properties associated with anionic species, which mostly include the comparatively large size of the anion, variable geometries, higher free energies of solvation, existence in narrow pH window and its coordinative saturation.[1.2,1.16] Despite these inherent difficulties, research on anion coordination gently started to achieve its momentum apace. In order to overcome the anion binding challenges, the primary approach is to strategically employ a positively charged receptor unit. However, most of these electrostatic interactions are found to be non-directional. Anion binding with neutral receptors is also feasible, as there exists an electrostatic charge difference, even if the forces between anions and cations are greater. The neutral receptors, without a competing counter-anion, offer a better prospect for amplified selectivity. The development of a Lewis-acidic site (e.g. organoboron, mercury or tin compounds) in an anion receptor has accomplished directionality as well as stronger interaction in the binding with the anionic species. The polarisable nature of the anions is taken into account, particularly during its encapsulation within the host cavity where van der Waals forces play a vital role in binding.[1.3] Thus, the foundation of anion binding principle is based upon electrostatic interactions, hydrogen bonding, hydrophobicity, coordination to a metal ion and amalgamations of these interactions working together.[1.17]

Delving into anion receptors in biology, an assortment of channels and anion transport proteins with at least 14 mitochondrial anion transport systems has been investigated so far, and these

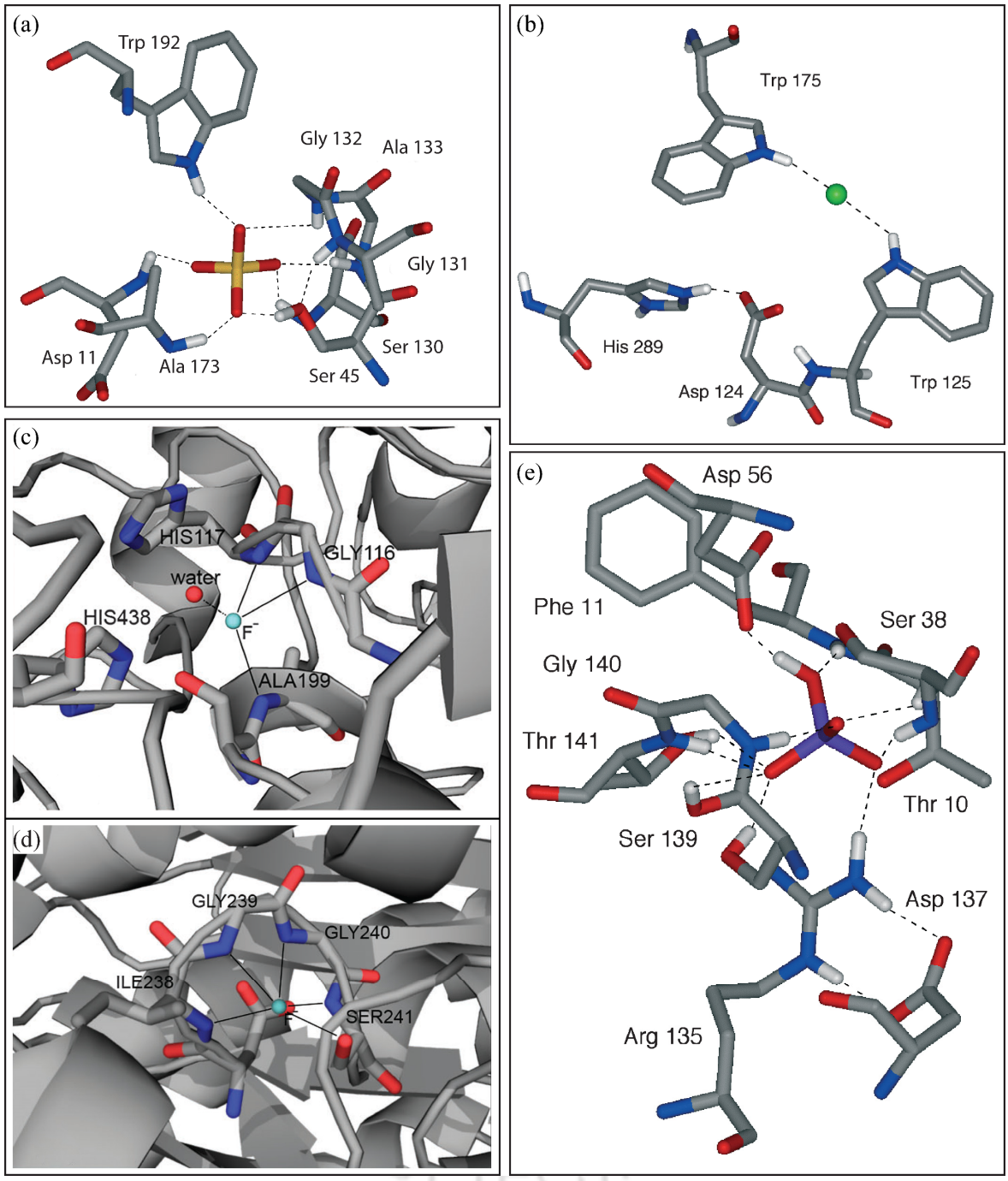

Figure 1.1 Anion binding in biology portrayed by (a) sulfate binding site in sulfate-binding protein where the sulfate ion is bound by seven hydrogen bonds donated by neutral –NH and –OH containing groups.[1.18a] (b) active site of haloalkane dehalogenase where the indole -NH protons interact with the bound chloride anion.[1.18b] (c) binding of mono hydrated fluoride anion in human butyrylcholinesterase complex (PDB code = 2XMC).[1.18c] (d) fluoride bound to Fatty acid amide hydrolase complex with fluoride (PDB code = 3PPM).[1.18d] (e) binding environment of phosphate in phosphate-binding protein where twelve hydrogen bonds are contributed by a combination of charged and neutral peptide residue interactions.[1.18e]

facilitate the transport of anions through the cell phospholipid bilayers. These biological systems (among others) are accountable for the trafficking of biological anionic species like ADP, ATP,

phosphate, fumarate, maleate, oxaloacetate, citrate, glutamate, sulfate, and halides. Over the last few years, structural elucidation by X-ray crystallography has enabled the direct visualisation of the enzyme–anionic substrate complexes where multiple hydrogen bonding interactions are involved (Figure 1.1).

The designing of abiotic receptors with enriched anion recognition properties is often challenging largely due to the charge to radius ratio of the target anion, its geometry and protonation state.[1.19-1.20] An orthodox approach for the synthesis of either of neutral or positively charged anion receptors usually comprises of the development of organic frameworks comprising of appropriate functionalities with suitable hydrogen bond donors. Lately, the halogen bonding non-covalent interactions (∠D−X—A close to linear) are also taken into account for their similar behaviour like hydrogen bonds as well as for its directional nature. The design of anion receptors with multiple hydrogen bonding sites alongside the subsequent topological contemplations prompts the idea of double valence for both anion and metal transition ions. For anions, however, negative charge on the anion is considered to be the primary valence while hydrogen bonds to the anion compensate the secondary valence.[1.21] Bowman-James has highlighted the primary factors that influence strength, selectivity and structures witnessed in the binding event between the receptor and the anion to be hydrogen bonding, topology, dimensionality and charge (or electrostatic interactions) (Scheme 1.1).

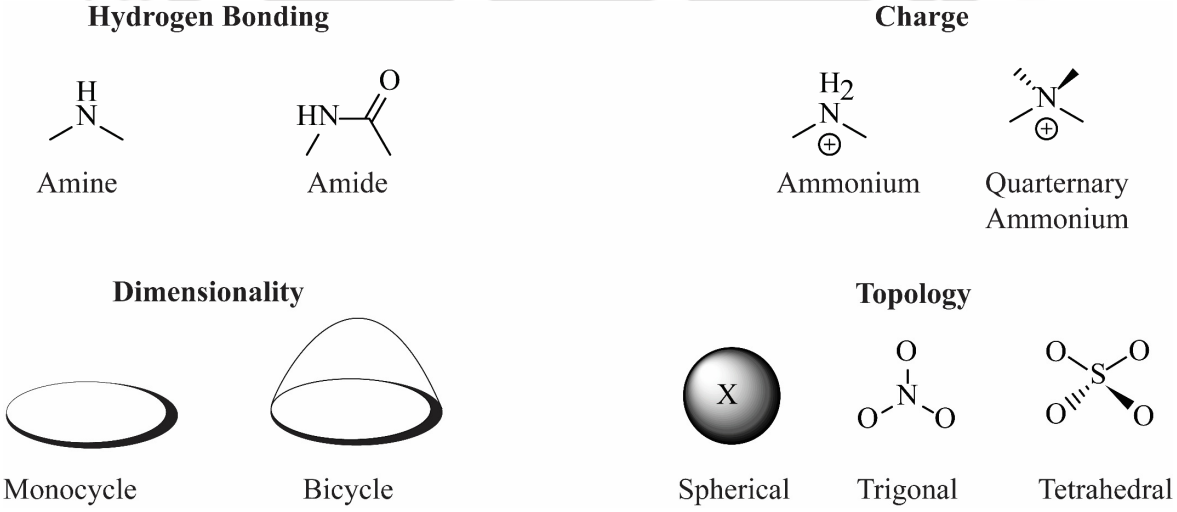

Scheme 1.1 Depiction of four factors, which mostly influence anion binding.[1.22]

The ceaseless efforts to accomplish selective anion sensing or separation has necessitated the recognition of anions by molecular receptors both in solid state as well as in solution phase. If we dive into the realm of anion binding in solid state, another distinctive feature of supramolecular chemistry lies in its ability to assimilate areas with apparently widely differing perceptions, which

is included in the domain of crystal engineering. This encompasses the design and synthesis of crystalline materials by virtue of self-assembly of molecular building blocks and thereby proceed towards functional materials. In contrast to molecular synthesis, crystal engineering comprises feeble intermolecular interactions and shallow potential energy surfaces, which are usually essential for assuring fast and reversible formation of self-assembly finally leading to a crystalline solid. The demerit lies in difficulty in structural predictability and control due to the minimal difference in energy among alternative crystal structures. However, comprehensive apprehension of intermolecular interactions involved, based on precedent empirical observations may lead to partial structure prediction as well as control during crystal engineering. In case of inorganic anions, the high charge density associated with small anions gives rise to comparatively stronger interactions in crystal. Conversely, this high charge density is also accountable for the strong solvation of these anions. This, in turn, causes difficulty in stripping out the solvating molecules during crystallisation, which muddles the crystal design process. To assess the design of crystal structures and their related properties, proper cognisance of the intermolecular interactions are necessary. Specifically, in anionic crystals, the following interactions are involved which is depicted in Scheme 1.2: [1.23]

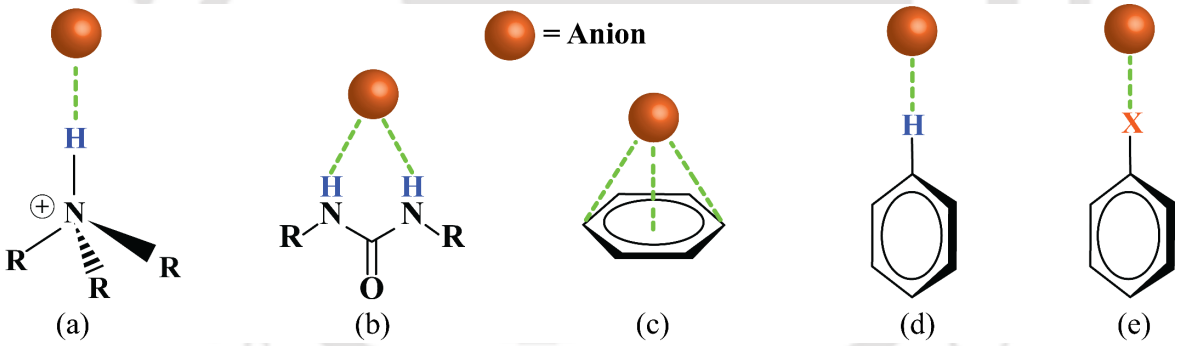

Scheme 1.2 Different types of non-covalent interactions present in anion binding; (a) electrostatic interaction by quaternary ammonium cation; (b) (i) complementary N–H···A^- interaction by a urea functionality ; (ii) C–H···A^- interaction between aryl group and an anion; (c) C–X···A^- halogen bonding where X = F^-, Cl^-, Br^- and I^-; (d) anion–π interaction.

(a) *Coulombic and van der Waals interactions*: Though these interactions are most abundant and completely electrostatic in nature, the non-directional behaviour does not assist in exploiting these interactions for controlling the crystal structure.

(b) *Metal coordination bonds* (M^+–A^-): These Lewis acid–base type interactions are comparatively strong and specific with elevated directionality. Consequently, they influence the structural design of the crystals directly.

(c) *Hydrogen bonds* (D–H·····A^-): Hydrogen bonds are primarily electrostatic and very much directional ($\angle D$–H·····A^- close to linear) and hence commonly utilized in crystal design. Apart

from the conventional use of O–H or N–H groups as hydrogen bond donors, recent studies have also revealed the use of C–H groups as another effective contributor of hydrogen bonds to the anions.

(d) *Halogen bonds (D–X·····A⁻)*: Though somewhat newer, halogen bonding interactions exist between an electrophilic halogen atom (X = Br, I) and a rich electron density centre (the anion). Similar to the hydrogen bonds, halogen bonds exhibit high directionality (∠*D–H·····A*⁻ close to linear).

(e) *Anion·····π interactions*: These interactions are purely electrostatic in nature and arises due to the existing attractions between the anions and electron deficient arene centres.

Anions may play various roles in crystals with respect to structural perspectives. Custelcean has pointed out four significant roles played by the anions in an anionic crystal (Scheme 1.3).[1.23]

(a) *Spectator*: The presence of anion is meant for merely balancing the charge where it does not contribute to the structural motif in the crystal. The typical example lies in the crystals of cationic frameworks (MOFs) having large pores or channels occupied with feebly interacting, yet muddled counter ions and solvent molecules.

(b) *Structure-directing*: The anion plays a significant role in structural formation in the crystal. The anion does not take an active part in building the assembly; instead, it actively performs as a templating agent around which the structure develops.

(c) *Building unit*: The active participation of the anion has been perceived as it directly involves a structural component to framework assembly by bridging the other components in the crystal expending well-defined and directional interactions.

(d) *Secondary building unit (SBU)*: The anion plays the role of a central constituent of an aggregate that acts as building block framework assembly in the crystal. Lately, anions have been extensively used as SBU components for the design and synthesis of hydrogen-bonded frameworks, MOFs or molecular crystals.

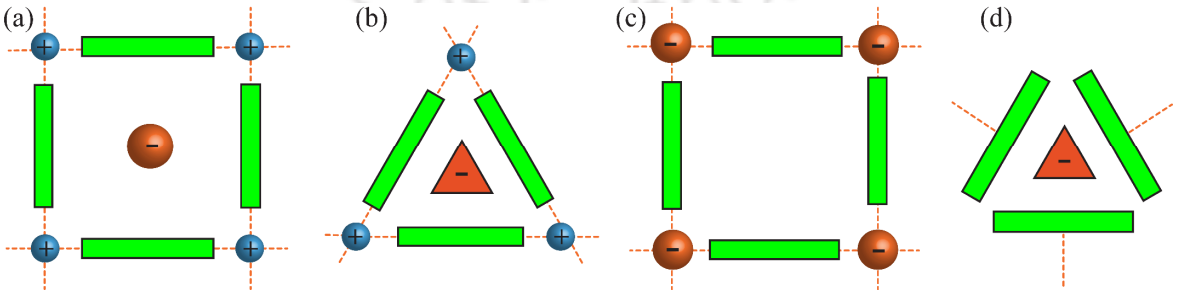

Scheme 1.3: Various Structural roles played by anions in crystals (a) spectator; (b) structure-directing (templating); (c) building unit; (d) SBU component.

Another attractive development of supramolecular chemistry is the optical detection or recognition of analytes. These signalling devices constitute the area of supramolecular chemistry, which is termed as semiochemistry. The most palpable area of application where semiochemistry focusses is the fabrication of molecular sensor devices, which amalgamates both the functions of molecular recognition as well as sensing in a single molecule. In broader terms, chemosensors can be defined as chemical systems that can convert chemical stimuli into easily detectable and simply interpretable responses. Essentially, a suitable chemosensor must contain a receptor unit that is in communication with a signalling unit. During guest binding, the chemosensor should exhibit sensitivity by generating a particular signal in the form of emission related to electromagnetic radiation (photochemical sensing), current (electrochemical sensing) or otherwise externally measurable change (e.g. in colour or pH). However, among these various types of sensing methods, optical sensors are often favoured due to their simplicity, facile handling, cheaper cost, prompt response time and reliable signal interpretation capacity.[1.24-1.26, 1.2]

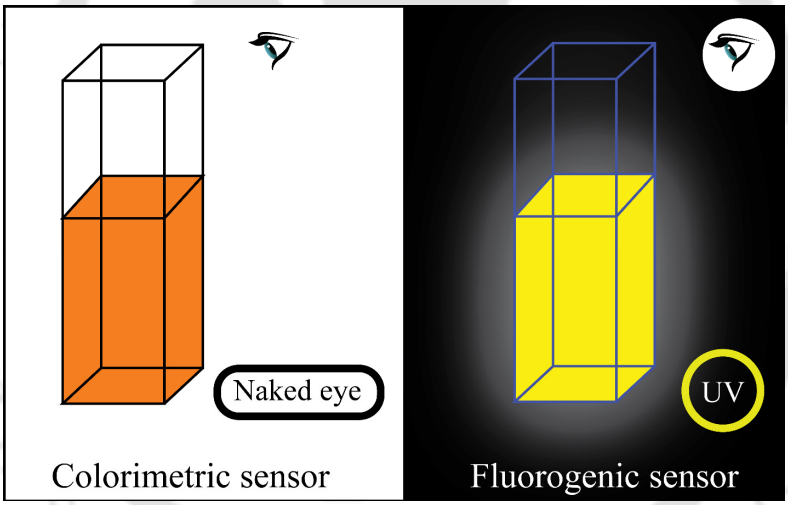

Scheme 1.4: A representative figure of optical chemosensor (Colorimetric and Fluorogenic).

Optical sensors are primarily categorised into two types (1) colorimetric or chromogenic sensors (2) luminescent sensors (Scheme 1.4). In general, the receptor (the recognition site) is attached to a signal emitting chromophore and/or fluorophore unit, which could translate the recognition event by exhibiting detectable colorimetric and/or fluorescence signal. The design principle of these chemosensor devices incorporates three major processes: (i) separation of targeted analytes, (ii) capturing a specific analyte from a complex mixture, and (iii) emanating output signal from a [chemosensor-analyte] complex.[1.27-1.29]

In case of anion sensing by discrete molecular receptors, recognition event is characterised by similar responses which include optical (colorimetric or fluorescence), an electrochemical, or a

sol-gel transition which in turn, helps in monitoring the presence as well as the concentration in some of anionic guests.[1.30] This approach facilitates the fruitful detection of various potentially toxic, environmentally deleterious anionic species. Subsequently, anion sensing has been developed to be one of the most dynamic research areas of supramolecular chemistry due to high sensitivity associated with either of the discrete colorimetric or fluorescence (optical) anion sensors. Many of these systems have the potential to detect anionic species with low concentrations along with the prospective for monitoring the anions in biological systems (bioimaging) accompanied by the added benefit of straightforward detection with the naked eye. Optical chemosensors find its widespread use in medical diagnosis, process control, food safety, detection of environmentally harmful analytes, molecular catalysis and fluorescence imaging. Fluorescence signal inducing chemosensors are beneficial with enhanced selectivity and sensitivity supplemented by real-time detection, non-destructive determination and economical instrumentation.[1.31] Owing to the additional benefits of spatial and temporal resolutions, fluorescence signals have been expediently used in analytical supramolecular chemistry to track many *in vitro* and *in vivo* biological processes to comprehend their various functions. The detailed study of the complex biological processes, signal transduction and intricate environmental systems becomes more feasible as fluorescence-based chemosensor utilises weak supramolecular interactions.[1.32] Fascinating features of the fluorescence-based chemosensor lie in the fact that neither it requires any reference nor consumes any extent of analytes which make it one of the most crucial sensing tools. Different sensing strategies of fluorescence-based chemosensor are obtained by tuning three essential constituents- the receptor unit, the signalling unit and the spacer units. Based on the sensing approaches, these chemosensors could be categorised into four broad classes (a) Turn Off; (b) Turn On; (c) Ratiometric and (d) Chemodosimeter. “Turn On” chemosensors are striking to the eyes of the observer as well as desirable due to their reduced false-positive responses as compared to their “Turn Off” counterparts. Beneficial aspects of the ratiometric probe are established by its ability to measure the emission intensities at two distinct wavelengths, increase in the dynamic range of emission and detection of analyte independent of the concentration of the receptor.[1.33] On the other hand, chemodosimeter based chemosensors can offer remarkably high selectivity and sensitivity compared to coordination based sensors. Selective sensing of a specific analyte by fluorescence-based chemosensors is usually attained by utilising one or more common photophysical mechanisms, including intramolecular charge transfer (ICT), photoinduced electron transfer (PET), excimer/exciplex formation, chelation induced enhanced fluorescence (CHEF), twisted intramolecular charge transfer (TICT), fluorescence resonance energy transfer (FRET), C=N isomerisation, electronic energy transfer

(EET) and aggregation induced emission (AIE).[1.34-1.35]

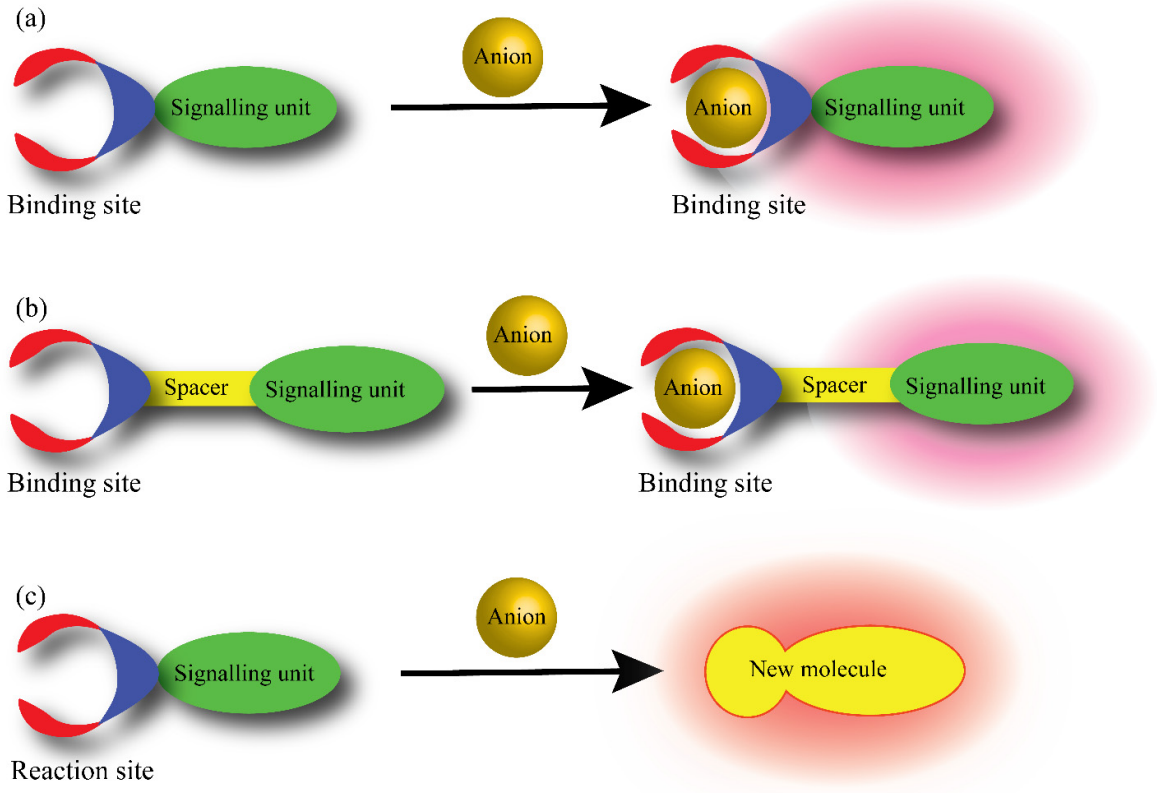

Scheme 1.5 Different kinds of single-molecule based optical anion sensors. (a) Receptor where the binding site is integrated with the signalling unit. (b) The binding site is separated from the signalling unit by a covalently linked spacer. (c) Chemodosimeter approach where a new molecule is formed due to anion induced irreversible reaction. (Above are the examples of "Turn-on" fluorescent chemosensors, although "Turn-OFF" and colorimetric sensors are also possible)

Chemosensors for anionic species consist of either discrete single molecule or molecular ensemble based platform. Optical sensing by a single discrete molecule can be achieved in several ways (Scheme 1.5). Typically, the anion sensors are made up two fragments where an anion binding site is covalently linked to a signalling unit (e.g., fluorophore or other dye). The signalling unit can be directly connected to the receptor for better conjugation with the π system of the chromophore. Otherwise, deliberate separation is provided in chemosensor design between the receptor unit and signalling unit through a short covalent linker.[1.36] Another tactic used in designing a discrete anion sensor is chemodosimeter approach. Rather than using non-covalent interactions to create supramolecular anion-receptor complex for anion sensing, the receptor is allowed to react with the anion or is catalysed by the anion to form a novel molecular entity with dissimilar optical properties.[1.37]

Comprehensive studies reveal that the chemosensor can sense the presence of the guest analyte using any of the four reactions mechanisms:[1.38] (1) protonation-deprotonation (2) complexation (including direct and displacement complexation) (3) cleavage and formation of covalent bonds and (4) redox reactions. Development of chromogenic and fluorogenic pH probes are usually based on protonation-deprotonation reactions while redox reactions based chemosensors selectively sense analytes such as metal ions, reactive oxygen species, small molecules and enzymes through redox reactions without the release of fluorochromes.

In anion sensing, the other two strategies are widely explored and employed likewise. Complexation-based chromogenic and fluorogenic probes are categorised into two types: direct complexation and competitive displacement complexation. In case of direct complexation approach, there exist a covalent linkage between the recognition unit (receptor) and the signalling unit (reporter) and complexation occurs between the resulting probe and the analyte (anion) via the following means: coordination, electrostatic interaction, or hydrogen bonding. The designing of chemosensor with high sensitivity and selectivity for anions in an aqueous system is a stimulating task because of the strong hydration effects exhibited by the anions. Molecular recognition based on hydrogen bonding is predominant in organic solvents only. The significant interactions based on direct complexation in anion chemosensor are mainly (i) electrostatic interactions via positively charged receptors comprised of polyamines and imidazolium groups and (ii) complexation with metal centres wherein a metal ion complex acts the dual role of a receptor as well as a reporter. In competitive displacement complexation approach, the receptor and the reporter constitute a molecular ensemble, which itself functions as a probe. Because of the stronger interaction with the analyte, the receptor in the ensemble releases the reporter unit, thereby bringing about the photophysical signal response of the system. Nucleophilic reaction with certain anions (e.g., F^- and SO_3^{2-}) may lead to the cleavage of the covalent bond between a removable group (usually electron-deficient groups) and a fluorochrome. This releases the fluorochrome, which eventually recovers its fluorescence signal leading to the development of a specific class of fluorogenic probe for the aforementioned anions. For anions such as HS^-, HSO_3^-, SO_3^{2-} and CN^- recognition approach has been developed lately based on the formation of the covalent bond.

In order to recognize and selectively bind the anions in an appropriate framework, most neutral artificial receptors establish hydrogen-bonding interactions expending the hydrogen bonds offered by specific binding sites from amide,[1.39-1.40] urea/thiourea,[1.41-1.42] pyrrole/indole[1.43-1.47], imidazole/benzimidazole[1.48-1.51] and triazole[1.52-1.53] functionalities.

1.3.3 *Why benzimidazole or benzothiazole based receptors are used in anion recognition*

The utter apprehension of the notion of expending binding sites in heterocyclic rings or functional groups in simple organic molecules has led to the development of one type of selective and effective synthetic receptor that can selectively recognise ions and act as sensors. Thus, heterocyclic chromophores have become one of the most investigated classes of optical chemosensor moiety owing to their exceptional spectral properties with simultaneous ability to detect different analytes. Amongst these, the benzimidazole moiety has grasped immense attention, as these are therapeutically active and broadly used in drug discovery and medicinal research.[1.54] The imidazole ring in benzimidazole moiety is ubiquitous in nature and plays a critical role in structural architecture inside the human body, mostly encountered as histamine and histidine. Furthermore, marine sponges harvest a plethora of remarkable, structurally complex secondary metabolites, which typically contain imidazole moiety. More interestingly, imidazole ring from the histidine residue can be located as the most common ligand at the active sites of various metalloproteins.[1.55] In synthetic anion receptor chemistry, the imidazole ring acts as an outstanding hydrogen bond donor while the acidity of the imidazole –NH proton can also be modified by altering the electronic properties of the imidazole substituents. Moreover, the presence of a donor pyridine-like nitrogen atom within the ring enables the selective binding of metal ions that may help in metal assisted anion recognition. Additional beneficial aspects of this nitrogen atom lie in the fact that it can be the charged positively to get supplementary assistance in anion binding as well as water solubility. The benzimidazole moieties are somewhat similar to biological protein residues tryptophan as the latter consist of indole ring instead of imidazole ring in the former. The tryptophan residues are found to be actively participating in anion binding in biological system portrayed by sulfate binding site in sulfate binding proteins and binding of chloride anion by active site of haloalkane dehalogenase (Figure 1.1a and 1.1b). Besides having all the above properties, benzimidazole moiety is fluorescence active and can therefore function as a fluorogenic antenna. Apart from its photochemical properties, the notable difference between the two heterocycles involves the different acidity of the benzimidazole –NH proton caused by the electronic effect of the benzene ring. The resemblance of structural features of benzimidazole to certain biological compounds like vitamin B_{12} nucleus and purine base of DNA makes it an interesting candidate for the pharmaceutical industry. Being isosteric with the indole and purine nuclei, benzimidazole bind reversibly and irreversibly to enzymes while making its presence in certain fundamental cellular components and bioactive compounds. Benzimidazole selectively binds parasite β-tubulin and has been demonstrated as a specific binding unit towards the DNA

minor groove, serotonin receptors (5-HT), histamine (H4) receptors, dopamine (D4) receptors, VEGFR, G protein coupled receptors (GPCRs) and act as inhibitor of certain kinase enzymes such as anaplastic lymphoma kinase, c-Abl kinase, casein kinase 2, ATR kinase, tyrosine kinase, thymidylate kinase.[1.56] They also act as ubiquitination inhibitors, TCS inhibitors, PARP-1 inhibitor, NK2 antagonist as well as a prominent inhibitor towards a large array of DNA and RNA processing enzymes exemplified by topoisomerase, DNA and RNA polymerases. They also possess excellent activity against the Coxsackie virus B3 and also target specific hepatitis C virus enzymes.[1.56] Benzimidazole ring is present in a number of essential drug molecules as proton pump inhibitors (omeprazole), antihypertensives (candesartan, telmisartan), antihelmintics (albendazole, mebendazole) and antihistaminics (astemizole), Antitumorals and antiviral ability of the benzimidazole containg drugs are still under investigation.[1.56] Substitution by nitro, amino or halogen groups at the 4, 5, 6 or 7 positions in the benzimidazole moiety introduces other functional groups feasible for targeting biomolecules as well as improving the electronic properties, which in turn, influence directly on the chemical, photochemical and spectroscopic properties. Thus, the inherent electron accepting and π-bridging properties along with fluorogenic responses, pH sensitivity and switching, presence of ringed nitrogen atom for chelating metal ion and its biocompatibility have made the benzimidazole moiety a principal candidate for its use as chemosensor functionality.[1.49,1.51]

Benzothiazole unit, on the other hand, is the combination of two rings: thiazole and benzene. The presence of sulfur and nitrogen atoms in the thiazole core is significant as benzothiazole unit plays a vital role as a template in the development of derivatives of thiazole that act as pharmacologically and biologically active compounds. Although it is stable because of its aromaticity, but being a heterocycle it has reactive sites too that allow for functionalization. In fact, the 2-substituted benzothiazole has emerged itself to be the core structure in the diversified therapeutic applications.[1.57] Benzothiazole derivatives find its importance in medicinal chemistry due to their numerous yet potential applications as antimicrobial, anticancer, antidiabetic, anti-inflammatory, antiviral and antileishmanial.[1.58] Benthiazole based ethoxzolamide drug is used as diuretic agent, frentizole as antiviral agent and immunosuppressive agent, halethazole as antiseptic agent, perospirone as antipsychotic agent, pramipexole as antiparkinson's agent, tiaramide as anti-inflammatory agent and zopolrestat as antidiabetic agent. 2-(4-aminophenyl)benzothiazole derivatives have been shown to possess potent antitumour activity rendering their perspective role.[1.59] During anion recognition, if linked to a chromophore, the benzothiazole unit improves photophysical properties extending conjugation in the chemosensor. Benzothiazole containing

motifs are also considered as a suitable competitor in the field of anion recognition as they show large molecular hyperpolarizability.[1.60]

1.3.4 Anion recognition using Benzimidazole and Benzothiazole based receptor: a thorough literature review of solid state and solution phase studies

With the developments in anion recognition in the recent past, anion supramolecular chemistry has flourished to a superlative extent. Benzimidazole and benzothiazole based receptors have also grasped keen attention in both solid state and solution phase recognition of anionic species due to the aforementioned properties. Exploring the anion recognition properties and sensing behaviour of these receptors has enriched the wisdom of chemical science fraternity as a whole. Hence, it is necessary to have a closer review on the recent advancement in the field of recognition and sensing of anionic guest with benzimidazole and benzothiazole based receptors so that newer challenges can be tackled with plausible improvements in receptor design.

P. A. Gale and his co-workers have reported a series of benzimidazole based anion receptors which exhibit tautomeric switching upon addition of basic anions (Figure 1.2).[1.61] The crystal structure elucidates the solid-state recognition of benzoate anion by one of the tautomers **1** in which the benzimidazole –NH is directed convergently with the urea –NH groups. The intermolecular hydrogen bonding interactions exist between the two receptors, two anions and two water molecules to form a dimer maintaining a ratio of receptor: anion: water = 2: 2: 2.

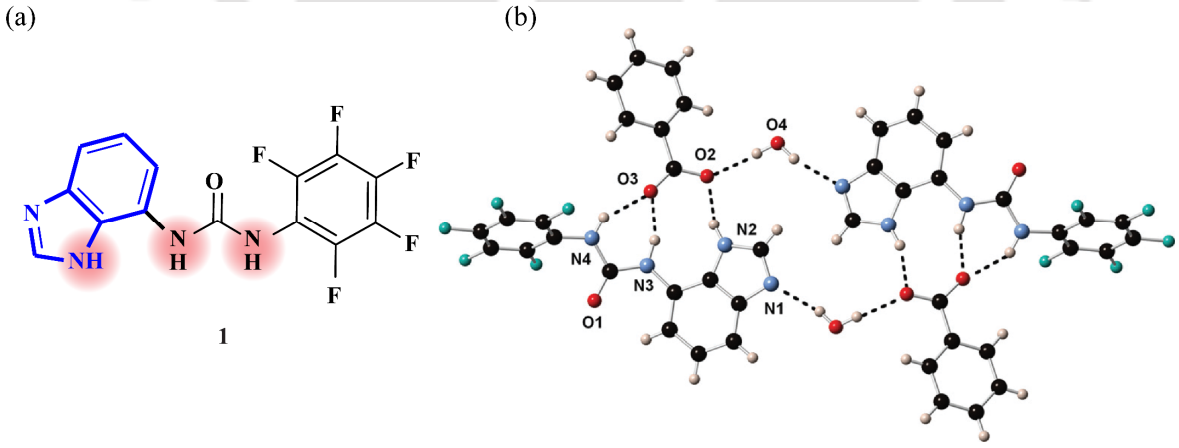

Figure 1.2 (a) Molecular structure of the receptor **1.** (b) Hydrogen bonded benzoate complex of the receptor **1**.

Another instance of the influence of anions on tautomerism in benzimidazole containing anion receptors (Figure 1.3a) has been reported by P. A. Gale *et al.*[1.62] Single crystal structural elucidation and ^{1}H NMR studies suggest that hydrogen bonding interactions between the receptors and guests contribute immensely to the nature of the tautomer present as shown in Fig. 1.3b. Single crystal structures were obtained for tetrabutylammonium benzoate complex of receptor **2a** and

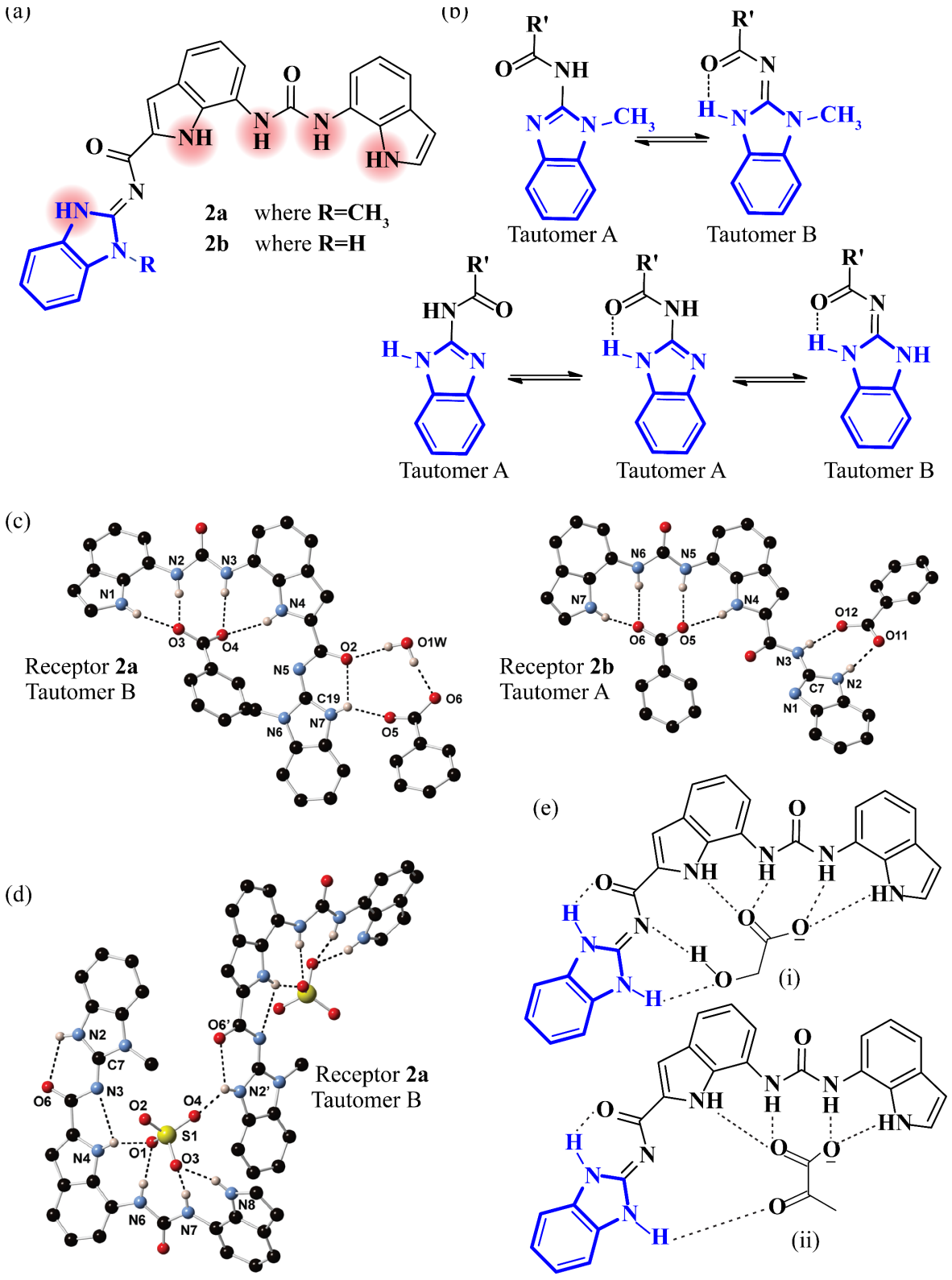

Figure 1.3 (a) Molecular structure of the receptors. (b) Tautomers exhibited by the receptors and their intramolecular hydrogen bond stabilisation. (c) Crystal structure of the benzoate complex with receptor **2a** and receptor **2b** in different tautomeric forms. (d) Sulphate complex of receptor **2a** adopting tautomeric B form. (e) Proposed binding modes of receptor **2b** with (i) lactate and (ii) pyruvate anion where it acts as tautomer B.

receptor **2b** as depicted in Figure 1.3c. Structural elucidation discloses that the receptor **2a** binds to two equivalents of the benzoate anions. The central diindolylurea group plays a pivotal role in binding the first benzoate anion using four hydrogen bonds while the receptor adopts tautomeric B form. The benzimidazole –NH assisted by the hydrogen bonding interaction from bridged water molecule binds the other benzoate anion. In the benzoate complex of receptor **2b**, the first anion is coordinated to the receptor via the hydrogen bonds donated by the central diindolylurea group. The benzimidazole group assumes tautomeric A form allowing the two –NH groups to donate two parallel hydrogen bonds to a second benzoate anion. Receptor **2a** also binds sulphate anion in its neutral form where it exhibits as tautomer B and offers four hydrogen bonds to the coordinated sulfate anion (Figure 1.3d). The fifth hydrogen bonding interaction is from the benzimidazole –NH of an adjacent complex, which also links the sulfate complexes into a chain in the solid state. In solution state, ^{1}H and ^{13}C NMR studies confirm the receptors are exhibiting tautomeric B structure, as depicted in Figure 1.3e, during the preferential binding of lactate over pyruvate anion.

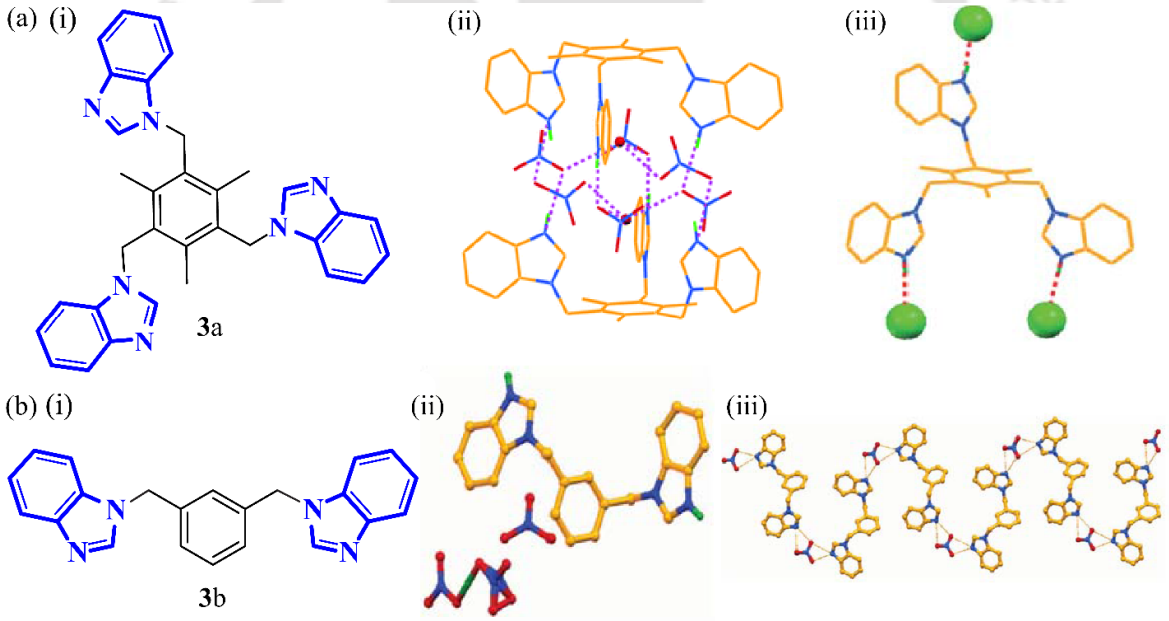

Figure 1.4 (a) (i) Molecular structure of the tripodal receptor **3**a. (ii) Single crystal X-ray structure of the nitrate complex by the protonated receptor. (iii) Single crystal structure of the chloride complex. (b) (i) Molecular structure of the dipodal receptor **3**b. (ii) Single crystal structure of the hydrogen dinitrate complex with nitrate anion assisted 1D-zigzag polymeric chain (iii).

Tripodal and dipodal receptors based on benzene platform with heterocyclic benzimidazole terminals have been chosen to coordinate with anions of different dimensionality in its protonated form. Ghosh and his co-workers have reported the nitrate and chloride ion-dependent aggregation properties of the protonated receptors.[1.63] In its triprotonated state, the receptor **3**a forms a dimeric capsule with the help of six hydrogen bonded NO_3^- ions, which encapsulates two water molecules

as guests (Figure 1.4a ii). The protonated receptors give rise to a bowl shaped cavity with all benzimidazole binding sites protruding in one direction. In contrast, the receptor fails to form a capsular aggregate with spherical chloride ion, as two of the three arms are oriented in a different direction (Figure 1.4a iii). A rare yet fascinating solid state binding of hydrogen dinitrate anion $(O_2N–O\cdots H\cdots O–NO_2)^-$ takes place in the nitrate complex of the dipodal receptor **3**b as shown in Figure 1.4b ii. The dinitrate anion where the central hydrogen atom bridges the two nitrate oxygen atoms is located in crystal lattice whereas NO_3^- ion participates to link the two receptors. Both the benzimidazole podant of the receptor **3**b are projected in opposite direction, which helps in the formation of a zigzag polymeric chain upon NO_3^- ion binding (Figure 1.4b iii).

The employment of benzimidazole based tripodal receptors in anion binding has been further presented by Das *et al*. where they have reported an isolated water chloride cluster $[Cl_3(H_2O)_4]^{3-}$ formation on addition of excess hydrochloric acid to a methanol–water (2:1) solution of the receptor **4** (Figure 1.5a).[1.64] The benzimidazole arms are oriented in such a way that it forms a bowl shape along with its –NHs for suitable space and binding site which favours the development of the chloride–water cluster. Structural exposition of the chloride cluster suggests that binding of three different chloride anions occurs in the lattice through several O–H···Cl and N–H···Cl hydrogen bonds (Figure 1.5b). Interestingly, three different π–π interactions: one intramolecular and other two intermolecular; are also present. Each pentameric cluster comprising two Cl^- ions

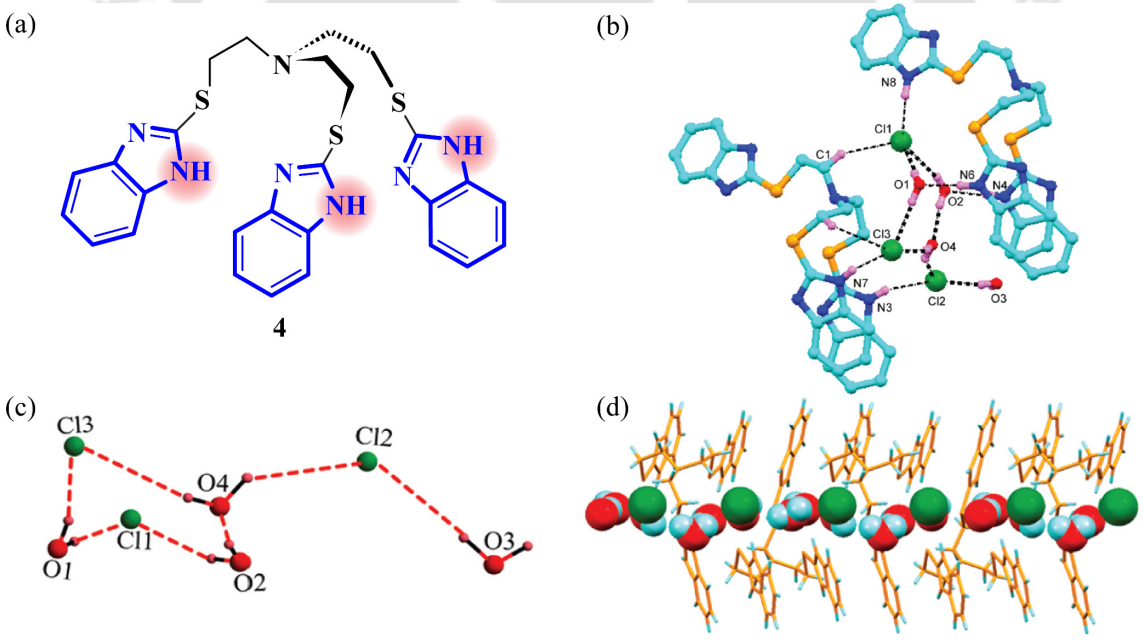

Figure 1.5 (a) Molecular structure of the tripodal receptor **4**. (b) Different binding environments of chloride ions in the crystal. (c) Chloride–water pentamer $[Cl_2(H_2O)_3]$adopting a half chair conformation. (d) Propagating Chloride–water channels through the hydrophobic channel formed by the receptor units.

and three water molecules, attaches itself to the next analogous unit by the tail, having one chloride and one water molecule as illustrated in Figure 1.5c. The dichloride pentamer leads to the formation of a heteroatomic water−cluster channel with the help of its tail in the hydrophobic framework created by the protonated receptor **4** (Figure 1.5d).

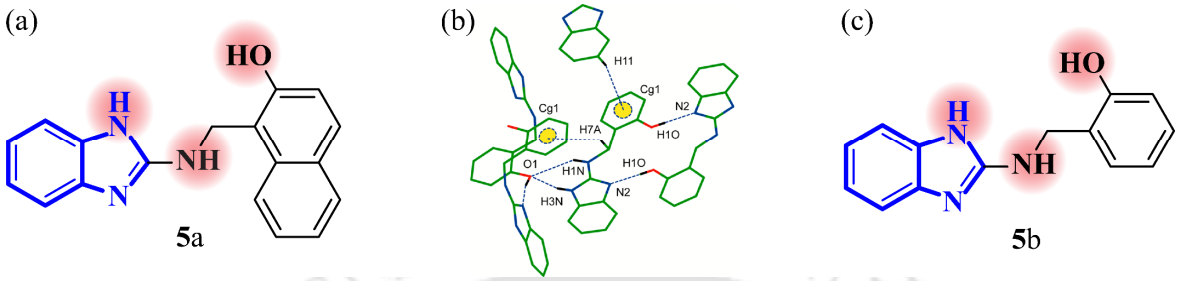

Figure 1.6 (a) Molecular structure of the tripodal receptor **5a**. (b) Crystal structure of the receptor **5**a depicting aromatic and aliphatic C−H···π interactions along with other hydrogen bonding interactions. (c) Molecular structure of the tripodal receptor **5b**.

Das and his co-workers have also demonstrated two charge assisted benzimidazole based receptors (**5**a and **5**b) bearing –NH and –OH functionalities which bind anions of varying dimensionality in the solid state (Figure 1.6).[1.65] Structural elucidation from single-crystal X-ray analysis reveals apposite binding topology of the anions pertaining to variable dimensionality with the protonated receptor molecules. With the spherical chloride ion, two of the benzimidazole –NHs (both protonated and neutral) and one –OH belonging to receptor **5**a take part in binding as shown in Figure 1.7a. The planar nitrate anion is stabilized by eight hydrogen bonding interactions from four protonated receptors **5**a consisting of several N−H···O and C−H···O bonding (Figure 1.7b). The asymmetric unit of the acetate complex consists of one protonated receptor accompanied by one acetate anion. Acetate anion is stabilized via six hydrogen bonding interactions from five protonated receptors consisting of three N−H···O, two C−H···O and one O−H···O interactions as presented in Figure 1.7c. Four of these five interacting receptors in conjunction with another receptor unit, interact with another acetate ion anti to the first acetate ion leading to a molecular barrel type structure. The aromatic acid based 3,5-dinitrobenzoate (DNB) anion is stabilized with the help of several N−H···O, C−H···O, O−H···O, C−H···π, and π···π interactions resulting in the crystal structure of molecular salt as in Figure 1.7d. With tetrahedral dihydrogen phosphate anion, the receptor **5**a also crystallizes one methanol unit as co-crystal in the asymmetric unit. From the single crystal study in Figure 1.7e, it is apparent that both the neutral −NH as well as protonated nitrogen of the benzimidazole moiety donate hydrogen bonding interactions to the dihydrogen phosphate anion. The hydrogen bonding between dihydrogen phosphate anion and the co-crystallized methanol oxygens, −NH and −OH groups of the receptor

5a give rise to a ladder-type H-bonding structure.

In case of the receptor **5**b, the encapsulated acetate ion exhibits different coordination environment and faces toward two interlocked receptors in the same plane. The asymmetric unit contains one monoprotonated benzimidazole receptor neutralized by the acetate anion and one acetic acid as co-crystal in the solid structure. Seven hydrogen bonding interactions are present in the acetate crystal which are donated by two protonated receptors and an acetic acid with the help of two N−H···O, one O−H···O and three C−H···O interactions comprising of both aliphatic and aromatic hydrogens (Figure 1.7f). Similar to earlier DNB crystal, the DNB ion crystallizes with two protonated receptors **5**b and the charge neutralization is accomplished by two deprotonated DNB molecules (Figure 1.7g). The DNB crystal by **5**b exhibits conformation isomorphs but misses π···π interactions. The structural exposition of the single crystal of the tetrahedral hydrogen sulfate anion (Figure 1.7h) divulges each hydrogen sulfate ion to be interacting with two protonated receptor molecules and two water molecules experiencing four hydrogen bond coordination from two NH···O and two OH···O interactions.

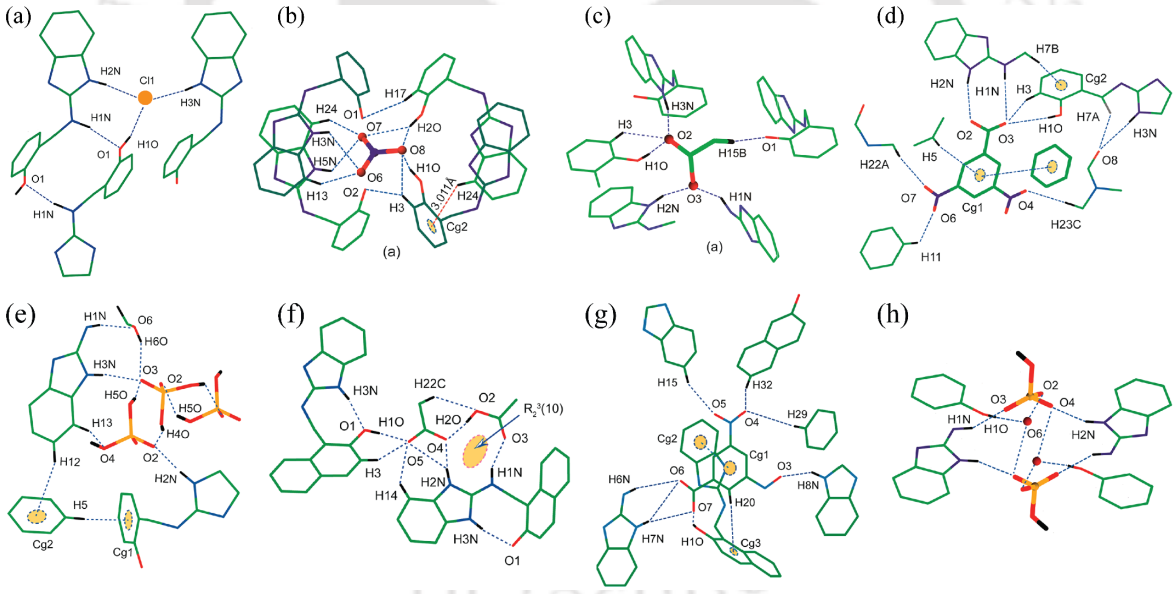

Figure 1.7 (a) Coordination environment of spherical chloride anion in [**5**aH$^+$][Cl$^-$] complex (b) Coordination environment of NO_3^- anion in the complex by protonated **5**a. (c) Crystal structure of [**5**aH$^+$][OAc$^-$] complex. (d) Binding of DBA anion in the salt by protonated **5**a. (e) Crystal structure of [**5**aH$^+$][$H_2PO_4^-$] complex. (f) Coordination environment of acetate anion in salt by protonated **5**b. (g) Coordination mode of 3,5-dinitrobenzoate anion in the molecular salt by protonated **5**b. (h) Binding of HSO_4^- anion in the complex by protonated **5**b.

Parallel to the solid state anion binding by the benzimidazole receptors, the solution phase recognition has also been emerging and seeking immense attention in the recent past. Nevertheless, it is noteworthy that the information derived from comparing solid state structural analysis with anion binding in solution phase can be ambiguous. Although low entropy and high

concentration are characteristics of crystal lattices, yet their enthalpic signature is highly noticeable and can be determined even with simple metric analyses. The crystalline anion-receptor complexes can be extremely useful for illustrating unique binding patterns, steric factors and preferential conformations. Anion recognition in solution phase, on the other hand, is expedient because of the rapid response time, intrinsic flexibility of the receptor and better selectivity amongst various anions. Strong hydration effects of anions in the aqueous system make the designing of highly sensitive and selective chromogenic and fluorogenic probe very challenging. Benzimidazole and benzothiazole based receptors can be employed in the solution phase as well because of the presence of the fluorogenic antenna in addition to the supplementary electrostatic assistance by the charged moiety. Both −NH and nitrogen (if protonated) functionalities of the benzimidazole can afford hydrogen bonding interactions to stabilize the host-guest complex. Apart from this, hydrogen bonding interactions from benzimidazole or benzothiazole −CH is also feasible.

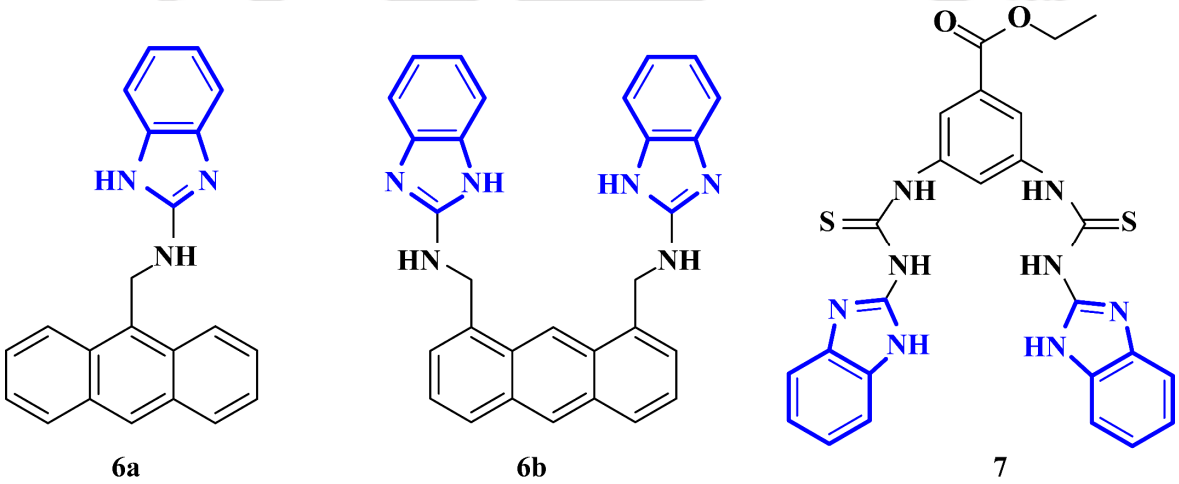

Figure 1.8 Molecular structures of PET-based chemosensors **6**-**7**.

Two neutral acyclic benzimidazole based anthracene containing fluorescent chemosensors **6a** and **6b** are reported by Jang *et al.*, which recognize multiple ions through PET caused fluorescence quenching (Figure 1.8).[1.66] Upon addition of halides, acetate and $H_2PO_4^-$ anions to the monopodal receptor **6a** which exhibits strong fluorescence in acetonitrile, experienced quenching via photoinduced electron transfer (PET) mechanism. The binding stoichiometry is found to be 1: 1 for halides, acetate and dihydrogen phosphate. Anion binding to the acidic N– H hydrogens in the receptor leads to an increase in reduction potential of the N–H bonds that in turn, augment the affinity of fluorescence quenching via PET mechanism. However, chemosensor **6b** with two benzimidazole functionalities exhibits stronger interactions towards the targeted anions because of the participation of all four –NH groups in the anion binding. The same is reflected in the

substantial increase in association constant values of chemosensor **6b** during the binding of acetate and dihydrogen phosphate. Another thiourea and ester modified dipodal benzimidazole probe **7** has been shown to have selective recognition of PO_4^{3-} in mixed DMSO/H_2O (8:2, v/v) solvent system by the same research group (Figure 1.8).[1.67] The fluorescence of the receptor decreases due to PET process upon binding the anion in 1:1 stoichiometry. The preference for the PO_4^{3-} ion is due to the complementarity of the pseudocavity of receptor **7** with the size and tetrahedral geometry of the anion. The benzimidazole core acts as the signalling unit as well as hydrogen bond donor, which determines the selectivity of the chemosensor.

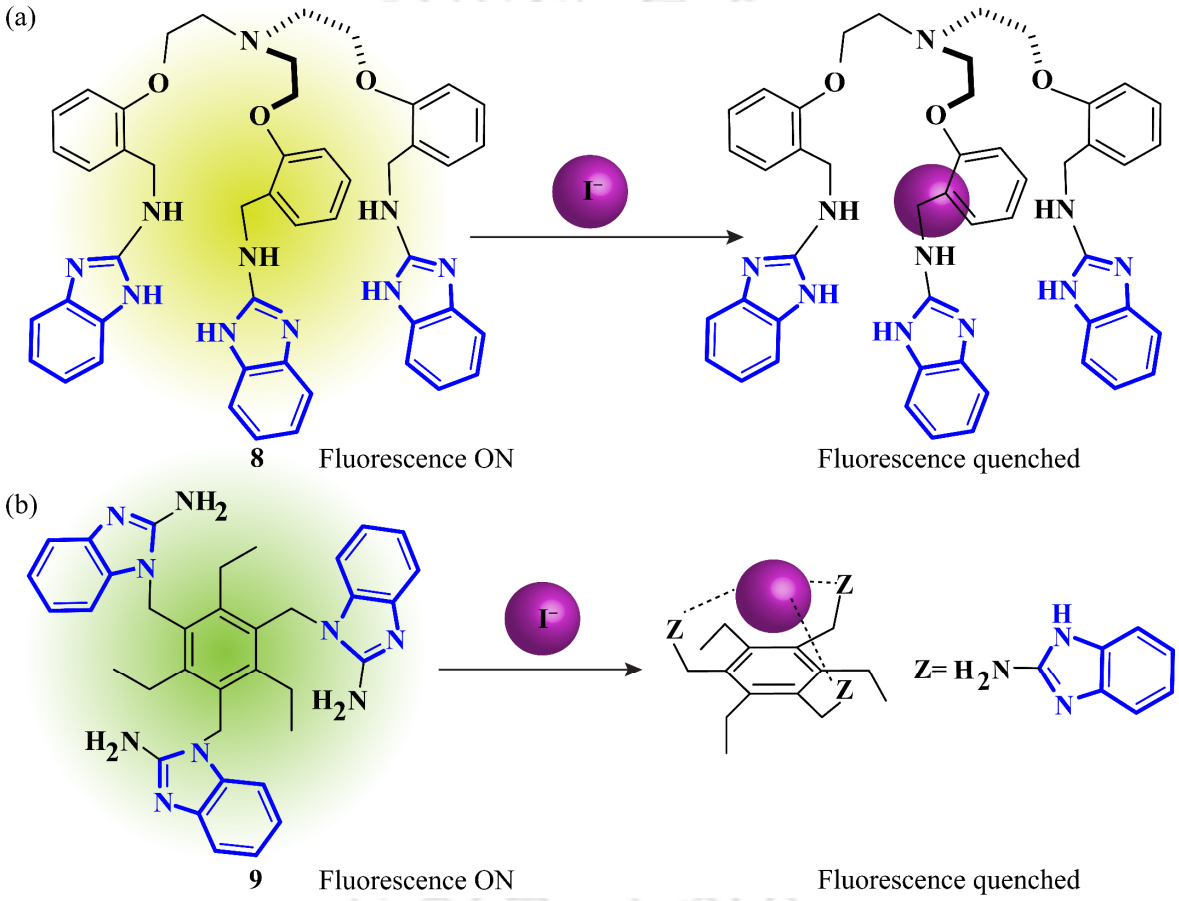

Figure 1.9 Molecular structures of the chemosensors **8**-**9** and their respective sensing mechanism.

In another instance, a benzimidazole based neutral receptor **8** in tripodal framework illustrates excellent selectivity for iodide ion without interference from other tested anions including F^-, Cl^-, Br^-, NO_3^-, CH_3COO^-, HSO_4^- and $H_2PO_4^-$ (Figure 1.9a).[1.68] The probe **8**, exhibits quenching in the intensity maximum at 495 nm in CH_3CN/H_2O (9:1, v/v) solution upon addition of I^- ion. The parallel alignment of N–H bonds in the receptor, its flexibility as well as the complimentary size of the anion are shown to govern the encapsulation of the anion in the preorganized pseudocavity. The continuous effort to synthesize benzimidazole based anion receptor is also reflected in another

encapsulation of iodide ion by a 1,3,5-substituted triethylbenzene derivative with a 2-aminobenzimidazole moiety, **9** where the latter is found to be the binding and signalling unit (Figure 1.9b).[1.69] The sensitivity and selectivity towards the iodide ion are obtained via absorption spectroscopy and a quenching in fluorescence intensity of the receptor in a buffered CH_3CN/H_2O (99:1, v/v) solution. Binding of the iodide ion in the receptor's pseudocavity via hydrogen bonding of $–NH_2$ protons leads to the static quenching of the fluorescence intensity of receptor **9**.

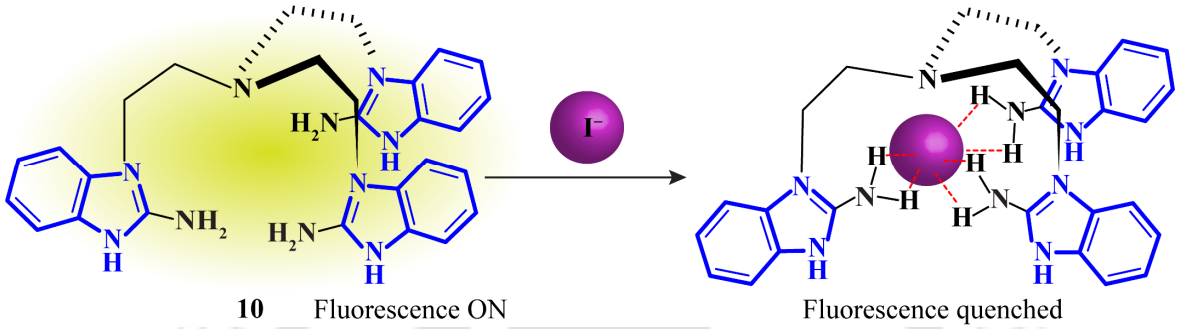

Figure 1.10 Molecular structures of the chemosensors **10** and its sensing mechanism.

Das and co-workers have also reported similar recognition of iodide ion by a novel benzimidazole based tripodal receptor (Figure 1.10).[1.70] The fluorescent receptor **10** can selectively bind iodide anion with concurrent quenching in its fluorescence intensity and with a 10 nm blue shift in UV/Vis spectra in CH_3CN/H_2O (99:1, v/v, pH = 7.91 HEPES buffer). Addition of other anions (F^-, Cl^-, Br^-, OAc^-, $H_2PO_4^-$, SO_4^{2-}, NO_3^- and CN^-) to the receptor **10** bring about no characteristic changes either in emission or absorption spectroscopy.

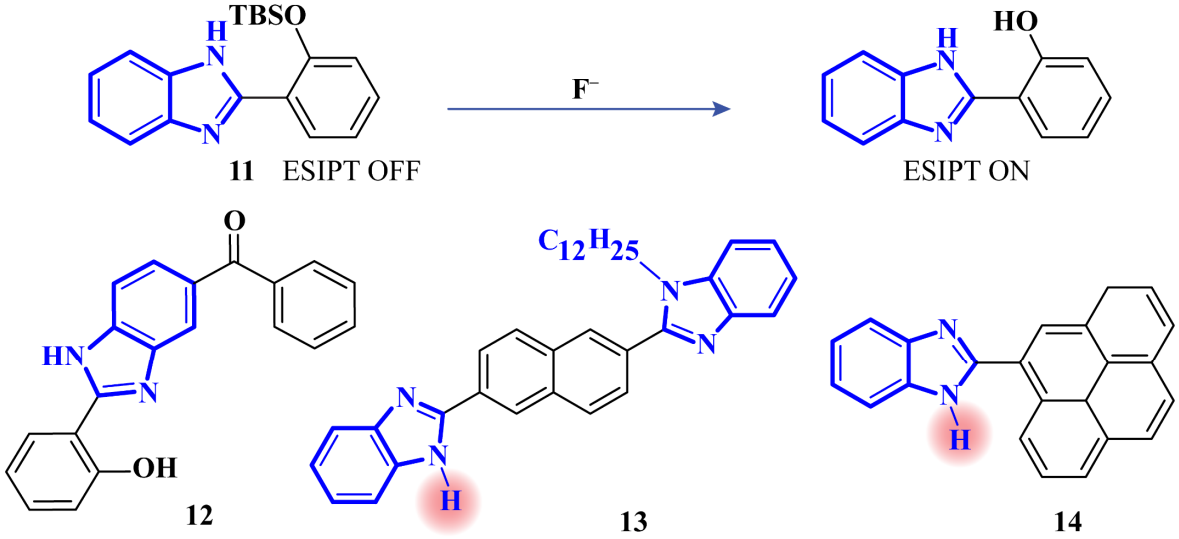

Figure 1.11 Molecular structures of ratiometric benzimidazole based chemosensors **11-14**.

Ratiometric chemosensors for anion sensing are mostly favoured as these can measure emission intensities at two different wavelengths which overcome the disadvantages related with intensity-

based measurements owing to the inherent correction for environmental effects and also escalate the selectivity, sensitivity and dynamic ranges of measurement (Figure 1.11). The first use benzimidazole based receptor for ratiometric anion sensing was based on 2-(2-hydroxyphenyl)benzimidazole framework.[1.71] The sensing of fluoride ions over other anions by receptor **11** is based on the modulation of the excited-state intramolecular proton transfer (ESIPT) process. Treatment with fluoride ions in aqueous DMF solution leads to the removal of the TBS protecting group of probe **11** thereby switching on the ESIPT process apparent in the decrease in emission band at 360 nm with a simultaneous increase in newly formed emission maximum around 454 nm. Another benzimidazole derivative **12** also acts as a selective chemosensor for selective recognition of F^- ions in acetonitrile.[1.72] The ESIPT based binding event is confirmed by the bathochromic shift absorption maxima at 360 nm and a ratiometric shift in fluorescence spectrum where the emission band at 420 nm shifts to 540 nm.

Chemosensors **13** and **14** are reported as fluoride ion sensors where the receptors expend hydrogen bonding via the acidic benzimidazole –NH during fluoride binding which gets deprotonated on excess addition of the targeted anion.[1.73-1.74] Addition of F^- to the chemosensor **13** results in colorimetric change from colourless to pale green under ambient light and green fluorescence under 365 nm UV light. Upon addition of fluoride ion, receptor **14** experiences a ratiometric shift from 366 nm to 402 nm in UV-Vis and 433 to 502 nm in the emission spectrum.

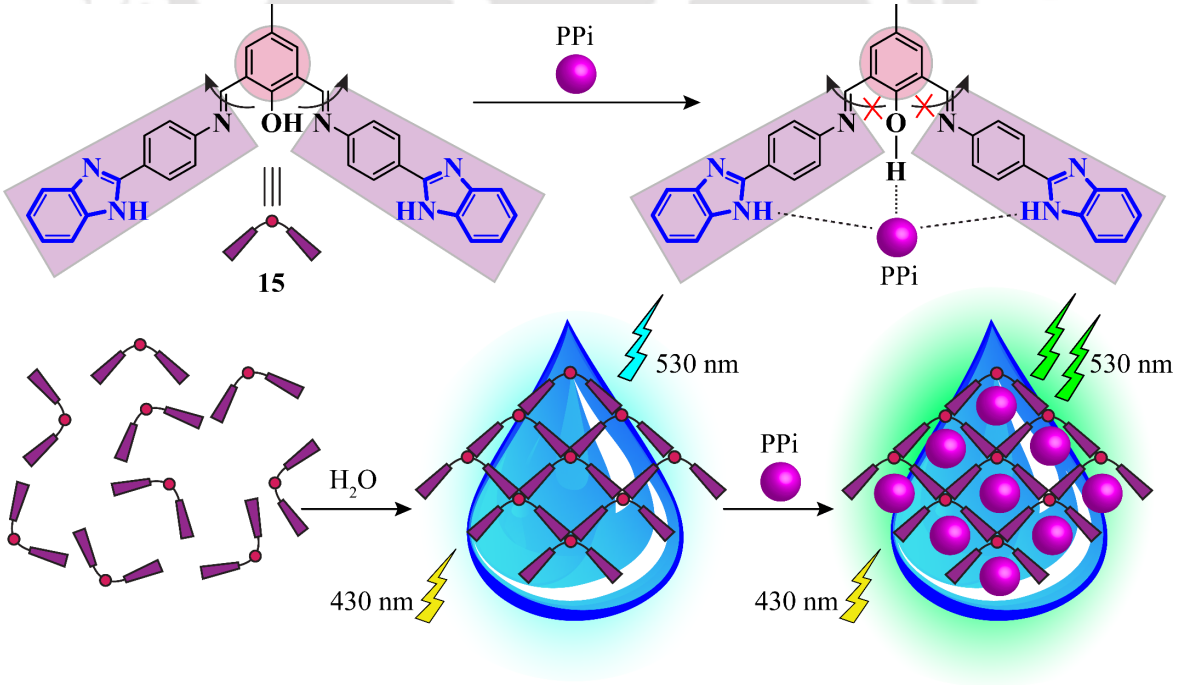

Figure 1.12 Aggregation induced emission of benzimidazole-based derivative **15** and its mechanism for detection of PPi.

A captivating novel AIE system based on a benzimidazole derivative **15** has been reported by Das and co-workers for detection of pyrophosphate (PPi) in physiological medium (Fig. 1.12).[1.75] The benzimidazole moiety plays the functional role in assembling the aggregated structures as well as recognition of the PPi ion in a competitive medium through 'turn-on' colorimetric and fluorimetric responses. Addition of H_2O into the probe solution in THF results in self-assembly of nanostructures with distinct emission at λ = 530 nm. PPi addition induces the manifold enhancement of the emission intensity of the probe which remains unaffected by other anions. The detection of PPi by the chemosensor can also be achieved in a mixed aqueous medium with similar photophysical changes.

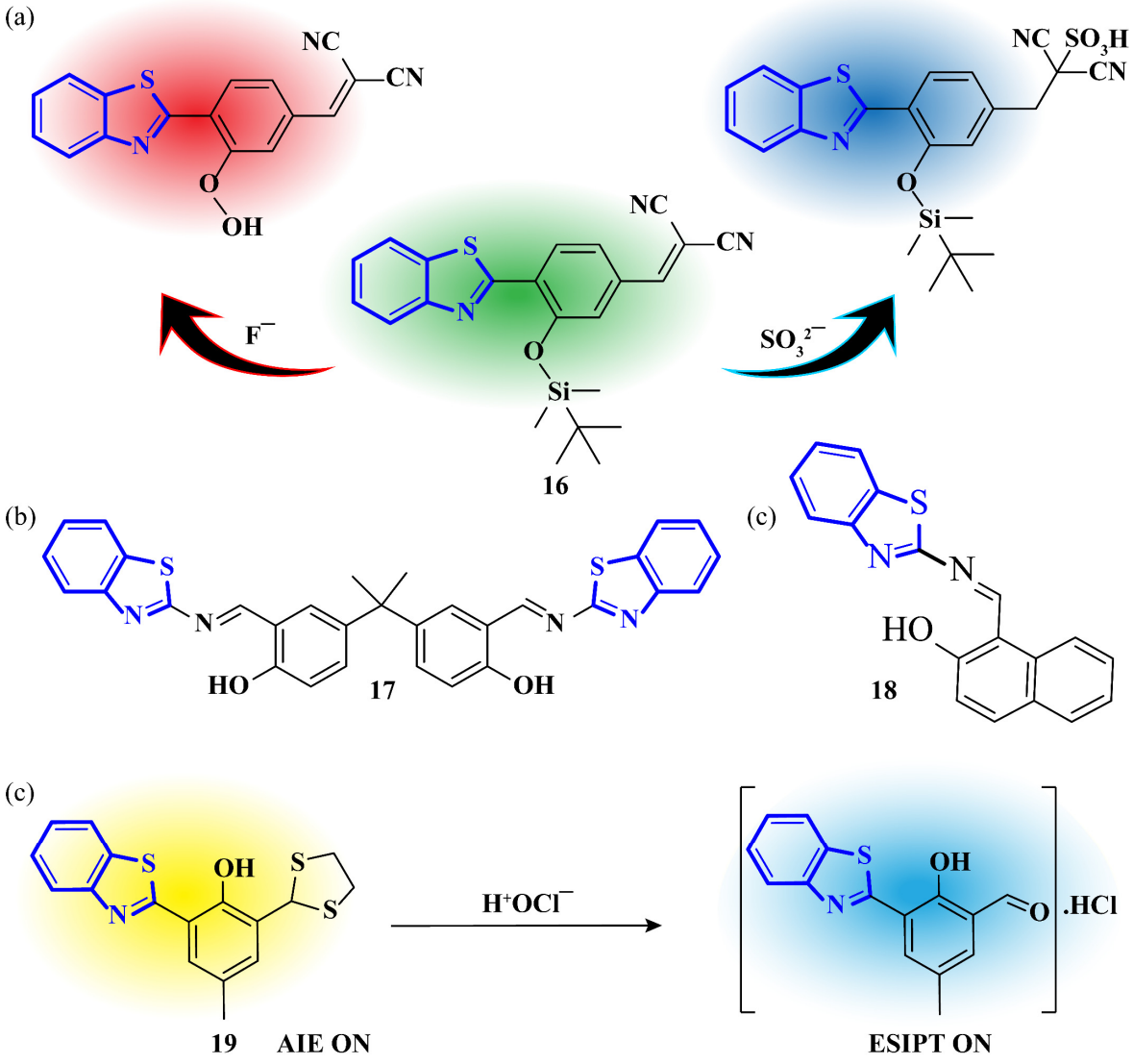

Figure 1.13 Molecular structures of benzothiazole based chemosensors **16-19** and their sensing mechanism.

Song and co-workers have reported a benzothiazole based bifunctional ratiometric fluorescent probe **16**, which can selectively bind both F^- and SO_3^{2-} anions with high sensitivity.[1.76] As shown in Figure 1.13a, the probe **16** exhibits a green fluorescence at I_{max}= 498 nm when excited at 410 nm in HEPES buffer solution. On addition of fluoride ion to the chemosensor **16** results in red fluorescence with a shift in emission maxima to 634 nm. Addition of fluoride ion to chemosensor **16** selectively cleaves the tertbutyldimethylsilyl ether bond and thereby, restores the ESIPT process. On the other hand, the addition of SO_3^{2-} ion induces Michael addition to the C=C double bond of the probe, which decreases the ICT process resulting in a blue shifted emission maxima at 371 nm. Another attractive Benzothiazole based dipodal Schiff base chemosensor **17** has been shown to have selective colorimetric as well as 'turn-on' fluorescent sensing ability towards fluoride ions in the presence of other anions in acetonitrile medium (Figure 1.13b).[1.77] Chemosensor **18** reported by Kim and co-workers acts a cyanide sensor through fluorogenic and colorimetric response based on a deprotonation event with subsequent nucleophilic addition.[1.78] Interestingly, it is a highly selective colorimetric acetate sensor based on a deprotonation process. Chemosenor **18** is the first reported chemosensor for the aforesaid anions with two different detection modes. Chen *et al.* illustrate a benzothiazole based chemosensor **19** for selective and sensitive detection of hypochlorite anion.[1.79] As depicted in Figure 1.13c, the probe **19**, upon addition of hypochlorite, swiftly turns into its oxidized form accompanied by a change in fluorescence from yellow to blue. The probe **19** initially exhibits emission at a longer wavelength (546 nm) in PBS buffer (pH=7.4), due to aggregation induced emission (AIE) mechanism. On addition of the hypochlorite ion, the dithiolane moiety in probe **19** changes to aldehyde unit and forms an adduct with HCl which emits blue fluorescence at 464 nm owing to ESIPT process.

Relatively cheaper synthetic procedure, high selectivity, prompt sensitivity, and easy handling have made small molecular chemosensors as the most broadly studied and extensively used chemosensors to target various hosts both *in vivo* and *in vitro*. Thus, we decided to synthesize benzimidazole and benzothiazole functionalized small molecular probes for sensing anionic species.

1.4 Concluding Remarks and objective of the thesis

From the thorough exploration of the literatures, it can be concluded that the acyclic receptors containing benzimidazole moiety in rigid or flexible scaffolds with appropriately positioned binding sites can recognize anionic guest either in solid or in the solution state. Despite their profound abundance in biological systems, imidazole core based benzimidazole or similar class of compounds has yet to go through in-depth assessment as chemosensor design for anionic

species. Blessed with the amphoteric behaviour of the imidazole ring, benzimidazole functionalities possess the additional benefits of a fluorogenic antenna, which has been discussed in the mentioned literatures. The electronic and fluorogenic assistance by the benzothiazole moiety is also presented in the reported literatures. Nevertheless, simultaneous detection of anions in solid as well as solution phase is what most of the literatures have been missing. With the help of the benzimidazole moiety, our aim is to develop anion receptors in a tripodal framework so as to obtain selective anion binding in both solid as well as solution phase. Tripodal receptors are favoured for anion binding because of the following features: (i) The flexibility of the tripodal receptors allows the formation of host-guest complexes with anionic guest of varying geometry and dimensions. (ii) These can accommodate an adequate number of neutral electron deficient groups or positively charged moiety as an interaction site. (iii) The classical complexation mechanism or non-covalent interaction can also be achieved.[1.80] In case of the symmetric acyclic tripodal receptors, the similar arms expend hydrogen bonding with targeted anionic species with multi-armed functionalities (urea/thiourea/ amide) leading to the formation of capsular and/or non-capsular assemblies. For simultaneous anion binding, we have planned to develop novel non-symmetric tripodal receptors consisting of two similar benzimidazole functionalized arms and the third arm for deliberate modification in order to augment the anion binding in solution phase as well as in solid state.

Anionic species are omnipresent in nature having diverse chemical and physiological impacts on the environment, biology, medicine and defence. Within this frame of reference, colorimetric and fluorescent probes which can emit differential signal output towards different anions are always admired. However, the reliability upon selectivity is questioned whenever anions with analogous chemical properties are also present, like the case of fluoride and acetate. We would expect shape and size complementary based discrimination of the anions based on our novel benzothiazole based receptors. Thus, the objective of the thesis can be summarized as-

- To design and synthesize of novel tripodal, dipodal and monpodal receptors based on benzimidazole and benzothiazole frameworks for better selectivity and sensitivity towards anions.
- Tailoring of non-symmetric tripodal receptor molecules to facilitate recognition of anions in both solution phase as well as solid state.
- To achieve selective sensing of single analyte among two or three competitive anions.
- To provide simultaneous breakthroughs by improving the optical properties of the receptors towards anions in solution phase.

References

1.1 J. M. Lehn, Supramolecular chemistry—scope and perspectives molecules, supermolecules, and molecular devices (Nobel Lecture), *Angew. Chem., Int. Ed. Engl.*, 1988, **27**, 89–112.

1.2 J. W. Steed and J. L. Atwood, Supramolecular chemistry, John Wiley and Sons Ltd., Chichester, 2nd ed, 2009, pp 2-3, 225-226,731.

1.3 J. W. Steed, D. R. Turner and K. J. Wallace, Core concepts in supramolecular chemistry and nanochemistry, John Wiley & Sons, Chichester, 2007, pp 1-4, 52-53.

1.4 D. J. Cram, Preorganization – from solvents to spherands, *Angew. Chem., Int. Ed. Engl.*, 1986, **25**, 1039–1134.

1.5 J. M. Lehn, Perspectives in supramolecular chemistry—from molecular recognition towards molecular information processing and self-organisation, *Angew. Chem., Int. Ed. Engl.*, 1990, **29**, 1304–1319.

1.6 C. A. Schalley, Analytical methods in supramolecular chemistry (Vol. 1), John Wiley & Sons, Chichester, 2012, pp 5–6.

1.7 S. M. Rowe, S. Miller and E. J. Sorscher, Mechanisms of disease; cystic fibrosis, *N. Engl. J. Med.*, 2005, **352**, 1992–2001.

1.8 F. Delange, The Disorders Induced by Iodine Deficiency, *Thyroid*, 1994, **4**, 107–128.

1.9 M. Cametti and K. Rissanen, Recognition and sensing of fluoride anion, *Chem. Commun.*, 2009, 2809–2829.

1.10 M. Kleerekoper, The role of fluoride in the prevention of osteoporosis, *Endocrinology and Metabolism Clinics*, 1998, **27**, 441–452.

1.11 S. G. Chang, D. Littlejohn and K. Y. Hu, Disulfate ion as an intermediate to sulfuric acid in acid rain formation, *Science*, 1987, **237**, 756–758.

1.12 B. Moss, A land awash with nutrients—the problem of eutrophication, *Chem. Ind.*, 1996, **11**, 407–411.

1.13 E. T. Urbansky, Perchlorate as an environmental contaminant, *Environ. Sci. Pollut. Res.*, 2002, **9**, 187–192.

1.14 K. Yoshihara, Technetium in the environment, *Top. Curr. Chem.*, 1996, **176**, 17–35.

1.15 S. L. W. D. E. Carter, Arsenate toxicity in human erythrocytes: characterisation of morphologic changes and determination of the mechanism of damage, *J. Toxicol. Environ. Health Part A*, 1998, **53**, 345–355.

1.16 N. H. Evans and P. D. Beer, Advances in anion supramolecular chemistry: from recognition to chemical applications, *Angew. Chem., Int. Ed. Engl.,* 2014, **53**, 11716–11754.

1.17 P. D. Beer and P. A. Gale, Anion recognition and sensing: the state of the art and future perspectives, *Angew. Chem., Int. Ed. Engl.,* 2001, **40**, 486–516.

1.18 (a) J. W. Pflugrath and F. A. Quiocho, Sulphate sequestered in the sulphate-binding protein of Salmonella typhimurium is bound solely by hydrogen bonds, *nature*, 1985, **314**, 257–260. (b) K. H. Verschueren, F. Seljée, H. J. Rozeboom, K. H. Kalk and B. W. Dijkstra, Crystallographic analysis of the catalytic mechanism of haloalkane dehalogenase, *Nature*, 1993, **363**, 693–698. (c) F. Nachon, E. Carletti, M. Wandhammer, Y. Nicolet, L. M. Schopfer, P. Masson and O. Lockridge, X-ray crystallographic snapshots of reaction intermediates in the G117H mutant of human butyrylcholinesterase, a nerve agent target engineered into a catalytic bioscavenger, *Biochem. J.*, 2011, **434**, 73–82. (d) M. Mileni, J. Garfunkle, C. Ezzili, B. F. Cravatt, R.C. Stevens and D. L. Boger, Fluoride-mediated capture of a non-covalent bound state of a reversible covalent enzyme inhibitor: X-ray crystallographic analysis of an exceptionally potent α-ketoheterocycle inhibitor of fatty acid amide hydrolase, *J. Am. Chem. Soc,* 2011, **133**, 4092–4100. (e) Z. Wang, H. Luecke, N. Yao and F. A. Quiocho, A low energy short hydrogen bond in very high resolution structures of protein receptor-phosphate complexes, *Nat. Struct. Biol.*, 1997, **4**, 519–522.

1.19 K. Bowman-James, A. Bianchi, and E. Garcia-España, Anion Coordination Chemistry; Eds.; Wiley-VCH: New York, 2011; Chapters 1–2.

1.20 P. D. Beer and P. A. Gale, Anion Recognition and Sensing: The State of the Art and Future Perspectives, *Angew. Chem. Int. Ed.*, 2001, **40**, 486–516.

1.21 D. J. Mercer and S. J. Loeb, Metal-based anion receptors: an application of second-sphere coordination, *Chem. Soc. Rev.*, 2010, **39**, 3612–3620.

1.22 K. Bowman-James, Alfred Werner Revisited: The Coordination Chemistry of Anions*, Acc. Chem. Res.* 2005, **38**, 671–678.

1.23 R. Custelcean, Anions in crystal engineering, *Chem. Soc. Rev.*, 2010, **39**, 3675–3685.

1.24 A. T. Wright and E. V. Anslyn, Differential receptor arrays and assays for solution-based molecular recognition, *Chem. Soc. Rev.*, 2006, **35**, 14–28.

1.25 R. Martinez-Manez and F. Sancenon, Fluorogenic and chromogenic chemosensors and reagents for anions, *Chem. Rev*., 2003, **103**, 4419–4476.

1.26 M. Vendrell, D. Zhai, J. C. Er and Y. T. Chang, Combinatorial strategies in fluorescent probe development, Chem. Rev., 2012, **112**, 4391–4420.

1.27 C. Suksai, and T. Tuntulani, Chromogenic anion sensors, *Chem. Soc. Rev*., 2003, **32**, 192–202.

1.28 T. Gunnlaugsson, M. Glynn, G. M. Tocci, P. E. Kruger and F. M. Pfeffer, *Coord. Chem. Rev*., 2006, **250**, 3094–3117.

1.29 G. Fukuhara, Analytical supramolecular chemistry: Colorimetric and fluorimetric chemosensors, *J. Photochem. Photobiol. C*, 2020, **42**, 100340.

1.30 P. A. Gale and C. Caltagirone, Anion Sensing by Small Molecules and Molecular Ensembles. *Chem. Soc. Rev*., 2015, **44**, 4212–4227.

1.31 C. Lodeiro, J. L. Capelo, J. C. Mejuto, E. Oliveira, H. M. Santos, B. Pedras and C. Nunez, Light and Colour as Analytical Detection Tools: A Journey into the Periodic Table Using Polyamines to Bio-Inspired Systems as Chemosensors. *Chem. Soc. Rev.*, 2010, **39**, 2948–2976.

1.32 H. Kobayashi, M. Ogawa, R. Alford, P. L. Choyke and Y. Urano, New Strategies for Fluorescent Probe Design in Medical Diagnostic Imaging. *Chem. Rev*., 2009, **110**, 2620–2640.

1.33 J. Fan, M. Hu, P. Zhan and X. Peng, Energy transfer cassettes based on organic fluorophores: construction and applications in ratiometric sensing, *Chem. Soc. Rev*., 2013, **42**, 29–43.

1.34 D. Wu, A. C. Sedgwick, T. Gunnlaugsson, E. U. Akkaya, J. Yoon and T. D James, Fluorescent chemosensors: the past, present and future, *Chem. Soc. Rev*., 2017, **46**, 7105–7123.

1.35 A. Gupta and N. Kumar, A review of mechanisms for fluorescent ''turn-on'' probes to detect Al^{3+} ions, *RSC Adv.,* 2016, **6**, 106413–106434

1.36 R. M. Duke, E. B. Veale, F. M. Pfeffer, P. E. Kruger, T. Gunnlaugsson, Colorimetric and Fluorescent Anion Sensors: An Overview of Recent Developments in the use of 1,8-Naphthalimide- Based Chemosensors, *Chem. Soc. Rev*., 2010, **39**, 3936–3953.

1.37 R. Martinez-Manez, F. Sancenon, Chemodosimeters and 3D Inorganic Functionalized Hosts for the Fluoro-Chromogenic Sensing of Anions, *Coord. Chem. Rev*., 2006, **250**, 3081–3093.

1.38 X. Li, X. Gao, W. Shi and H. Ma, Design Strategies for Water-Soluble Small Molecular Chromogenic and Fluorogenic Probes, *Chem. Rev*., 2014, **114**, 590–659.

1.39 S. O. Kang, R. A. Begum, and K. Bowman-James, Amide-based ligands for anion coordination, *Angew. Chem. Int. Ed.,* 2006, **45**, 7882–7894.

1.40 S. O. Kang, M. A. Hossain, and K. Bowman-James, Influence of dimensionality and charge on anion binding in amide-based macrocyclic receptors, *Coord. Chem. Rev.,* 2006, **250**, 3038–3052.

1.41 A. F. Li, J. H. Wang, F. Wang and Y. B. Jiang, Anion complexation and sensing using modified urea and thiourea-based receptors, *Chem. Soc. Rev.,* 2010, **39**, 3729–3745.

1.42 V. B. Bregovic, N. Basaric and K. Mlinaric-Majerski, Anion binding with urea and thiourea derivatives, *Coord. Chem. Rev.,* 2015, **295**, 80–124.

1.43 I. Saha, J. T. Lee and C. -H. Lee, Recent Advancements in Calix[4]pyrrole-Based Anion-Receptor Chemistry, *Eur. J. Org. Chem.*, 2015, **2015**, 3859–3885.

1.44 G. I. Vargas-Zuniga and J. L. Sessler, Pyrrole N–H anion complexes, *Coord. Chem. Rev.*, 2017, **345**, 281–296.

1.45 P. A. Gale, J. R. Hiscock, C. Z. Jie, M. B. Hursthouse and M. E. Light, Acyclic indole and carbazole-based sulfate receptors, *Chem. Sci.*, 2010, **1**, 215–220.

1.46 R. Manivannan, A. Satheshkumar, E. H. El-Mossalamy, L. M. Al-Harbi, S. A. Kosa and K.P. Elango, Design, synthesis and characterisation of indole based anion sensing receptors, *New J. Chem.*, 2015, **39**, 3936–3947.

1.47 S. Juanjuan, W. Linlin and H. Yangfeng, Colorimetric, turn-on fluorescence detection of fluoride ions using simple indole-based receptors in living cells, Analytical Methods, *Anal. Methods*, 2019, **11**, 2585–2590

1.48 Z. Xu, S. K. Kim and J. Yoon, Revisit to imidazolium receptors for the recognition of anions: highlighted research during 2006–2009, *Chem. Soc. Rev.,* 2010, **39**, 1457–1466.

1.49 P. Molina, A. Tárraga and F. Otón, Imidazole derivatives: A comprehensive survey of their recognition properties, *Org. Biomol. Chem.*, 2012, **10**, 1711–1724.

1.50 M. Alfonso, A. Tarraga and P. Molina, Pyrrole, imidazole, and triazole derivatives as ion-pair recognition receptors, *Tetrahedron Lett.*, 2016, **57**, 3053–3059.

1.51 E. Horak, P. Kassal and I. Murković Steinberg, Benzimidazole as a structural unit in fluorescent chemical sensors: the hidden properties of a multifunctional heterocyclic scaffold, *Supramol. Chem.*, 2018, **30**, 838–857.

1.52 V. Haridas, S. Sahu, P. P. Kumar and A. R. Sapala, Triazole: a new motif for anion recognition, *RSC Adv.*, 2012, **2**, 12594–12605.

1.53 B. Schulze and U. S. Schubert, Beyond click chemistry–supramolecular interactions of 1, 2, 3-triazoles, *Chem. Soc. Rev.*, 2014, **43**, 2522–2571.

1.54 R. S. Keri, A. Hiremathad, S. Budagumpi, B. M. Nagaraja, Comprehensive review in current developments of benzimidazole-based medicinal chemistry, *Chem. Biol. Drug Des.*, 2015, **86**, 799–845.

1.55 I. Bertini, A. Sigel and H. Sigel, Handbook on Metalloproteins, Marcel and Dekker, New York, 2001.

1.56 P. Singla, V. Luxami and K. Paul, Benzimidazole-biologically attractive scaffold for protein kinase inhibitors, *RSC Adv.*, 2014, **4**, 12422–12440.

1.57 B. Khan, U. Ashraf and A. Tariq, Synthesis and Characterization of Ter-Butyl Chloride and Its Derivatives (Ter-Butyl Zinc Chloride and Ter-Butyl Lead Chloride) By Using TLC, FTIR, UV/VIS and GC/MS Techniques. *Asian J. Research Chem*., 2010, **3**, 1011–1014.

1.58 R. Ali and N. Siddiqui, Biological aspects of emerging benzothiazoles: a short review, *Journal of chemistry*, 2013.

1.59 P. C. Sharma, A. Sinhmar, A. Sharma, H. Rajak, and D. P. Pathak, Medicinal significance of benzothiazole scaffold: an insight view. *Journal of Enzyme Inhibition and Medicinal Chemistry*, 2013, **28**, 240–266

1.60 R. Kaur, G. Dhaka, P. Singh, S. Rana and N. Kaur, Optical and electrochemical recognition studies of anions via novel benzothiazole azo-derivative, *Arabian Journal of Chemistry*, 2020.(in press)

1.61 P. A. Gale, J. R. Hiscock, N. Lalaoui, M. E. Light, N. J. Wells and M. Wenzel, Benzimidazole-based anion receptors: tautomeric switching and selectivity, *Org. Biomol. Chem.*, 2012, **10**, 5909–5915.

1.62 J. R. Hiscock, P. A. Gale, N. Lalaoui, M. E. Light and N. J. Wells, Benzimidazole-based anion receptors exhibiting selectivity for lactate over pyruvate, *Org. Biomol. Chem.*, 2012, **10**, 7780–7788.

1.63 M. Arunachalam and P. Ghosh, Nitrate directed organized assemblies of protonated arene based tripodal receptors, *Cryst Eng Comm.*, 2010, **12**, 1621–1627.

1.64 M. N. Hoque, A. Basu and G. Das, Cyclic Pentameric Puckered Hybrid Chloride–Water Cluster $[Cl_3(H_2O)_4]^{3-}$ in the Hydrophobic Architecture, *Cryst. Growth Des*., 2012, **12**, 2153−2157.

1.65 A. Gogoi and G. Das, Charge-assisted complexation of anions of different dimensionality by benzimidazole-based receptors bearing-OH functionality, *Cryst. Growth Des.*, 2012, **12**, 4012−4021.

1.66 J. Kang, H. S. Kim and D. O. Jang, Fluorescent anion chemosensors using 2-aminobenzimidazole receptors, *Tetrahedron Lett.*, 2005, **46**, 6079–6082.

1.67 G. W. Lee, N. Singh and D. O. Jang, Benzimidazole and thiourea conjugated fluorescent hybrid receptor for selective recognition of PO_4^{3-}, *Tetrahedron Lett.,* 2008, **49**, 1952–1956.

1.68 N. Singh and D. O. Jang, Benzimidazole-based tripodal receptor: highly selective fluorescent chemosensor for iodide in aqueous solution, *Org. Lett*., 2007, **9**, 1991–1994.

1.69 D. Y. Lee, N. Singh, M. J. Kim, and D. O. Jang, Chromogenic and fluorescent recognition of iodide with a benzimidazole-based tripodal receptor, *Org. Lett*., 2011, **13**, 3024–3027.

1.70 C. Kar, A. Basu and G. Das, Benzimidazole functionalized tripodal receptor for selective recognition of iodide, *Tetrahedron Lett.*, 2012, **53**, 4754–4757.

1.71 X. F., Yang, Qi, H. Wang, L. Z. Su, and G. Wang, A ratiometric fluorescent probe for fluoride ion employing the excited-state intramolecular proton transfer, *Talanta,* 2009, **80**, 92–97.

1.72 A. S. Gupta, K. Paul and V. Luxami, Ratiometric fluorescent chemosensor for fluoride ion based on inhibition of excited state intramolecular proton transfer, *Spectrochim. Acta A Mol. Biomol. Spectrosc.*, 2015, **138**, 67–72.

1.73 Y. C. Wu, J. Y. You, K. Jiang, J. C. Xie, S. L. Li, D. Cao and Z. Y. Wang, Colorimetric and ratiometric fluorescent sensor for F-based on benzimidazole-naphthalene conjugate: reversible and reusable study & design of logic gate function, *Dyes Pigm*, 2017, **140**, 47–55.

1.74 A. Kushwaha, S. K. Patil, and D. Das, A pyrene-benzimidazole composed effective fluoride sensor: potential mimicking of a Boolean logic gate, *New J. Chem.*, 2018, **42**, 9200–9208.

1.75 A. Gogoi, S. Mukherjee, A. Ramesh, and G. Das, Aggregation-induced emission active metal-free chemosensing platform for highly selective turn-on sensing and bioimaging of pyrophosphate anion, *Anal. Chem*., 2015, **87**, 6974−6979.

1.76 F. Qi, F. Zhang, L. Mo, X. Ren, Y. Wang, Xi Li, X. Liu, Y. Zhang, Z. Yang, and X. Song, A HBT-based bifunctional fluorescent probe for the ratiometric detection of fluoride and sulphite in real samples, *Spectrochim. Acta A Mol. Biomol. Spectrosc.*, 2019, **219,** 547–551.

1.77 S. Erdemir and O. Kocyigit, Reversible "OFF–ON" fluorescent and colorimetric sensor based benzothiazole-bisphenol A for fluoride in MeCN, *Sens. Actuators B Chem.*, 2015, **221**, 900–905.

1.78 G. R.You, G. J.Park, S. A. Lee, Y. W. Choi, Y. S. Kim, J. J. Lee and C. Kim, A single chemosensor for multiple target anions: the simultaneous detection of CN^- and OAc^- in aqueous media, *Sens. Actuators B Chem.*, 2014, **202**, 645–655.

1.79 C. Chang, F. Wang, J. Qiang, Z. Zhang, Y. Chen, W. Zhang, Y. Wang and X. Chen, Benzothiazole-based fluorescent sensor for hypochlorite detection and its application for biological imaging, *Sens. Actuators B Chem.,* 2017, **243**, 22–28.

1.80 B. Kuswandi, W. Verboom and D.N. Reinhoudt, Tripodal receptors for cation and anion sensors*, Sensors*, 2006, **6**, 978–1017.

Chapter 2

Experimental Methods & Characterization

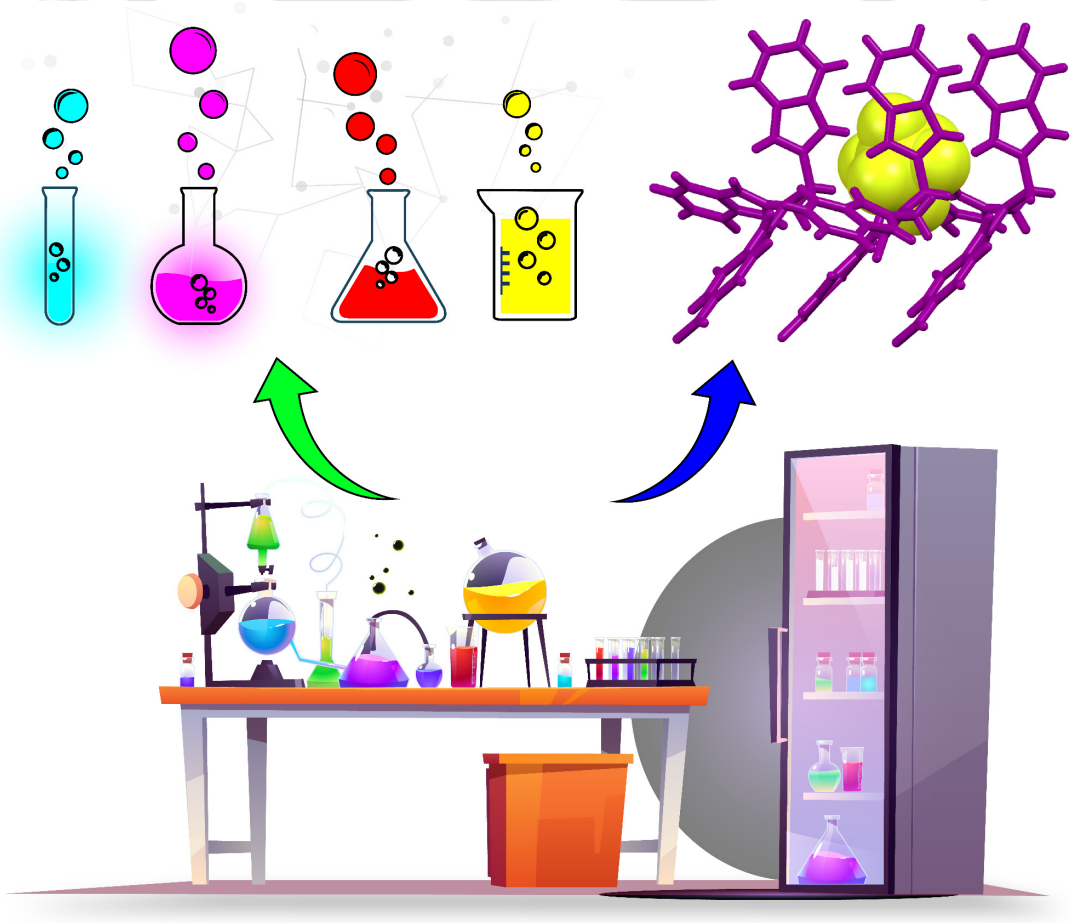

Chapter 2

This chapter incorporates comprehensive information about the various materials and methodology employed in the synthesis and characterization of the acyclic receptors/probes (**L_1-L_5**). Specifics of general equipments, binding studies, minutes of crystallization along with different experimental setups and calculations used to study the interaction with different analytes are elaborately described.

2.1 Materials

All of the reagents and solvents were commercially available and used henceforth without further purification. Iminodiacetic acid, *ortho*-Phenylenediamine, 4-nitrophenylisocyanate, 1-naphthyl isocyanate, 4-Chloro-3-formylcoumarin, 2-Mercaptobenzothiazole, Hydrazine monohydrate, 2-Hydroxy-1-naphthaldehyde, 4-Methylphenol, Hexamethylenetetramine were purchased from Sigma-Aldrich (U.S.A). All quaternary ammonium salts were purchased from Sigma-Aldrich (U.S.A) whereas, organic and inorganic acids such as CH_3COOH, CF_3COOH, HF, H_2SO_4, HCl, HBr, HI, HNO_3 were obtained either from Merck or LOBA chemicals (India). All sodium, potassium salts and deuterated solvents such as DMSO-d_6, $CDCl_3$ for NMR studies were acquired from Merck chemicals (India) and used as received. Solvents used in the synthesis and crystallization experiments were procured either from Merck, India and dried using standard techniques, wherever mentioned in the synthetic procedures.

2.2 Experimental methods

During absorption studies, Perkin-Elmer Lambda-25 UV–Vis spectrophotometer was used to achieve the absorption spectra which were recorded using quartz cuvette of path length 10 mm in the wavelength range of 250–750 nm. Horiba Fluoromax-4 spectrofluorometer was used to obtain the fluorescence spectra with quartz cuvettes of 10 mm path length at 298 K in the emission spectroscopy studies. The mass spectra were obtained using an Agilent Technologies 6520 Accurate mass spectrometer. The infrared spectra were recorded on a Perkin-Elmer Spectrum One FT-IR spectrometer with KBr pellets in the range 4000–400 cm^{-1}. Bruker-D8 Advance X-ray diffractometer with Cu-Kα radiation at λ = 0.15418 nm was used to record the powder X-ray diffraction patterns of dried crystalline powder of the crystal complexes. NMR spectra were recorded and documented on a Varian FT-400 MHz as well as Bruker 600 MHz instruments. Parts per million (ppm) were used to represent the value of the chemical shift on the delta scale. The

abbreviated vocabularies were used to describe spin multiplicities in ^{1}H NMR spectra viz. 's' for singlet; 'd' for doublet; 't' for triplet; 'm' for multiplet.

2.3 Synthesis and characterization of the receptors

2.3.1 Synthesis of L_1 [1,1-bis((1H-benzo[d]imidazol-2-yl)methyl)-3-(4-nitrophenyl)urea]:
The receptor **L_1**, was synthesized by refluxing and stirring 4-nitrophenyl isocyanate (328 mg, 2 mmol) with previously reported ligand Bis(2-benzimidazylmethyl)amine[2.1-2.2] (554 mg, 2 mmol) in dry DCM for 24 hours maintaining a molar ratio of 1:1 (Scheme 2.1). The brown coloured solution was evaporated to dryness and extracted with $CHCl_3/H_2O$. Then the solvent was removed under reduced pressure and finally dried in vacuum over silica gel. The product **L_1** was obtained as a brown coloured solid (723.5 mg) which was characterized by NMR, FT-IR and ESI-MS.

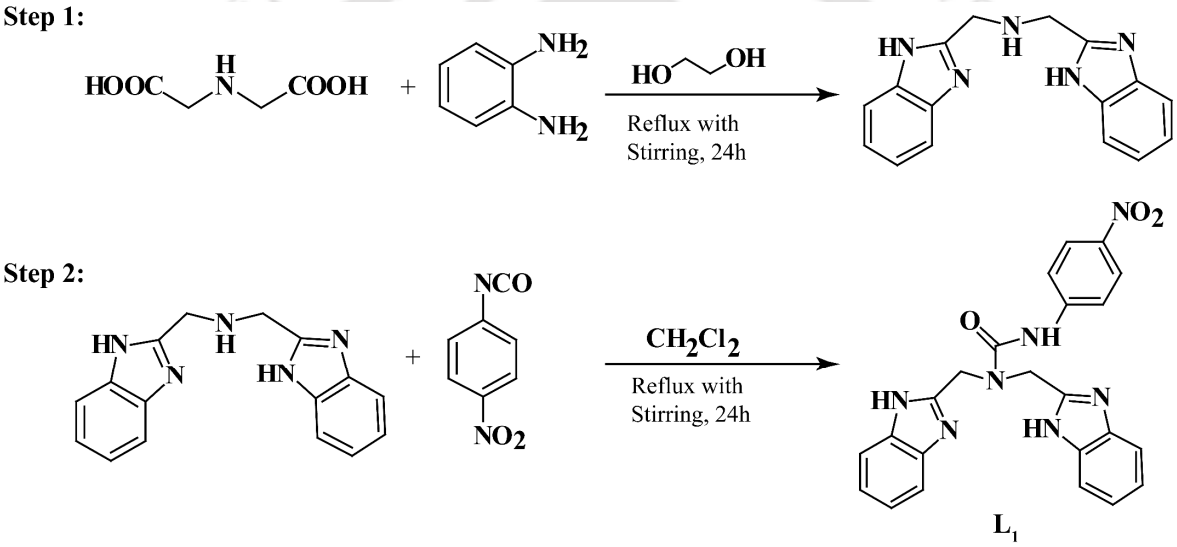

Scheme 2.1 Synthesis of the receptor **L_1**

Receptor **L_1**: Yield= 82%; Mp: 262-265°C. ^{1}H NMR (400 MHz, $CDCl_3$, $SiMe_4$) δ (ppm): 10.163 (s, amide –NH), 8.175 (d, 2H, aromatic –CH), 7.678 (d, 2H, aromatic –CH), 7.632 (d, 2H, benzimidazole –CH), 7.292 (d, 2H, benzimidazole –CH), 4.912 (s, 1H, aliphatic $-CH_2$). ^{13}C NMR (100 MHz, $CDCl_3$) δ (ppm): 156.628, 150.672, 145.806, 142.916, 138.012, 125.177, 123.644, 119.122, 115.514 and 46.473. FT-IR (KBr pellet, cm^{-1}): 3243 (N–H), 2922 (C–H_{alp}), 1664 (C=O), 1502 (NO_2 –*asym*), 1329 (NO_2 –*sym*) 1249(C–N); Calculated for [**L_1**+ H^+]= 442.16, ESI-MS (positive mode, m/z)= 442.16.

2.3.2 Synthesis of L_2 [1,1-bis((1H-benzo[d]imidazol-2-yl)methyl)-3-(naphthalen-1-yl)urea]:
Initially, 1-Naphthyl isocyanate (338 mg, 2 mmol) was refluxed and stirred with previously reported ligand Bis(2-benzimidazylmethyl)amine[2.1-2.2] (554 mg, 2 mmol) in dry DCM for 24 hours maintaining a molar ratio of 1:1. Evaporation of the brown coloured solution and work up with

$CHCl_3/H_2O$ yields the receptor **L_2**, 1,1-bis((1H-benzo[d]imidazol-2-yl)methyl)-3-(naphthalen-1-yl)urea (Scheme 2.2). The compound was finally dried in vacuum over silica gel. The product **L_2** was obtained as brown coloured solid (882.3 mg). Later, it was recrystallized from DMSO-MeOH (2:3) mixture and left for slow evaporation. Red block type crystal were obtained after 4-5 weeks which were characterised by NMR, FT-IR, ESI-MS and single crystal X-ray analysis.

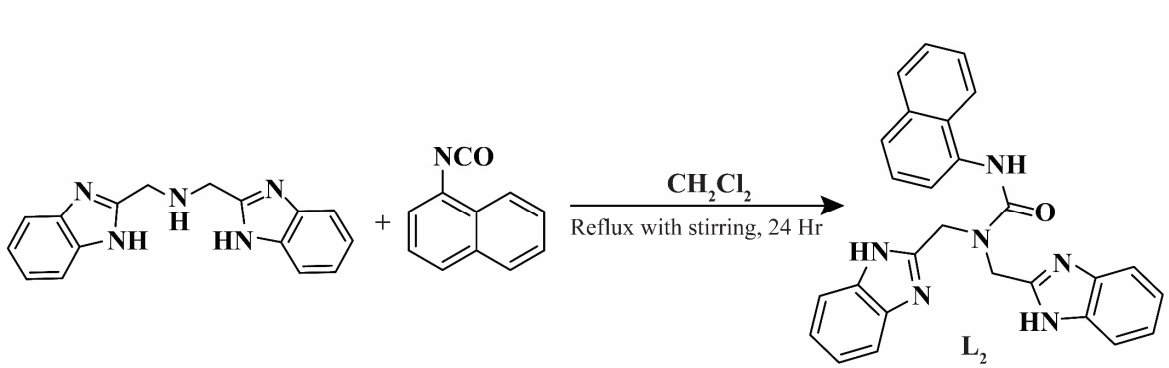

Scheme 2.2 Synthesis of the receptor **L_2**.

Receptor **L_2**: Yield=75%; ^{1}H NMR (600 MHz, DMSO-d_6, $SiMe_4$) δ (ppm): 13.02 (s, 2H, Benzimidazole–NH), 9.28 (s, 1H, amide –NH), 8.17-8.16 (d, 1H, ~8.4 Hz, Ar_H), 7.88-7.87 (d, 1H, ~8.4Hz, Ar_H), 7.73-7.71 (d, 2H, ~6Hz, Ar_H), 7.68-7.67 (d, 1H, ~7.8 Hz, Ar_H), 7.60-7.57 (m, 3H, Ar_H), 7.48-7.43 (m, 2H, Ar_H), 7.39-7.37 (t, 1H, ~7.8 Hz, Ar_H), 7.23-7.22 (d, 4H, ~6Hz, Ar_H), 5.04 (s, 4H, aliphatic -CH_2). ^{13}C NMR (100 MHz, DMSO-d_6) δ (ppm): 156.85, 152.99, 135.64, 134.17, 128.66, 128.42, 126.24, 125.99, 125.87, 124.72, 123.65, 121.56 and 46.61 FTIR (KBr pellet, cm^{-1}): 3243 (N–H), 3049 (C–H_{alp}), 1645 (C=O), 1515 (C=C), 1448 (C=C), 1274 (C–N); Calculated for [**L_2** + H^+]= 447.19, ESI-MS (positive mode, m/z)= 447.21.

2.3.3 Synthesis of **L_3** [(E)-1-((2-(benzo[d]thiazol-2-yl)hydrazineylidene)methyl)naphthalen-2-ol]:

The chemosensor **L_3** was synthesized by slightly modifying the previously reported procedure.[2.3] As shown in Scheme 2.3, 2-hydrazinobenzothiazole (330 mg, 2 mmol) and 2-hydroxyl-1-naphthaldehyde (344 mg, 2 mmol) are dissolved in 50 mL of methanol and refluxed for 6 hours. The yellow paper type precipitate is then filtered and washed with cold methanol to give a pure form of **L_3** (510.5 mg) (Scheme 2.3).

L_3: Yield: 80%; ^{1}H NMR (600 MHz, DMSO-d_6, $SiMe_4$) δ(ppm): 12.19 (bs, 1H, hydrazone –NH), 9.19 (s, 1H, imine –CH), 8.66-8.65 (d, 1H, ~ 8.4 Hz, Ar_H), 7.91-7.87 (m, 2H, Ar_H), 7.75-7.72 (m, 1H, Ar_H), 7.60-7.57 (t, 1H, ~ 8.4Hz, Ar_H), 7.42-7.39 (t, 1H, ~7.2Hz Ar_H), 7.32-7.29 (t, 2H, ~7.2Hz

, Ar_H), 7.25-7.24 (d, 1H, ~8.8Hz, Ar_H), 7.12-7.10 (t, 1H, ~7.8Hz, Ar_H). ESI-MS (m/z): Calculated for $C_{18}H_{13}N_3OS$: 319.08. Found: 318.15 (**L_3** - H^+, Negative mode).

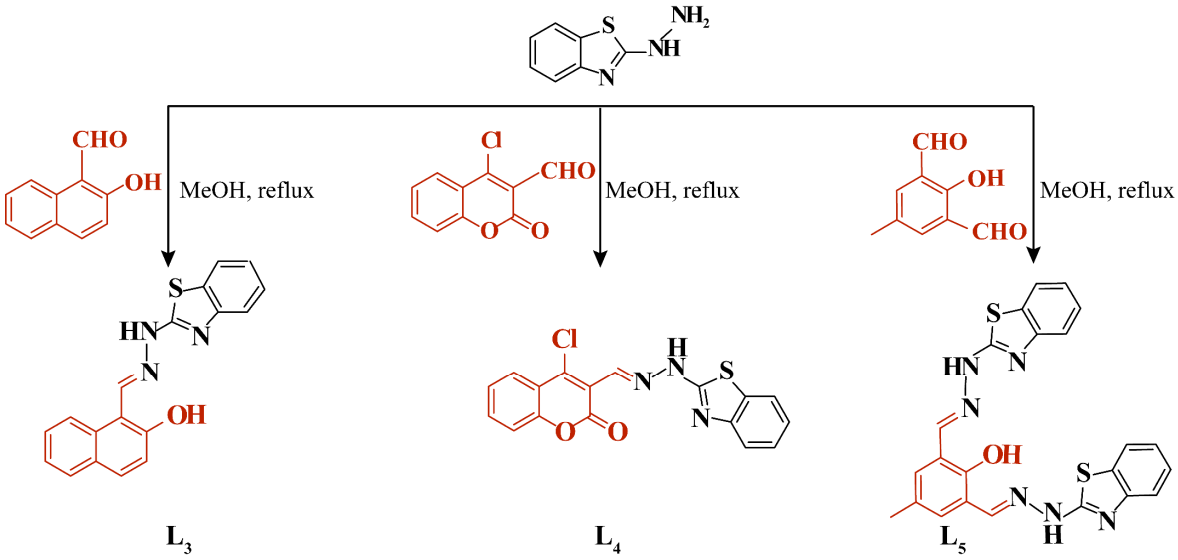

Scheme 2.3 Synthesis of the receptor **L_3**, **L_4** and **L_5**.

2.3.4 Synthesis of **L_4** [(E)-3-((2-(benzo[d]thiazol-2-yl)hydrazineylidene)methyl)-4-chloro-2H-chromen-2-one]:

For the preparation of **L_4**, 208.6 mg (1 mmol) of 4-Chloro-3-formylcoumarin was condensed with 165 mg (1 mmol) of 2-hydrazinobenzothiazole in methanol. After 4 hours of stirring, a yellowish precipitate was formed which after washing with cold methanol gave pure **L_4** (298.2 mg) (Scheme 2.3).

L_4: Yield:84%; ^{1}H NMR (600 MHz, DMSO-d_6, $SiMe_4$) δ(ppm): 12.75 (bs, 1H, hydrazone –NH), 8.32 (s, 1H, imine –CH), 8.06-8.05 (d, 1H, ~ 8.4Hz, Ar_H), 7.83 (d, 1H, Ar_H), 7.75-7.72 (t, 1H, ~ 7.6 Hz, Ar_H), 7.53-7.48 (m, 3H, Ar_H), 7.34-7.32 (t, 1H, ~ 7.6 Hz, Ar_H), 7.17-7.14 (t, 1H, ~ 7.6 Hz, Ar_H). ^{13}C NMR (150 MHz, DMSO-d_6) δ (ppm): 168.31, 161.18, 157.55, 151.18, 150.44, 142.23, 137.73, 130.92, 128.62, 125.56, 125.41, 124.83, 121.62, 121.20, 118.30, 118.20, 116.01. ESI-MS (m/z): Calculated for $C_{17}H_{10}ClN_3O_2S$: 355.02. Found: 354.10 (**L_4** - H^+, Negative mode).

2.3.5 Synthesis of **L_5** [2,6-bis((E)-(2-(benzo[d]thiazol-2-yl)hydrazono)methyl)-4-methylphenol]: The chemosensor **L_5** was synthesized following the previously reported procedure.[2.4] Freshly prepared 2,6-Diformyl-4-methylphenol (164 mg, 1 mmol) was condensed with 2-hydrazinobenzothiazole (330 mg, 2 mmol) in Methanol for 4 hours. The yellowish precipitate was then filtered and washed 3/4 times with cold methanol to obtain pure **L_5** (380.5 mg) (Scheme 2.3).

L_5: Yield = 83 %; ^{1}H NMR (600 MHz, DMSO-d_6, $SiMe_4$) δ(ppm):12.31 (bs, 1H, hydroxyl–OH), 11.57 (bs, 2H, hydrazone –NH), 8.49 (s, 2H, imine –CH), 7.77-7.76 (d, 2H, Ar_H), 7.50 (s, 2H, Ar_H), 7.32-7.29 (m, 4H, Ar_H), 7.13-7.10 (t, 2H, ~ 7.6 Hz, Ar_H), 2.32 (s, 3H, aliphatic –CH_3). ESI-MS (positive mode, m/z) Calculated [$\mathbf{L_5}$ + H^+] = 459.11, found mass: 459.10.

2.4 Synthesis and characterization of anion complexes of the protonated receptors $(\mathbf{L_1}H_2)^{2+}$-$(\mathbf{L_2}H_2)^{2+}$

2.4.1 Hexafluorosilicate complex of receptor $\mathbf{L_1}H_2^{2+}$, $[(\mathbf{L_1}H_2)^{2+}.SiF_6^{2-}]$: 55 mg (0.15mmol) of the receptor $\mathbf{L_1}$ was suspended in a mixture of DMSO-MeOH (2:3) and to this, 3-4 drops (0.5 mL) of HF was added. After being stirred for about an hour, the clear solution was left for crystallization in a glass vial at room temperature. Slow evaporation of the solvent mixture afforded colorless needle like small crystal after 2-3 weeks suitable for x-ray analysis (57 mg). Yield: 65%, m.p.: 278-280°C. ^{1}H NMR (400 MHz, DMSO-d_6) δ (ppm): 9.759 (s, amide –NH), 8.1585 (d, 2H, aromatic –CH), 7.7525 (d, 2H, aromatic –CH), 7.622 (d, 2H, benzimidazole –CH), 7.223 (d, 2H, benzimidazole –CH), 5.017 (s, 1H, aliphatic –CH_2). FT-IR (KBr pellet, cm^{-1}): 3437(N–H), 1676 (–C=O), 1508 (NO_2 –*asym*), 1329 (NO_2 –*sym*), 743 (Si–F).

2.4.2 Sulfate-Bisulfate cluster complex of receptor $\mathbf{L_1}H_2^{2+}$, $[2(\mathbf{L_1}H_2)^{2+}.2HSO_4^-.SO_4^{2-}.H_2O]$: Similar to the preparation of the complex 1, 55 mg (0.15mmol) of ligand $\mathbf{L_1}$ was dissolved in DMF in a glass vial and 3-4 drops of concentrated H_2SO_4 was added and stirred for an hour. On getting a clear solution, the vial was kept at room temperature for 2-3 weeks to get small needle-like colourless crystals of complex 2 (68 mg). Yield: 76%, m.p.: 282-285°C. ^{1}H NMR (400 MHz, DMSO-d_6) δ (ppm): 9.664(s, amide –NH), 8.154 (d, 2H, aromatic –CH), 7.818 (d, 2H, aromatic –CH), 7.722 (d, 2H, benzimidazole –CH), 7.467 (d, 2H, benzimidazole –CH), 5.279 (s, 1H, aliphatic –CH_2). IR (KBr pellet, cm^{-1}): 3420 (N–H), 2926 (C–H_{alp}), 1687 (–C=O), 1505 (NO_2 –*asym*), 1332 (NO_2 –*sym*), 1117 (S=O).

2.4.3 Sulfate Complex of receptor $\mathbf{L_2}H_2^{2+}$, $[2(\mathbf{L_2}H_2)^{2+}.2SO_4^{2-}]$: In 5 mL DMSO, 67 mg (0.15 mmol), the receptor $\mathbf{L_2}$ was added and solubilized. After addition of 4-6 drops (0.5 mL) of concentrated H_2SO_4, the clear blue coloured solution was kept under stirring for 1 hour. The solution was filtered out and allowed for slow evaporation at room temperature in a glass vial. Slow evaporation of the solvent mixture afforded blue coloured block like small crystal after 8-10 weeks which were suitable for X-ray analysis (31 mg). Yield: 75%. ^{1}H NMR (400 MHz, DMSO-d_6) *δ* (ppm): 9.20 (s, amide –NH), 7.88-7.84 (m, 6H, Ar_H), 7.73-7.71 (d, 1H, ~7.6Hz, Ar_H), 7.45-7.38 (m, 7H, Ar_H), 7.31-7.27 (t, 1H, Ar_H), 5.30 (s, 4H, ~7.6Hz aliphatic –CH_2). IR (KBr pellet, cm^{-1}): 3330 (N–H), 3058 (C–H alp), 1672 (C=O), 1520 (C=C), 1462 (C=C), 1119 (S=O).

2.5 Single crystal X-ray crystallography

For each case of single crystal XRD experiment, a suitable crystal for single crystal determination was selected carefully from the mother liquor. After being immersed in silicone oil, the appropriate sized crystal was selected. With the help of epoxy resin, it was attached to the top end of a glass fiber and glued. The intensity data were accumulated using a Bruker SMART APEX II CCD diffractometer, fortified with a fine focus 1.75 kW sealed tube Mo−Kα radiation (λ = 0.71073 Å) at 298(2) K, with increasing ω (width of 0.3° per frame) at a scan speed of 3s per frame. Consequently, the X-ray crystallographic intensity data were also collected using a Supernova, single source at offset, Eos diffractometer using Mo-Kα radiation (λ = 0.71073 Å) fortified with a CCD area detector, and the corresponding data refinement and cell reduction were carried out by CrysAlisPro.[2.5] The SMART software was utilized for data acquisition. SAINT and XPREP software[1] were utilized for crystal data integration and reduction.[2.6] Corrections related to Multi-scan empirical absorption were applied to the data using the program SADABS.[2.7] Crystal structures were resolved by direct methods using SHELXTL-2014 and were subjected to refinement on F^2 by the full matrix least-squares technique using the SHELXL-2014 program.[2.8] In the crystal structure, non-hydrogen atoms are refined anisotropically. Hydrogen atoms attached to all carbon atoms are geometrically fixed. Structural illustrations of the crystal structures were created using MERCURY 2.3[2.9] and MERCURY 4.0[2.10] for Windows. PLATON/SQUEEZE was used to refine the host framework in some host-guest complexes excluding the disordered counter-cation or solvent molecules.[2.11] All the crystallographic data have been deposited in the CCDC. The CCDC numbers assigned to the complexes $[(\mathbf{L_1}H_2)^{2+}.SiF_6^{2-}]$, $[2(\mathbf{L_1}H_2)^{2+}.2HSO_4^{-}.SO_4^{2-}.H_2O]$ and $[2(\mathbf{L_2}H_2)^{2+}.2SO_4^{2-}]$ are respectively 1020478, 1020477 and 1920833. The ligand crystal ($\mathbf{L_2}$) bears CCDC number 1920832. Crystallographic parameters for data collection and crystallographic refinement details of the receptors and their anion complexes are summarized in the respective chapters.

2.6 UV−Vis and Fluorescence Spectral Studies

Stock solutions of various anions (50 $\times 10^{-3}$ M) were prepared in deionized water. Tetrabutyl/tetraethyl or sodium salts of the corresponding anions were used to make all the stock solutions of the studied anions. The stock solutions (5×10^{-3} M) of the probes $\mathbf{L_{1\text{-}2}}$ were prepared in dry DMSO while those of $\mathbf{L_{3\text{-}5}}$ were in dry DMF respectively. For the selectivity study and titration experiment in both absorption and emission studies, each chemosensor solutions were then diluted to 10×10^{-6} mol L^{-1} in the required experimental medium. For the titration experiments in each case, a 10×10^{-6} M solution of the probe solution was taken in a quartz optical

cell of 1 cm optical path length and then titrated with an incremental concentration of concerned anion stock solutions in pure acetonitrile.

2.7 Evaluation of the Apparent Binding Constant

In each case of evaluation, an effective chemosensor concentration of 10.0×10^{-6} M was used for the absorption as well as emission titration studies with the sensed guest anions. The probe solutions (10 μM) in acetonitrile were titrated with the increasing concentrations of the guest anions (F^- and OAc^-). The effective guest anion concentration was varied. The apparent binding constant for the formation of the respective host-guest complex was evaluated using the Benesi−Hildebrand (B−H) plot (Equation 1 and Equation 2).[2.12-2.13]

$$1/(A-A_0) = 1/\{K(A_{max}-A_0)C^n\} + 1/(A_{max}-A_0) \quad (1) \quad \text{or}$$

$$1/(I-I_0) = 1/\{K(I_{max}-I_0)C^n\} + 1/(I_{max}-I_0) \quad (2)$$

A_0 is the absorbance of the free probe, A_{max} is the absorbance treated with an excess amount of titrated anion, A is the absorbance associated with a certain concentration of fluoride or acetate ion, K is the binding constant (M^{-1}) and C is the concentration of fluoride or acetate ion. Similarly, I_0 is the emission intensity of host at emission maximum (λ_{max}), I is the observed emission intensity at that particular wavelength in the presence of a certain concentration of the analyte *(C)*, I_{max} is the maximum emission intensity value that was obtained at λ_{max} during titration with varying analyte concentration, K is the apparent binding constant (M^{-1}) and was determined from the slope of the linear plot. In case of **L_3**, **L_4** and **L_5**, the apparent binding constants for the formation of respective host-guest complexes based on absorption spectroscopy were calculated using equation 1 while in case of **L_2** and **L_5**, emission spectroscopy based apparent binding constants for the formation of respective Host-guest complexes were evaluated using equation 2.

2.8 Calculation of the Detection Limit

The detection limit for the specific chemosensor was calculated based on the fluorescence or UV-Vis titration. In case of the two probes (**L_2** and **L_5**), a continuous measurement of emission spectrum of the blank chemosensor was carried out 10 times and the standard deviation of blank measurement was determined. Similarly, for the three probes (**L_3**, **L_4** and **L_5**), the same procedure was repeated using absorption spectroscopy and standard deviation of the blank measurement was determined. To gain the slope, the ratio of the fluorescence emission or absorbance at a specific wavelength was plotted as a concentration of guest anion. Finally, the detection limit was calculated using the following equation:

$$\text{Detection limit} = 3\sigma/k \quad (3)$$

where σ is the standard deviation of blank measurement, and k is the slope between the ratio of fluorescence emission versus respective analyte concentration.

References

2.1 R. Cariou, J. J. Chirinos, V. C. Gibson, G. Jacobsen, A. K. Tomov, G. J. P. Britovsek, and A. J. P. White, The effect of the central donor in bis (benzimidazole)-based cobalt catalysts for the selective cis-1, 4-polymerisation of butadiene, *Dalton Trans.*, 2010, **39**, 9039–9045.

2.2 L. K. Thompson., B. S. Ramaswamy, and E. A. Seymour, Cobalt (II) and zinc (II) complexes of the'tripod'ligand tris (2-benzimidazylmethyl) amine. Some five-coordinate derivatives and some with mixed stereochemistries, *Can. J. Chem.*, 1977, **55**, 878−888.

2.3 A. Gogoi, S. Samanta, and G. Das, A benzothiazole containing CHEF based fluorescence turn-ON sensor for Zn^{2+} and Cd^{2+} and subsequent sensing of $H_2PO_4^-$ and $P_4O_7^{4-}$ in physiological pH, *Sens. Actuators B Chem.*, 2014, **202**, 788–794.

2.4 A. Gogoi, S. Mukherjee, A. Ramesh and G. Das, Nanomolar Zn(II) sensing and subsequent PPi detection in physiological medium and live cells with a benzothiazole functionalized chemosensor, *RSC Adv.,* 2015, **5**, 63634–63640.

2.5 CrysAlisPro, version 1171.33.34d, Oxford Diffraction Ltd. [release 27-02-2009 CrysAlis 171. NET]

2.6 *SMART, SAINT and XPREP*; *Siemens Analytical X-ray Instruments Inc*.: Madison, WI, 1995.

2.7 G. M. Sheldrick, SADABS: *Software for Empirical Absorption Correction*; University of Gottingen, Institute fur Anorganische Chemieder Universitat: Tammanstrasse 4, D-3400, Gottingen, Germany, 1999−2003.

2.8 G. M. Sheldrick, *Crystal structure refinement with SHELXL*, *Acta Crystallogr., Sect. C: Struct. Chem*., 2015, **71**, 3−8.

2.9 Mercury 2.3, Supplied with Cambridge Structural Database; CCDC, Cambridge, U.K., 2007.

2.10 Mercury 4.0, Supplied with Cambridge Structural Database; CCDC, Cambridge, U.K., 2019

2.11 P. Van der Sluis and A. L. Spek, PLATON/SQUEEZE, *Acta Crystallogr., Sect. A: Found. Crystallogr.,* 1990, **46**, 194–201.

2.12 H. A. Benesi and J. H. Hildebrand, A spectrophotometric investigation of the interaction of iodine with aromatic hydrocarbons, *J. Am. Chem. Soc.*, 1949, **71**, 2703–2707.

2.13 I. D. Kuntz, F. P. Gasparro, M. D. Johnston, and R.P. Taylor, Molecular interactions and the Benesi-Hildebrand equation., *J. Am. Chem. Soc.*, 1968, **90**, 4778–4781.

Appendix 1

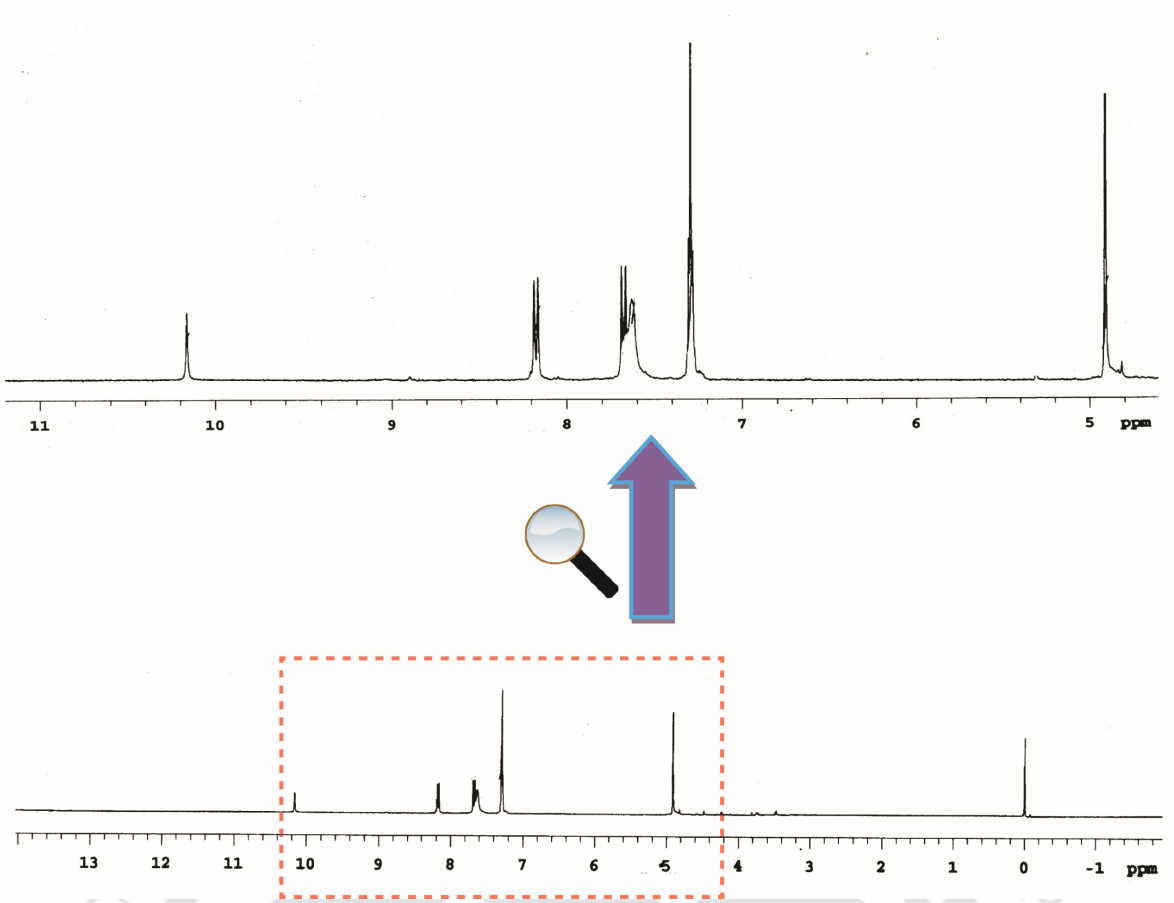

Figure A2.1 ^{1}H NMR spectrum of receptor $\mathbf{L_1}$ in $CDCl_3$ at 298 K.

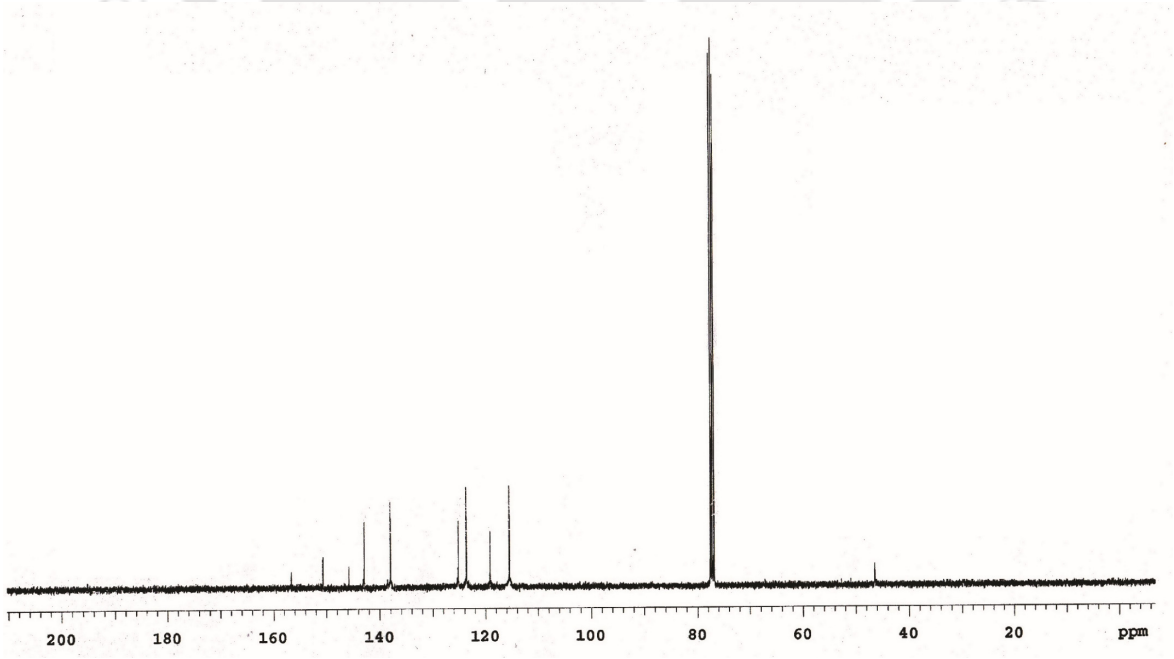

Figure A2.2 ^{13}C NMR spectrum of receptor $\mathbf{L_1}$ in $CDCl_3$ at 298 K.

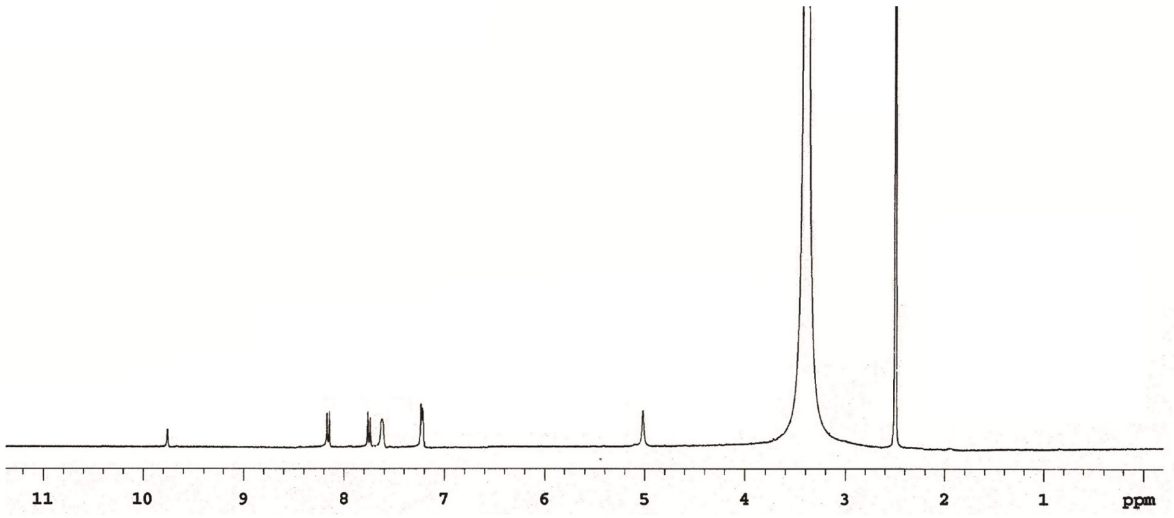

Figure A2.3 ^{1}H NMR spectrum (400 MHz, DMSO-d_6, 298 K) of complex 1[$(\mathbf{L_1}H_2)^{2+}.SiF_6^{2-}$].

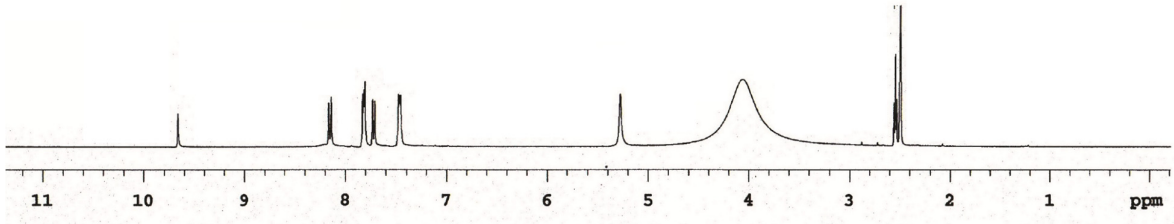

Figure A2.4 ^{1}H NMR spectrum (400 MHz, DMSO-d_6, 298 K) of complex 2 [2$(\mathbf{L_1}H_2)^{2+}.2HSO_4^{-}.SO_4^{2-}.H_2O$].

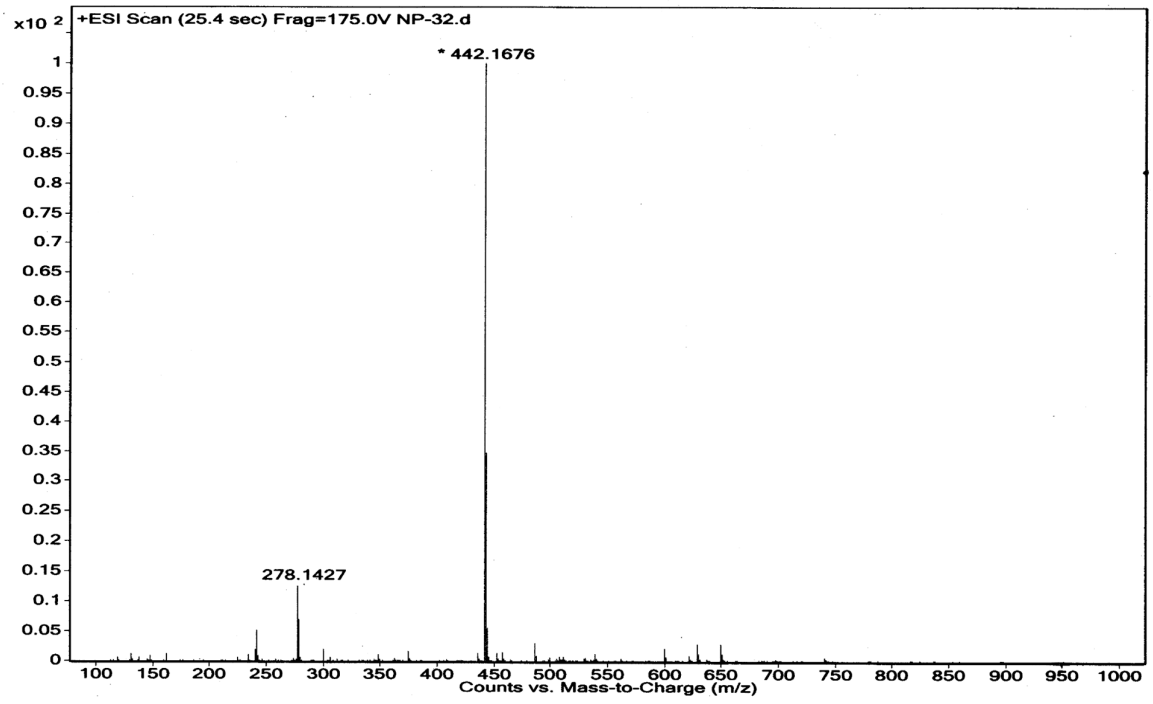

Figure A2.5 ESI-Mass spectrum of receptor $\mathbf{L_1}$ in acetonitrile.

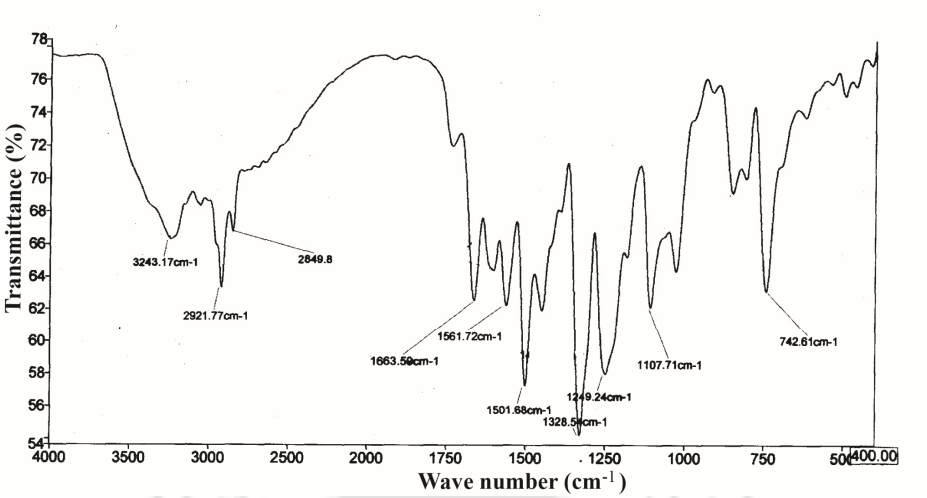

Figure A2.6 FT-IR spectrum (KBr pellet) of the receptor $\mathbf{L_1}$.

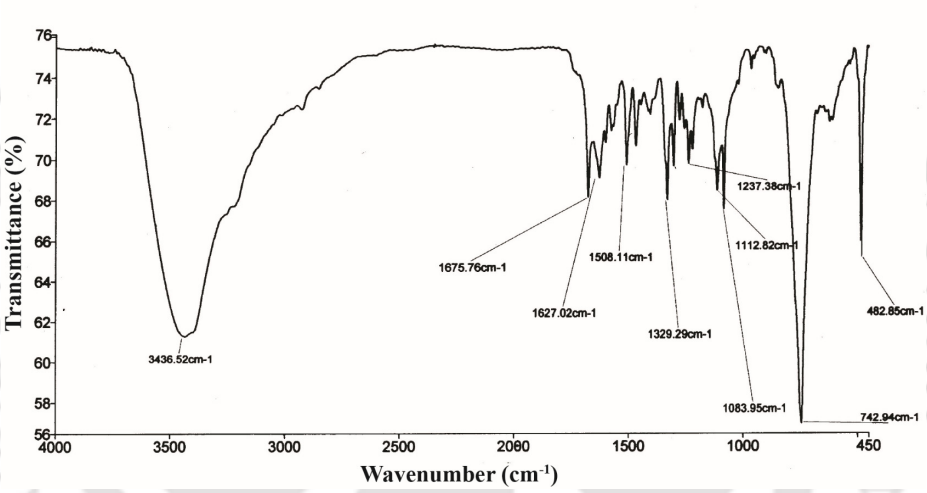

Figure A2.7 FT-IR spectrum (KBr pellet) of the complex **1** $[(\mathbf{L_1}H_2)^{2+}.SiF_6^{2-}]$.

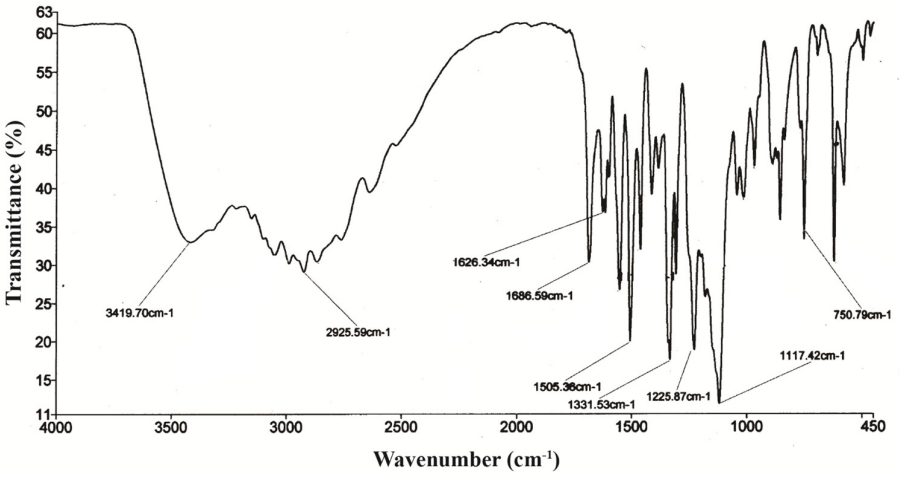

Figure A2.8 FT-IR spectrum (KBr pellet) of the complex **2** $[2(\mathbf{L_1}H_2)^{2+}.2HSO_4^-.SO_4^{2-}.H_2O]$.

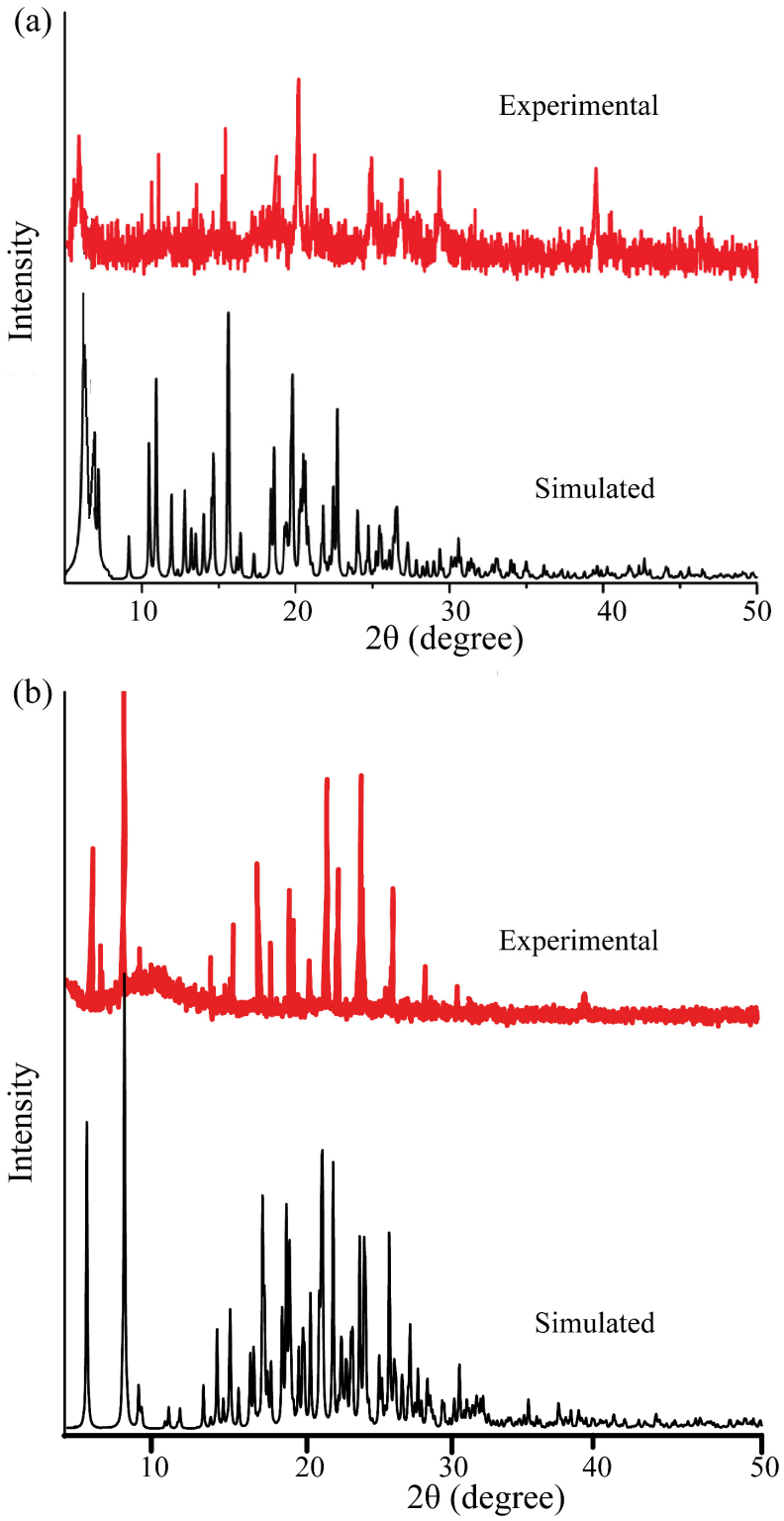

Figure A2.9 Powder X-ray diffraction patterns for the anion complexes: as-synthesized (red) and simulated from the single-crystal diffraction data (black); **(a)** Complex **1**[$(\mathbf{L_1}H_2)^{2+}.SiF_6^{2-}$]**,** (**b**) Complex **2**[$2(\mathbf{L_1}H_2)^{2+}.2HSO_4^{-}.SO_4^{2-}.H_2O$].

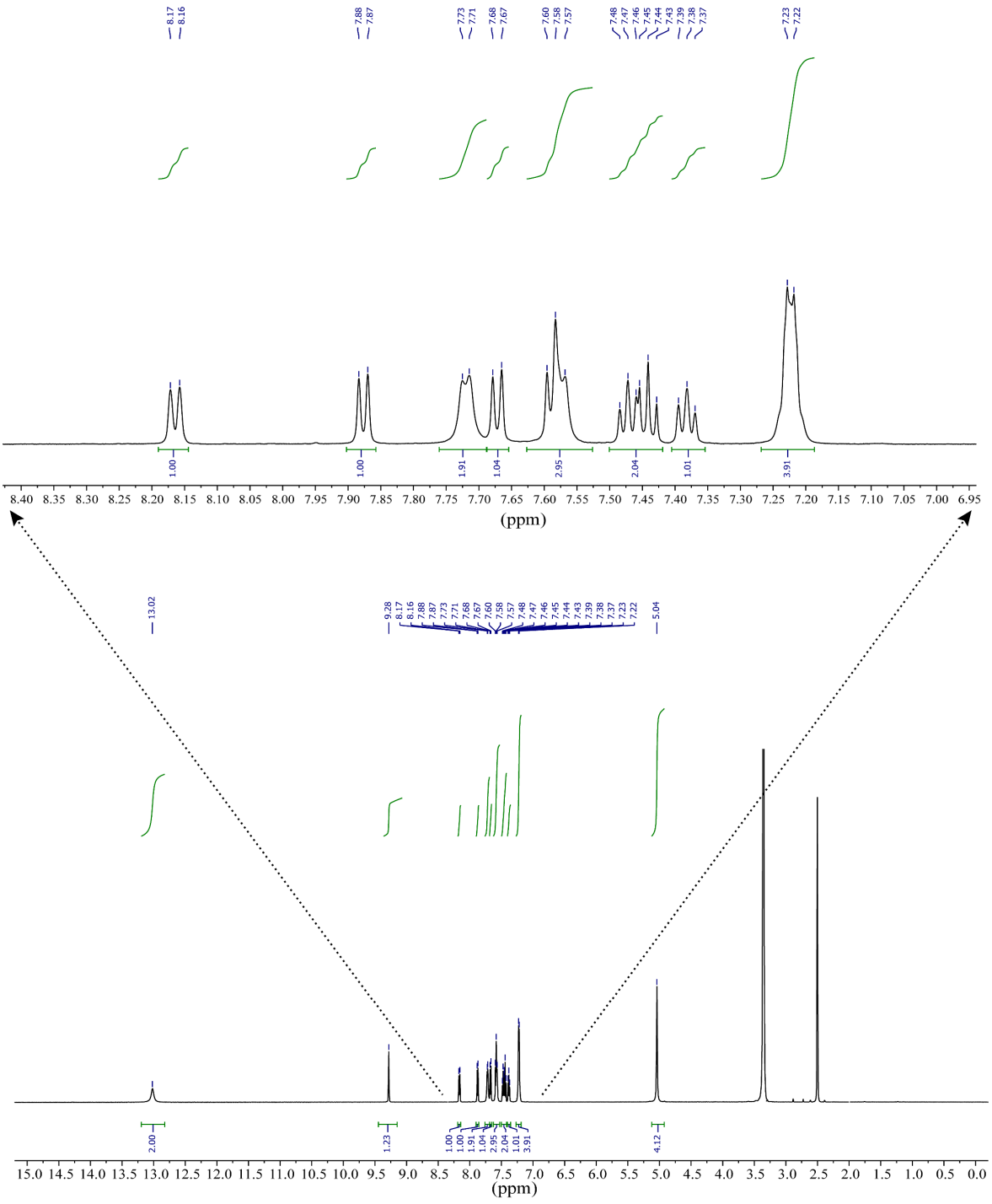

Figure A2.10 Integrated ^{1}H-NMR spectrum (full as well as expanded) of free receptor **L_2** in DMSO-d_6 at 298 K.

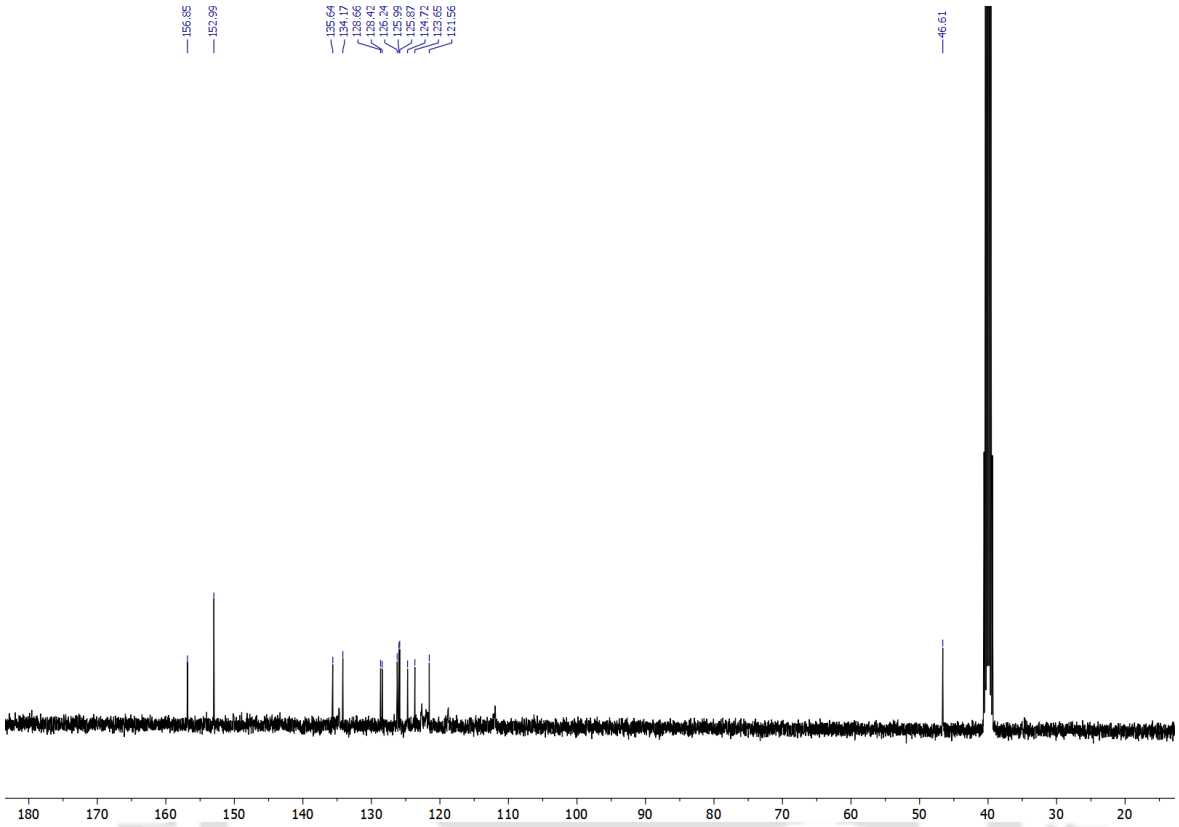

Figure A2.11 ^{13}C-NMR spectrum of free receptor $\mathbf{L}_2$ in DMSO-d_6 at 298 K.

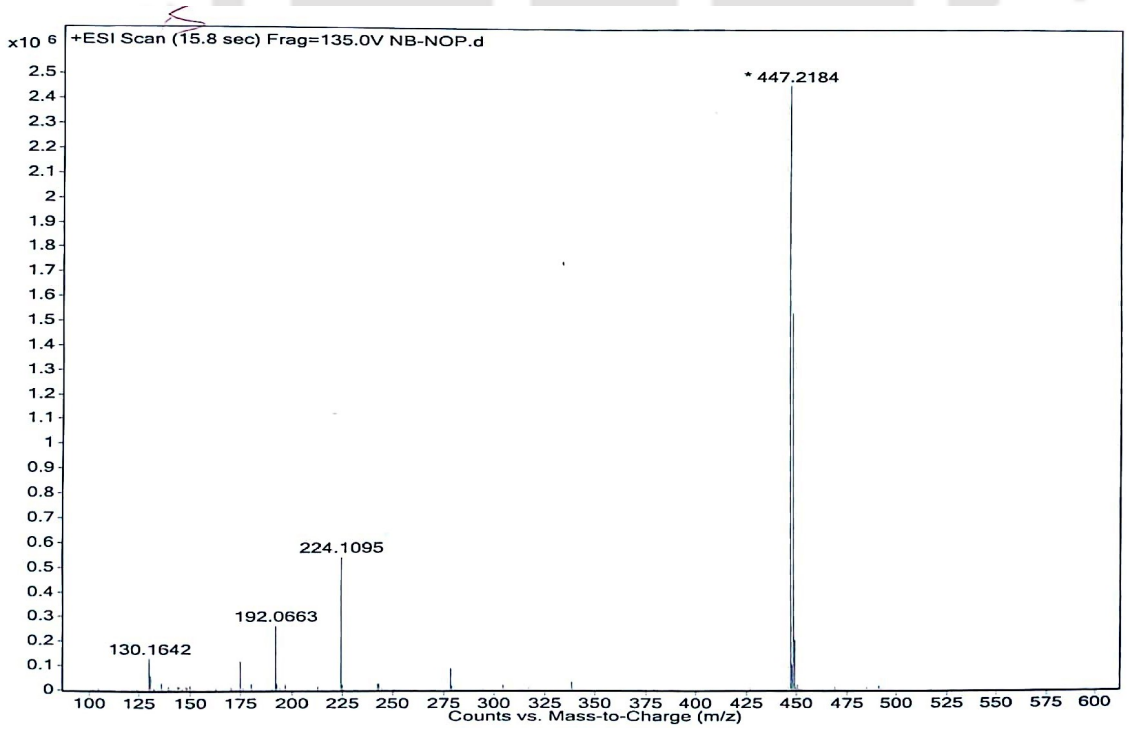

Figure A2.12 ESI-Mass spectrum of receptor $\mathbf{L}_2$ in acetonitrile.

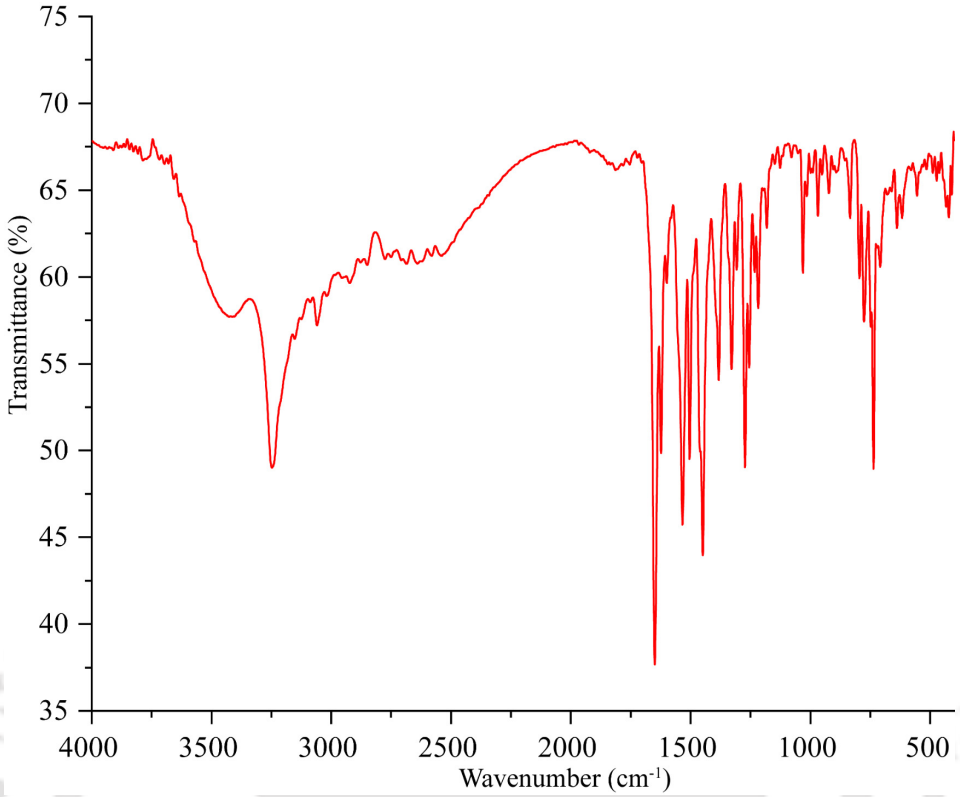

Figure A2.13 FT-IR spectrum (KBr pellet) of the receptor **L**$_2$.

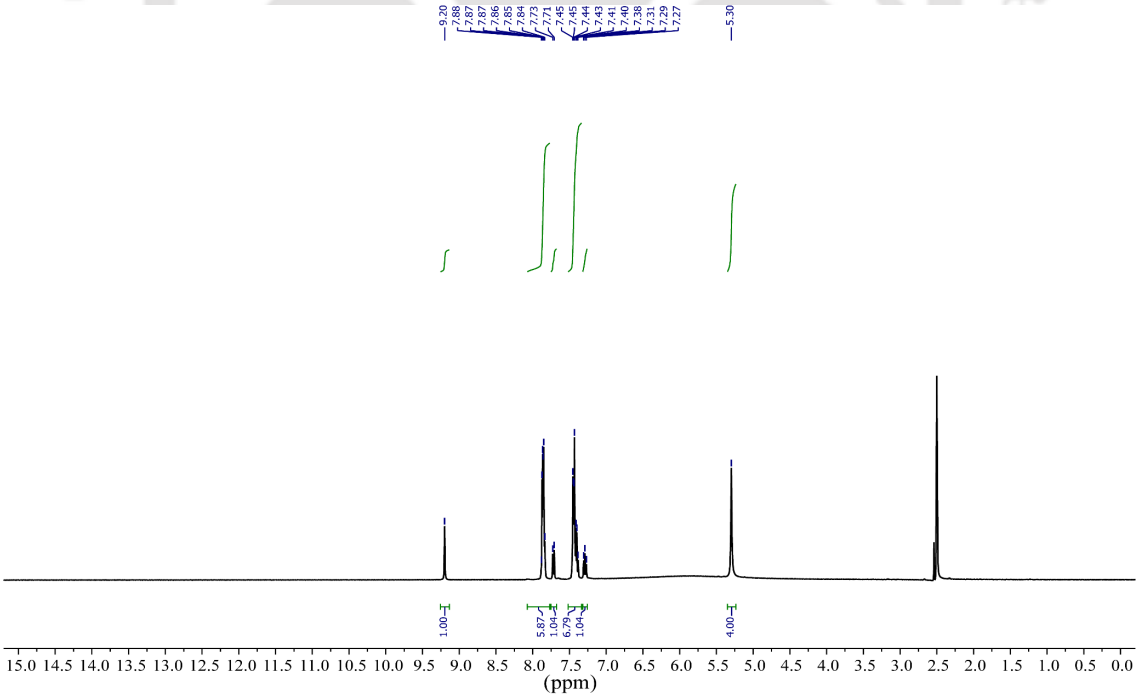

Figure A2.14 ^{1}H NMR spectrum (400 MHz, DMSO-d$_6$, 298 K) of sulfate complex of **L**$_2$ [2(**L**$_2$H$_2$)$^{2+}$.2SO$_4^{2-}$]

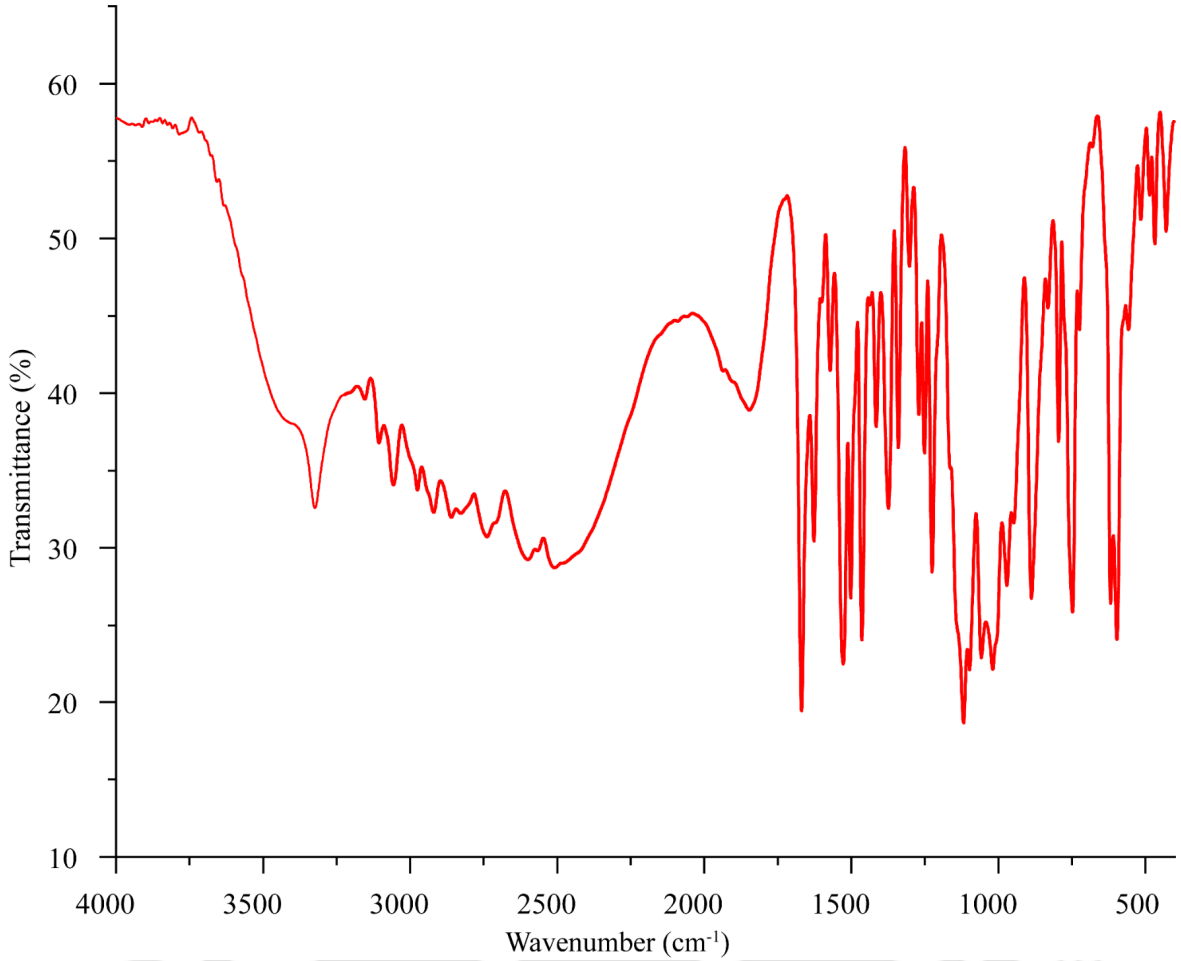

Figure A2.15 FT-IR spectrum (KBr pellet) of the sulphate complex **of L_2** $[2(\mathbf{L_2}H_2)^{2+}.2SO_4^{2-}]$

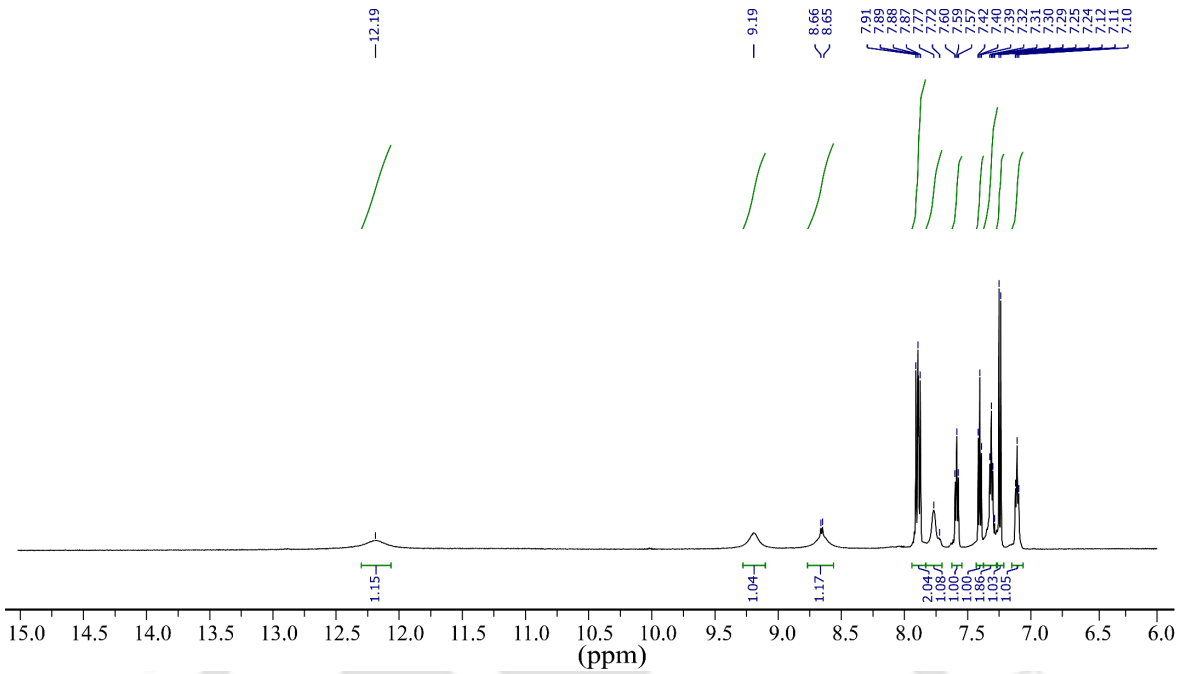

Figure A2.16 ^{1}H NMR of **L$_3$** in DMSO at 298 K.

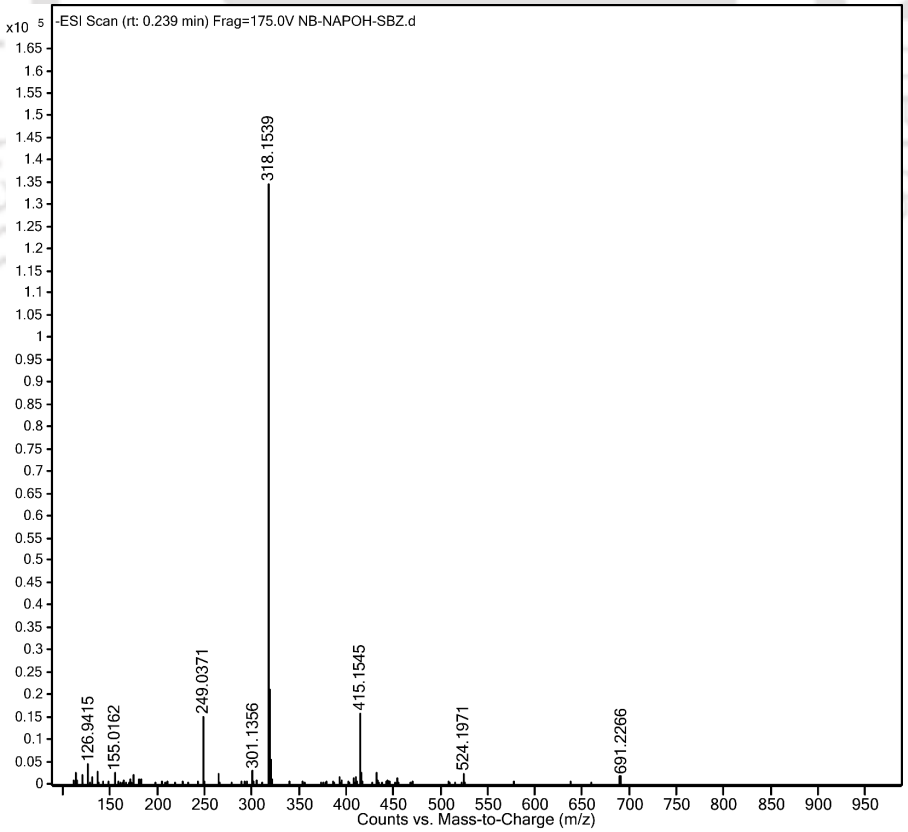

Figure A2.17 ESI-Mass spectrum of receptor **L$_3$** in acetonitrile (negative mode).

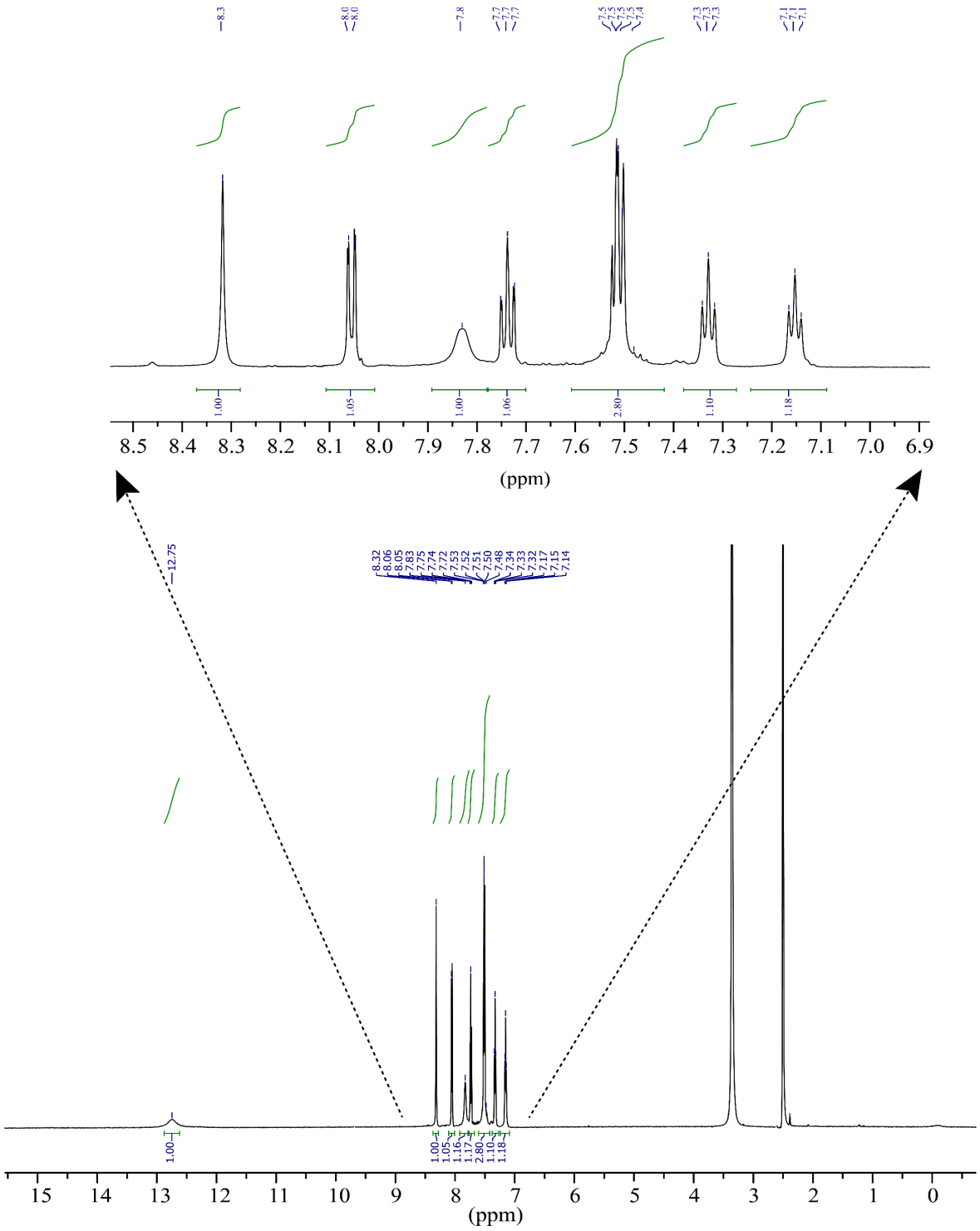

Figure A2.18 Expanded ^{1}H NMR of **L$_4$** in DMSO-d$_6$ at room temperature.

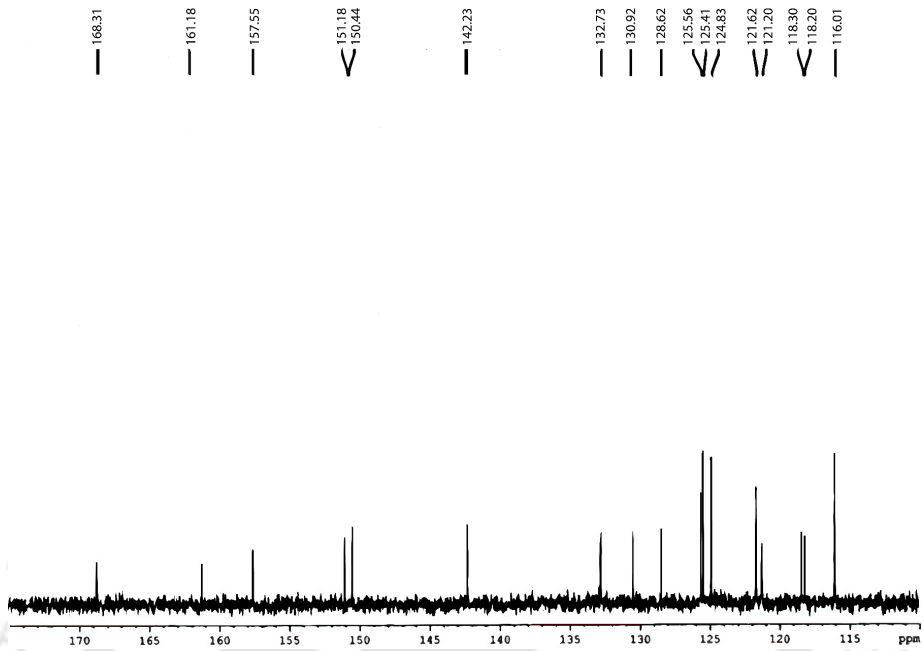

Figure A2.19 ^{13}C NMR of **L4** in DMSO-d_6

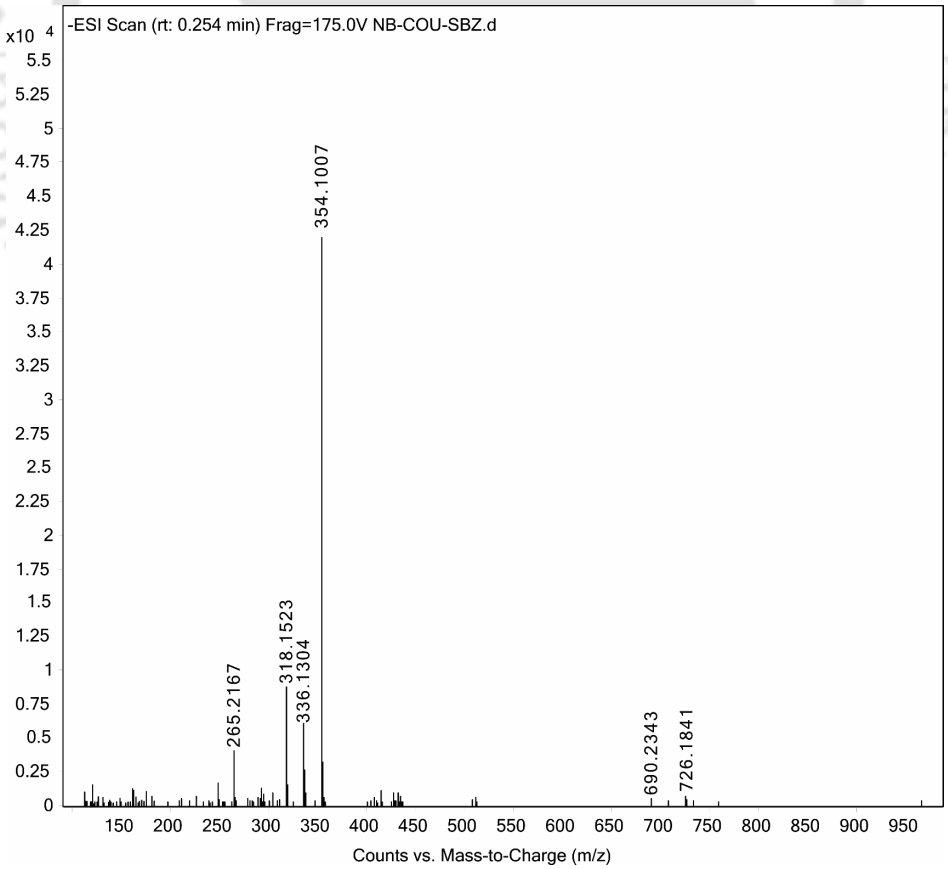

Figure A2.20 ESI-Mass spectrum of receptor **L4** in acetonitrile (negative mode).

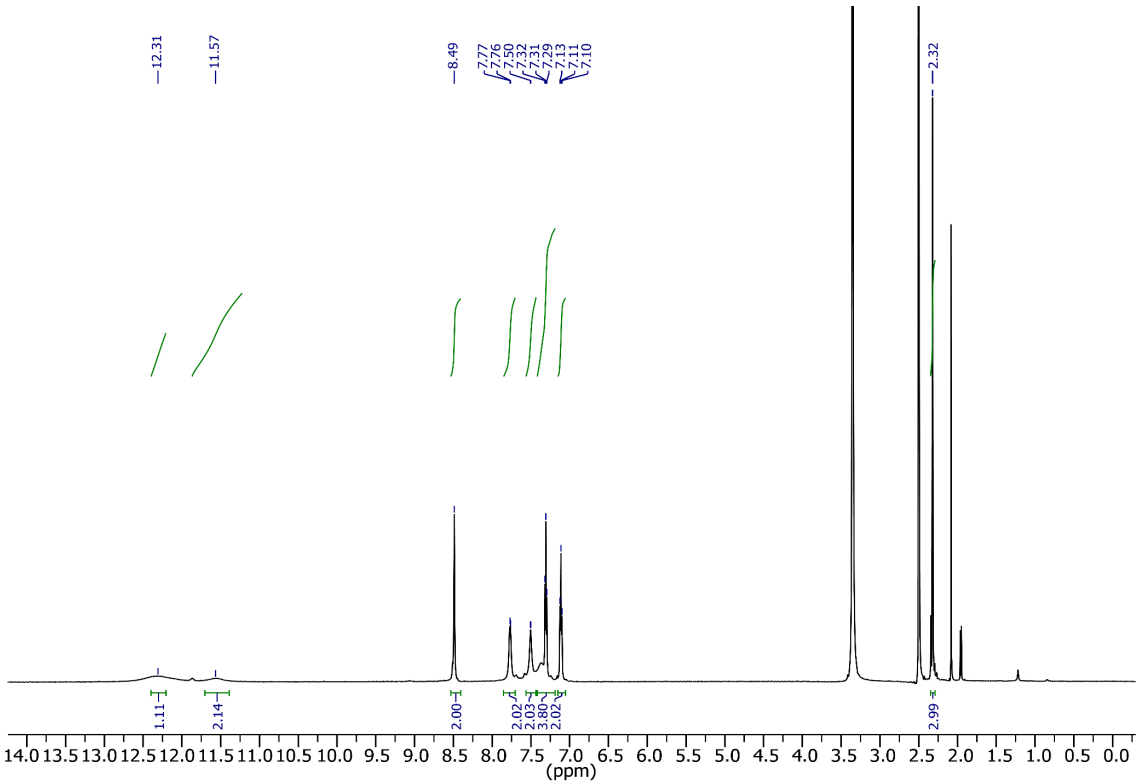

Figure A2.21 ^{1}H NMR of $\mathbf{L_5}$ in DMSO at 298 K.

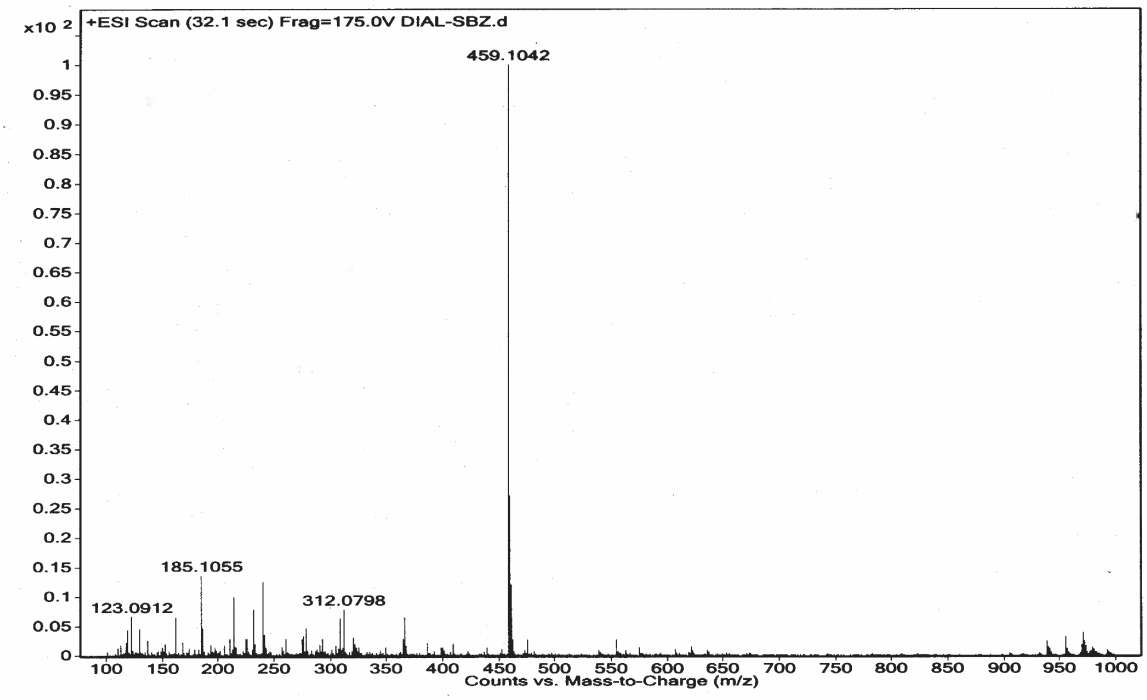

Figure A2.22 ESI-Mass spectrum of receptor $\mathbf{L_5}$ in acetonitrile (positive mode).

Chapter 3

Anion binding aptitude of a benzimidazole and amide functionalized non-symmetrical tripodal receptor

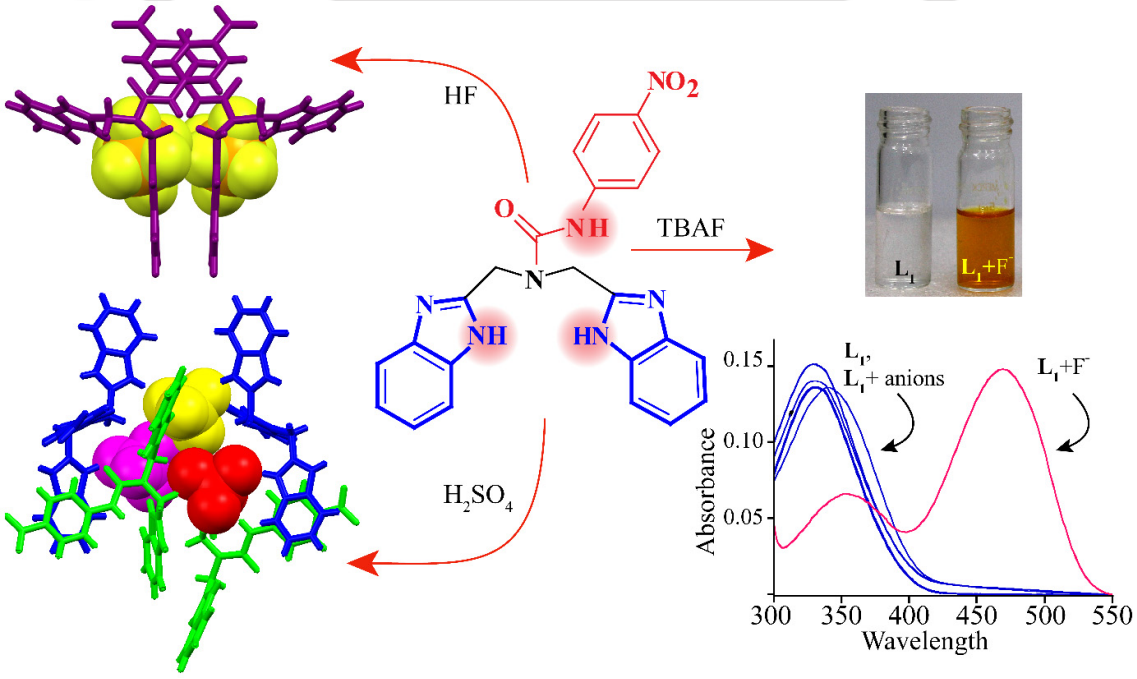

Chapter 3

3.1 Background and focus of the chapter

Molecular recognition of anions plays the pivotal role at the roots of numerous fundamental chemical and biological phenomena relevant to the field of sensing, transport and catalysis and thus comprises the theme of chief importance in supramolecular chemistry. Along with the comprehensive analysis of the various functions associated with these anions, the field of anion recognition, either in solution phase or in solid state, has become more vibrant and continues to grow apace recently. As reversible, non-covalent interactions constitute the central strategy used in supramolecular chemistry, anion coordination by abiotic species expending hydrogen bonding interactions has grasped a significant and active area of research.[3.1-3.2] Consequently, the design principle of appropriate receptors containing flexible and preorganized cavities has gradually encompassed the tripodal scaffolds. These have been developed, modified and extensively studied across the last two decades to investigate their coordination behaviour with anions of different dimensions.[3.3-3.4] In the progressive effort of synthesizing and developing newer anion receptors, our group have reported several acylic symmetric tripodal receptors.[3.5-3.8] Such symmetric acyclic receptors with multi-armed hydrogen bonding functionalities (urea/thiourea/ amide) were found to interact with targeted anionic species via the formation of capsular and/or non-capsular assemblies. Among these, benzimidazole based tripodal receptors for anion binding have not been explored much and remained scanty in number.[3.9-3.10]

Among the polyatomic anions, the binding and recognition of fluorosilicate anions are rather less investigated.[3.11-3.14] Hexafluorosilicate (SiF_6^{2-}) ion, an octahedral anion with six Si–F bond distances of 1.71 Å,[3.15] has found its ubiquitous use in diverse fields lately. Selective binding and recognition of fluorosilicate anions have gained attention due to their environmental impact[3.16], biomedical impact with noteworthy potential for health damage[3.17] along with the implementation of fluorosilicates for the fluoridation of drinking water[3.18]. The hexafluorosilicate salts are strongly dependent on cations for its solubility[3.19]and thus reveal wide-ranging physicochemical properties utilized in numerous applications such as leather and wood preservation agents, two-solution fluoride mouth rinse, commercial laundry, insecticide, pediculicide and rodenticide, enamels for bone china and porcelain and in vitreous enamel frits, aluminium and beryllium metallurgy, aluminium etchants and opalescent glass.[3.20-3.22]

Recognition of sulfate ions in an aqueous medium is always a challenging task with artificial receptors. Difficulty in sulfate binding can be attributed to the large hydration energy ($\Delta G = -1090$ kJmol^{-1}), relatively larger size and similarity to other tetrahedral anions, such as phosphates. However, sulfate ion secures the fourth place as the most abundant anion in the human circulatory system (about 300 μmol L^{-1}) and plays several roles in human physiology.[3.23] SO_4^{2-} conjugation helps in building the typical structure and function of tissues. Sulfation and sulfate conjugate hydrolysis, catalysed by certain sulfotransferases and sulfatase enzyme superfamilies, play a pivotal role in the metabolism and disposition of many xenobiotics. Activation of various endogenous compounds such as heparin, heparan sulfate, dermatan sulfate, and bile acids is also regulated in the presence of sulfate anion.[3.24-3.25] The most concerning health effect related to sulfate ingestion is laxative action. [3.26] Sulfate is naturally present in the environment as a consequence of the sulfur cycle. Alternatively, the methylation of mercury by sulfate-reducing bacteria leads to its most toxic and bioaccumulative form, methylmercury cation. Mercury methylation can be troublesome as it is lethal and bio-magnified through the food web, promoting the internal eutrophication of water ecosystems and augmenting the biodegradation of organic soils.[3.27] Apart from its occupancy at the end of the Hofmeister series due to its strong ability to decrease protein solubility, sulfate anions also play a remarkable role in sulfate binding proteins, nucleation of ice in the upper atmosphere. Also, they are the reason for the complexity involved in nuclear waste separations. Use of ferrous sulfamate [$Fe(NH_2SO_3)_2$] as a reducing agent for converting Pu^{4+} to Pu^{3+} at the portioning stage of the actinides reprocessing leads to the formation of sulphate waste. Another sulphate source is the use of barium sulphate for the coprecipitation process of strontium to treat the contaminated streams selectively. Molecular recognition approaches are employed for sulfate removal from radioactive wastes which comprise anion-sequestering systems selective for sulfate, liquid−liquid extraction or crystallization.[3.28-3.29] It is also accountable for the permanent hardness of water. Designing of selective receptors for binding sulfate ion in a highly competitive environment is rather challenging.[3.30] As sulfate can occur in more than one type of charged state in aqueous media depending on the pH of the medium; the binding selectivity is affected. The high hydration energies and hydrophilicity also hinder the transport of the anion across the organic phase. The theoretical calculation reveals that sulfate ion can be associated with twelve hydrogen bonding interactions from water molecules in the first hydration shell.[3.31]

On the other hand, fluoride ion, a hard Lewis base in nature, possesses the smallest ionic radius and highest charge density. It has become an attractive candidate for chemosensor designers, as it is associated with various biological, medical and technological processes. The role that fluoride

ions play in dental health is noteworthy as it is utilized in dental caries[3.32] and also applied in the treatment for osteoporosis.[3.33-3.34] Because of the slow excretion from the human body, overexposure to fluoride can cause acute gastrointestinal and nephrological disorders.[3.35] In several underdeveloped countries, the root cause of devastating bone disease fluorosis is found to be the excessive fluoride levels in drinking water.

Our focus is to employ benzimidazole based tripodal receptor for anion binding and study the anion binding aptitude in both solid state as well as solution phase. Unlike the conventional symmetrical tripodal receptor, herein, we have introduced a non-symmetrical tripodal receptor and study the host-guest interaction in both phases. This chapter describes the synthesis of a novel non-symmetric tripodal receptor, **L_1** with benzimidazole and amide –NH functionalities and a comparative study for anion binding aptitude of those functionalities has been performed in solid state and solution phase. The protonated receptor **L_1** in solid state tends to form a pseudo-cavity around the octahedral hexafluorosilicate anions whilst in the second complex, binding of one sulfate and two bisulfates in unison by two protonated units arises. The benzimidazole –NHs are the strongest hydrogen bond donors in both the crystals controlling dominance over amide –NHs. The neutral receptor being selective towards fluoride anion induces a naked eye visible colorimetric change. The ^{1}H NMR studies with the neutral and protonated form of the receptor suggest the strong involvement of amide –NH in anion binding in the solution phase.

3.2 Structural aspects of the receptor L_1

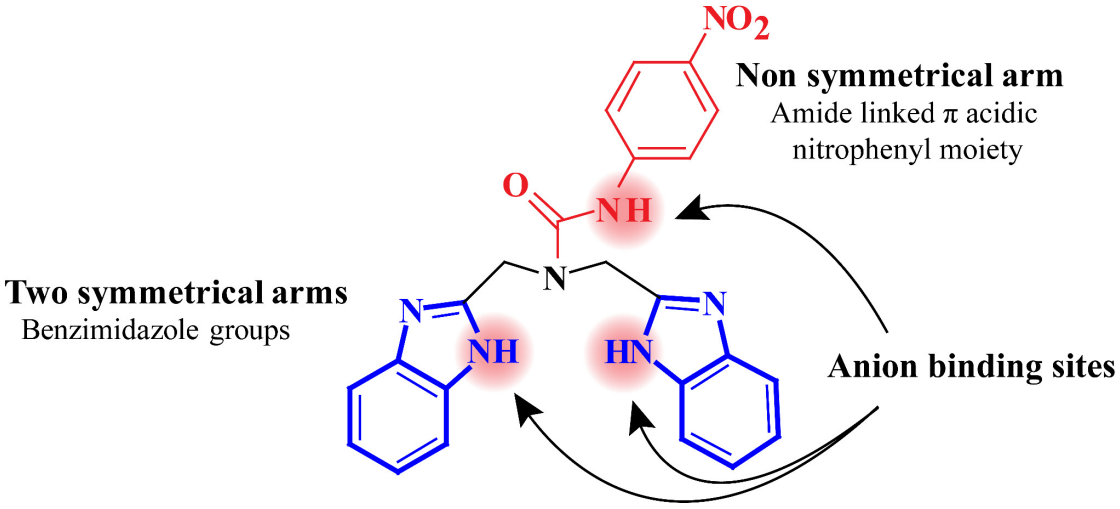

Scheme 3.1 Molecular Structure of the Receptors **L_1**.

To coordinate with the anions of varied dimensionality, the receptor should be flexible enough and must involve preorganized orientation of the functional group and terminal substituents with hydrogen bond donor groups. Keeping the prerequisites in mind, the non-symmetric tripodal

receptor $\mathbf{L_1}$ was functionalized with benzimidazole and amide –NHs (Scheme 3.1). The two similar podants were fabricated with benzimidazole functionalities for electronic assistance while the third arm was deliberately modified with amide functionality. The propensity towards higher valent anion coordination was supposed to increase by the presence of protonation sites on the two benzimidazole moieties along with the apparent protonation on the apical nitrogen. Anion receptors in nature often involve amide linkages as hydrogen bond donors hence the third podant was functionalized with a π acidic nitrophenyl moiety connected by the amide linkage which was expected to enhance the binding ability of the receptor towards anions.

3.3 Solid state anion recognition

A suitable receptor for ionic guests demands proper binding sites tailored to a definite framework/platform. The binding ability of the receptor $\mathbf{L_1}$ towards anions was augmented by the protonation sites on the two benzimidazole groups along with the π acidic nitrophenyl moiety connected by the amide linkage on the non-symmetric arm. Binding of polyatomic anions with $\mathbf{L_1}H_2^{2+}$ was studied as protonated salts of HF and H_2SO_4. These results in the single crystals of complex **1** and **2** which were characterized by X-ray crystallography.

3.3.1 Structural study of the Complex 1 $[(\mathbf{L_1}H_2)^{2+}.SiF_6^{2-}]$

Silicon hexafluoride salt **1** was formed as a result of the reaction of the ligand with HF in DMSO/MeOH apparently because of glass corrosion during crystal formation.

$$6HF + SiO_2 \longrightarrow H_2SiF_6 + 2H_2O$$

Structural elucidation suggested that complex **1** crystallizes in the monoclinic system with a space group $P2_1/a$. Exposition of the crystal structure reveals that due to the unsymmetrical receptor design and restriction in flexibility in the amide podand, the two benzimidazole containing arms are adjusted inside the cavity holding the SiF_6^{2-} through the NH···F bonds while the third podand points outside the cavity. Further, two more receptor molecules interact in a sideway fashion through amide –NH, benzimidazole –NH, aromatic and aliphatic –CHs. The fluoride atoms display monofurcated, bifurcated, trifurcated and tetrafurcated nature of hydrogen bonding acceptance. The complete coordination environment of SiF_6^{2-} suggests that it has been stabilized *via* thirteen hydrogen bonding interactions with three protonated receptors having average donor to acceptor distance of 3.067 Å consisting of eight N−H···F (seven from the benzimidazole groups and one from the amide –NH), two C_{Ar}–H···F (one from the ortho hydrogen of nitrophenyl ring and the other from the aryl group of one benzimidazole moiety) and three C_{Alp}–H···F (from the $-CH_2$ groups adjacent to the benzimidazole groups) (Figure 3.1a). The strongest hydrogen bond

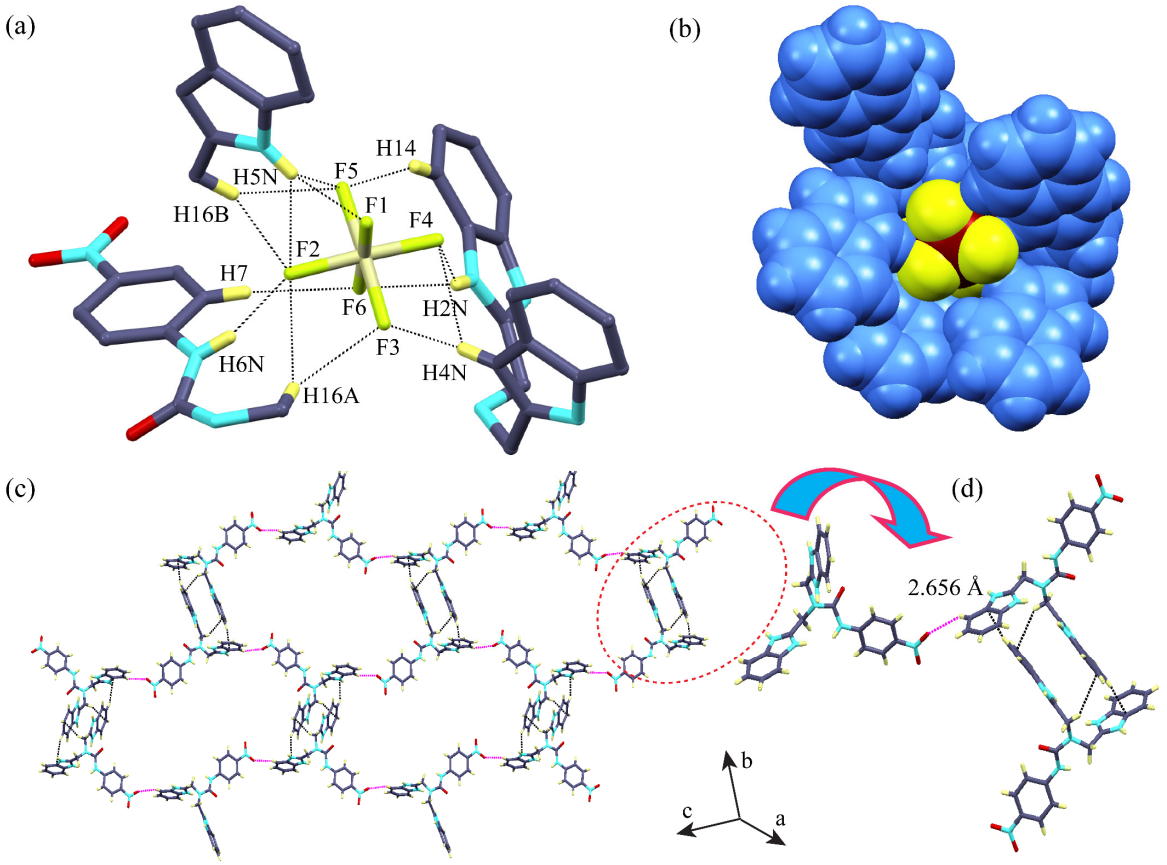

Figure 3.1 (a) Coordination environment of single SiF_6^{2-} anion in complex **1**. (b) Spacefill view of pseudo-cavity around SiF_6^{2-} anion. (c) π---π and CH---NO_2 induced three dimensional hydrogen bonding framework with (d) magnified view (SiF_6^{2-} units are omitted for clarity).

is offered by the benzimidazole –NH of one symmetric arm to F3 atom of SiF_6^{2-} (1.846 Å, ∠N4−H···F3= 155.3º, Table A3.2). Three protonated receptors are oriented in such a way that one SiF_6^{2-} anion is enclosed within the pseudo-cavity formed by the benzimidazole side arms (Figure 3.1b). Previously reported SiF_6^{2-} encapsulation from our group with C_{3v} symmetric tren based amide receptor exhibits average donor to acceptor distance of 3.112 Å.[3.36] Other cases of SiF_6^{2-} encapsulation by protonated symmetric flexible tren based tripodal receptor was reported by Ghosh *et al.* showing a coordination environment of twelve bonds around the SiF_6^{2-} anion with an average donor to acceptor distance of 2.887 Å.[3.37] The oxygen atom of the π acidic nitrophenyl moiety and two CH---π interactions play the pivotal role in forming the three dimensional structure along the crystallographic '***c***' axis (Figure 3.1c). The oxygen atom of the nitro group forms a hydrogen bond with the aryl –CH group of benzimidazole moiety with a separation of 2.656 Å. The two arms, one containing the benzimidazole moiety and the other with amide linkage are oriented in a similar direction to donate hydrogen bonding to two SiF_6^{2-} anions while the third arm containing the other benzimidazole unit runs parallel to the benzimidazole containing arm of another $\mathbf{L_1}H_2^{2+}$ receptor. This characteristic orientation leads to two kinds of CH---π interactions.

One interaction is from the aryl −CH of the benzimidazole moiety of one $\mathbf{L_1}H_2^{2+}$ unit to the π cloud of the benzimidazole group of other protonated ligand which is oriented in a similar fashion like that of the amide linked p-nitrophenyl group. The other consists of interaction between the two parallel benzimidazole containing arms; the $-CH_2$ of one $\mathbf{L_1}H_2^{2+}$ unit to the π cloud of the benzimidazole group of other $\mathbf{L_1}H_2^{2+}$ unit and *vice versa*. The difference in separation distance is apparent as the former interaction is of 3.983 Å while the latter is shorter by 0.922 Å i.e. its separation is of 3.061 Å.

3.3.2 Structural study of the Complex 2 $[2(\mathbf{L_1}H_2)^{2+}.2HSO_4^-.SO_4^{2-}.H_2O]$

The complex crystallises in the orthorhombic system with $P2_12_12_1$ space group. Structural elucidation reveals that the asymmetric unit comprises two units of protonated receptor $\mathbf{L_1}H_2^{2+}$, two units of hydrogen sulfate ions, one sulfate ion along with one molecule of water of crystallization. In the asymmetric unit, each protonated receptor of $\mathbf{L_1}$ is oriented in two different orientations in response to the stabilizing surrounding species in the crystal pattern leading to remarkable distinction from the view of symmetry equivalence (c′=2).

In supramolecular chemistry, the existence of more than one molecular conformer in the same crystal structure has been described by the term conformational isomorphism. The occurrence of such isomorphism elucidates concepts like kinetic and thermodynamic crystal stability as it is found to be the outcome of interrupted crystallization, as illustrated by Desiraju *et al*.[3.38]

The two conformational isomorphs (***C1*** and ***C2***) are interlinked by hydrogen bond interactions between themselves and also with the anions. The two benzimidazole arms of the ***C1*** (C_{39}-N_8-C_{31}-C_{32} = 88.90˚) are connected to ***C2*** (C_8-N_1-C_{16}-C_{17} = -104.96˚) through one hydrogen sulfate and one sulfate anion, while H22 and H6A of ***C2*** are in direct contact with the nitro group and amide carbonyl O4 of ***C1*** conformer (Figure 3.2a). This, in turn, makes the aromatic H37 to interact with the π cloud of benzimidazole moiety of ***C2*** conformer (Figure A3.2a). Another interesting behaviour is exhibited by the nitro groups in the three dimensional decoration of the conformers. The nitro group of ***C1*** conformer interacts strongly with aliphatic −CHs through three −CH···O interaction (average distance 2.447Å) forming a '**T**' like structure and elongates the structure along crystallographic '*b'* axis. The ***C2*** conformer, in contrast, draws out along the crystallographic '*c'* axis with 'zigzag' motion using only one −CH···O interaction between the oxygen atom of the p-nitro group of one conformer and the aryl hydrogen of the benzimidazole group of analogous species (D−H···A = 2.603Å) (Figure A3.2b).

Both the benzimidazole groups of ***C1*** are nearly in the same plane and interact with three hydrogen

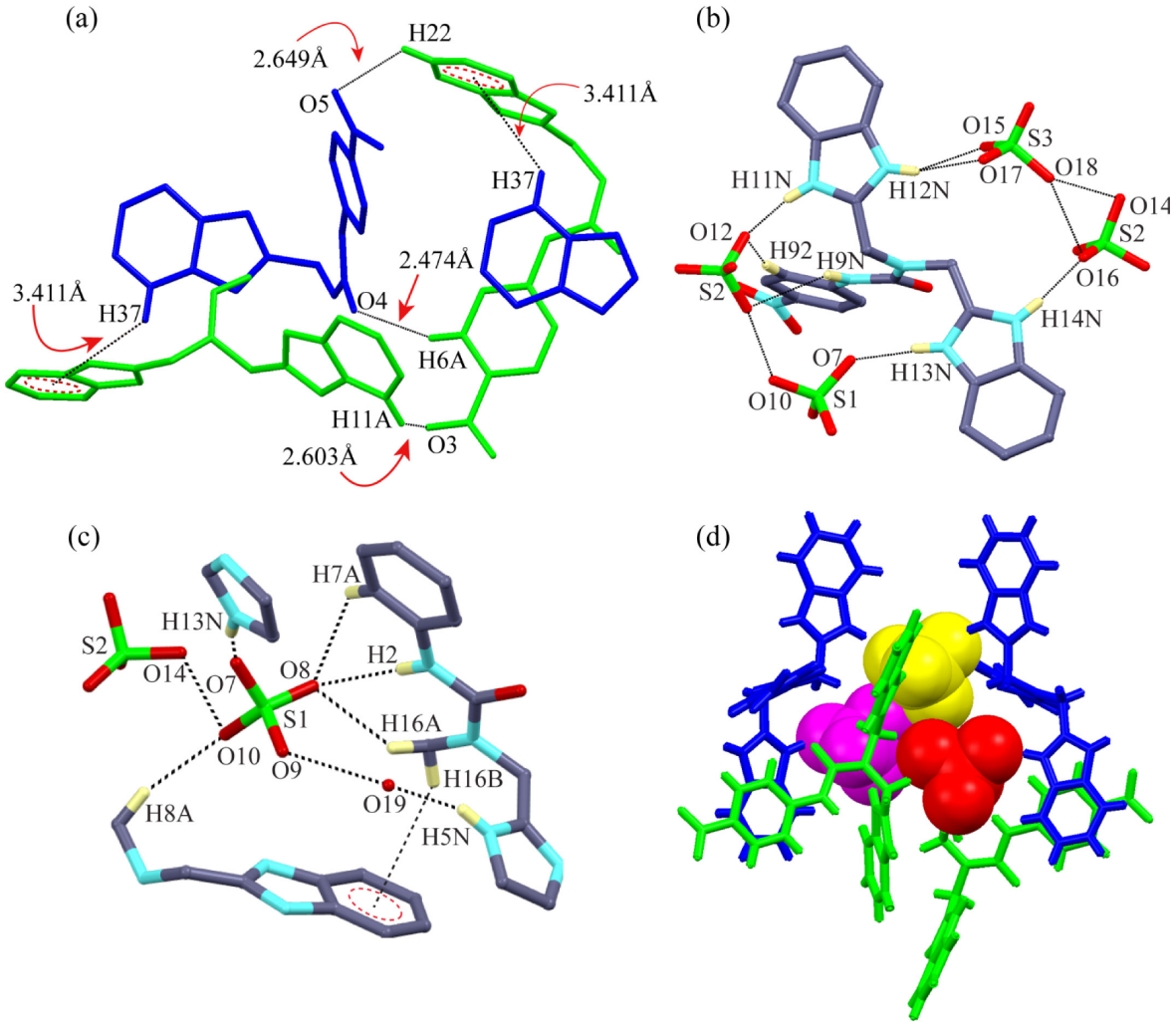

Figure 3.2 (a) The two conformational isomers of $\mathbf{L_1H_2}^{2+}$ with intramolecular and intermolecular interactions. (b) The coordination environment of $\mathbf{L_1H_2}^{2+}$ (***C1***) with hydrogen sulfate and sulfate. (c) Coordination environment of S1 centered sulfate. (d) Spacefill presentation of the interacting anions in a pseudo-cavity formed by the protonated receptors.

sulfate and one sulfate anion through the involvement of both neutral as well as protonated −NHs (Figure 3.2b). The S1 centred hydrogen sulfate is hepta coordinated as it is linked to three receptors, one hydrogen sulfate and one water molecule with five moderately strong hydrogen bonds (Figure 3.2c). O8 belonging to S1 is trifurcated and satisfied with two −CHs and one amide –NH interactions. The strongest hydrogen bond interaction is the one with benzimidazole –NH and O7 with H13N···O7=1.877Å, ∠169.05˚, while O9 interacts with the oxygen atom of the water molecule. The bifurcated O10 involves in hydrogen bonding with the $-CH_2$ group adjoining to the benzimidazole group and S2 centred hydrogen sulfate anion (C8H···O10 = 2.397Å, O10···O14 = 2.686Å).

The significant coordinations in the S2 centred hydrogen sulfate anion are from four −NH···O

(average N−O = 2.8375Å), three O···O (average O−O = 2.82 Å) and one −CH···O interaction (Figure 3.3a). O12, as well as O13, are bifurcated hydrogen bond acceptor as the former forms bonds with benzimidazole –NH group and aryl –CH of the p-nitrophenyl group while the latter receives hydrogen bonds from one benzimidazole –NH of ***C1*** conformer and S3 centred sulfate anion. The trifurcated nature of O14 is interpreted from its contact with the amide –NH of ***C1*** conformer and the two oxygen atoms of coordinated S1 and S3 centred hydrogen sulfate and sulfate anion respectively. The remaining O11 is monofurcated acceptor as only the benzimidazole group belonging to ***C2*** conformer renders hydrogen bond to it. Among these S1 and S2 centred coordination, the strongest hydrogen bond in each case is from the protonated –NH functionality of the benzimidazole group (O7···H13N = 1.877 Å, O12···H12N = 1.821 Å) proving its dominance over the amide –NH functionality.

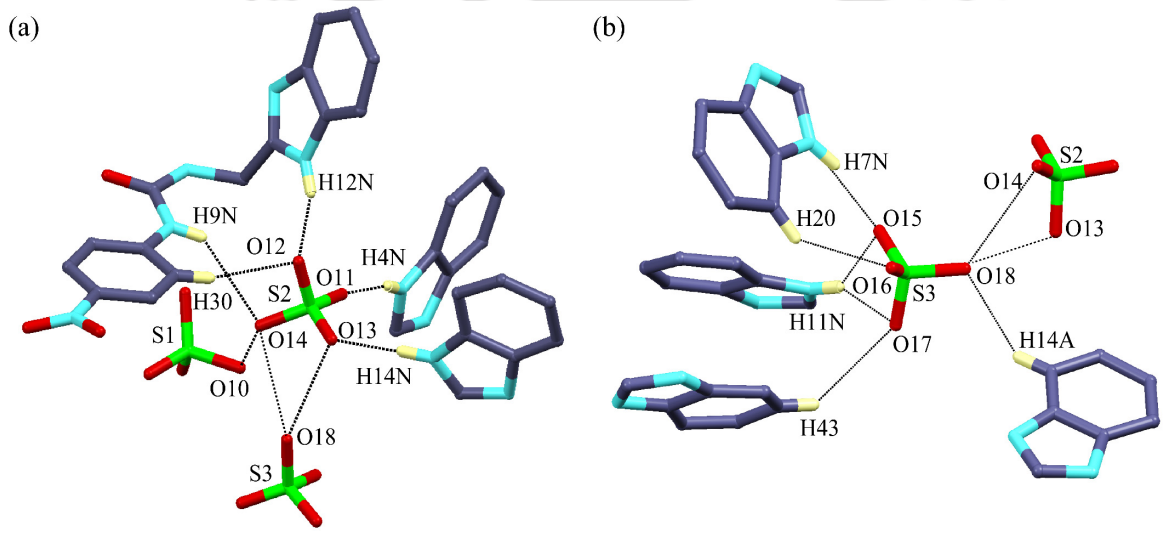

Figure 3.3 The coordination environment of the (a) S2 and (b) S3 centered hydrogen sulfate anion.

As depicted in (Figure 3.3b), another octa-coordinated environment is evident on the S3 centred sulfate which is satisfied by three –NH···O, three C_{Ar}–H···O and two O···O interactions. Two of the protonated benzimidazole groups from conformer ***C1*** and ***C2*** and the O15 atom of S3 sulfate construct two of the three NH···O interactions. The third interaction incorporates the bonding between O17 and benzimidazole –NH group from ***C1*** conformer along with the aryl −CH of benzimidazole group of another ***C1*** conformer leads to the bifurcated nature in O17. The only hydrogen bonding pattern associated with O16 comprises the second C_{Ar}–H···O interaction in which the aryl −CH of benzimidazole group of ***C2*** conformer provides the same. The residual O18 atom is a trifurcated acceptor as it has two O···O interactions with S2 centred hydrogen sulfate anion together with final C_{Ar}–H···O interaction in which the aryl −CH of benzimidazole group of another ***C2*** conformer plays the crucial role. Two units of each ***C1*** and ***C2*** conformers of $\mathbf{L_1}H_2^{2+}$

assemble forming a pseudo-cavity to stabilize the [$(HSO_4^-)_2.SO_4^{2-}$] anionic cluster, as shown in Figure 3.2d. A comparative study of our work with other literatures on sulfate and bisulfate binding has been prepared and presented in Table A3.4.

3.4 Solution phase anion recognition

The interesting solid state anion recognition property of the **L_1**, insisted us to investigate its solution phase anion sensing ability in acetonitrile solution. For this, the 10 μM **L_1** solution was treated with tetrabutyl/tetraethyl salts of various anions such as F^-, Cl^-, Br^-, I^-, $PO4^{3-}$ $H_2PO_4^-$, HSO_4^-, $SO4^{3-}$, NO_3^-, HCO_3^-, and CH_3COO^-. As evident from Figure 3.4a, the ligand **L_1** exhibited a characteristic absorption maximum at 333 nm probably due to π–π* transition. However, among the aforesaid anions, only the addition of fluoride (10 equivalents) led to develop a new red shifted (138 nm) absorption peak at 471 (±3) nm with a concomitant visual colour change of the solution from colourless to orange-red type (Figure 3.4a, Inset). The titration spectra with escalating fluoride concentration further revealed a progressive increase in absorbance at 471 nm with a new isobestic point at 363 nm (Figure 3.4b), which clearly suggests the formation of a new complex. It was interesting to note that addition of other anions including basic $CH_3CO_2^-$, $H_2PO_4^-$ etc. had no effect on the absorption spectrum of the receptor and caused no visible colour change to the solution (Figure A3.4). To support the standing of this result, a comparative study of the sensing affinity of few recent benzimidazole and amide based receptors with the present chemosensor is listed in Table A3.5.

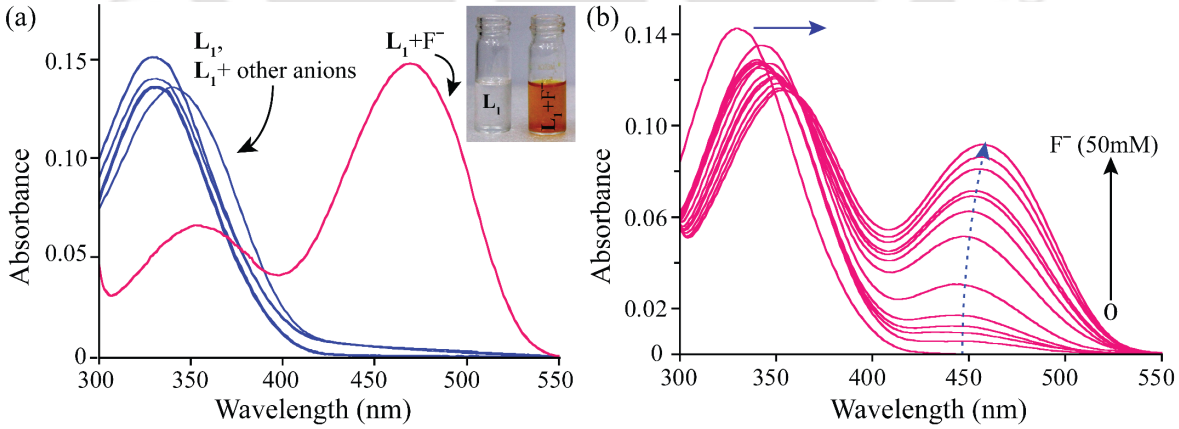

Figure 3.4 UV-visible changes of **L_1** with the (a) various anions and (b) with increasing fluoride concentration in acetonitrile solution. Inset: visible colorimetric change upon the addition of F^- to **L_1**.

Interaction with fluoride anion can cause deprotonation of the host. Thus, to unveil the reason behind the observed colour change, tetrabutylammonium hydroxide was added to the acetonitrile solution of **L_1**. The analogous spectroscopic output (Figure A3.5) strongly suggested the possibility of anion-induced deprotonation of the receptor **L_1**, i.e. either the benzimidazole or the

amide −NH was deprotonated. Electron withdrawing nitro group increases the acidity of the amide −NH and thus the fluoride anion or hydroxide anion could probably deprotonate the amide –NH. Such type of deprotonation event is also reported by Gunnlaugsson *et al.*[3.39] and Magri *et al.*[3.40] with urea/thiourea type of receptors.

To confirm the deprotonation event, we also recorded the ^{1}H NMR spectra of the ligand with excess F^- ion in DMSO-*d*$_6$ (the solvent was chosen for better solubility). As shown in Figure 3.5, the highly downfield amide –NH signal, H_a at 9.8 ppm disappeared after the addition of an excess of fluoride solution and subsequently, other aromatic protons H_b, H_d and H_e experienced upfield shift due to the induced negative charge on the ligand. Interestingly, the doublet of aromatic –CH, H_c at 7.678 ppm showed downfield shift suggesting its interaction with the fluoride ion.

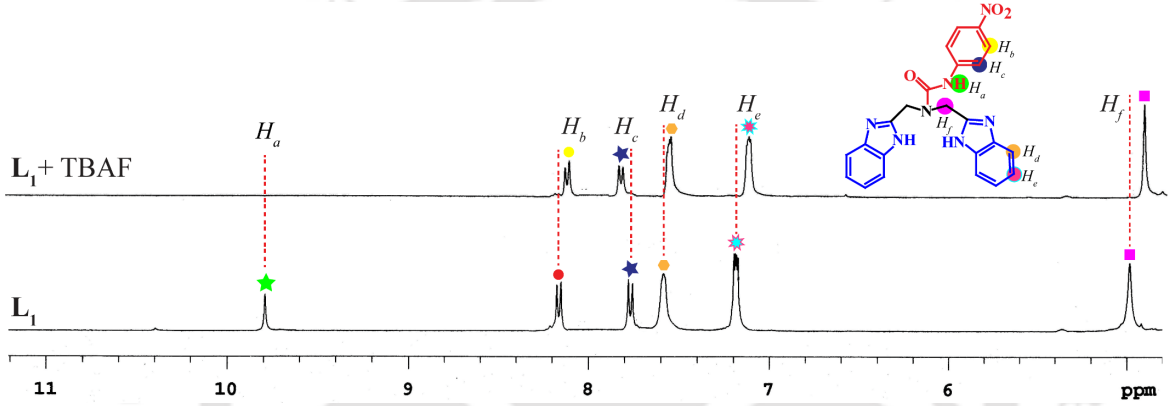

Figure 3.5 ^{1}H NMR Stacked plot comparing the chemical shifts of the receptor **L**$_1$ before and after addition of TBAF solution in DMSO-d$_6$.

However, dissimilar results were obtained when ^{1}H NMR spectra were recorded in DMSO-*d*$_6$ (Figure A3.6) for both the complexes. The upfield shift was observed for amide −NH proton and all the aromatic −CHs and aliphatic −CHs for the complexes were shifted downfield. For complex **2**, the aliphatic −CH underwent the maximum downfield shift of 0.293 ppm, proving its dominance in anion binding in solution phase.

3.5 Practical paper strip application

Finally, for the realistic application of the chemosensor **L**$_1$, we performed the paper strip test. A simple and straight forward way for the instant sensing of fluoride ions as their tetrabutyl salts in aqueous solution was done by easily prepared test papers. A 1 mM solution of **L**$_1$ in DCM was prepared and coated on a few Whatman paper strips and dried in vacuum at 100–110 ºC. The pale yellow coloured strips thus obtained were dipped in aqueous solutions of TBAF of varying concentration. On increasing the concentration of the F^-, the colour of the strip changed from faint yellow to darker yellow as shown in Figure A3.7. It can be clearly observed that the receptor **L**$_1$

can detect up to a lower concentration limit down to 10 mg/L. However, for wider implementation, a sample containing a mixture of various anions was prepared and colour change was tested. It was found to be effective even in the presence of other anions, which suggests that the interactions of other anions were absent leading to selective detection of F^- in the mixture of anions.

3.6 Conclusion

A novel non-symmetric tripodal receptor with two similar arms along with an arm with different functionality was prepared and characterized. Three units of protonated receptors tend to form a pseudo-cavity around the hexafluorosilicate anion with its symmetric arms while the oxygen atom of the π acidic nitrophenyl moiety of the non-symmetric arm plays a pivotal role in forming the three-dimensional array. The hexafluorosilicate anion was stabilised via a total of thirteen interactions comprising of mono to tetrafurcated nature of hydrogen bonding acceptance. In addition, the receptor exhibits simultaneous binding of two bisulfates and one sulfate anion along with a water molecule with its two protonated counterparts. Interestingly, solid state study of this crystal reveals the existence of two conformational isomers ($c' = 2$) and both are different in their corresponding torsional angles and hydrogen bonding aptitude. In both the crystals, the benzimidazole –NH groups are prominent hydrogen bond donors. The neutral receptor was highly sensitive to fluoride anion and impelled a naked eye visible colorimetric change from colourless to orange-red type, which was established via UV absorption study with a red shift of 138 nm upon addition of excess fluoride. The ^{1}H NMR studies with the neutral and protonated form of the receptor suggested the strong involvement of amide –NH in anion binding. The anion-induced deprotonation of the seldom observed amide proton was proved by the NMR studies as the addition of fluoride rendered disappearance of the amide –NH peak. In qualitative practical approach, the receptor **L_1** was found to detect a lower concentration limit down to 10 mg/L of fluoride ions as their tetrabutyl salts in aqueous solution, which was mentioned as a practical application for a simple and straightforward way for the instant sensing of fluoride ions.

References

3.1 L. Adriaenssens, and P. Ballester, Hydrogen bonded supramolecular capsules with functionalized interiors: the controlled orientation of included guests, *Chem. Soc. Rev.*, 2013, **42**, 3261−3277.

3.2 L. Chen, S. N.Berry, X. Wu, E. N. Howe, and P. A. Gale, Advances in anion receptor chemistry, *Chem*, 2020, **6**, 61−141.

3.3 S. K. Dey, A. Basu, R. Chutia, and G. Das, Anion coordinated capsules and pseudocapsules of tripodal amide, urea and thiourea scaffolds, *RSC Adv.*, 2016, **6**, 26568−26589.

3.4 R. Dutta and P. Ghosh, Recent developments in anion induced capsular self-assemblies, *Chem. Commun.,* 2014, **50**, 10538−10554.

3.5 S. K. Dey and G. Das, A selective fluoride encapsulated neutral tripodal receptor capsule: solvatochromism and solvatomorphism, *Chem. Commun.*, 2011, **47**, 4983−4985.

3.6 A. Basu and G. Das, A C_{3v}-Symmetric Tripodal Urea Receptor for Anions and Ion Pairs: Formation of Dimeric Capsular Assemblies of the Receptor during Anion and Ion Pair Coordination, *J. Org. Chem*., 2014, **79**, 2647−2656.

3.7 S. K. Dey, R. Chutia and G. Das, Oxyanion-Encapsulated Caged Supramolecular Frameworks of a Tris (urea) Receptor: Evidence of Hydroxide-and Fluoride-Ion-Induced Fixation of Atmospheric CO_2 as a Trapped CO_3^{2-} Anion, *Inorg. Chem*., 2012, **51**, 1727−1738.

3.8 A. Basu and G. Das, Encapsulation of divalent tetrahedral oxyanions of sulfur within the rigidified dimeric capsular assembly of a tripodal receptor: first crystallographic evidence of thiosulfate encapsulation within neutral receptor capsule, *Dalton Trans*., 2012, **41**, 10792−10802.

3.9 N. Singh and D. O. Jang, Benzimidazole-based tripodal receptor: highly selective fluorescent chemosensor for iodide in aqueous solution, *Org. Lett.*, 2007, **9**, 1991–1994.

3.10 M. N. Hoque, A. Basu and G. Das, Cyclic Pentameric Puckered Hybrid Chloride–Water Cluster $[Cl_3(H_2O)_4]^{3-}$ in the Hydrophobic Architecture, *Cryst. Growth Des*., 2012, **12**, 2153−2157.

3.11 A. S. Degtyarenko, E. B. Rusanov, A. Bauzá, A. Frontera, H. Krautscheid, A. N. Chernega, A. A. Mokhir and K. V. Domasevitch, Self-assembly cavitand precisely recognizing hexafluorosilicate: a concerted action of two coordination and twelve CH··· F bonds, *Chem. Commun*., 2013, **49**, 9018–9020.

3.12 I. Ravikumar, P. S. Lakshminarayanan, E. Suresh, and P. Ghosh, Structural studies on encapsulation of tetrahedral and octahedral anions by a protonated octaaminocryptand cage, *Beilstein J. Org. Chem*., 2009, **5**, 1−8.

3.13 A. Pramanik, D. R. Powell, B. M. Wong and M. A. Hossain, Spectroscopic, structural, and theoretical studies of halide complexes with a urea-based tripodal receptor, *Inorg. Chem.* **2012**, 51, 4274–4784.

3.14 B. Nayak, S. Halder, S. De and G. Das, Binding consistency of anions by the effect of aromatic meta-substitution of bis-urea receptors: entrapment of hexafluorosilicate clusters, *CrystEngComm*, 2019, **21**, 7172−7181.

3.15 A. F. Holleman and E. Wiberg, Inorganic Chemistry, Academic Press, San Diego, USA, 2001.

3.16 R. D. Masters and M. J. Coplan, Water treatment with silicofluorides and lead toxicity, *Int. J. Environ. Stud*., 1999, **56**, 435–449.

3.17 B. Machalinski, M.Baskiewicz-Masiuk, B. Sadowska, A. Machalinska, M. Marchlewicz, B. Wiszniewska and I.Stecewicz, The influence of sodium fluoride and sodium hexafluorosilicate on human leukemic cell lines, *Fluoride*, 2003, **36**, 231–240.

3.18 E. T. Urbansky, Fate of fluorosilicate drinking water additives, *Chem. Rev*., 2002, **102**, 2837–2854.

3.19 J. Frayret, A. Castetbon, G. Trouve and M. Potin-Gautier, Solubility of $(NH_4)_2SiF_6$, K_2SiF_6 and Na_2SiF_6 in acidic solutions, *Chem. Phys. Lett.*, 2006, **427**, 356−364.

3.20 L. C. Chow, S. Takagi, C. M. Carey and B. A. Sieck, Remineralization effects of a two-solution fluoride mouthrinse: an in situ study, *J. Dent. Res.*, 2000, **79**, 991−995.

3.21 H. Amouri, C. Desmarets, J. Moussa, Confined Nanospaces in Metallocages: Guest Molecules, Weakly Encapsulated Anions, and Catalyst Sequestration, *Chem. Rev.* 2012, **112**, 2015−2041.

3.22 J. Lee, S. Park, D. Kim, Y. A. Lee, and O. S. Jung, Hexafluorosilicate anion in the formation of a coordination cage: anion competition, *Inorg. Chem. Front.*, 2020, **7**, 1546−1552.

3.23 P. A. Dawson, S. Petersen, R. Rodwell, P. Johnson, K. Gibbons, A. McWhinney, F. G. Bowling and D. McIntyre, *BMC Pregnancy Childbirth*, 2015, **15**, 96.

3.24 P. A. Dawson, L. Beck and D. Markovich, *Proc. Natl. Acad. Sci. U. S. A.*, 2003, **100**, 13704.

3.25 K. M Bąk, M. Krystyna, and M. J. Chmielewski. "Selective turn-on fluorescence sensing of sulfate in aqueous–organic mixtures by an uncharged bis (diamidocarbazole) receptor, *Org. Biomol. Chem.*, 2017, **15**, 5968–5975.

3.26 W. D. Heizer, R. S. Sandler, E. Seal, S. C. Murray, M. G. Busby, B. G. Schliebe and S. N. Pusek, Intestinal effects of sulfate in drinking water on normal human subjects, Digestive diseases and sciences, 1997, 42, 1055–1061.

3.27 L. P. M. Lamers, H. B. M. Tomassen and J. G. M. Roelofs, *Environ. Sci. Technol.*, 1998, **32**, 199–205.

3.28 G. J. Lumetta, B. A. Moyer and R. P. Singh, Eds, Fundamentals and Applications of Anion Separations; Kluwer Academic: New York, 2004; pp 107–114.

3.29 B. A. Moyer, R. Custelcean, B. P. Hay, J. L. Sessler, K. Bowman-James, V. W. Day and S. -O. Kang, A case for molecular recognition in nuclear separations: sulfate separation from nuclear wastes, *Inorg. Chem.*, 2013, **52**, 3473–3490.

3.30 I. Ravikumar and P. Ghosh, Recognition and separation of sulfate anions, *Chem. Soc. Rev.*, 2012, **41**, 3077–3098.

3.31 B. Gao and Z. Liu, A first principles study on the solvation and structure of $SO_4^{2-}(H_2O)n$, n=6 –12, *J. Chem. Phys.*, 2004, **121**, 8299–8306.

3.32 L. K. Kirk, Biochemistry of the Halogens and Inorganic Halides; Plenum Press: New York, 1991.

3.33 M. Kleerekoper, The role of fluoride in the prevention of osteoporosis, *Endocrinol. Metab. Clin. North Am.*, 1998, **27**, 441–452.

3.34 D. Briancon, Fluoride and osteoporosis: an overview, *Rev. Rhum.*, 1997, **64**, 78–81.

3.35 Y. Michigami, Y. Kuroda, K. Ueda and Y. Yamamoto, Determination of urinary fluoride by ion chromatography, *Anal. Chim. Acta*, 1993, **274**, 299–302.

3.36 A. Basu, R. Chutia and G. Das, Dual modes of binding on the hexafluorosilicate anion by a C_{3v} symmetric flexible tripodal amide ligand in solid state, *Cryst Eng Comm*., 2014, **16**, 4886–4891.

3.37 P. Bose, I. Ravikumar and P. Ghosh, Anion Binding in the C_{3v}-Symmetric Cavity of a Protonated Tripodal Amine Receptor: Potentiometric and Single Crystal X-ray Studies, *Inorg. Chem.*, 2011, **50**, 10693–10702.

3.38 G. R. Desiraju, Crystal engineering a holistic view, *Angew. Chem, Int. Ed.*, 2007, **47**, 8342−8356.

3.39 T. Gunnlaugsson, P. E. Kruger, P. Jensen, J. Tierney, H. D. P. Ali and G. M. Hussey, Colorimetric "naked eye" sensing of anions in aqueous solution, *J. Org. Chem*., 2005, **70**, 10875−10878.

3.40 K. N. Farrugia, D. Makuc, A. Podborska, K. Szacitowski, J. Plavec and D. C. Magri, *Org. Biomol. Chem.*, 2015, **13**, 1662−1672.

Appendix 2

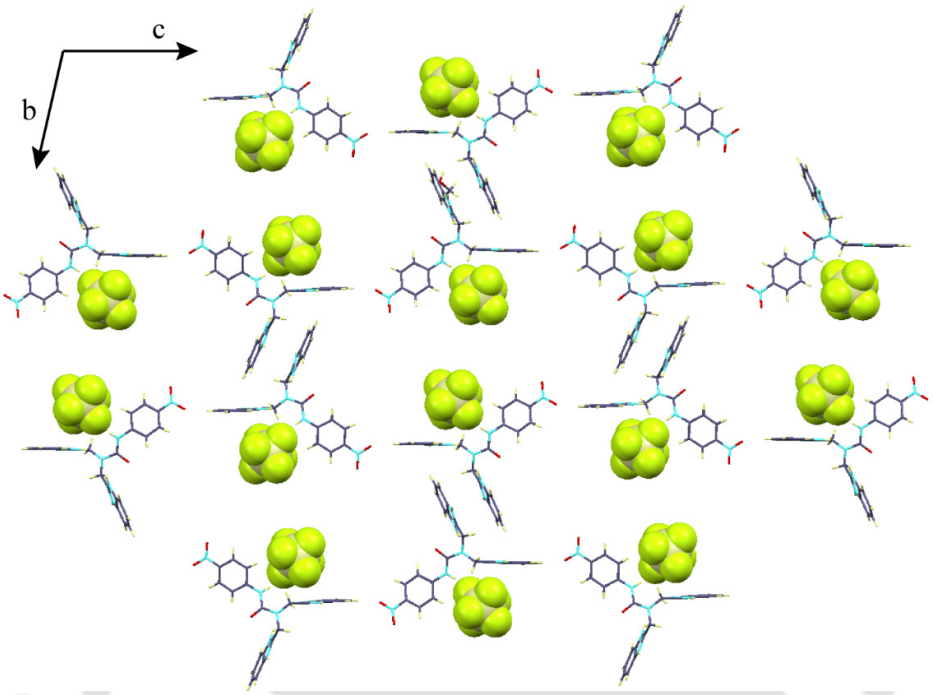

Figure A3.1 Extended sheet-like framework structure of the $\mathbf{L_1}$ with spacefill presentation of SiF_6^{2-}.

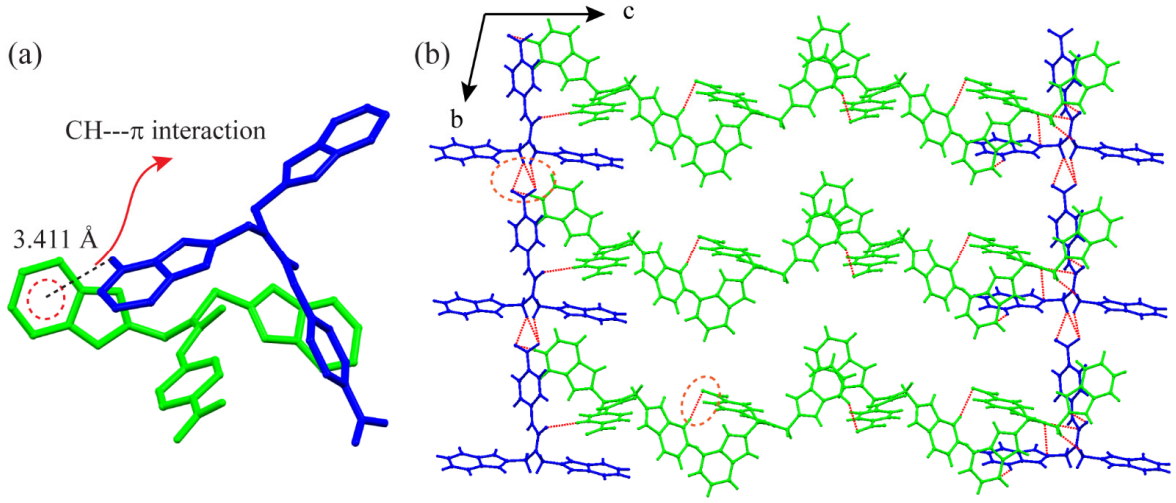

Figure A3.2 (a) The interacting isomorphs represented in different colors (blue = ***C1***, green = ***C2***). (b) The –CH (aliphatic)···$\mathbf{NO_2}$ and –CH(aromatic)···$\mathbf{NO_2}$ interactions extending the ***C1*** chain and ***C2*** in perpendicular ***b*** and ***c*** directions.

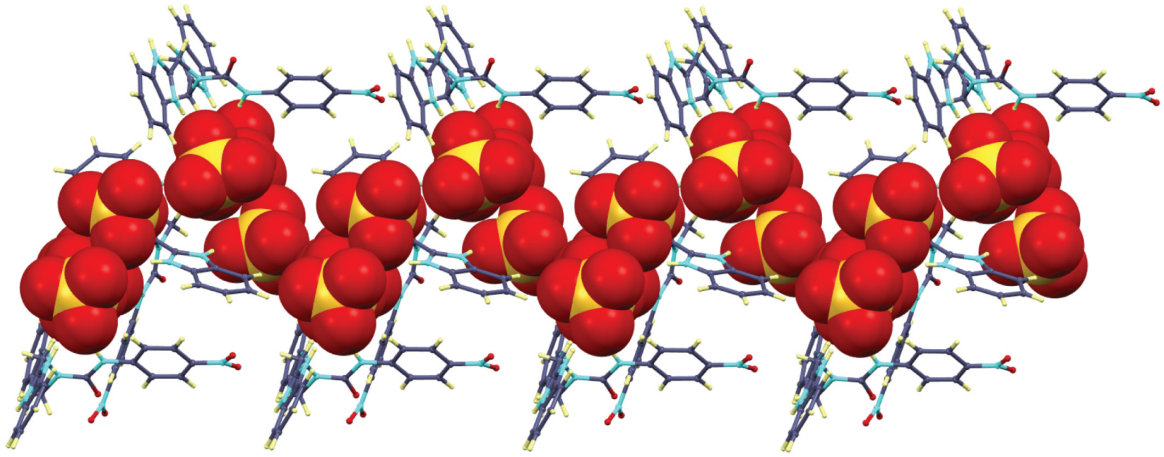

Figure A3.3 Hydrogen bonded network structure of complex **2** $[2(\mathbf{L_1}H_2)^{2+}.2HSO_4^-.SO_4^{2-}.H_2O]$ with spacfill guest anions.

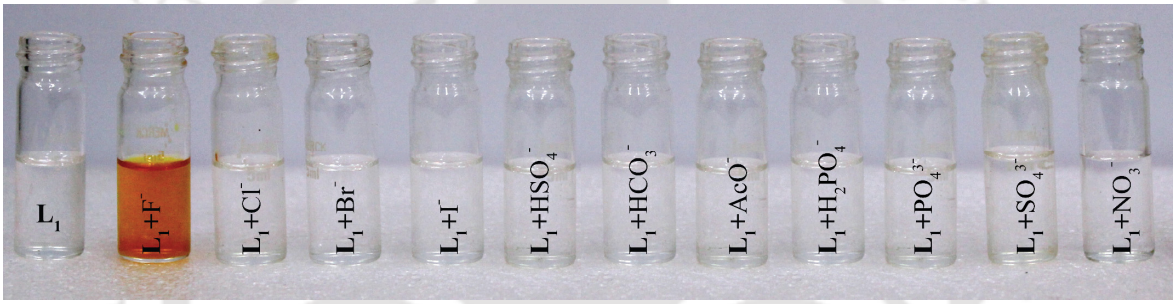

Figure A3.4 Corresponding colorimetric changes of $\mathbf{L_1}$ upon addition of various anions.

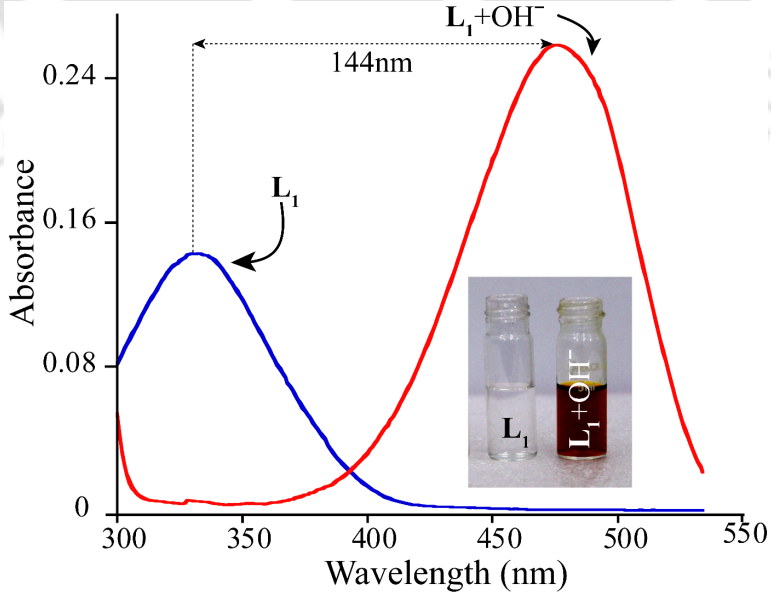

Figure A3.5 Absorption spectra of TBOH addition to the receptor $\mathbf{L_1}$ and the corresponding colour change.

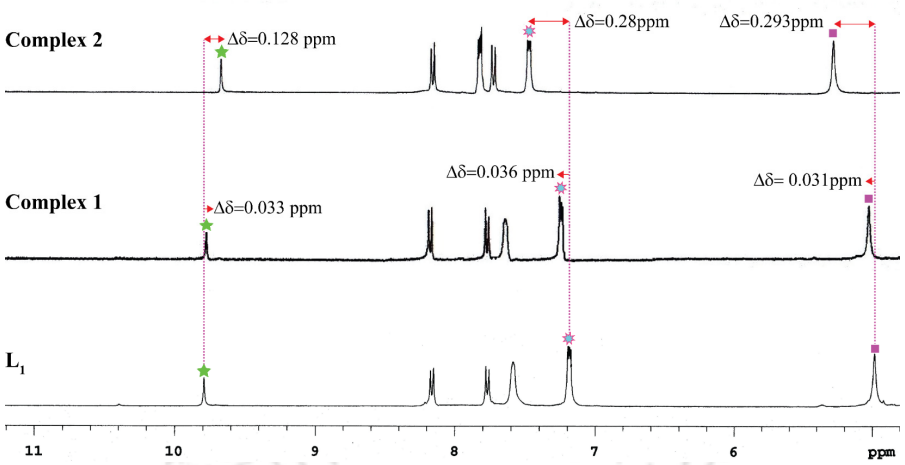

Figure A3.6 The stacked NMR plot comparing the receptor $\mathbf{L_1}$ with the complex **1** $[(\mathbf{L_1}H_2)^{2+}.SiF_6^{2-}]$ and complex **2** $[2(\mathbf{L_1}H_2)^{2+}.2HSO_4^{-}.SO_4^{2-}.H_2O]$.

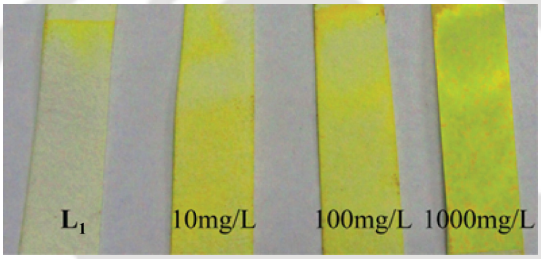

Figure A3.7 Qualitative anions detection: visual colour change of paper-made test strips of $\mathbf{L_1}$ with different concentrations of fluoride anion.

Table A3.1 Crystallographic data and refinement details of the anion complexes.

Parameters	$[(\mathbf{L_1}H_2)^{2+}.SiF_6^{2-}]$	$[2(\mathbf{L_1}H_2)^{2+}.2HSO_4^{-}.SO_4^{2-}.H_2O]$
Empirical formula	$C_{23}\ H_{21}\ F_6\ N_7\ O_3\ Si$	$C_{46}\ H_{42}\ N_{14}\ O_{19}\ S_3$
Formula Weight	585.56	1190.12
Crystal system	monoclinic	orthorhombic
a (Å)	9.1589(7)	20.5191(10)
b (Å)	26.8890(18)	12.0434(6)
c (Å)	14.2575(10)	21.2997(10)
α (°)	90.00	90
β (°)	104.209(7)	90
γ (°)	90	90
V(Å^3)	3403.8(4)	5263.6(4)
Z	4	4
ρ (cal) (g/cm^3)	1.143	1.502
μ (Mo Kα) (mm^{-1})	0.133	0.231
T(K)	298 K	298 K
R_1; wR2 [I >2σ(I)]	0.0718; 0.1617	0.0951; 0.1823
R_1; wR2 (all)	0.1309; 0.1813	0.2201; 0.2065
Residual electron density (e/Å^3)	0.277/-0.252	0.768/-0.367
Goodness-of-fit	1.096	1.130
Reflection collected	8619	13021
Independent reflection	6783	10210
CCDC no.	1020478	1020477

Table A3.2 Relevant Hydrogen Bonding Parameters for Complex 1 and complex 2 of receptor $\mathbf{L_1}$.

Complex 1	D−H···A	*d*(H···A)/Å	*d*(D···A)/ Å	∠ D−H···A/º
	N2H···F4	2.051	2.795(3)	144.3
	N2H···F6	2.213	2.822(4)	127.7
	N4H···F3	1.846	2.652(4)	155.3
	N4H···F4	2.568	3.186(3)	129.5
	N5H···F1	1.988	2.829(4)	165.8
	N5H···F2	2.550	3.201(3)	133.3
	N5H···F5	2.552	3.132(3)	125.6
	N6H···F2	1.957	2.788(3)	162.5
	C7H···F6	2.624	3.550(5)	172.9
	C14H···F5	2.574	3.455(4)	158.4
	C16HA···F2	2.535	3.197(4)	125.5
	C16HB···F2	2.296	3.015(4)	130.1
	C16HB···F5	2.436	3.282(4)	145.4
Complex 2	**D−H···A**	***d*(H···A)/Å**	***d*(D···A)/ Å**	**∠ D−H···A/º**
S1 Centred	N13H···O7	1.877	2.727(6)	169.05
	N2H···O8	2.216	3.00(1)	151.48
	C7H···O8	2.696	3.35(1)	128.49
	C16···O8	2.473	3.26(1)	138.67
	O19···O9	NA	2.85(1)	NA
	O14··· O10	NA	2.69(1)	NA
	C8H···O10	2.397	3.34(1)	163.09
	N5H···O19	1.959	2.761(7)	158.71
S2 Centred	N4H···O11	1.835	2.65(1)	161.15
	N12H··O12	1.821	2.64(1)	158.45
	C30H···O12	2.529	3.41(1)	157.72
	N14H···O13	1.846	2.70(1)	173.06
	O18···O13	NA	2.81(2)	NA
	O10···O14	NA	2.69(1)	NA
	N9H···O14	2.639	3.36(1)	141.91
	O18···O14	NA	2.96(1)	NA
S3 Centred	N7H···O15	2.001	2.844(8)	166.26
	N11H···O15	2.195	2.915(9)	141.16
	C20H···O16	2.535	3.32(1)	142.03
	N11H···O17	2.465	3.23(1)	148.37
	C43H···O17	2.698	3.42(1)	135.74
	C14H···O18	2.523	3.35(1)	147.53
	O14···O18	NA	2.96(1)	NA
	O13···O18	NA	2.81(2)	NA

Table A3.3 Comparison of solid state study of the present work with other literatures covering SiF_6^{2-}.

Reference	Guest Anion	No. and types of Hydrogen bond donors	Average *d*(D···A)/ Å
Present work	SiF_6^{2-}	13, Benzimidazole –NH, Amide –NH and –CH	3.067 Å
Cryst Eng Comm., 2014, **16**, 4886–4891	SiF_6^{2-}	18, amide –NH and –CH	3.112 Å

Dalton Trans., 2015, **44**, 15220–15231	SiF_6^{2-}	10, amide –NH and –CH	3.052 Å

Table A3.4 Comparison of solid state study of the present work with other literatures covering SO_4^{2-} and HSO_4^-.

Reference	Guest Anion	No. and types of Hydrogen bond donors	Average *d*(D···A)/ Å
Present work	One SO_4^{2-} and two HSO_4^-	23; Benzimidazole–NH, Amide –NH and –CH	3.0019
Cryst. Growth Des., 2014, **14**, 2962−2971	One SO_4^{2-} and two HSO_4^-	19; Ammonium –NH and –CH	3.077
Inorg. Chem., 2007, **46**, 5817−5819	One SO_4^{2-}	2; Urea –NH	3.1483
Cryst. Growth Des., 2012, **12**, 4012−4021	One HSO_4^-	4; Benzimidazole–NH, Aliphatic –NH	2.7785
Dalton Trans., 2015, **44**, 2138-2149	One SO_4^{2-}	12; Urea –NH	3.0308

Table A3.5: Comparison of Solution phase study of the present work with other literatures with similar functionalities as in $\mathbf{L_1}$.

Reference	System	λ_{max}	Guest
Present work	Acetonitrile	453nm	F^-
Talanta, 2010, **81**, 967-971.	DMSO	672 nm	F^-
Tetrahedron Letters, 2011, **52**, 6919–6922	CH_3CN:DMSO:HEPES (93:1:6, v/v/v)	520 nm	CN^-
Tetrahedron, 2009, **65**, 3480-3485	1:1 DMSO–H_2O	441 nm	CN^-
Spectrochimica Acta Part A: Molecular and Biomolecular Spectroscopy, 2014, **121**, 662–669	Acetone	425 nm	F^-
Tetrahedron Letters, 2005, **46**, 7255-7258.	Acetonitrile	427 nm	F^-

Chapter 4

A case study of ratiometric fluorescent sensing of fluoride ions and solid state recognition of sulfate ions by a benzimidazole based non-symmetrical tripodal receptor

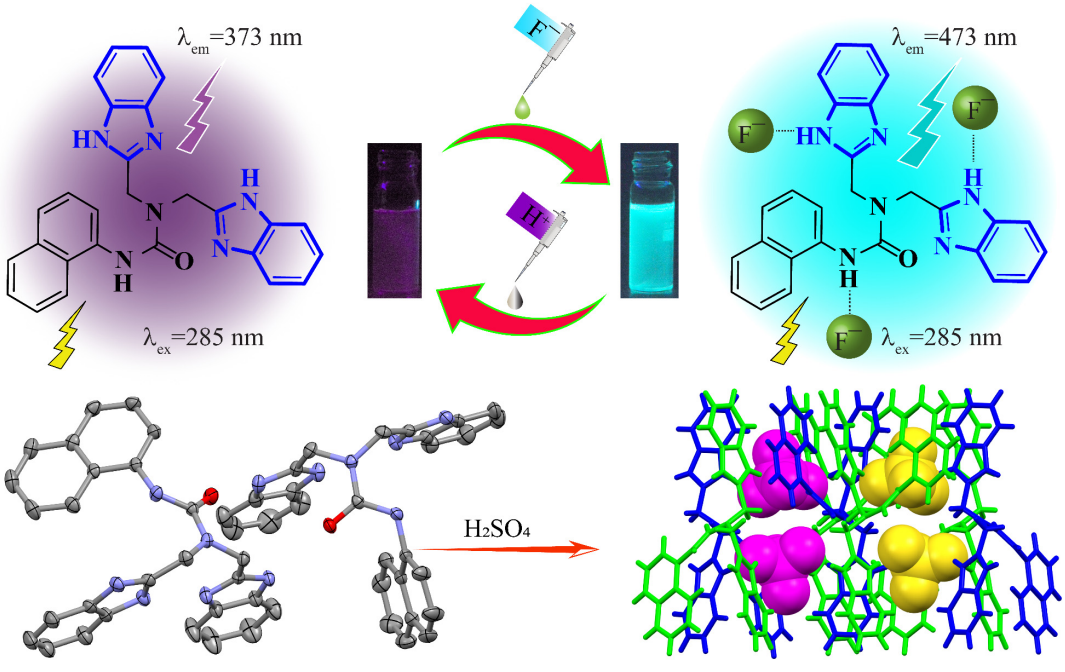

Chapter 4

4.1 Background and focus of the chapter

As selective anion recognition has emerged to be a vanguard research topic in the recent past owing to the vital role it plays in chemical, biological, and ecological processes, [4.1-4.4] the contest for designing apposite abiotic receptors with enriched anion recognition properties has reached its peak although the process is always stimulating primarily because of the charge to radius ratio of the target anion, in addition to its geometry and protonation state.[4.5-4.6] Recognition of fluoride anion seeks vast importance among the spherical halides, as it possesses the highest hydration energy among the mono negative species (ΔG_h = -465 kJ mol^{-1} and $\Delta H°$= 100-110 kcal mol^{-1}).[4.7] With high solvation enthalpy, the fluoride anion boasts of possessing the highest electronegativity, the maximum charge density as a chemical entity and a relatively smaller ionic radius (1.47 Å). As mentioned earlier in Chapter 3, excessive fluoride ions in drinking water may lead to skeletal and dental fluorosis. The presence of fluoride at toxic levels leads to osteosarcoma in the human body[4.8] while treatment of osteoporosis can be achieved by fluoride itself.[4.9] In recent years, designing of highly sensitive and selective receptors for the detection and monitoring of fluoride ions has grasped a colossal interest.[4.10-4.13] The colorimetric changes or emission quenching are the major events observed for most of the fluoride sensors while receptors with emission intensity enhancement are significantly few in number.[4.14-4.16] One major aspect of fluorescence sensing is to synthesize small molecules capable of quantitative determination of a specific analyte with an evident selectivity. Analysis by a probe with fluorescence measurement at a single wavelength may be impeded by a variety of analyte-independent features starting with instrumental parameters, the surrounding microenvironment of the probe, and the native concentration of the probe molecule as well as photobleaching. In contrary to this, ratiometric fluorescent sensors come handy by allowing emission intensity measurement at two different wavelengths, which ensures integrated rectification for environmental effects as well as an upturn in the dynamic range of emission.[4.17-4.21] This, in turn, makes it an interesting research area to develop ratiometric fluorescent sensors for fluoride anions. As Chapter 3 discusses, the characteristics of tetrahedral oxyanion sulfate being prominently present in the nuclear wastes can interfere in their treatment processes. This anion is also accountable for the permanent hardness of water in addition to the ice nucleation phenomenon in the upper atmosphere. In nature, the selective binding, as well as transport of sulfate ion, is accomplished by sulfate binding proteins (SBPs) found in *Salmonella*

typhimurium, a gram-negative bacterium while many other criteria govern the selective binding of sulfate to synthetic receptors.[4.22]

Our constant effort to synthesize non-symmetric tripodals having different podants have also been carried out with the prospect of anion binding in both solid and solution phase. Introduction of both benzimidazole and amide –NH in a single tripodal receptor for anion binding was a fairly newer idea keeping in mind the probability of anion selectivity in both the phases. In our earlier work in Chapter 3, we have demonstrated a non-symmetrical tripodal **L_1** fabricated with two symmetric arms containing benzimidazole moiety along with an amide linked π acidic nitrophenyl moiety. In this work, we have modified the third amide linked arm with a naphthyl residue in order to improve the photophysical properties.

This chapter reports the synthesis of novel non-symmetric tripodal receptor **L_2** which is shown as fluorescent chemosensors for the fluoride ion. The receptor **L_2** is designed with benzimidazole and amide –NH functionalities to get assistance in fluorescence signals during anion sensing. The recognition behaviour of the probe **L_2** towards fluoride ion using emission spectroscopy is accompanied by ratiometric change as well as a visual change in colour from violet to cyan under UV light. In addition, INHIBIT type logic gate at the molecular level is fabricated using the reversibility and reusability of the probe towards F^- and H^+ ions. In the protonated form, the asymmetric unit encompasses two molecules of the non-symmetrical receptor which bind two molecules of sulfate anion where the benzimidazole –NHs are found to be the potent source of hydrogen bond donors.

4.2 Structural aspects of the receptor L_2

Considering the advantages of non-symmetric tripodals, **L_2** was synthesized to enrich the photophysical property of our previously reported receptor **L_1** and solid state structural variation was also analyzed with various anions of the same. Our former ligand **L_1** contained a nitrophenyl moiety along with the two benzimidazole containing symmetric arms while the newly synthesized receptor **L_2** possessed amide linked naphthyl group as the non-symmetric arm which was supposed to augment the anion binding in solution phase as well as solid state. Thus, apart from executing electronic assistance, the two similar benzimidazole arms were expected to provide binding propensity towards the anions with its acidic –NH protons along with its apparent protonation sites. The third non-symmetric amide linked arm was assumed to upsurge the anion binding aptitude while the naphthyl part was decorated with an idea of improving fluorogenic responses of **L_2** which the receptor **L_1** missed in the earlier case.

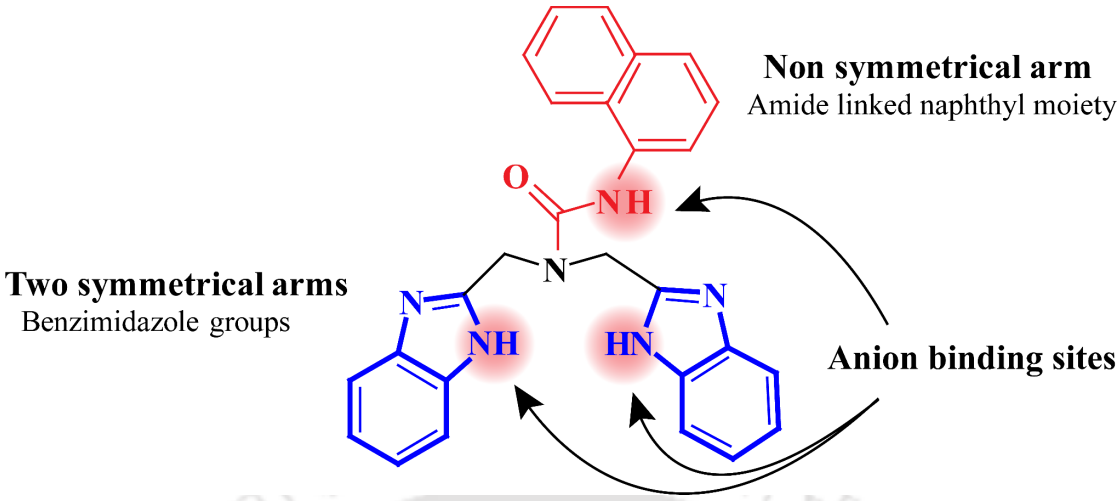

Scheme 4.1 Molecular Structure of the Receptors L_2.

4.3 Solution phase anion binding studies of the receptor L_2

4.3.1 UV-Vis study

The probe L_2 solution (10 μM) was taken in quartz optical cell having an optical path length of 1 cm and the anion binding properties of the probe were studied by UV/Vis spectroscopy in acetonitrile solution. The UV-Visible spectrum of the probe exhibited two absorption maxima at 276 nm and 282 nm characteristic to $\pi-\pi^*$ transitions in the system. Upon addition of 10 equivalents of various anions such as $CH_3CO_2^-$ (OAc^-), Cl^-, Br^-, I^-, NO_3^-, HCO_3^-, HSO_4^-, SO_4^{2-}, ClO_4^-, PPi, $H_2PO_4^-$, PO_4^{3-}, SCN^-; no characteristic change was observed in the original spectrum of the probe. Upon addition of highly basic TBAF, absorbance at 282 nm rendered a diminutive change (Figure A4.1). During the addition of this highly basic anion, the corresponding visual colour change occurs with the pink coloured ligand solution turns colourless. Having a preview of the colorimetric behaviour of the tripodal probe L_2 with different anions, we emphasized our impetus to explore the fluorescence sensing ability of the receptor comprehensively.

4.3.2 Fluorescence studies

The tripodal probe L_2 exhibits a distinct emission maximum at 373 nm in acetonitrile solution upon excitation at 285 nm. Likewise the UV-Visible spectral study, the receptor interacts only with the fluoride anion in the excited state and upon addition of 10 equivalents of TBAF, a new red shifted emission maxima was observed at 473 nm with a remarkable stokes shift of 100 nm (Figure 4.1a). The resulting solution thus emits intense cyan fluorescence which is easily detectable under the 365 nm UV lamp. However, this selectivity was solvent dependent and the sensitivity was negligible in the presence of water or other protic solvents (Figure A4.2).

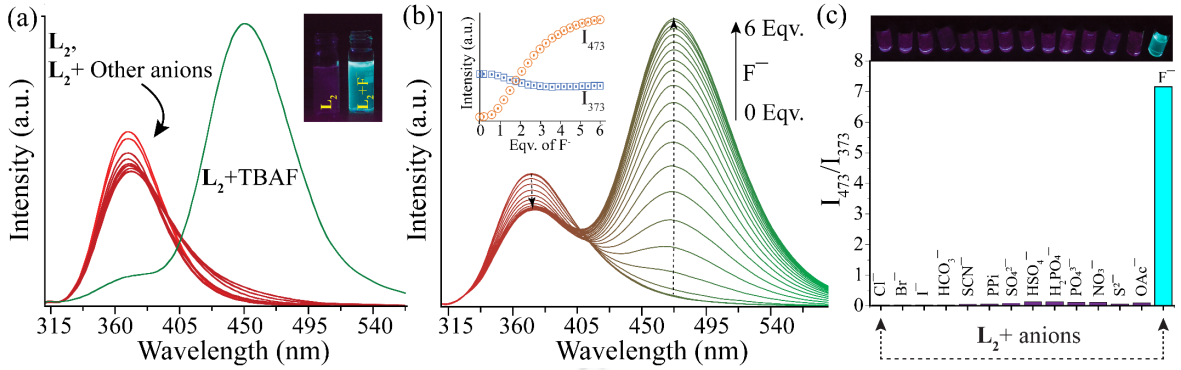

Figure 4.1 (a) Changes in emission spectra of **L2** (10 μM) with the incremental addition of TBAF and other anions (10 equivalents) in acetonitrile. Inset: visible colour change upon the addition of F^- to **L2** under UV lamp (λ_{ex} = 365 nm). (b) Fluorescence titration spectra of **L2** upon incremental addition of 6 equiv. of TBAF in acetonitrile. Inset: changes in the fluorescence intensity at 373 nm and 473 nm with the incremental addition of TBAF. (c) Bar diagram representing the fluorescence intensity ratio I_{473}/I_{373} upon the addition of 10 equivalents of various anions. The inset shows the corresponding visual fluorescence colour under the UV lamp.

To get a quantitative appraisal of the interaction between F^- and the probe **L2**, fluorescence titration experiments were carried out in acetonitrile. The emission intensity at 473 nm increased with the gradual increase in the concentration of fluoride anion. The intensity of the peak at 473 nm kept increasing until it reached saturation value with the addition of 6 equivalents of F^- ion. Interestingly, the intensity maximum at 473 nm surpassed the original intensity at 373 nm. As shown in Figure 4.1b, the incremental addition of TBAF solution created a coinciding scenario where intensity at 473 nm was switched "on" while intensity at 373 nm was switched "off" leading to the construction of a ratiometric probe. The ratio between the intensity maximum at 373 nm and 473 nm were evaluated and are plotted against their respective anions in Figure 4.1c. However, the fluoride induced resulting spectra are similar to the hydroxide added spectra along with their equivalent fluorescence intensity ratio I_{473}/I_{373}, which suggests the deprotonation of the receptor at higher concentration of fluoride (Figure A4.3a and A4.3b). Thus, the ratiometric fluorescence change may occur via an enhancement in the extent of intramolecular charge transfer (ICT). Beneficial aspects of the ratiometric probe are established by its signal rationing and its ability to detect the analyte irrespective of the probe concentration. As the probe **L2** involved deprotonation, we also carried out the fluorescence pH titration experiment in an aqueous medium. The ratiometric change akin to the addition of TBAF in acetonitrile was apparent at higher pH value of the aqueous medium while in acidic medium, the intensity of the peak at 373 nm diminished (Figure A4.3c).

Job's plot derived from the fluorescence titration in acetonitrile suggested the formation of a 1:3 (receptor**:** fluoride) binding stoichiometry which corroborated the three apparent binding sites of the receptor (Figure A4.4a). The binding constant evaluated from the Benesi–Hildebrand equation

was found to be 1.25x10^{17} M^{-3} for fluoride anions (Figure A4.4b). The limit of detection (LOD) of the tripodal receptor towards the fluoride anion was evaluated and found to be as low as 4.63x10^{-8} M (Figure A4.5). This LOD value was comparable to or lower than the previously reported receptors towards fluoride anions which are summarised in Table A4.4.

4.3.3 ^{1}H NMR titration studies with fluoride anion

Based on the fluorescence studies, it was postulated that the selectivity of the probe towards fluoride was the result of the interaction of the anions with acidic benzimidazole and amide –NHs and subsequent deprotonation of the probe **L$_2$** by excess fluoride concentration. To confirm the aforementioned postulate and study the mechanistic features of the interaction between the probe **L$_2$** and fluoride ions, ^{1}H NMR titration experiments were conducted in DMSO-d$_6$ at 10 mM concentration of the probe solution with TBAF.

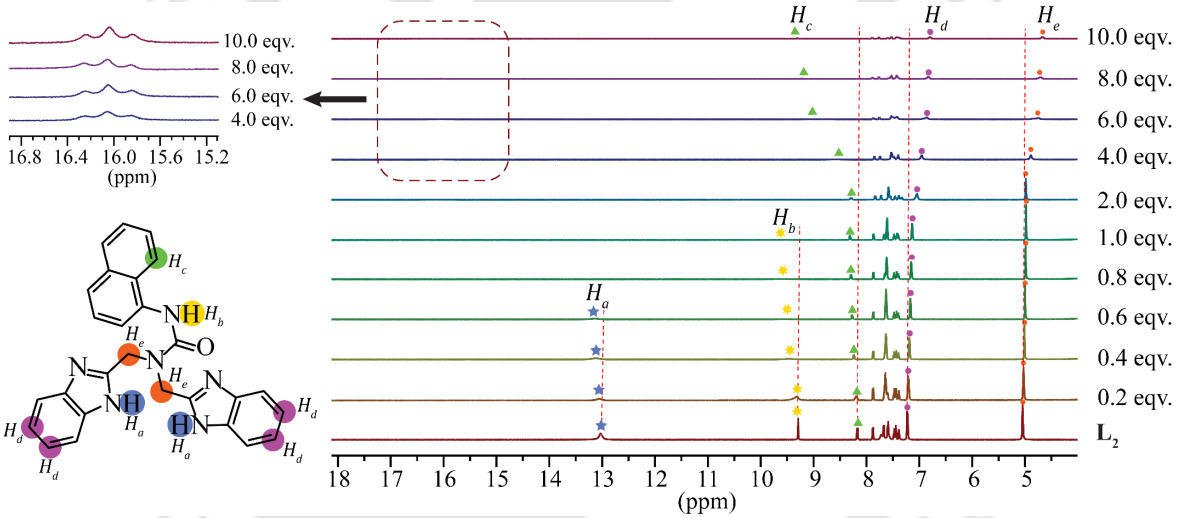

Figure 4.2 Stack plot of the ^{1}H NMR spectra of receptor **L$_2$** in the presence of increasing amounts of TBAF (0.2–10 equiv.) recorded in DMSO-d$_6$.

Initially, as shown in Figure 4.2, upon addition of fluoride anions at low concentration (up to 0.8 eqv.), the benzimidazole –NHs, *Ha* (13.02 ppm), and amide –NH, *Hb* (9.28 ppm) proton signals showed considerable broadening with significant downfield shifts (Δδ=0.32 ppm and Δδ=0.35 ppm) indicating the initial interaction of fluoride ions to the acidic benzimidazole and amide −NH protons. The benzimidazole –NH signal vanished first on addition of 0.8 equivalent of TBAF, followed by the disappearance of amide –NH with 2.0 equivalent of TBAF (Figure A4.6). As complexation of **L$_2$**–H···F$^-$ occurred, it gradually increased the electron density of the complex. This, in turn, triggered the minute upfield shift of the other aromatic –CH proton signals of *Hd* and the methylene –CH proton signals of *He* via through-bond effects with the increasing amount of fluoride anion till 2.0 equivalent. Beyond the addition of 2.0 equivalents of

TBAF, deprotonation of the probe **L_2** may have started which is reflected in the more pronounced upfield shift of the two proton signals viz. H_d and H_e as depicted in the stacked figure. Meanwhile, the deprotonation of the probe **L_2** upon addition of excess TBAF can be further supported by the occurrence of a triplet proton signal at 16.02 ppm conforming the formation of HF_2^- species which is the most stable hydrogen bonded complex formed by the fluoride ion.[4.23-4.25] Interestingly, the doublet of naphthyl –CH, H_c at 8.17 ppm shows a gradual downfield shift, which escalated in the presence of excess TBAF. Again, the changes were more pronounced after the addition of 2.0 equivalents of fluoride anion. This, thereby, suggests the interaction of the probe **L_2** with fluoride anion after the commencement of its deprotonation. This, in turn, suggests the prominent interaction of the probe with fluoride anion in solution phase. Based on the outcomes from ^{1}H NMR study, the sensing mechanism for fluoride ion can be established with the following observations: (i) initially at lower fluoride concentration, the benzimidazole and amide –NHs form hydrogen bonded complex with the fluoride anions, and then (ii) when excess fluoride is introduced into the receptor-fluoride complex, due to its a high affinity towards hydrogen, fluoride can easily bring about the cleavage of acidic N–H bond, which thereby increases the electron density on both benzimidazole and naphthyl moiety.

4.3.4 Reversible binding and interpretation of related logic gate

With the purpose to scrutinize the reversibility and reusability of the probe towards the fluoride anion, fluorescence studies of the probe **L_2**-F^- with an incremental amount of TFA (Trifluoroacetic acid) were carried out (Figure A4.7a). On addition of TFA, an obvious decrease in intensity at 473 nm along with a simultaneous increase in original intensity at 373 nm are observed. The fluorescence spectra of the probe **L_2**-F^- complex could revert to their free sensor state upon the addition of seven equivalents of TFA. Upon addition of TFA, the probe finally recovered its original optical properties. Recently, Optical switches have grasped a keen interest for its capability in information processing and manipulation of Boolean type logic gates at the molecular level.[4.26-4.27] The probe **L_2** exhibited reversibility and recyclability towards F^- and H^+ ions (Figure 4.3a and Figure A4.7b) which encouraged us to frame logic gate based on its distinctive behaviour. Based on the ratiometric fluorescence responses of the probe, a molecular "INHIBIT" type logic gate was constructed. Addition of F^- and H^+ was considered to be the chemical inputs and denoted as Input 1 (Inp1) and Input 2 (Inp2) respectively. Consequently, as shown in Figure 4.3b, I_{473}/I_{373}, the ratiometric response between intensity maximum at 373 nm and 473 nm was taken as the output. As F^- anion induced "ON" signal in the output, while H^+ regulated the "OFF" signal in the optical output, the ratio I_{473}/I_{373} with values greater than 4 were

considered to be '1' and that with the values less than 4 was considered to be '0'. Again when either of the inputs, F^- and H^+ were missing, '0' was assigned and in their presence, the inputs were denoted as '1' (Figure 4.3c). Accordingly, an "INHIBIT" (an amalgamated AND and NOT logic gates) logic gate can be fabricated considering a threshold value of 4 for the ratio I_{473}/I_{373} (Figure 4.3d).

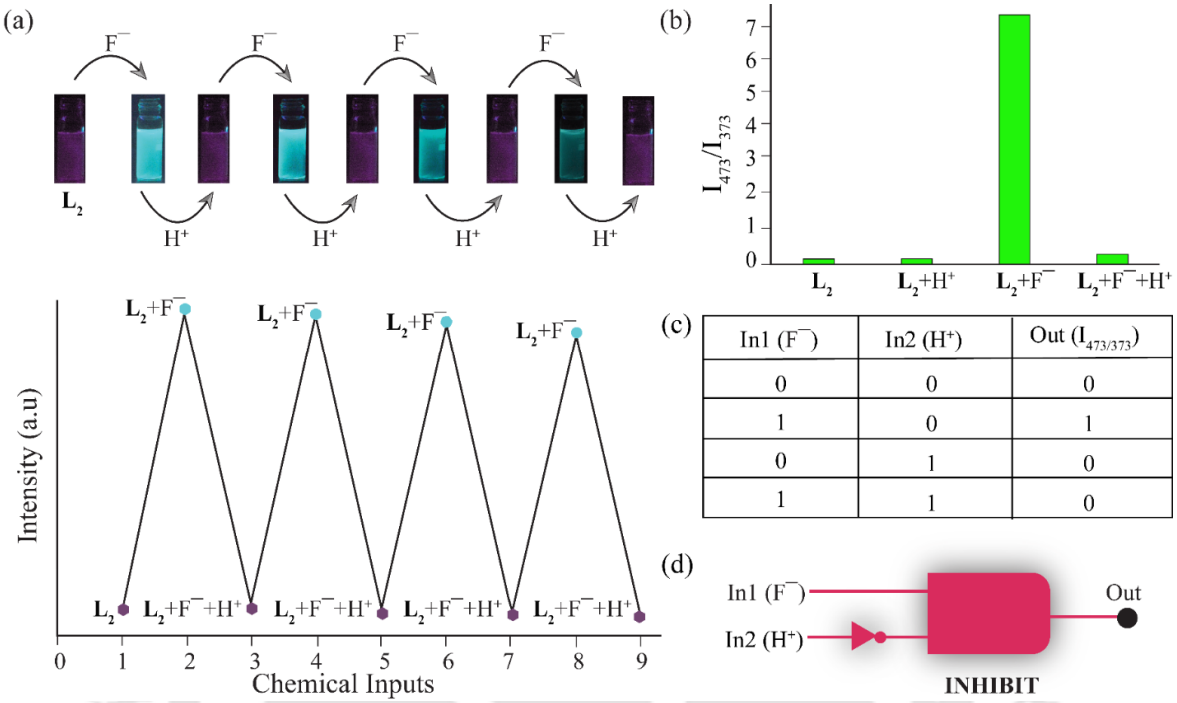

In1 (F^-)	In2 (H^+)	Out ($I_{473/373}$)
0	0	0
1	0	1
0	1	0
1	1	0

Figure 4.3 (a) Reversible and recyclable behaviour of probe **L2** on addition of TBAF and TFA. Inset: The corresponding colour changes during alternate cycles. (b) The I_{473}/I_{373} values for the alternate cycles. (c) The truth table for the reversible behaviour. (d)The fabricated 'INHIBIT' logic gate based on the probe behaviour towards F^- and H^+.

4.4 Solid state studies of L2 and its corresponding anion binding studies

4.4.1 Structural elucidation of the Ligand L2

The non-symmetric tripodal **L2** crystallizes in the P-1 space group in the triclinic system. Two units of ligands are present in the asymmetric unit where each unit adopts a distorted '**T**' like structure and is arranged in alternate 'up-down' fashion mainly due to three types of hydrogen bonding (Figure 4.4a). In response to the stabilization imposed by the surrounding species, each receptor differs in symmetry equivalence (c′ = 2) making them two distinct conformational isomorphs viz. C1 (blue coloured) and C2 (green coloured). Generally, conformational isomorphism is a result of kinetic and thermodynamic crystal stability factors, which are mostly considered to be the consequences imposed by erratic crystallization, first demonstrated by Desiraju *et al.*[4.28] The C1 isomorphs exhibits intramolecular hydrogen bonding between the two benzimidazole arms while it links to

another similar unit through hydrogen bonding between benzimidazole nitrogen and amide –NH. In case of C2 units, intramolecular −NH···N bondings between the two benzimidazole arms have forced them to reside in a single plane, while the third arm which is adorned with an amide –NH protrude itself out of the plane. The remaining −NH fragment from the second benzimidazole arm along with one methylene−CH of the same ligand tugs the carbonyl oxygen of the second similar unit of the isomorph and trusses up the two units together (Figure 4.4b). The interactions between C1 and C2 units are composed of the hydrogen bonding between the carbonyl oxygen of amide group and the benzimidazole −NH along with the two fascinating –CH···π interactions associated with the benzimidazole and naphthyl – CHs of two different C1 units with the naphthyl ring of C2 unit. These interactions, in turn, play a crucial role in the development of three dimensional structure (Figure 4.4c). Among these hydrogen bonding interactions, the intramolecular −NH···N bonding interaction between the benzimidazole arms in a single unit is the strongest.

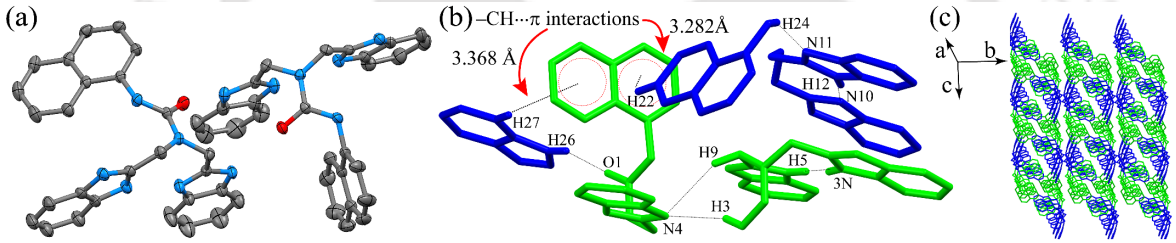

Figure 4.4 (a) Ortep diagram of the asymmetric unit of **L₂**. (b) Various hydrogen bonding interactions between the different isomorphs in the ligand crystal. (c) Packing diagram of **L₂** units along crystallographic *b* axis.

4.4.2 Study of binding of polyatomic anions with $L_2H_2^+$:

All the attempts to study the interactions of the probe $\mathbf{L_2}$-F^- in solid state with the neutral receptor were unsuccessful due to its deprotonation. Along with the acidic –NH protons, the receptor **L₂** contains apparent protonation sites at the benzimidazole nitrogen atoms. Therefore, attempts were made with the protonated probe to bind anions in solid state also. Among all the anions, only protonated salt of H_2SO_4 was obtained.

4.4.2.1 Structural study of the sulfate complex $[2(L_2H_2)^{2+}\cdot 2SO_4^{2-}]$:

The blue coloured crystal appropriate for single crystal XRD analysis was obtained by the reaction of receptor **L₂** and H_2SO_4 in DMSO. Structural elucidation by single crystal XRD discloses the complex to be crystallized in a triclinic system involving space group P-1 with Z=4. The asymmetric unit comprises of two units of protonated receptors and two units of SO_4^{2-} anions. A

total of seven numbers of protonated receptors are involved in forming the pseudocapsular cavity wherein two pairs of sulfate anions are encapsulated (Figure 4.5b). The protonated receptors also exhibit conformational isomorphism like as in the ligand crystal. The two isomorphs links to one another through intermolecular hydrogen bond interactions between the receptor units and the conjugated anions. C1 isomorph (blue coloured) attaches itself directly to the C2 isomorph (green coloured) using one –CH···π interaction between the methylene bridge and the naphthyl group. Apart from this, C1 isomorph offers two hydrogen bonding interactions while C2 donates four hydrogen bonds to the two S2 centred sulfates which bridges both the conformational isomorphs. Interestingly, in the vicinity of the S1 centred sulfates, all these bonding patterns altered between C1 and C2. Solitary hydrogen bonding interaction exists between C1 and C2 as the amide –C=O of one unit attaches itself to the methylene –CH of the benzimidazole arm. In case of both the isomorphs, one connects to another similar unit using one –CH···π interaction between the naphthyl and benzimidazole moiety (Figure A4.8) while the hydrogen bond between amide –C=O and naphthyl –CH plays the pivotal role in decorating the three dimensional structure (Figure 4.5c).

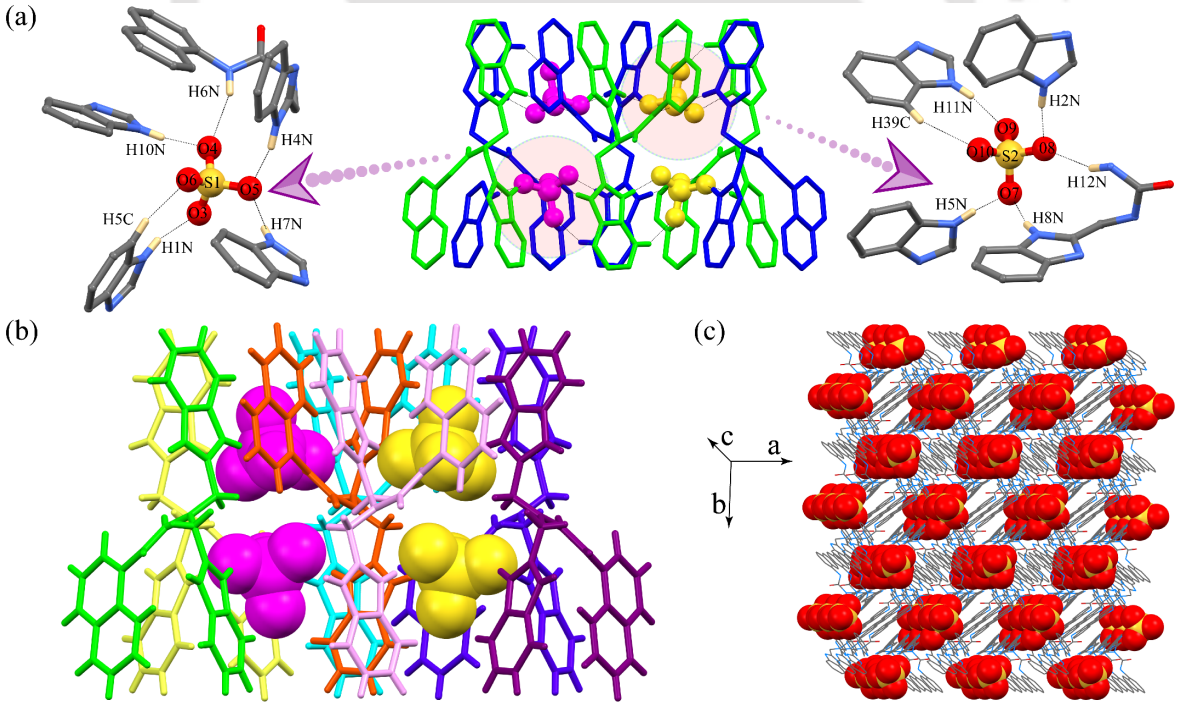

Figure 4.5 X-ray structures depicting (a) Hydrogen bonding coordination environment of two sulfate anions surrounded by the protonated receptors $\mathbf{L_2H_2^{2+}}$. (b) Space-fill representation of sulfate anions in the pseudo encapsulated cavity of the protonated receptor. (c) The packing motifs of the sulfate complex as viewed down along the crystallographic *c* axis.

As evident from Figure 4.5a, the two sulfates experience different binding environment surrounded by three units of C1 isomorph and four units of C2 isomorph. Considering the binding

environment of S1 centred sulfate in the crystal structure, it is apparent that it is coordinated by six valid hydrogen bonding interactions. The significant interactions are from five benzimidazole and amide linked −NH···O (average N−O = 2.750 Å) and one −CH···O interactions (C−O = 3.264 Å). O3 of the bound sulfate is coordinated to one benzimidazole arm with its single −NH···O interaction. The O4 binding interactions are composed of one unit of benzimidazole −NH and one unit of amide –NH. The bifurcated O5 incorporates hydrogen bonding from two benzimidazole –NHs while the solely monofurcated O6 is hydrogen bonded to one aromatic –CH of benzimidazole group. Among these hydrogen bonding interactions, the stronger hydrogen bonds are donated by the benzimidazole –NH interactions (N10H···O4=1.82Å, ∠N−H···O=171.0°; N7H···O5=1.83 Å, ∠N−H···O=163.0°; N4H···O5=1.83Å, ∠N−H···O=163.0°; N1H···O3=1.87Å, ∠N−H···O=163.0°; shadowing the amide –NH interaction N6H···O4=2.22 Å, ∠N−H···O= 158.0°. The surrounding environment of S2 also depicts a total of six valid binding interactions primarily from five −NH···O (average N−O = 2.748 Å) and one −CH···O interactions (C−O = 3.274 Å). O7 of the bound Sulfate is bifurcated with two benzimidazole –NHs. The bifurcated nature of O8 is contributed by the hydrogen bonds donated by one benzimidazole –NH and one amide –NH. O9 is connected to the protonated receptor solely through one benzimidazole –NH. O10 atom of the bound S2 is offered one single hydrogen bond from the one −CH from benzimidazole group of the protonated receptor. Similarly, as in the case of S1 environment, benzimidazole –NHs prevail to be the stronger hydrogen bond donor towards bound S2 centred oxygen atoms. Four benzimidazole –NHs interactions *viz.* N5H···O7=1.85 Å, ∠N−H···O=163.0°; N8H···O7=1.81 Å, ∠N−H···O=165.0°; N2H···O8=1.82 Å, ∠N−H···O=168.0°; N11H···O9=1.86 Å, ∠N−H···O=164.0° show greater hydrogen bonding aptitude towards the encapsulated anion than the potential amide –NH interaction (N12H···O8=2.24 Å, ∠N−H···O=157.0 Å). All the oxygen atoms of the S1 and S2 centred sulfates are consistent with the electronic structure calculations by Hay *et al.* suggesting the involvement of maximum of three hydrogen bonds for each oxygen atom of an oxo anion.[4.29]

4.5 Visual detection of fluoride ion in solid state

In solid state, visual detection of F^- under UV light was also accomplished following the methods published in the literature.[4.30-4.31] As shown in Figure 4.6a, a quantifiable 100 mM solution of the receptor **L_2** was adsorbed on a thin layer chromatography (TLC) plate and revealed a violet emission under UV light. On adding a fluoride ion spot (10 mM), it was adsorbed on the plate changing the colour to cyan in the centre. Thus, the receptor adsorbed TLC plate serves a prospective sensor to detect F^- ions. To check the feasibility of using the sensor coated Whatman

filter paper strips, these strips were dipped into the sensor solution in DMSO (50 mM) and then dried under vacuum.[4.32-4.34] Introduction of the coated strips into a 0.1 mM F^- solution induced a swift change in its fluorescence colour to cyan under the 365 nm UV light (Figure 4.6b). Thus, it also paves a way towards the development of quick and cheap sensors for fluoride ion in solid state. These studies strengthen the possible candidature of the probe **L_2** towards faster and convenient detection of fluoride ions.

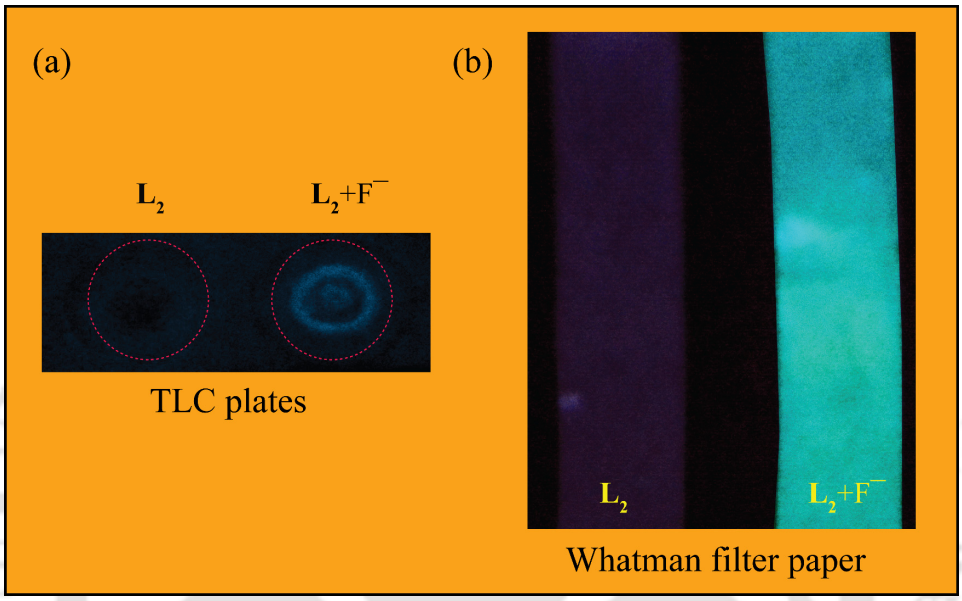

Figure 4.6 (a) Fluorescence image (under 365 nm UV light) of the chemosensor **L_2** adsorbed on a TLC plate and the spot of TBAF solution on it. (b) Fluorescence changes (under 365 nm UV light) of test strips in presence of TBAF solution.

4.6 Conclusion

In brief, we efficaciously designed and synthesized a novel non-symmetric tripodal receptor **L_2** which acts as a selective fluoride ion sensor in solution phase. The recognition behaviour of the probe towards fluoride ion using emission spectroscopy in acetonitrile was accompanied by a visual change in colour from violet to cyan blue. Selectivity towards fluoride anion was achieved through the selective formation of hydrogen bonded host-guest complex with consequent deprotonation of the probe. We have successfully achieved better photophysical properties in **L_2** than **L_1** by introducing the naphthyl group. Thus, it enables us to obtain a quantitative detection of fluoride ions as a ratiometric sensor with evaluation of stoichiometry, binding constant and lowest limit of detection. The ^{1}H NMR experiments with F^- ion indicated that deprotonation of the probe was facilitated by the inherent acidity of benzimidazole and amide −NH, the basic nature of fluoride ion and the polarity of acetonitrile solvent. The reversibility and reusability of probe towards F^- and H^+ led to fabricate INHIBIT type molecular logic gate. Fluoride ion detection in

solid state was also accomplished via TLC plate and solution coated paper strips. With the deprotonation of the probe playing a pivotal role in solution phase detection of fluoride ions, protonation of the probe led to detection of sulphate anions in solid state study. In solid state study, the asymmetric unit incorporates one pair of non-symmetrical protonated receptor which exist as conformational isomorphs tending to bind two units of sulfate anions. Two different binding environments were present in case of the two bound sulfates where the strongest hydrogen bonds are offered by the benzimidazole –NH moiety. Thus, we can conclude that non-symmetric receptors like **L_1** and **L_2** in its protonated form tend to encapsulate tetrahedral sulphate molecules inside the pseudo-cavity.

References

4.1 P. A. Gale, Anion receptor chemistry: highlights from 2008 and 2009, *Chem. Soc. Rev.*, 2010, **39**, 3746−3771.

4.2 M. Wenzel, J. R. Hiscock, and P. A. Gale, Anion receptor chemistry: highlights from 2010, *Chem. Soc. Rev.*, 2012, **41**, 480−520.

4.3 P. A. Gale, E. N. W. Howe, and X. Wu, Anion Receptor Chemistry, *Chem*., 2016, **1**, 351–422.

4.4 P. A. Gale, E. N. W. Howe, X. Wu, and M. J. Spooner, Anion receptor chemistry: Highlights from 2016, *Coordin. Chem. Rev.*, 2018, **375**, 333–372.

4.5 K. Bowman-James, A. Bianchi, and E. Garcia-España, Anion Coordination Chemistry; Eds.; Wiley-VCH: New York, 2011; Chapters 1−2.

4.6 P. D. Beer and P. A. Gale, Anion Recognition and Sensing: The State of the Art and Future Perspectives, *Angew. Chem. Int. Ed.*, 2001, **40**, 486−516.

4.7 Y. Marcus, Thermodynamics of solvation of ions. Part 5.—Gibbs free energy of hydration at 298.15 K, *J. Chem. Soc., Faraday Trans.*, 1991, **87**, 2995−2999.

4.8 S. Ayoob and A. K. Gupta, Fluoride in Drinking Water: A Review on the Status and Stress Effects, *Crit. Rev. Environ. Sci. Technol.,* 2006, **36**, 433−487.

4.9 K. L. Kirk, *Biochemistry of the Elemental Halogens and Inorganic Halides*; Plenum Press: New York, 1991, pp 221–238.

4.10 M. Cametti and K. Rissanen, Highlights on contemporary recognition and sensing of fluoride anion in solution and in the solid state, *Chem. Soc. Rev.*, 2013, **42**, 2016–2038.

4.11 Y. Zhou, J. F. Zhang, and J. Yoon, Fluorescence and Colorimetric Chemosensors for Fluoride-Ion Detection, *Chem. Rev*., 2014, **114**, 5511–5571.

4.12 The curious case of salicylidene-based fluoride sensors: chemosensors or chemodosimeters or none of them, S. K. Dey and C. Janiak, *RSC Adv*., 2020, **10**, 14689-14693.

4.13 A. M. John, J. Jose, R. Thomas, K. J. Thomas and S. P. Balakrishnan, Spectroscopic and TDDFT investigation of highly selective fluoride sensors by substituted acyl hydrazones, *Spectrochim. Acta A Mol. Biomol. Spectrosc.*, 2020, **236**, 118329.

4.14 B. Sui, B. Kim, Y. Zhang, A. Frazer, and K. D. Belfield, Highly Selective Fluorescence Turn-On Sensor for Fluoride Detection, *ACS Appl. Mater. Interfaces*, 2013, **5**, 2920–2923.

4.15 M. Hirai, M. Myahkostupov, F. N. Castellano, and F. P. Gabbaï, 1-Pyrenyl- and 3-Perylenyl-antimony(V) Derivatives for the Fluorescence Turn-On Sensing of Fluoride Ions in Water at Sub-ppm Concentrations, *Organometallics*, 2016, **35**, 1854–1860.

4.16 Y. Jo, N. Chidalla, and D. -G. Cho, Bis-ureidoquinoline as a Selective Fluoride Anion Sensor through Hydrogen-Bond Interactions, *J. Org. Chem.*, 2014, **79**, 9418–9422.

4.17 B. C. Zhu, F. Yuan, R. X. Li, Y. M. Li, Q. Wei, Z. M. Ma, B. Du, and X. L. Zhang, A highly selective colorimetric and ratiometric fluorescent chemodosimeter for imaging fluoride ions in living cells, *Chem. Commun.,* 2011, **47**, 7098–7100.

4.18 Y. Kubo, M. Yamamoto, M. Ikeda, M. Takeuchi, S. Shinkai, S. Yamaguchi, and K. Tamao, A colorimetric and ratiometric fluorescent chemosensor with three emission changes: fluoride ion sensing by a triarylborane- porphyrin conjugate, *Angew. Chem. Int. Ed.*, 2003, **42**, 2036–2040.

4.19 K. Mahapatra, P. Karmakar, J. Roy, S. Manna, K. Maiti, P. Sahoo, and D. Mandal, Colorimetric and ratiometric fluorescent chemosensor for fluoride ions based on phenanthroimidazole (PI): spectroscopic, NMR and density functional studies, *RSC Adv.*, 2015, **5**, 37935–37942.

4.20 S. Biswas, M. Gangopadhyay, S. Barman, J. Sarkar, and N. D. P. Singh, Simple and efficient coumarin-based colorimetric and fluorescent chemosensor for F^- detection: An ON^1–OFF–ON^2 fluorescent assay, *Sens. Actuators B Chem.*, 2016, **222**, 823–832.

4.21 X. Wu, H. Wang, S. Yang, H. Tian, Y. Liu and B. Sun, Highly sensitive ratiometric fluorescent paper sensors for the detection of fluoride ions, *ACS omega*, 2019, **4**, 4918-4926.

4.22 J. W. Pflugrath and F. A. Quiocho, The 2 Å resolution structure of the sulfate-binding protein involved in active transport in Salmonella typhimurium., *J. Mol. Biol.*, 1988, **200**, 163–180.

4.23 B. Descalzo, K. Rurack, H. Weisshoff, R. Martínez-Máñez, M. D. Marcos, P. Amorós, K. Hoffmann, and J. Soto, Rational Design of a Chromo- and Fluorogenic Hybrid Chemosensor Material for the Detection of Long-Chain Carboxylates, *J. Am. Chem. Soc.*, 2005, **127**, 184–200.

4.24 X. Zheng, W. Zhu, D. Liu, H. Ai, Y. Huang and Z. Lu, Highly selective colorimetric/ fluorometric dual-channel fluoride ion probe, and its capability of differentiating cancer cells, *ACS Appl. Mater. Interfaces,* 2014, **6**, 7996–8000.

4.25 Saravanan, S. Easwaramoorthi, C. -Y. Hsiow, K. Wang, M. Hayashi and L. Wang, Benzo-selenadiazole fluorescent probes-near-IR optical and ratiometric fluorescence sensor for fluoride ion, *Org. Lett.*, 2014, **16**, 354–357.

4.26 A. P. De Silva, H. Q. N. Gunaratne, and C. P. McCoy, A molecular photoionic AND gate based on fluorescent signalling, *Nature*, 1993, **364**, 42–44.

4.27 Kumar, M. A. Kaloo, A. R. Sekhar, and J. Sankar, A selective fluoride sensor and a digital processor with "Write–Read–Erase–Read" behaviour, *Dalton Trans*., 2014, **43**, 16164–16168.

4.28 G. R. Desiraju, Crystal Engineering: A Holistic View, *Angew. Chem. Int. Ed.*, 2007, **47**, 8342−8356.

4.29 P. Hay, T. K. Firman, and B. A. Moyer, Structural Design Criteria for Anion Hosts: Strategies for Achieving Anion Shape Recognition through the Complementary Placement of Urea Donor Groups, *J. Am. Chem. Soc.*, 2005, **127**, 1810–1819.

4.30 Y. -C. Wu, J. -P. Huo, L. Cao, S. Ding, L. -Y. Wang, D. -R. Cao, and Z. -Y. Wang, Design and application of tri-benzimidazolyl star-shape molecules as fluorescent chemosensors for the fast-response detection of fluoride ion, *Sens. Actuators B Chem.*, 2016, **237**, 865–875.

4.31 Y. -C. Wu, J. -Y. You, K. Jiang, J. -C. Xie, S. -L. Li, D. Cao, and Z. -Y. Wang, Colorimetric and ratiometric fluorescent sensor for F^- based on benzimidazole-naphthalene conjugate: Reversible and reusable study & design of logic gate function, *Dyes Pigm*, 2017, **140**, 47–55.

4.32 J. -F. Xiong, J. -X. Li, G. -Z. Mo, J. -P. Huo, J. -Y. Liu, X. -Y. Chen, and Z. -Y. Wang, Benzimidazole derivatives: selective fluorescent chemosensors for the picogram detection of picric acid, *J. Org. Chem.*, 2014, **79**, 11619–11630.

4.33 Sui, B. Kim, Y. Zhang, A. Frazer, and K.D. Belfield, Highly selective fluorescence turn-on sensor for fluoride detection, *ACS Appl. Mater. Interfaces*, 2013, **5**, 2920–2923.

4.34 X. Wu, H. Wang, S. Yang, H. Tian, Y. Liu, and B. Sun, Highly Sensitive Ratiometric Fluorescent Paper Sensors for the Detection of Fluoride Ions, *ACS Omega* 2019, **4**, 4918–4926.

Appendix 3

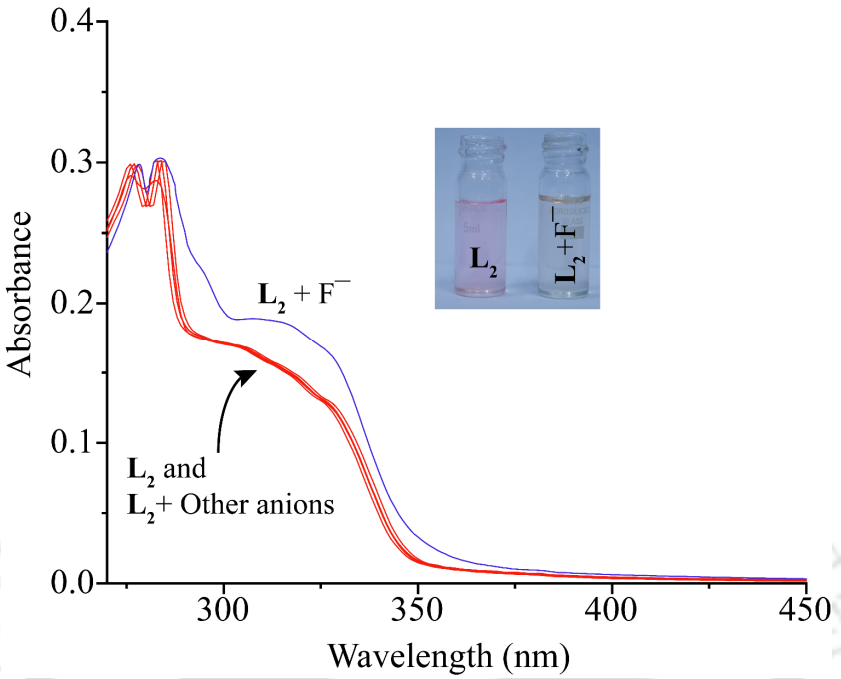

Figure A4.1 Change in absorption spectra of **L₂** (10 mM) with different anions (50 mM) in acetonitrile solution. Inset: Corresponding change in the colour of the probe solution after the addition of F^-.

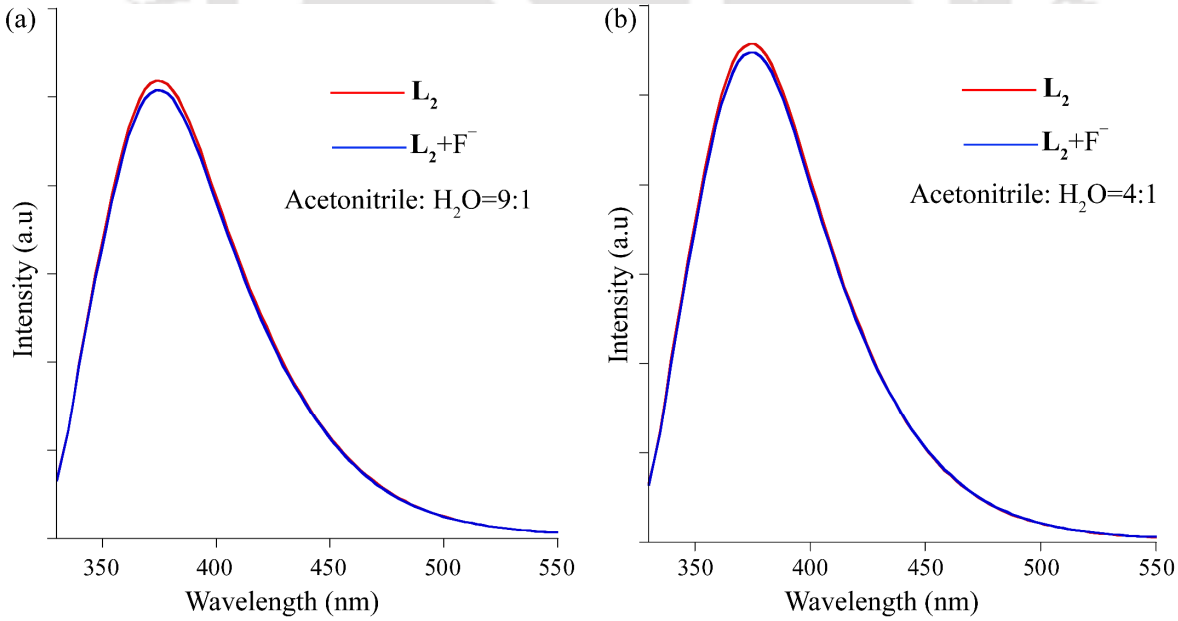

Figure A4.2 (a) Change in emission spectra of **L₂** (10 mM) with fluoride anion (50 mM) in (a) Acetonitrile: H_2O=9:1 (b) Acetonitrile: H_2O=4:1solution.

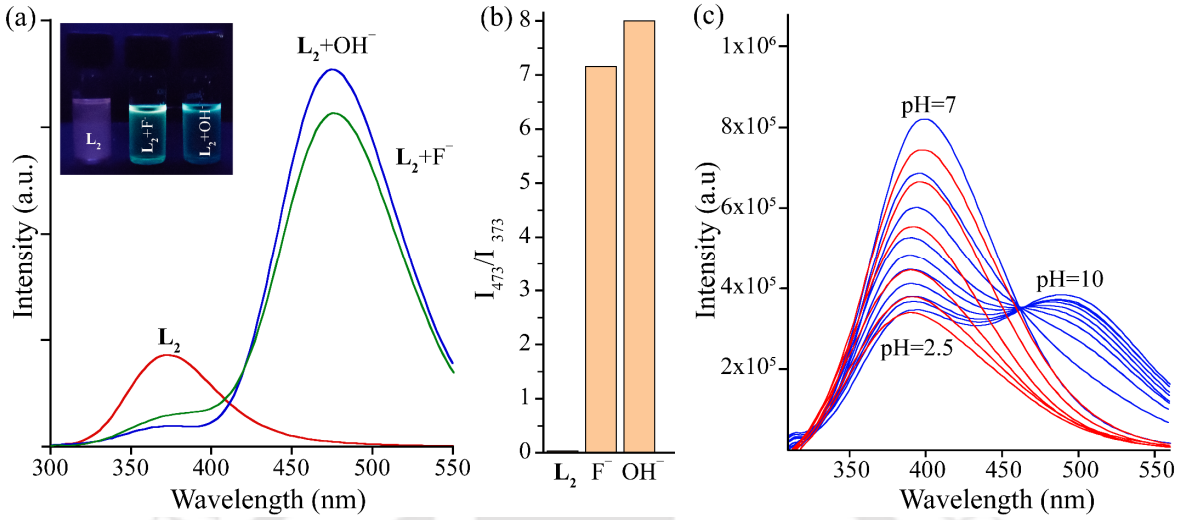

Figure A4.3 (a)The comparative emission spectra of TBOH and TBAF addition to the receptor **L₂** in acetonitrile. Inset: Visible colour change upon addition of the two anions F^- and OH^- under UV lamp (λ_{ex} = 365 nm). (b) Relative fluorescence intensity ratio I_{473}/I_{373} upon the addition of 10 equivalents of F^- and OH^- anions. (c) Change of the fluorescence spectra of **L₂** (5 mM) with decreasing pH from 10 to 2.5 (λ_{ex} = 285 nm) in aqueous medium.

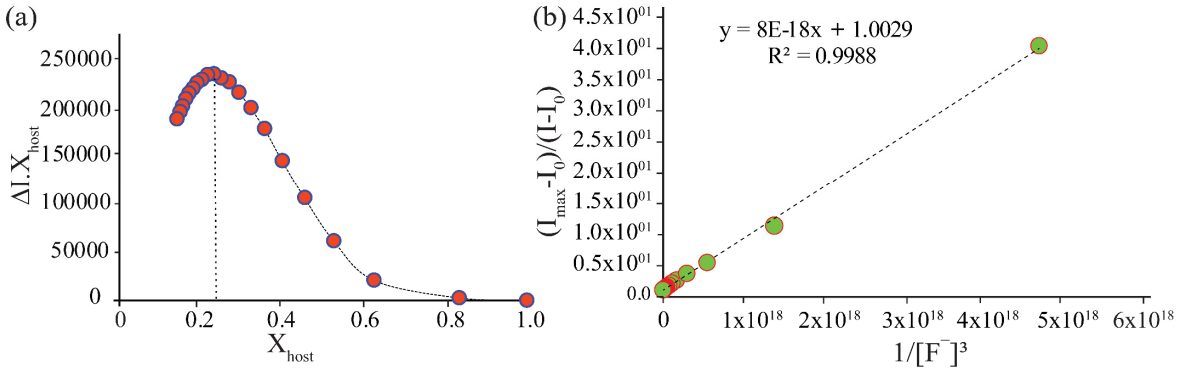

Figure A4.4. (a) Job's plot for determining the stoichiometry of the probe **L₂** and F^- ion and (b) the corresponding Benesi−Hildebrand plot for binding constant determination.

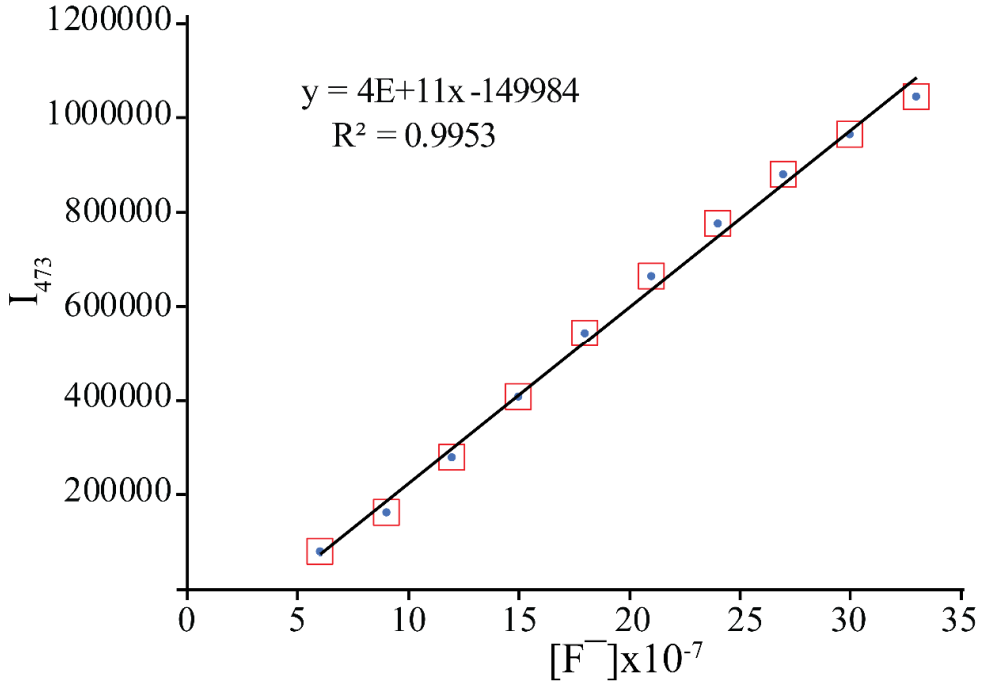

Figure A4.5 Ratio of fluorescence emission intensity change at 473 nm versus concentrations for lowest detection limits (LOD) calculation.

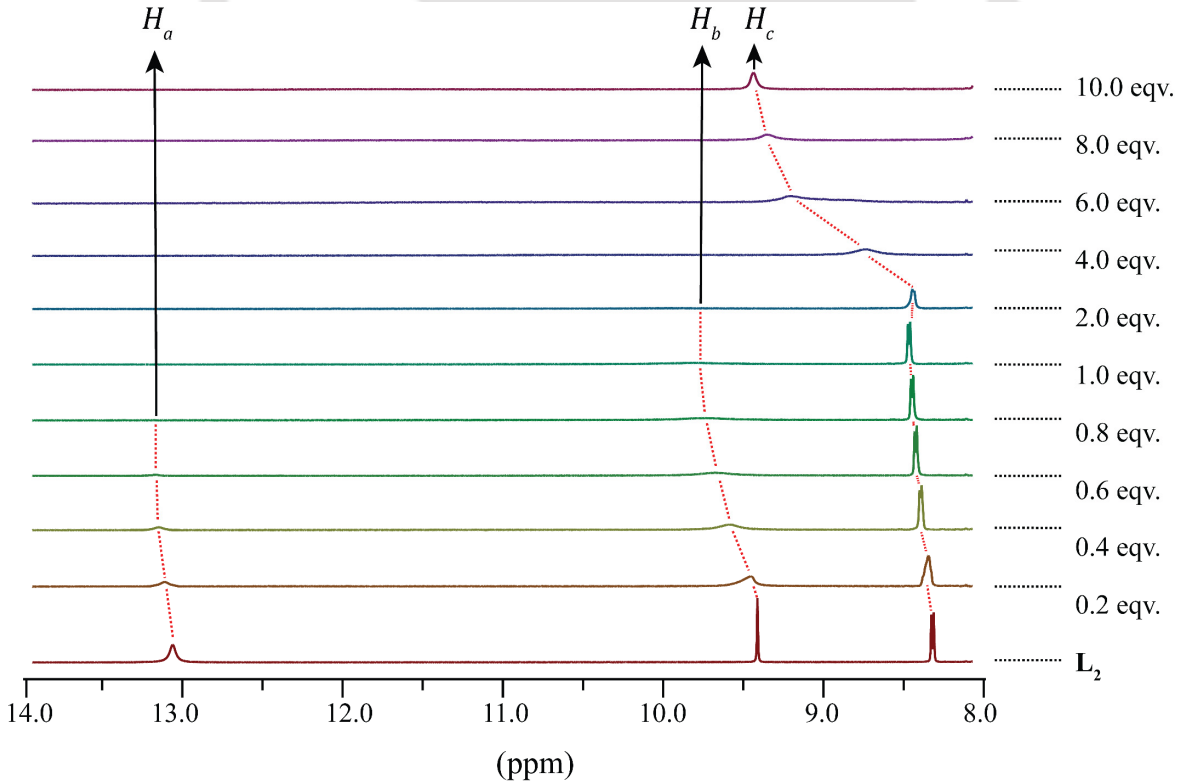

Figure A4.6 Enhanced view (8–14ppm) of stack plot of ^{1}H NMR spectra of receptor **L**$_2$ in the presence of increasing amounts of TBAF (1–10 equiv.) recorded in DMSO-d_6.

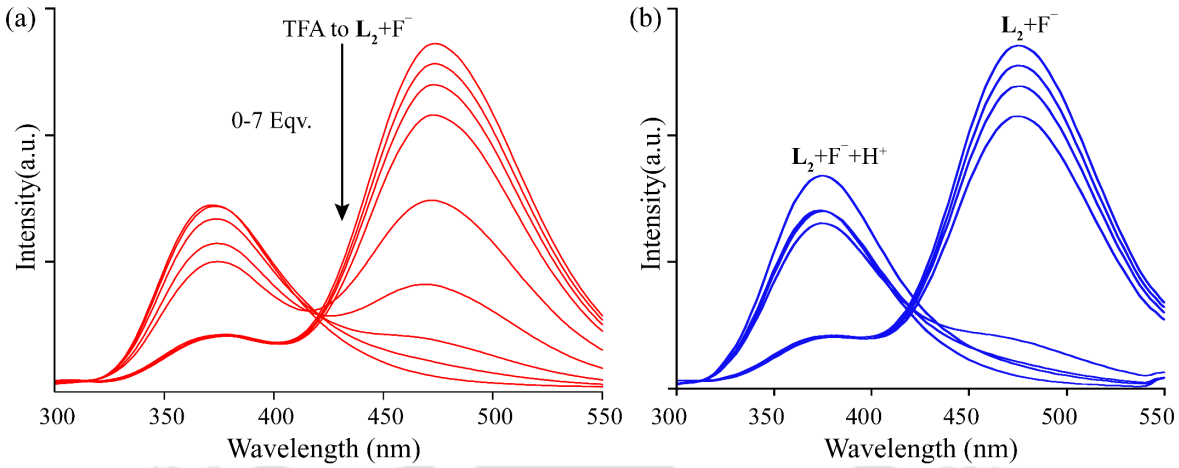

Figure A4.7 (a) Titration of L_2-F⁻ complex with Trifluoroacetic acid. (b) Reversibility test of the probe: Ratiometric shift of 100 nm with the addition of fluoride ions (F⁻) and reversed back to the original upon addition of TFA.

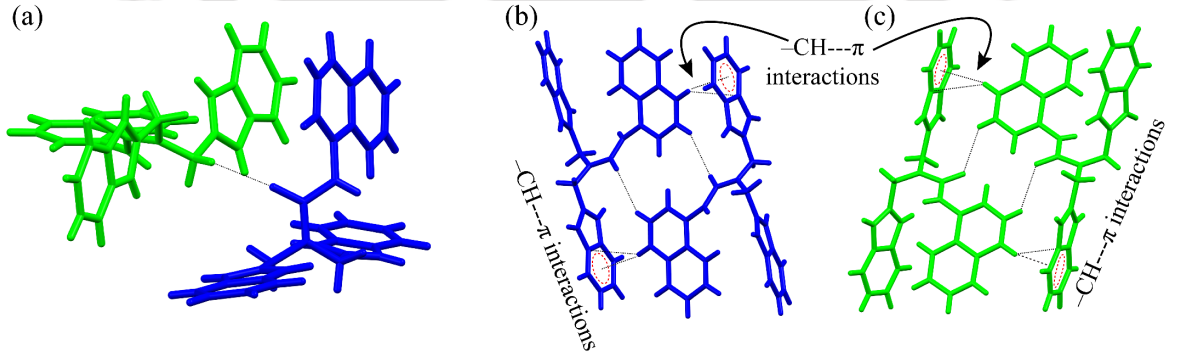

Figure A4.8 (a) The interacting isomorphs represented in different colors (blue = C1, green = C2). The –CH (aliphatic)···π interactions and –CH (aromatic)··· amide C=O interactions extending the (b) C1 chain and (c) C2 chain.

Tabele 4.1 Crystallographic data and refinement details of the receptor $\mathbf{L_2}$ and the sulfate complex.

Parameters	$C_{27}H_{22}N_6O$	$C_{27}H_{24}N_6O_5S$
CCDC No.	1920832	1920833
Fw	446.51	544.58
Crystal system	triclinic	triclinic
Space group	*P -1*	*P -1*
a/Å	11.3681(7)	12.349(4)
b/Å	14.1597(10)	13.224(4)
c/Å	15.0368(9)	16.924(6)
α/°	82.533(3)	99.628(12)
β/°	76.926(3)	108.857(11)
γ/°	77.221(3)	90.120(11)
V/Å^3	2291.2(3)	2573.9(14)
Z	4	4
D_c/(g cm^{-3})	1.294	1.405
μ (Mo K_α)/mm^{-1}	0.083	0.177
T/K	298(2)	298(2)
θ max.	28.95	20.28
Total no. of reflections	40988	91599
Independent reflections	12256	9080
Observed reflections	8485	567
Parameters refined	614	704
R_1, I > 2σ(I)	0.0772	0.1529
wR_2 (all data)	0.2312	0.3318
GOF (F^2)	0.997	1.800

Table A4.2: Hydrogen bonding distances (Å) and Bond angles (º) in the receptor crystal

D−H···A	d(D···H)/Å	d(H···A)/Å	d(D···A)/Å	<D−H···A/°	Symmetry codes
N1-H3···N4	0.860	2.232	2.944	140.12	[-x, -y, -z+1]
N3-H3N···N5	0.860	1.967	2.791	160.12	x,y,z
N5-H5N···N3	0.860	1.940	2.791	170.18	x,y,z
N7-H24···N11	0.860	2.222	2.971	145.64	[-x+2, -y, -z]
N9-H26···O1	0.860	1.992	2.788	153.45	x,y,z
N12-H12N···N10	0.860	1.947	2.796	169.00	x,y,z
C12-H9···N4	0.970	2.660	3.540	151.13	[-x, -y, -z+1]

Table A4.3: Hydrogen bonding distances (Å) and Bond angles (º) in the protonated complex

D−H···A	d(D···H)/Å	d(H···A)/Å	d(D···A)/Å	<D−H···A/°	Symmetry codes
N1--H1N···O3	0.86	1.87	2.699(8)	163	x,y,z
N2--H2N···O8	0.86	1.82	2.665(8)	168	[-x,1-y,1-z]
N4--H4N···O5	0.86	1.84	2.672(8)	163	[1-x,-y,1-z]
N5--H5N···O7	0.86	1.85	2.679(8)	163	x,y,z
N6--H6N···O4	0.86	2.22	3.035(8)	158	[1-x,-y,1-z]
N7--H7N···O5	0.86	1.83	2.668(8)	163	[1-x,-y,1-z]
N8--H8N···O7	0.86	1.81	2.650(8)	165	[1+x,y,z]
N10--H10N···O4	0.86	1.82	2.678(8)	171	[x,y,z]
N11--H11N···O9	0.86	1.86	2.696(8)	164	[1-x,1-y,1-z]
N12--H12N···O8	0.86	2.24	3.052(8)	157	[1+x,y,z]
Intra C14--H14···O2	0.93	2.48	2.896(10)	108	x,y,z
Intra C01--H1···N12	0.93	2.57	2.879(10)	100	x,y,z
C2--H2···O10	0.93	2.59	3.387(11)	144	[-x,1-y,1-z]
C5--H5···O6	0.93	2.43	3.264(11)	150	x,y,z
C8--H8A···O7	0.97	2.43	3.141(8)	130	x,y,z
C9--H9B···O2	0.97	2.28	2.956(9)	126	x,y,z
Intra C19--H19···O1	0.93	2.45	2.871(9)	108	x,y,z
C29--H29···O6	0.93	2.59	3.464(12)	156	[1-x,-y,1-z]
C35--H35B···O1	0.97	2.32	2.976(9)	124	[1+x,y,z]
C36--H36A···O5	0.97	2.44	3.147(9)	129	[1-x,-y,1-z]
C39--H39···O10	0.93	2.46	3.274(11)	147	[1-x,1-y,1-z]

Table A4.4. The comparison of our chemosensors **L_2** with F^- sensors available in recent literatures.

No.	Chemosensor type	Solvent	Reversibility and reusability	Detection limit	Ref.
1	BODIPY-benzimidazole	CH_3CN	Yes	0.093 μM	A4.1
2	Pyrene-benzimidazole	DMSO	Yes	1.63×10^{-5} M	A4.2
3	1,2-dioxetane derivative	DMSO	No	47 μM	A4.3
4	7-(diethylamino)-3-(2-(pyridin-4-yl)vinyl)-coumarin and triisopropylsilane ether	DMSO:PBS (7:3)	No	1.2×10^{-8} M	A4.4
5	BN-Embedded phenacenes	THF	No	1.8 x 10^{-8} M	A4.5
6	Tri-benzimidazolyl type	DMSO	Yes	0.284 μM	A4.6
7	**Our chemosensor**	**CH_3CN**	**Yes**	**4.63×10^{-8} M**	

References

A4.1 S. Madhu and M. Ravikanth, Boron-dipyrromethene based reversible and reusable selective chemosensor for fluoride detection, *Inorg. Chem.*, 2014, **53**, 1646–1653.

A4.2 A. Kushwaha, S. K. Patila, and D. Das, Pyrene-benzimidazole composed effective fluoride sensor: potential mimicking of a Boolean logic gate, *New J. Chem.*, 2018, **42**, 9200–9208.

A4.3 I. S. Turan and E. U. Akkaya, Chemiluminescence Sensing of Fluoride Ions Using a Self-Immolative Amplifier, *Org. Lett.*, 2014, **16**, 1680−1683.

A4.4 Y. Shen, X. Zhang, Y. Zhang, H. Li, and Y. Chen, An ICT-Modulated strategy to construct colorimetric and ratiometric fluorescent sensor for mitochondria-targeted fluoride ion in cell living, *Sens. Actuators B Chem.,* 2018, **258**, 544–549.

A4.5 Y. Han, W. Yuan, H. Wang, M. Li, W. Zhang, and Y. Chen, Dual-responsive BN-embedded phenacenes featuring mechanochromic luminescence and ratiometric sensing of fluoride ions, *J. Mater. Chem. C*, 2018, **6**, 10456–10463.

A4.6 Y. -C. Wu, J. -P. Huo, L. Cao, S. Ding, L.-Y. Wang, D. Cao, and Z. -Y. Wang, Design and application of tri-benzimidazolyl star-shape molecules as fluorescent chemosensors for the fast-response detection of fluoride ion, *Sens. Actuators B Chem.*, 2016, **237**, 865–875.

Chapter 5

Colorimetric detection of fluoride and acetate ions by benzothiazole based receptors: Fluorescence based selective acetate sensing

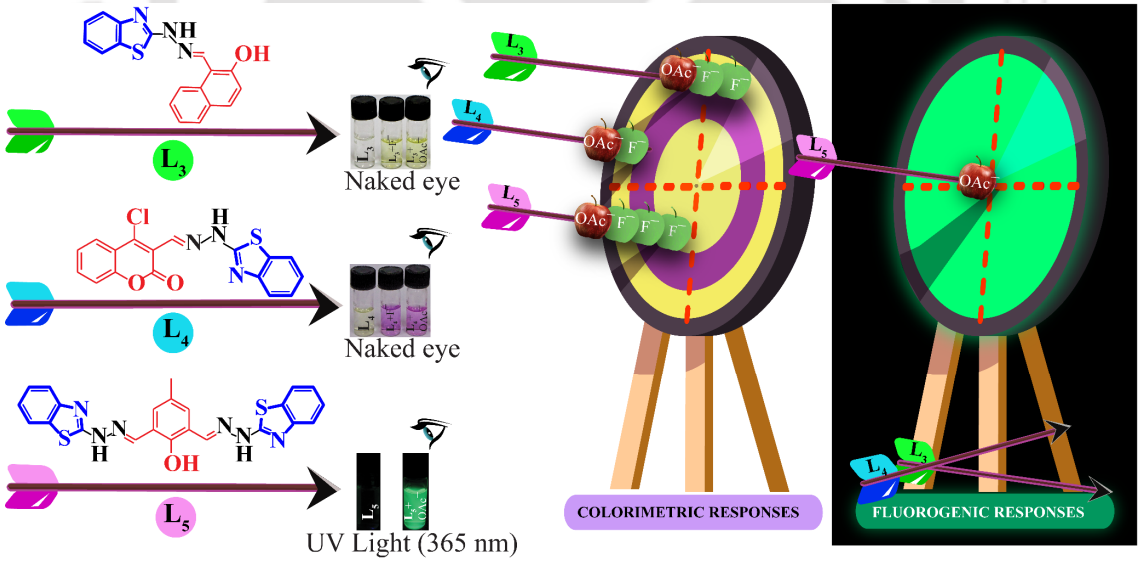

Chapter 5

5.1 Background and Focus of the Chapter

Along with the benefits extracted from its recognition and coordination in biological, clinical, catalysis and environmental milieu, anions can have damaging effects on the environment too, which can scarcely be underestimated. Among various anions, fluoride and acetate have been intensively studied owing to their significant roles in our everyday life. As summarised in earlier chapters, fluoride ion is helpful in fortifying dental health as it is used in the prevention of dental caries[5.1] and the treatment of osteoporosis[5.2-5.3]. However, high levels of fluoride in drinking water can cause fluorosis[5.4], nephrotoxic changes[5.5] and even urolithiasis[5.6] in organisms. The U.S. Environmental Protection Agency (EPA) has specified an enforceable drinking water regulation for the drinking water standards with a maximum level of 4 ppm (~200 μM) fluoride ions to avoid health hazards, while the Department of Health and Human Services has recommended an optimal dose of 0.7-1.2 ppm fluoride for community water systems.[5.7-5.8] Fluoride finds its use in military services as hydrolysis of sarin (isopropyl methylphosphonofluoridate), a chemical weapon, leads to fluoride release, which enables to track its presence in victims and natural environments.[5.9-5.10] On the other hand, acetate anion plays the pivotal role in numerous metabolic processes as well as regulates specific behaviours in several critical activities of enzymes, transport of hormones, protein synthesis and DNA regulation.[5.11-5.13] The production and oxidation rate of acetate has often been used as an indicator of organic decomposition in marine sediments as well as transmetalation of tetrapyrroles.[5.14-5.15] Acetate ion finds its importance in the medical field also due to its role as a possible tracer for malignancies and widespread use in prostate cancer and its metastases.[5.16-5.17] Therefore, substantial efforts have been devoted to the development of better sensors for the detection of fluoride[5.18-5.24] and acetate anion[5.25-5.27].

As our quest for designing non-symmetric tripodal receptors has met with the efficacious binding of anions in both solid as well as solution phase, we are trying to get better photophysical properties during anion binding event in our latest work. Most of the anion binding receptors involve multi-step synthetic procedures, extensive purification work along with an exhibition of delayed response for the anion recognition event. Alternatively, all these drawbacks could be circumvented by introducing Schiff bases containing acidic –OH and/or –NH protons for selective sensing of anionic species. Apart from their simple single step synthetic procedure, these Schiff bases are beneficial for both colorimetric as well as fluorometric detection of target anions due to their prompt optical changes by forming hydrogen bonded host-guest complex, deprotonation

event associated with polar –OH or −NH groups and seldom observed chemodosimeter type reaction with anions.[5.28-5.34]

In this present work, we have studied and improvised the selectivity and sensitivity of a series of Schiff base based chemosensor for fluoride and acetate sensing. The synthesized Schiff bases have achieved the burgeoning need of simple, sensitive, low-cost and easy-to-synthesize chemosensors for naked eye detection of fluoride and acetate ions. Three benzothiazole functionalized Schiff bases have been synthesized and applied as colorimetric sensors for fluoride and acetate ions in acetonitrile. Selectivity between the two anions are shown to be accomplished by using emission spectroscopy as one of the Schiff bases with its dimeric cage-like structure, can selectively sense acetate ion based on its shape complementarity emitting 'turn-on' fluorescence.

5.2 Design aspects of the chemosensors (L_3, L_4 and L_5)

The Schiff base probes were synthesized from one-step condensation reactions and were characterized entirely by ^1H, ^{13}C and mass analysis. In each case, the imine bond joins the chromophore and the benzothiazole unit extending conjugation. The probe **L_3**, reported earlier from our group[5.35], was based on naphthyl chromophore while **L_4** was decorated with the coumarin chromophore to enhance the chromogenic properties. The Chloro (Cl) group present in coumarin moiety of **L_4** was supposed to increase the acidity of the −NH proton, and it would help in charge transfer interactions leading to plausible enhancement in photophysical properties. Previously reported **L_5** was utilized as a modification to the probe **L_3** by introducing another similar imine linked benzothiazole arm to form a dimeric cage-like structure[5.36]. All of these probes were applied chronologically visualizing its sensing aptitude and selectivity studies towards the targeted anions in solution phase.

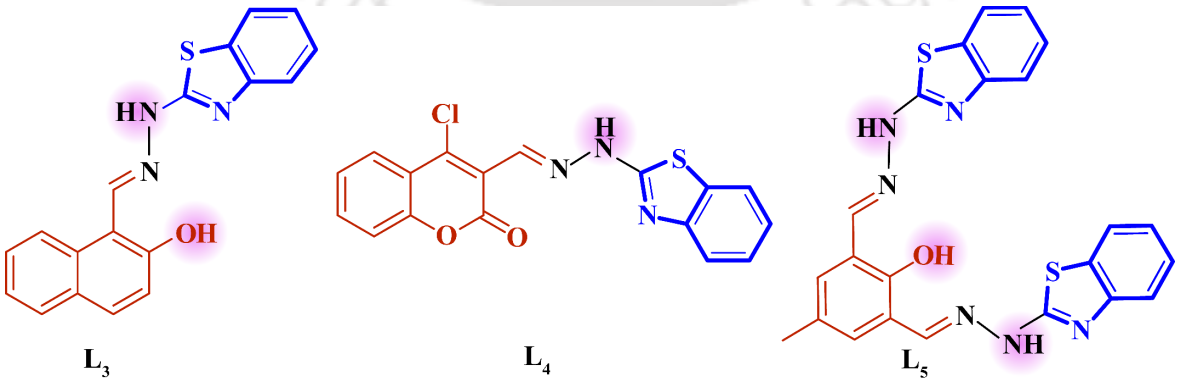

L_3 L_4 L_5

Scheme 5.1 Molecular Structure of the Receptors **L_3**, **L_4** and **L_5**.

5.3 Solution phase anion binding studies of the receptors L_3, L_4 and L_5

5.3.1 Absorption studies

The anion sensing aptitude of the probes (**$L_{3\text{-}5}$**) was elucidated by UV/Vis changes in acetonitrile solution upon addition of 10 equivalents of various anions such as F^-, Cl^-, Br^-, I^-, NO_3^-, $CH_3CO_2^-$ (OAc^-), HSO_4^-, SO_4^{2-}, HCO_3^-, PPi, $H_2PO_4^-$ and PO_4^{3-}. The monopodal naked probe **L_3** (10μM) displayed two distinct absorption peaks positioned at 340 nm and 384 nm, as shown in Figure 5.1a. The high energy absorption peaks might be attributed to π–π* transitions. Among the anions, chemosensor **L_3** was selective to both F^- and OAc^- and instigated an immediate colour change of the corresponding solutions from colourless to yellowish type. This colorimetric change was an outcome of a newly emerged nearly 72 nm red shifted absorption maximum at 456 nm. The isobestic points at 316 nm and 412 nm were also indicative of the formation of a new UV active complex. The colorimetric changes occurred after OAc^- addition were also accountable for similar host-guest complex formation. In all these cases, an intramolecular charge transfer (ICT) interaction might have occurred where the charge would propagate from the guest anions to the host **L_3** due to hydrogen bond interactions and/or plausible deprotonation event. To validate the deprotonation tenet, UV-Vis change of the probe solutions were also recorded after the addition of TBAOH and found to be similar to the addition of F^- or OAc^- (Figure A5.8a).

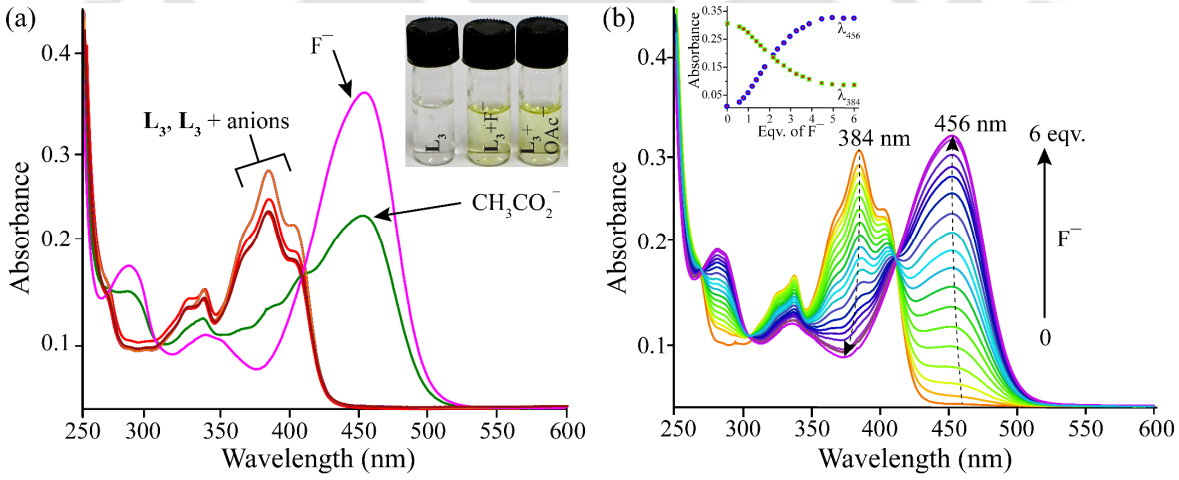

Figure 5.1 (a) Changes in absorption spectra of **L_3** (10 μM) with the incremental addition of TBAF, TBAOAc and other anions (10 equivalents) in acetonitrile. Inset: visible colour change upon the addition of F^- and OAc^- to **L_3**. (b) UV-Vis titration spectra of **L_3** upon incremental addition of 6 equiv. of TBAF in acetonitrile. Inset: changes in the absorption maxima at 384 nm and 456 nm with the incremental addition of TBAF.

Further to follow the formation of the host-guest complexes, UV-Vis titration studies of the probe solutions (10μM) were recorded with increasing concentrations of the guest anions. In case of fluoride addition, as depicted in Figure 5.1b, the **L_3**'s characteristic peak at 384 nm was bleached out and corresponding to it, a new peak at 456 nm was intensified with the progress of the titration

until its saturation with 6 equiv. of the aforementioned anion. The absorbance at 456 nm showed a linear dependence of their absorbance values over a wide range of fluoride concentrations. The titration data derived Job's plot suggested a 1:2 host-guest complex formation (Figure A5.1a). The binding constant evaluated from the Benesi–Hildebrand equation was found to be 3.33×10^{11} M^{-2} for the fluoride ions (Figure A5.1b). An analogous investigation was also performed for the binding nature of acetate to **L_3** (Figure A5.2a). The Job's plot from the titration profile suggested the formation of 1:1 **L_3**-acetate complex with the calculated binding constant of 1.67×10^6 M^{-1} from Benesi–Hildebrand equation (Figure A5.2b & A5.2c). Based on the UV-Vis changes, the lowest detection limit (LOD) of the host **L_3** for fluoride and acetate ions were evaluated to be 1.05×10^{-7} M and 2.57×10^{-7} M respectively (Figure A5.1c & A5.2d).

Scrutinizing the absorption study of the probe **L_3**, we modified the imine linked chromophore attached to the benzothiazole moiety in the probe **L_4** by introducing 4-Chloro-3-formylcoumarin moiety in order to attain better colorimetric response. The coumarin based Schiff base receptor **L_4** possessed a single –NH to interact with the anions. In the UV-Vis studies, as shown in Figure 5.2a, **L_4** exhibited two characteristic absorption peaks at 290 nm and 403 nm in acetonitrile which were replaced by new peaks at 322, 351 and 550 nm after the addition of F^- and OAc^- solution. The new isobestic points at 307 nm, 359 nm and 459 nm with fluoride and 303 nm, 353 nm and 460 nm with acetate ions were clear indicative of new complex formation with the two targeted anions. This 147 nm bathochromic shift also resulted in the formation of a beautiful purple colouration from the original light yellow solution. The probe probably interacted with the incoming fluoride or acetate anion through hydrogen bonds donated by –NH functionality and the charge propagation finally led to the formation of red shifted absorption maximum through an ICT process. However, a deprotonation event could not be ignored and to corroborate it like the earlier case, TBAOH was added to the fresh **L_4** solution (Figure A5.8b). It thus developed an absorption maximum at 550 nm with a visual change in colour to purple similar to the addition of F^- or OAc^- solution.

To understand the mechanistic details of the binding process, **L_4** was titrated with both F^- and OAc^- ions in acetonitrile. As apparent from Figure 5.2b, on perpetual addition of F^- concentration caused an increase in absorbance of the peak at 550 nm with a concomitant decrease in absorbance of the peaks at 290 nm and 403 nm in the UV spectra. The intensity of the peak at 550 nm was increasing until it reached saturation value with the addition of 3 equiv. of F^- ion. The Job's plot from the titration data suggested 1:1 binding stoichiometry, i.e. each probe **L_4** could bind one fluoride anion (Figure A5.3a). Again, the OAc^- ion induced changes were akin to that of the fluoride addition, which was visible in the titration spectra shown in Figure A5.4a, and it also

could bind in a 1:1 ratio to the probe **L4** (Figure A5.4b). However, **L4** could bind strongly with F^- than OAc^- as the binding constant for the former ($1.25x10^6$ M^{-1}) was higher than that for OAc^- ($5.0x10^5$ M^{-1}) based on Benesi-Hinderbrand equation (Figure A5.3b & Figure A5.4c). Based on the UV-Vis changes, the lowest detection limit of **L4** for fluoride and acetate anions were calculated to be as low as $3.35x10^{-8}$ M and $5.79x10^{-8}$ M respectively (Figure A5.3c & Figure A5.4d). **L4** was nonchalant to the presence of other tested anions and thus produced no visual colour change (Figure A5.5a).

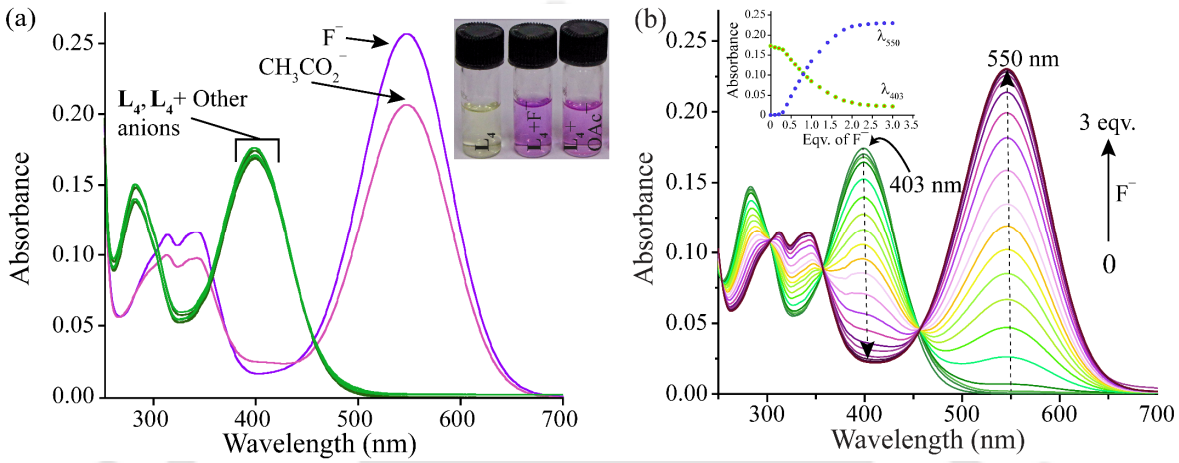

Figure 5.2 (a) Changes in absorption spectra of **L4** (10 μM) with the incremental addition of TBAF, TBAOAc and other anions (10 equivalents) in acetonitrile. Inset: visible colour change upon the addition of F^- and OAc^- to **L4**. (b) UV-Vis titration spectra of **L4** upon incremental addition of 3 equiv. of TBAF in acetonitrile. Inset: Changes in the absorption maxima at 384 nm and 456 nm with the incremental addition of TBAF.

Thus, modification of ligand functionality from **L3** to **L4** with the coumarin moiety resulted in swift colorimetric detection of the aforementioned anions. The naked eye colour changes were more pronounced in case of the probe **L4** which was apparent in the striking colour change from light yellow to purple in the presence of the targeted anions (Figure A5.5b). In comparison to 72 nm red shifted maxima in case of **L3** on interaction with the fluoride or acetate solution, a bathochromatic shift of 147 nm was observed with the probe **L4** with corresponding absorption maxima at 550 nm instead of earlier 456 nm. The chloro group present in **L4** was assumed to augment the photophysical properties by increasing the acidity of the −NH protons, which in turn, might help in charge transfer interactions leading to plausible enhancement in colorimetric responses towards the targeted anions.

Thus, as we improved the colorimetric responses of the probes from **L3** to **L4** towards both fluorides and acetate anions, what we were anxious about was the selectivity between the two competitive anions. Therefore, we moved towards **L5**, a dimeric cage-like dipodal probe with −OH and−NH functionalities to interact with the guest anions. However, the absorption study based properties of this new probe **L5** were more or less similar to that of **L3**. A 10 mM probe solution

in acetonitrile exhibited two absorption peaks at 332 nm and 386 nm where the peaks might be attributed to the π-π* transitions. As Figure 5.3a suggested, the yellow coloured solution formed after the addition of 10 equiv. of F^- ions to **L_5**, gave new absorption maximum at 445 nm with isobestic points at 296 nm and 403 nm, indicating a new host-guest complex.

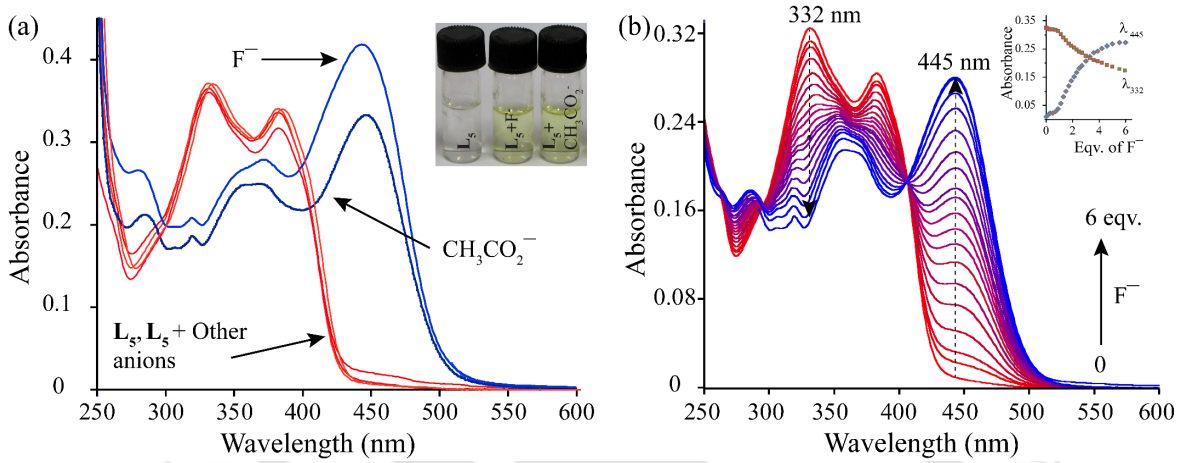

Figure 5.3 (a) Changes in absorption spectra of **L_5** (10 μM) with the incremental addition of TBAF, TBAOAc and other anions (10 equivalents) in acetonitrile. Inset: visible colour change upon the addition of F^- and OAc^- to **L_5**. (b) UV-Vis titration spectra of **L_5** upon incremental addition of 6 equiv. of TBAF in acetonitrile. Inset: changes in the absorption maxima at 332 nm and 445 nm with the incremental addition of TBAF.

For the quantitative appraisal of the interaction, titration experiment was carried out with incremental addition of fluoride aliquots, where the peak at 445 nm reached its saturation after addition of 6 equiv. of the aforesaid anion as depicted in Figure 5.3b. The Job's plot from the titration data suggested the formation 1:3 host-guest complex in case of F^- ions and the binding constant evaluated from the Benesi–Hildebrand equation was found to be 1.66×10^{17} M^{-3} for the fluoride ions (Figure A5.6a & A5.6b). Based on the UV-vis changes, the lowest detection limit (LOD) of **L_5** for fluoride ions was found to be as low as 9.33×10^{-6} M (Figure A5.6c). Similar changes in absorption spectra of **L_5** were also perceived with acetate anions, where the isobestic points at 294 nm and 406 nm indicated the formation of a new host-guest complex (Figure 5.3a).

To get a quantitative appraisal of the interaction, an analogous titration experiment was carried out with the incremental addition of acetate ions in acetonitrile (Figure A5.7a). Job's plot derived from the UV titration studies in acetonitrile suggested the formation of a 1:1 binding stoichiometry with the acetate ion (Figure A5.7b).

Deprotonation event of the probe **L_5** was also established by the similar TBAOH addition induced UV-Vis spectrum and corresponding colorimetric changes in **L_5** (Figure A5.8c). Thus, after the comprehensive appraisal of anion sensing via UV-Vis studies, we have emphasized our impetus to investigate the anion sensing aptitude of the three probes considering selectivity to be the

principal goal with the help of emission spectroscopy studies. However, this selectivity towards the anions exhibited by the three probes was solvent dependent and the sensitivity was negligible in the presence of water or other polar protic solvents (Figure A5.9).

5.3.2 Fluorescence studies

As the absorption studies suggested, UV-Vis analysis were quite sensitive towards the F^- ions and OAc^- ions, yet not selective enough to differentiate between the two competitive anions; hence fluorescence emission experiments were performed under the same experimental condition with the three probes **L**$_3$, **L**$_4$, and **L**$_5$. Interestingly, among the three probes, only **L**$_5$ could distinguish OAc^- ions from F^- ions through differential fluorescence output. Initially, the naked probe **L**$_5$ emitted a very weak emission band centred at 540 nm when excited at 385 nm. As depicted in Figure 5.4a, the emission maximum of **L**$_5$ was intensified nearly 14 times after interacting with only OAc^- ion. The yellowish coloured solution thus formed, emitted a greenish type fluorescence in the presence of OAc^- ion under the 365 nm UV lamp. However, no appreciable change in fluorescence emission intensity was witnessed after addition F^- ions to **L**$_5$. Interaction with other anions, including hydroxide ion, also failed to make any characteristic change to the fluorescence emission maxima of the probe **L**$_5$ (Figure A5.10a). Likewise, the titration experiment was performed with the incremental addition of acetate anion to have a quantitative appraisal of interaction with the probe, **L**$_5$. The C=N isomerisation might be accounted for the weak fluorescence of **L**$_5$.[5.36-5.38] However,

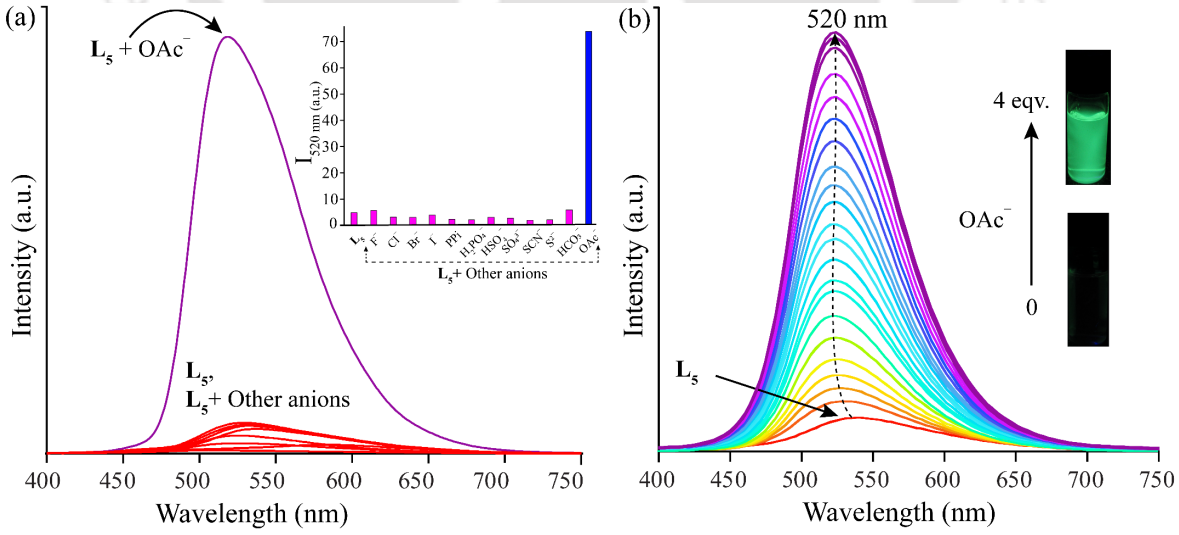

Figure 5.4 (a) Changes in emission spectra of **L**$_5$ (10 μM) with the incremental addition of TBAOAc and other anions (10 equivalents) in acetonitrile (λ_{ex} = 385 nm). Inset: Bar diagram represents the fluorescence intensity at I_{520} upon the addition of 10 equivalents of various anions. (b) Fluorescence titration spectra of **L**$_5$ upon incremental addition of 4 equiv. of TBAOAc in acetonitrile. Inset: The corresponding visual fluorescence colour change of **L**$_5$ upon addition of acetate ions under UV lamp (λ_{ex} = 365 nm).

with the initial few aliquots of OAc^- ion, the emission maximum was blue shifted to 520 nm and then intensified with a further addition of OAc^- ion concentration until it reached a saturation value after addition of 4 equiv. of OAc^- ions. The Job's plot from the titration data suggested a 1:1 host-guest complex (Figure A5.10b). The binding constant was evaluated with the Benesi–Hildebrand equation and found to be $3.0x10^6$ M^{-1} as in Figure A5.10c. The detection limit for acetate ion was determined using the $3\sigma/K$ method and found to be as low as $2.907x10^{-8}$ M (Figure A5.10d). The 'Y' shaped acetate ion possibly might fit well in the cavity of **L5** and blocked its non-radiative pathway, i.e. free rotation around the C=N bond by forming 1:1 complex with the acidic hydrogens of **L5**, which finally resulted in the enhanced fluorescence output.[5.32-5.33, 5.39] The other two probes, **L3** and **L4** were unable to distinguish F^- and OAc^- anions as both exhibited no characteristic changes in the presence of the aforementioned anions. **L3** was weakly fluorescent with I_{max}= 525 nm when excited at 385 nm and **L4** exhibited I_{max}= 502 nm when excited at 405 nm. The other anions also could not produce any distinctive changes in the fluorescence emissive behaviour of both **L3** and **L4** (Figure A5.11a and A5.11b).

We compared the smallest LOD values assessed for our Schiff bases, **L4** (for colorimetric fluoride sensing) and **L5** (for fluorescent acetate sensing) with recently reported Schiff base chemosensors and our limit of detection were found to be comparable or lower which are summarised in Table A5.1.

5.3.3 ^{1}H NMR titration studies with fluoride and acetate ion

Based on the outcome of absorption and emission studies, the interaction of the probes with the fluoride and acetate ions was postulated to be the initial hydrogen bond formation and further deprotonation of the acidic protons in **L3**–**L5** by addition of excess fluoride and acetate anions. This, in turn, may cause the unique absorption behaviour and visible changes in colour. Consequently, ^{1}H NMR titration experiments were performed in DMSO-d_6 at 10 mM concentration of each probe solution with TBAF and TBAOAc, to study the mechanistic nature of the interaction between three probes with the aforesaid anions.

Initially, upon addition of fluoride ions up to 6.0 equiv. to **L3** solution, the hydrazone –NH, *Ha* (12.19 ppm) proton signals displayed considerable broadening with significant downfield shifts ($\Delta\delta$=1.40 ppm) indicating the involvement of these –NH with the fluoride ions (Figure 5.5a). The hydroxyl –OH proton signals were not visible, possibly because of its exchangeable nature. The complexation of **L3**$\cdots F^-$ might have occurred via both –NH and –OH protons, thereby gradually increasing the electron density of the complex.

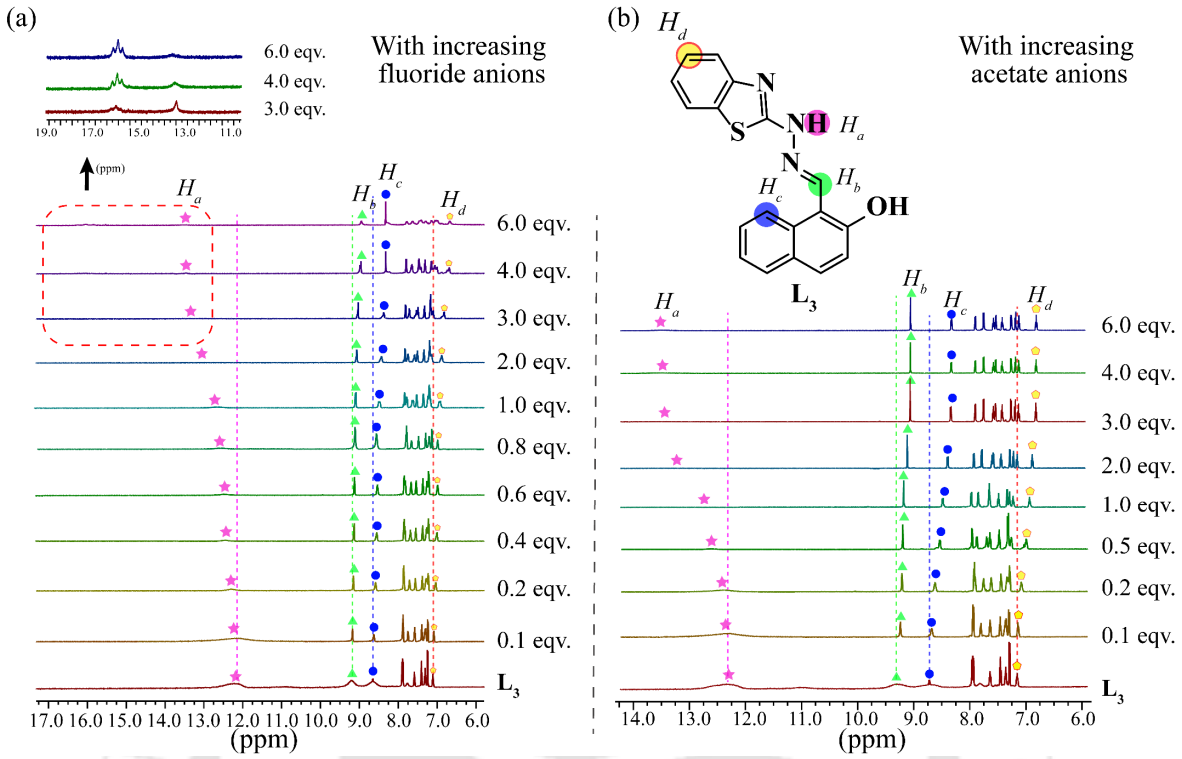

Figure 5.5 Stack plot of the ^{1}H NMR spectra of receptor **L$_3$** in the presence of increasing amounts of (a) TBAF (0.1-6.0 equiv.) and (b) TBAOAc (0.1-6.0 equiv.) recorded in DMSO-d_6.

The imine proton, *H$_b$* along with the sets of other aromatic –CH protons corresponding to signals ranging from *H$_c$* to *H$_d$* exhibited minute upfield shift via through-bond effects with the increasing amount of fluoride anion till 1.0 equivalent. The addition of TBAF beyond 1.0 equivalent might have induced deprotonation of the probe **L$_3$** which was reflected in the more pronounced upfield shift of the aromatic –CH proton signals viz. *H$_c$* to *H$_d$* as depicted in the stacked Figure. Further addition of TBAF beyond 4 equiv. could not render any shift in the resonance values of the proton signals. Thus, it can be resolved that fluoride ions formed a hydrogen bonded complex with the probe **L$_3$** at the acidic –NH group which resulted in the broadening of the –NH signal with a prominent downfield shift. Interestingly, the hydrazone –NH signal, *H$_a$* was still present as a weak signal even upon addition of 6 equiv. of TBAF solution. The occurrence of a triplet proton signal at 16.07 ppm conforming the formation of HF_2^- species suggested that the probe involved in a deprotonation event with the addition of excess TBAF solution.[5.40-5.42] The simultaneous presence of the hydrazone –NH signal along with the triplet proton signal suggested the plausible deprotonation of the more acidic –OH group on excess addition of TBAF solution.

In case of acetate addition to **L$_3$**, as shown in (Figure 5.5b), the addition of the former (up

to 3.0 equiv.) induced broadening as well as downfield shift (Δδ=1.27 ppm) of the hydrazone –NH, H_a (12.19 ppm) proton signals. The signals gradually diminished in between until it revived with excess addition of the TBAOAc solution (until 3.0 equiv.). Similar to the addition of TBAF solution, acetate solution also could not render deprotonation of the hydrazone –NH with the addition of excess acetate solution as its signal H_a was seemingly visible as a weak signal upon addition of 6 equiv. of TBAOAc solution. In this case, the imine proton, H_b exhibited considerable upfield shift (Δδ=0.26 ppm) along with the other aromatic –CH proton signals ranging from H_c to H_d as depicted in the stacked spectra. Until the addition of 6 equiv. of TBAOAc, H_c and H_d protons experienced an upfield shift of Δδ=0.42 ppm and 0.43 ppm respectively which could be ascribed to the deprotonation of the acidic –OH group.

For the probe **L4**, as shown in Figure 5.6a, with the addition of TBAF solution from 0 to 1.5 equivalents resulted in the downfield shift (Δδ=0.34 ppm) and broadening of the hydrazone –NH, H_a protons signal at 12.75 ppm. Simultaneously, the signals due to imine proton, H_b along with other aromatic proton signals (H_c to H_d) also experienced infinitesimal upfield shift due to through-bond effects with the increasing amount of fluoride anion till 1.0 equivalent. The deprotonation might have started after addition of 2.0 equivalent of TBAF, which was apparent in the more distinct upfield shift of the imine proton, H_b (Δδ=0.20 ppm) and aromatic –CH proton signals viz. H_c to H_d depicted in the stacked Figure. A similar occurrence of triplet proton signal at 16.10 ppm corresponding to HF_2^- species also confirmed the deprotonation event. Unlike as in **L3**, deprotonation of the hydrazone –NH took place in **L4** with excess addition of TBAF solution as its acidity was increased due to the presence of the chloro group in the coumarin moiety.

As presented in Figure 5.6b, the addition of initial aliquots of acetate anions (up to 1.0 equiv.) to the probe **L4** encouraged broadening as well as downfield shift (Δδ=0.26 ppm) of the hydrazone –NH, H_a (12.75 ppm) proton signals. Addition of acetate ions beyond 1.0 equiv. might have initiated deprotonation event of the acidic protons, which led to the considerable upfield shift (Δδ=0.25 ppm) of the imine proton. Apart from this, the other aromatic –CH proton signals ranging from H_c to H_d as depicted in the spectrum experienced the upfield shift via through-bond effect with the increasing amount of acetate ions. Till the addition of 4 equivalents of TBAOAc, H_c and H_d protons experienced pronounced upfield shift of Δδ=0.19 ppm and 0.40 ppm, respectively due to the increase in electron density as a result of subsequent deprotonation of the hydrazone –NH.

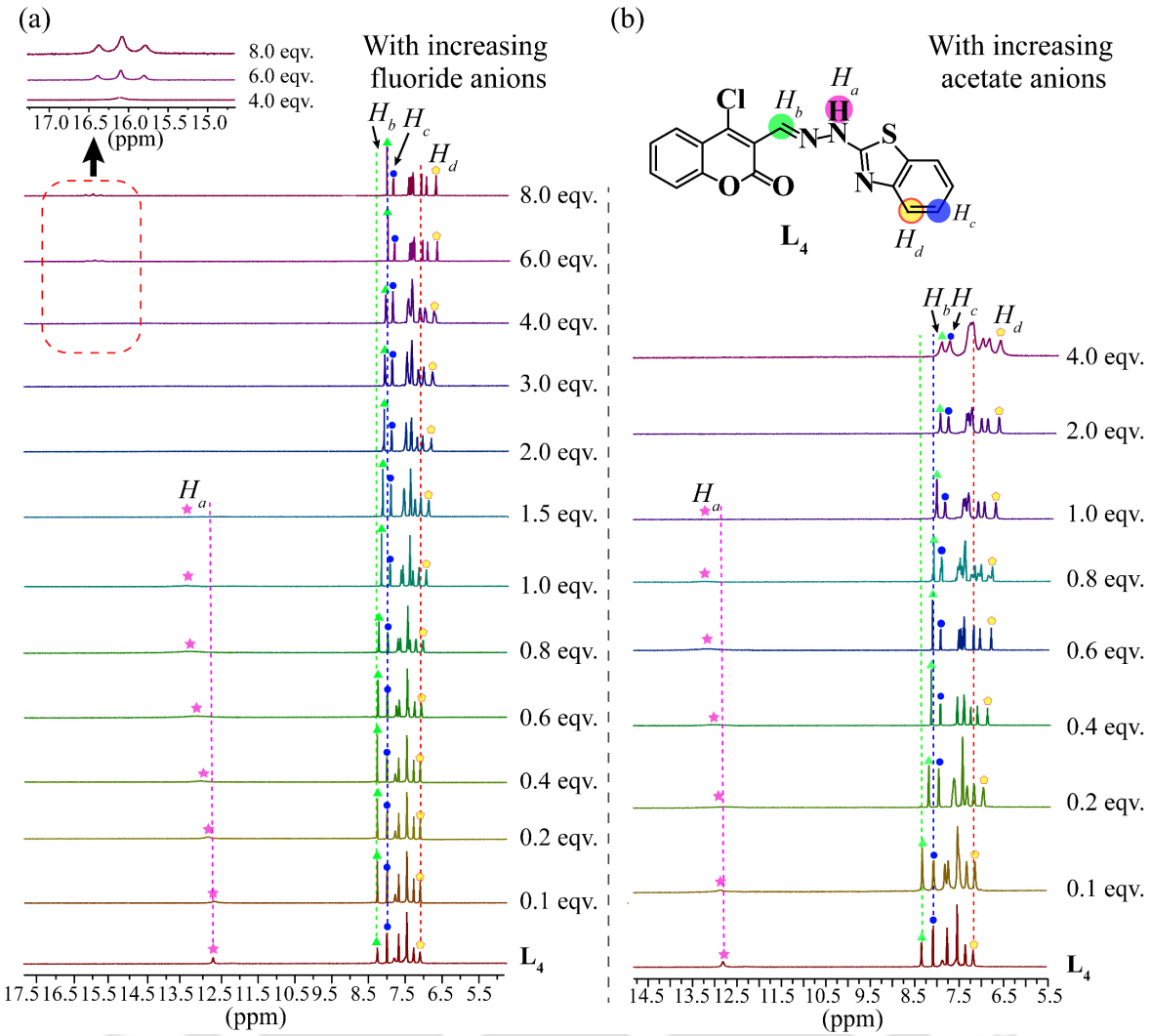

Figure 5.6 Stack plot of the ^{1}H NMR spectra of receptor **L$_4$** in the presence of increasing amounts of (a) TBAF (0.1-8.0 equiv.) and (b) TBAOAc (0.1-4.0 equiv.) recorded in DMSO-d_6.

As depicted in Figure 5.7a, the probe **L$_5$** exhibited singlets at 12.31 ppm and 11.57 ppm due to hydroxyl –OH, *Ho* and hydrazone –NH, *Ha* respectively. Addition of 0.2 equivalents TBAF solution resulted in the broadening of the –OH proton's signal, which eventually disappeared upon further addition of TBAF solution. Concurrently, the *Ha* signal experienced a significant downfield shift of Δδ=1.12 ppm until the addition of 3.0 equiv. of TBAF solution. Interestingly, *Ha* signals experienced minor upfield shift after addition of excess (5.0 equiv.) TBAF solution, which eventually became saturated at higher TBAF concentration. The occurrence of 1:2:1 triplet signal of the HF_2^- species at 16.07 ppm after the addition of excess equivalents of fluoride anion was coincident with the *Ha* proton signal at 12.22 ppm, which confirmed the single deprotonation event associated with the most acidic hydrogen, i.e. the hydroxyl –OH, *Ho* present in the probe **L$_5$**. Due to the initial through bond effect and increase in electron density due to consequent deprotonation, the

imine proton signal, H_b displayed considerable upfield shift of Δδ=0.36 ppm while other aromatic –CH proton signals ranging from H_c to H_d exhibited upfield shift of Δδ=0.44 ppm and Δδ=0.51 ppm respectively.

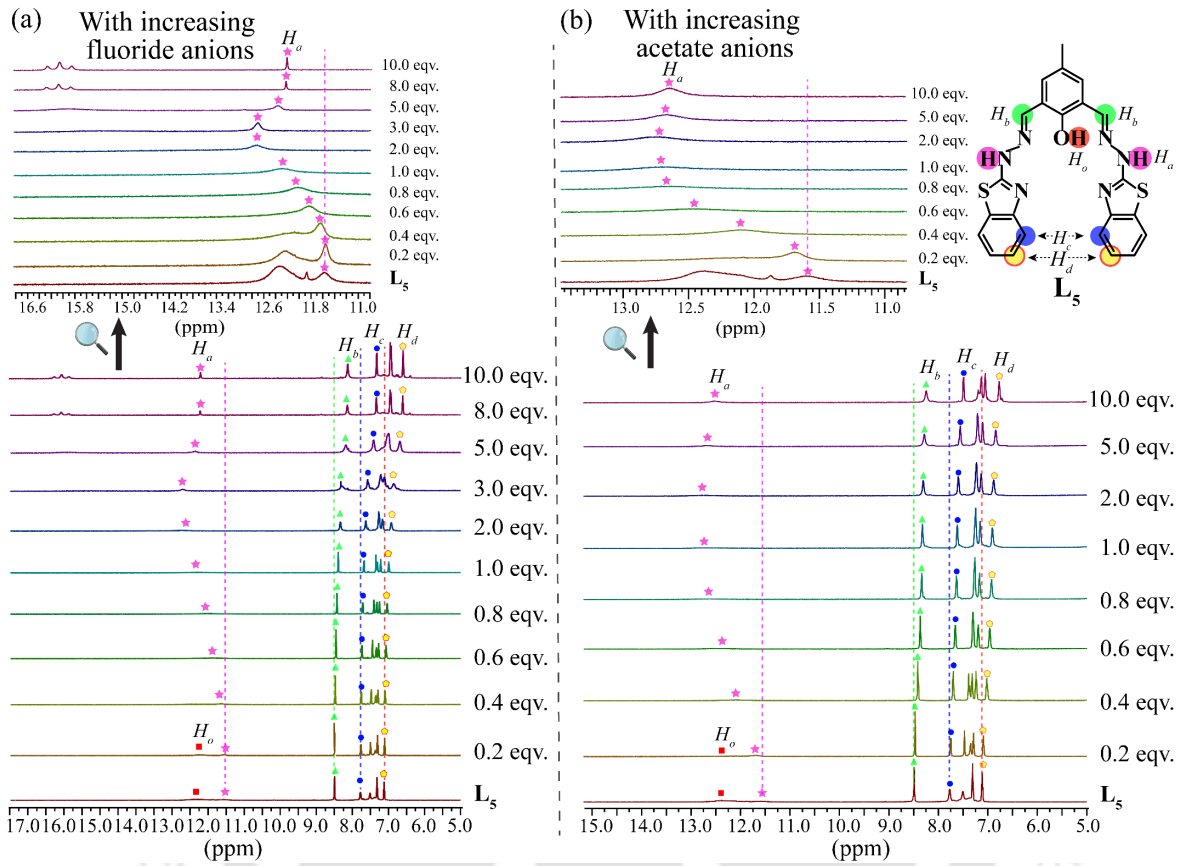

Figure 5.7 Stack plot of the ^{1}H NMR spectra of receptor **L5** in the presence of increasing concentrations of (a) TBAF (0.2-10.0 equiv.) and (b) TBAOAc (0.2-10.0 equiv.) recorded in DMSO-d_6.

Upon addition of acetate ions at low concentration (up to 0.2 equiv.), the acidic –OH proton, H_o experienced broadening and disappeared instantly, as shown in Figure 5.7b. The hydrazone –NH, H_a proton signals showed considerable broadening with substantial downfield shifts (Δδ=1.18 ppm) until the addition of 2.0 equivalents of TBOAc solution. The H_a proton signals displayed minor upfield shift after addition 2.0 equiv. of TBAOAc solution, which reached its saturation at higher TBAOAc concentration (10.0 equiv.). The complexation of acetate ions with acidic hydroxyl –OH and hydrazone –NH of **L5** gradually increased the electron density of the complex that triggered the upfield shift of the imine proton signal, H_b and the other aromatic –CH proton signals ranging from H_c to H_d. Again, these upfield shifts were more pronounced with the excess addition of acetate ions, which suggested the deprotonation of hydroxyl –OH rather than hydrazone –NH as the H_a proton signals still prevailed in the spectra. Until the addition of 10.0 equivalents of

acetate ions, H_b displayed an upfield shift of Δδ=0.25 ppm while the H_c to H_d protons showed upfield shifts of Δδ=0.29 ppm and Δδ=0.35 ppm respectively.

Based on the outcomes from ^{1}H NMR study, the sensing mechanism for fluoride and acetate ion can be established with the following observations: (i) Initially upon addition of lower concentration fluoride and acetate ions, the three probes with their acidic –OH proton (in **L$_3$** and **L$_5$**) and hydrazone –NH, formed hydrogen bonded complex with the incoming anions. (ii) Fluorides and acetates with high affinity towards the acidic hydrogens could easily result in the cleavage of either of O–H (in **L$_3$** and **L$_5$**) or N–H bond (in **L$_4$**) when the excess concentration of TBAF or TBAOAc was introduced to the receptor-anion complex.

5.3.4 Reversibility study and interpretation of related logic gate

Recently, optical switches have attracted much attention for its proficiency in information processing and construction of Boolean type logic gates at the molecular level.[5.43-5.45] In order to analyse the reversibility and reusability of the chemosensors towards the targeted anions, we have selected **L$_4$** for fluoride and **L$_5$** for acetate as they exhibited the smallest LOD values and captivating visual changes.

Initially, the probe **L$_4$**-F^- complex was treated with an incremental amount of TFA (Trifluoroacetic acid). When H^+ was added to the solution containing a **L$_4$**-F^- complex, the new response at 550 nm was gradually quenched with simultaneous generation of the original peak at 403 nm (Figure A5.12a). Upon addition of 4 equivalents of TFA, the chemosensor **L$_4$** finally regained its original optical properties. The absorption maxima of the chemosensor **L$_4$** at 403 nm was unchanged in the presence of the acid. From a chemical perspective, it can be concluded that the addition of TFA inhibited the hydrogen bonding interaction between the F^- ions and the host **L$_4$** as H^+ has a better affinity towards the basic F^- ions. Thus, the chemosensor **L$_4$** displayed repeatable reversibility and recyclability towards F^- and H^+ ions, which could be observed for more than five cycles (Figure 5.8a and A5.12b). The sensitivity and reversibility of the chemosensor **L$_4$** have instigated us to fabricate a combination of several interesting Boolean logic gates with molecular level arithmetic calculations. For the construction of the logic gate, the presence of the probe **L$_4$** was taken as Input 1 (Inp1) and the addition of F^- and H^+ ions were considered as Input 2 (Inp2) and Input 3 (Inp3) respectively. The emergence of the original peak at 403 nm with the addition of H^+ was taken as Output 1 (Out 1) while incremental additions of F^- gave us a response at 550 nm as Output 2 (Out 2). The output 1 (Out 1) was considered to be

ON or '1' if input 1 (Inp1) was ON or 1 which suggests the blank probe **L4** exhibited the Output at 403 nm without the addition of F^- ion. With the addition of F^-, the Output 1 was switched OFF and simultaneously Output 2 (Out2) at 550 nm was switched ON or '1'. This behaviour led to the implementation of AND logic gate here. The addition of H^+ ion which was considered as Input 3, acted as an inhibitor by preventing the hydrogen bonding interaction between the probe **L4** and the F^- ion. This behaviour was following the NOT gate. Overall, as per the truth table, the reversible behaviour led us to fabricate a combination of AND-OR-NOT logic gate which is depicted in Figure 5.8b and 5.8c.

(a)

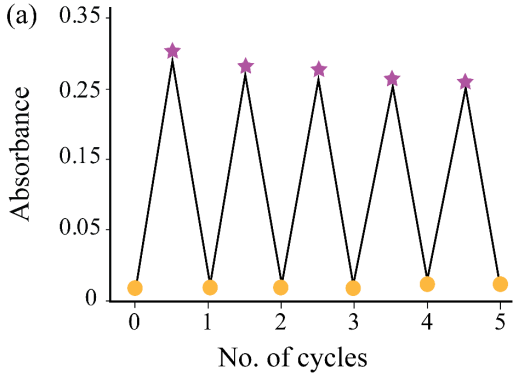

(b)

Inp1 (L_4)	Inp2 (F^-)	Inp3 (H^+)	Out1 $_{(403)}$	Out2 $_{(550)}$
0	0	0	0	0
0	0	1	0	0
0	1	0	0	0
0	1	1	0	0
1	0	0	1	0
1	0	1	1	0
1	1	0	0	1
1	1	1	1	0

(c)

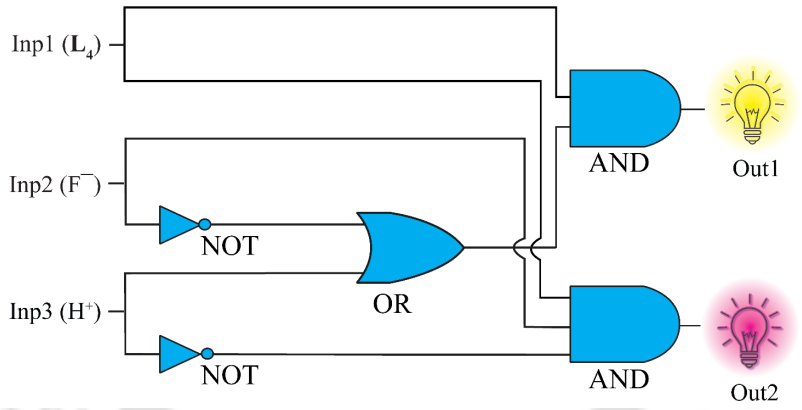

Figure 5.8 (a) Reversible and recyclable behaviour of probe **L4** upon addition of TBAF and TFA (absorption behaviour at λ= 550 nm; orange circle: initial optical density of **L4** or with H^+ ion while purple star: final optical density of with F^- ion). (b) The corresponding truth table. (c) The fabricated combination of basic AND-OR-NOT logic gate based on the reversible behaviour of **L4** towards F^- and H^+.

Similarly, we carried out the reversibility test for the probe **L5** in presence of TBAOAc and TFA as OAc^- ion has the propensity to form CH_3COOH binding with H^+ ions.[5.33] Reversibility studies of the probe **L5**-OAc^- with an incremental amount of TFA (Trifluoroacetic acid) were carried out as shown in Figure 5.9a. Accordingly, the probe **L5** was found to be reversible and recyclable toward OAc^- and H^+ ions over more than five cycles as depicted in Figure 5.9b. The addition of OAc^- ions to the probe solution resulted in fluorescence increase at 520 nm (ON state), while the addition of H^+ ions to the probe **L5**–OAc^- complex instigated recovery of original fluorescence intensity of the probe **L5**

(OFF state). This "Off–On–Off" switching behaviour led us to fabricate an INHIBIT logic gate where the output 'turn-on' fluorescence at 520 nm was assigned as '1' and the 'turn-off' behaviour was denoted as '0'. Again, when any one of the inputs; $\mathbf{L_5}$, OAc^- and H^+ was missing, then they were assigned as '0' and for their presence, the inputs were denoted as '1' (Figure 5.9c and 5.9d).

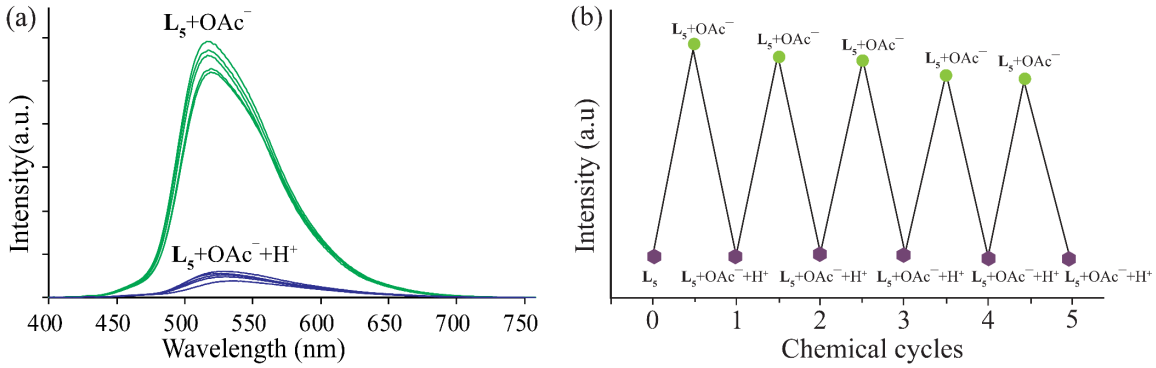

(c)

Inp1 ($\mathbf{L_5}$)	Inp2 (OAc^-)	Inp3 (H^+)	Out $_{(520)}$
0	0	0	0
0	0	1	0
0	1	0	0
0	1	1	0
1	0	0	0
1	0	1	0
1	1	0	1
1	1	1	0

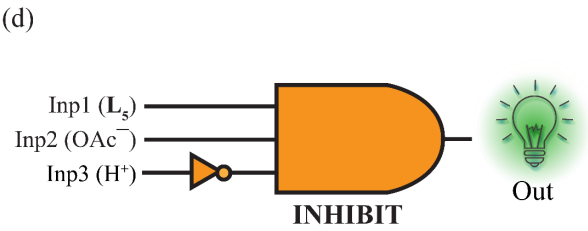

Figure 5.9 (a) Reversible and recyclable fluorescence response of probe $\mathbf{L_5}$ on addition of TBAOAc and TFA. (b) Reversibility of $\mathbf{L_5}$ (up to five cycles) with alternate addition of OAc^- and H^+. (c) and (d) The truth table for the fabricated 'INHIBIT' logic gate based on the probe behaviour towards OAc^- and H^+.

5.4 Conclusion

In essence, we have successfully synthesized and utilized a series of benzothiazole functionalized Schiff bases for sensing two competitive anions, i.e. fluoride and acetate. The colorimetric behaviour of the chemosensor $\mathbf{L_3}$ towards the targeted anions was improved by ligand functionality modification in $\mathbf{L_4}$ with improvement in colour and larger bathochromic shift of 147 nm. The emission spectroscopy based acetate selectivity was achieved by introducing another chemosensor $\mathbf{L_5}$ having a dimeric cage-like structure with two Benzothiazole arms. Among the three probes, $\mathbf{L_4}$ showed the lowest fluoride detection limit down to 3.35×10^{-8} M based on the UV-Vis studies while $\mathbf{L_5}$ exhibited the lowest LOD value for acetate ion with 2.907×10^{-8} M detection with the help of emission studies. ^{1}H NMR studies confirmed the initial formation –OH···F^-/OAc^- and/or –NH···F^-/OAc^- hydrogen bonds and subsequent deprotonation of the most acidic protons on excess addition of sensed anions.

References

5.1 L. K. Kirk, Biochemistry of the Halogens and Inorganic Halides; Plenum Press: New York, 1991.

5.2 M. Kleerekoper, The role of fluoride in the prevention of osteoporosis, *Endocrinol. Metab. Clin. North Am*., 1998, **27**, 441–452.

5.3 D. Briancon, fluoride and osteoporosis: an overview, *Rev. Rhum.*, 1997, **64**,78–81.

5.4 P. DenBesten and W. Li, Chronic fluoride toxicity: dental fluorosis, *Monogr Oral Sci*., 2011, **22**, 81–96.

5.5 P. Grandjean, Developmental fluoride neurotoxicity: an updated review, *Environ. Health*, 2019, **18**, 1–17.

5.6 P. P. Singh, M. K. Barjatiya, S. Dhing, R. Bhatnagar, S. Kothari and V. Dhar, Evidence suggesting that high intake of fluoride provokes nephrolithiasis in tribal populations, *Urol Res*., 2001, **29**, 238–244.

5.7 Environmental Protection Agency (US) Fluoride: dose-response analysis for non-cancer effects. Washington: EPA, Office of Water, Health and Ecological Criteria Division; 2010. EPA 820-R-10-019.

5.8 K. Sebelius, Proposed HHS Recommendation for Fluoride Concentration in Drinking Water for Prevention of Dental Caries, *Fed. Regist*., 2011, **76**, 2383–2388.

5.9 S. W. Zhang and T. M. Swager, Fluorescent Detection of Chemical Warfare Agents: Functional Group Specific Ratiometric Chemosensors, *J. Am. Chem. Soc*., 2003, **125**, 3420–3421.

5.10 T. K. Adams, B. R. Capacio, J. R. Smith, C. E. Whalley and W. D. Korte, The application of the fluoride reactivation process to the detection of sarin and soman nerve agent exposures in biological samples, *Drug Chem Toxicol*., 2004, **27**, 77–91.

5.11 T. Y. Joo, N. Singh, G. W. Lee and D. O. Jiang, Benzimidazole-based ratiometric fluorescent receptor for selective recognition of acetate, *Tetrahedron Lett*., 2007, **48**, 8846–8850.

5.12 S. Goswami, A. K. Das, D. Sen, K. Aich, H. K. Fun and C. K. Quah, A simple naphthalene-based colorimetric sensor selective for acetate, *Tetrahedron Lett*., 2012, **53**, 4819–4823.

5.13 L. Orzel, L. Fiedor, M.Wolak, A. Kania, R. van Eldik and G. Stochel, Interplay between Acetate Ions, Peripheral Groups, and Reactivity of the Core Nitrogens in Transmetalation of Tetrapyrroles, *Chem. Eur. J*., 2008, **14**, 9419–9430.

5.14 T. Y. Ho, M. I. Scranton, G. T. Taylor, R. Varela, R. C. Thunell and F. Muller-Karger, Acetate cycling in the water column of the Cariaco Basin: seasonal and vertical variability and implication for carbon cycling, *Limnol. Oceanogr*., 2002, **47**, 1119–1128.

5.15 S. Goswami, A. K. Das, K. Aich and A. Manna, Competitive intra- and inter-molecular proton transfer in hydroxynaphthyl benzothiazole: selective ratiometric sensing of acetate, *Tetrahedron Lett*., 2013, **54**, 4215–4220.

5.16 I. Grassi, C. Nanni, V. Allegri, J. J. Morigi, G. C. Montini, P. Castellucci and S. Fanti, The clinical use of PET with ^{11}C-acetate, *Am J Nucl Med Mol Imaging*., 2012, **2**, 33–47.

5.17 D. Sharma, A. Moirangthem, S. K. Sahoo, A. Basu, S. M. Roy, R. K. Pati, A. K. SK, J. P. Nandre and U. D. Patil, Anion selective chromogenic and fluorogenic chemosensor and its application in breast cancer live cell imaging, *RSC Adv*., 2014, **4**, 41446–41452.

5.18 Y. Zhou, J. F. Zhang and J. Yoon, Fluorescence and Colorimetric Chemosensors for Fluoride-Ion Detection, *Chem. Rev*., 2014, **114**, 5511−5571.

5.19 Dhillon, M. Nair and D. Kumar, Analytical methods for determination and sensing of fluoride in biotic and abiotic sources: a review, *Anal. Methods*, 2016, **8**, 5338–5352.

5.20 Sui, B. Kim, Y. Zhang, A. Frazer and K. D. Belfield, Highly Selective Fluorescence Turn-On Sensor for Fluoride Detection, *ACS Appl. Mater. Interfaces*, 2013, **5**, 2920–2923.

5.21 X. Yuan, X. Xu, C. Zhao, F. Zhang, Y. Lu, Y. Shen and C. Wang, A novel colorimetric and fluorometric fluoride ion probe based on photoinduced electron transfer signaling mechanism, *Sens. Actuators B Chem.*, 2017, **253**, 1096–1105.

5.22 Y. Xing, Q. Zhu, X. Zhou and P. Qi, A dual-functional smartphone-based sensor for colorimetric and chemiluminescent detection: A case study for fluoride concentration mapping, *Sens. Actuators B Chem.*, 2020, **319**, 128254.

5.23 S. Mukherjee, M. Shah, K. Chaudhari, A. Jana, C. Sudhakar, P. Srikrishnarka, M. R. Islam, L. Philip and T. Pradeep, Smartphone-based fluoride-specific sensor for rapid and affordable colorimetric detection and precise quantification at sub-ppm levels for field applications, *ACS Omega*, 2020, **5**, 25253−25263.

5.24 Coumarin functionalized molecular scaffolds for the effectual detection of hazardous fluoride and cyanide, A. Mondal, S. Nag and P. Banerjee, *Dalton Trans.*, 2021, Advance Article.

5.25 V. Puente-Munoz, J. M. Paredes, S. Resa, A. M. Ortuno, E. M. Talavera, D. Miguel, J. M. Cuerva and L. Crovetto, Efficient acetate sensor in biological media based on a selective Excited State Proton Transfer (ESPT) reaction, *Sens. Actuators B Chem.*, 2017, **250**, 623–628.

5.26 H. Matsumoto, Y. Nishimura and T. Arai, Excited-state intermolecular proton transfer dependent on the substitution pattern of anthracene–diurea compounds involved in fluorescent ON^1–OFF–ON^2 response by the addition of acetate ions, *Org. Biomol. Chem*., 2017, **15**, 6575–6583.

5.27 X. Pang, J. Ge, X. Yu, Y. Li, F. Shen, Y. Wang and J. Ren, An ''off–on'' fluorescent naphthalimide-based sensor for anions: its application in visual F^- and AcO^- discrimination in a self-assembled gel state, *New J. Chem*., 2019, **43**, 10554–10559.

5.28 Y. M. Hijji, B. Barare, A. P. Kennedy and R. Butcher, Synthesis and photophysical characterization of a Schiff base as anion sensor, *Sens. Actuators B Chem.*, 2009, **136**, 297–302.

5.29 S. Dalapati, S. Jana and N. Guchhait, Anion recognition by simple chromogenic and chromo-fluorogenic salicylidene Schiff base or reduced-Schiff base receptors, *Spectrochim. Acta A Mol. Biomol. Spectrosc.,* 2014, **129**, 499–508.

5.30 G. J. Park, Y. J. Na, H. Y. Jo, S. A. Lee, A. R. Kim, I. Noh and C. Kim, A single chemosensor for multiple analytes: fluorogenic detection of Zn^{2+} and OAc^- ions in aqueous solution, and an application to bioimaging, *New J. Chem.*, 2014, **38**, 2587–2594.

5.31 D. Sharma, S. K. A. Kumar and S. K. Sahoo, Vitamin B6 cofactor derived chemosensor for the selective colorimetric detection of acetate anions, *Tetrahedron Lett.*, 2014, **55**, 927–930.

5.32 D. Sharma, A. Kuba, R. Thomas, S. K. A. Kumar, A. Kuwar, H.-J. Choi and S. K. Sahoo, Acetate selective fluorescent turn-on sensors derived using vitamin B6 cofactor pyridoxal-5-phosphate, *Spectrochim. Acta A Mol. Biomol. Spectrosc.,* 2016, **157**, 110–115.

5.33 Q. Lin, X. Liu, T.-B. Wei and Y.-M. Zhang, TICT–ICT state change mechanism based acetate fluorescent sensor act as an "Off–On–Off" switch and logic gate, *Sens. Actuators B Chem.*, 2014, **190**, 459–463.

5.34 O. G. Tsay, S. T. Manjare, H. Kim, K. M. Lee, Y. S. Lee and D. G. Churchill, Novel reversible Zn^{2+}-assisted biological phosphate "turn-on" probing through stable aryl-hydrazone salicylaldimine conjugation that attenuates ligand hydrolysis, *Inorg. Chem.*, 2013, 52, 10052–10061.

5.35 A. Gogoi, S. Samanta and G. Das, A benzothiazole containing CHEF based fluorescence turn-ON sensor for Zn^{2+} and Cd^{2+} and subsequent sensing of $H_2PO_4^-$ and $P_4O_7^{4-}$ in physiological pH, *Sens. Actuators B Chem.*, 2014, **202**, 788–794.

5.36 A. Gogoi, S. Mukherjee, A. Ramesh and G. Das, Nanomolar Zn(II) sensing and subsequent PPi detection in physiological medium and live cells with a benzothiazole functionalized chemosensor, *RSC Adv*., 2015, **5**, 63634–63640.

5.37 J. S. Wu, W. M. Liu, X. Q. Zhuang, F. Wang, P. F. Wang, S. L. Tao, X. H. Zhang, S. K. Wu and S. T. Lee, Fluorescence turn on of coumarin derivatives by metal cations: a new signaling mechanism based on C= N isomerization, *Org. Lett.*, 2007, **9**, 33–36.

5.38 J. Wu, W. Liu, J. Ge, H. Zhang and P. Wang, New sensing mechanisms for design of fluorescent chemosensors emerging in recent years, *Chem. Soc. Rev.*, 2011, **40**, 3483–3495.

5.39 S. Goswami, S. Maity, A. K. Das and A. C. Maity, Single chemosensor for highly selective colorimetric and fluorometric dual sensing of Cu(II) as well as 'NIRF' to acetate ion, *Tetrahedron Lett.*, 2013, **54**, 6631–6634.

5.40 A. B. Descalzo, K. Rurack, H. Weisshoff, R. Martínez-Máñez, M. D. Marcos, P. Amorós, K. Hoffmann and J. Soto, Rational Design of a Chromo- and Fluorogenic Hybrid Chemosensor Material for the Detection of Long-Chain Carboxylates, *J. Am. Chem. Soc*., 2005, **127**, 184–200.

5.41 C. Saravanan, S. Easwaramoorthi, C. -Y. Hsiow, K. Wang, M. Hayashi and L. Wang, Benzo-selenadiazole fluorescent probes-near-IR optical and ratiometric fluorescence sensor for fluoride ion, *Org. Lett*., 2014, **16**, 354–357.

5.42 Y. L. Leng, J. H. Zhang, Q. Li, , Y. M. Zhang, Q. Lin, H. Yao and T. B. Wei, An easy prepared dual-channel chemosensor for selective and instant detection of fluoride based on double Schiff-base, *Spectrochim. Acta A Mol. Biomol. Spectrosc.*, 2016, **167**, 116–121.

5.43 M. Shahid, P. Srivastava, and A. Misra, An efficient naphthalimide based fluorescent dyad (ANPI) for F^- and Hg^{2+} mimicking OR, XNOR and INHIBIT logic functions, *New J. Chem.*, 2011, **35**, 1690–1700.

5.44 P. Ghosh, B. G. Roy, S. Jana, S. K. Mukhopadhyay, and P. Banerjee, Colorimetric and fluorimetric response of Schiff base molecules towards fluoride anion, solution test kit fabrication, logical interpretations and DFT-D3 study, *Phys. Chem. Chem. Phys.*, 2015, **17**, 20288–20295.

5.45 L. A.Trifoi, G. K. Hodgson, N. P. Dogantzis and S. Impellizzeri, A Reconfigurable, Dual-Output INHIBIT and IMPLICATION Molecular Logic Gate, *Frontiers in Chemistry*, 2020, **8**, 470.

Appendix 4

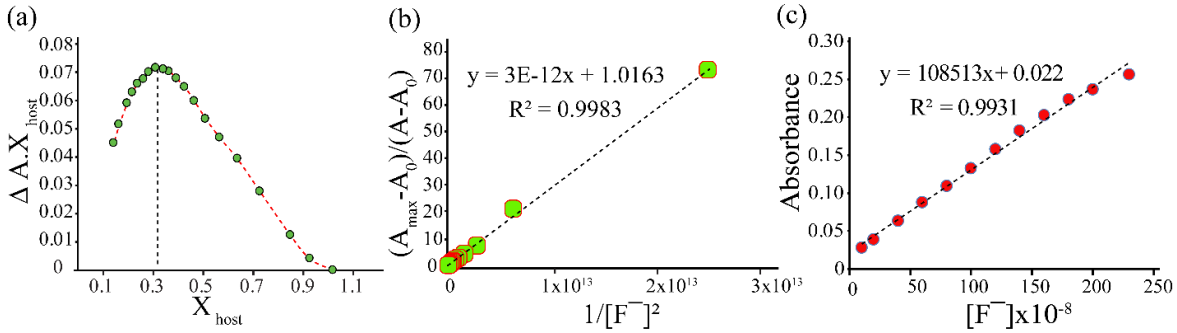

Figure A5.1 (a) Job's plot for determining the stoichiometry of the probe **L**$_3$ and F^- ion and (b) The corresponding Benesi–Hildebrand plot for binding constant determination. (c) Absorbance intensity at 456 nm versus F^- ion concentrations for lowest detection limits (LOD) calculation.

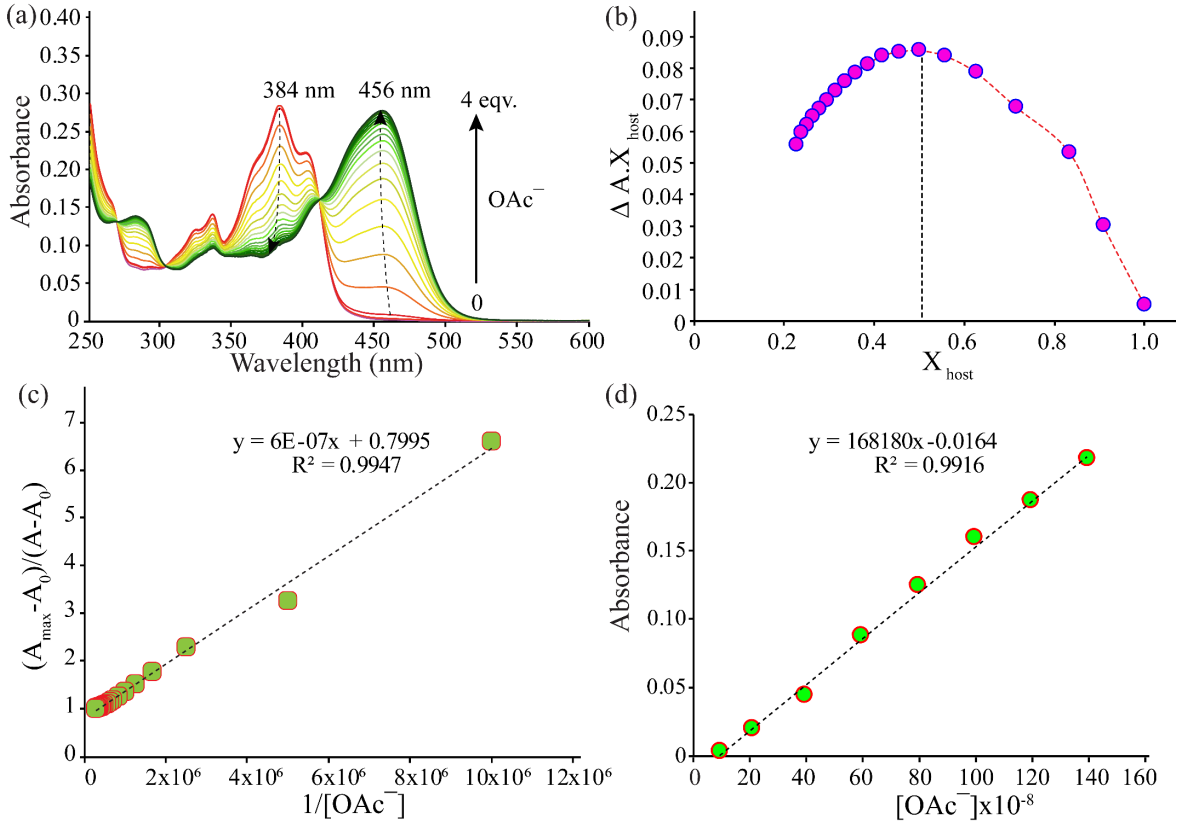

Figure A5.2 (a) UV–vis titration spectra of the probe **L**$_3$ upon incremental addition of OAc^- ion (0–4 equiv.) in CH_3CN. (b) Job's plot for determining the stoichiometry of the probe **L**$_3$ and OAc^- ion and (c) The corresponding Benesi–Hildebrand plot for binding constant determination. (d) Absorbance intensity at 456 nm versus OAc^- ion concentrations for lowest detection limits (LOD) calculation.

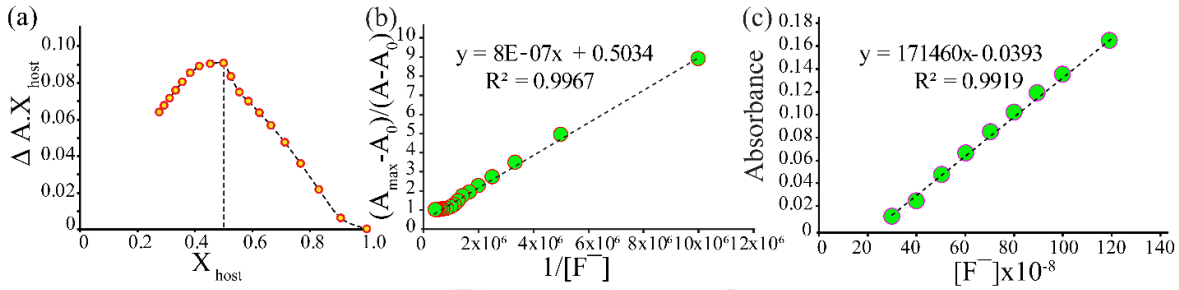

Figure A5.3 (a) Job's plot for determining the stoichiometry of the probe **L**4 and F^- ion and (b) The corresponding Benesi−Hildebrand plot for binding constant determination. (c) Absorbance intensity at 550 nm versus F^- ion concentrations for lowest detection limits (LOD) calculation.

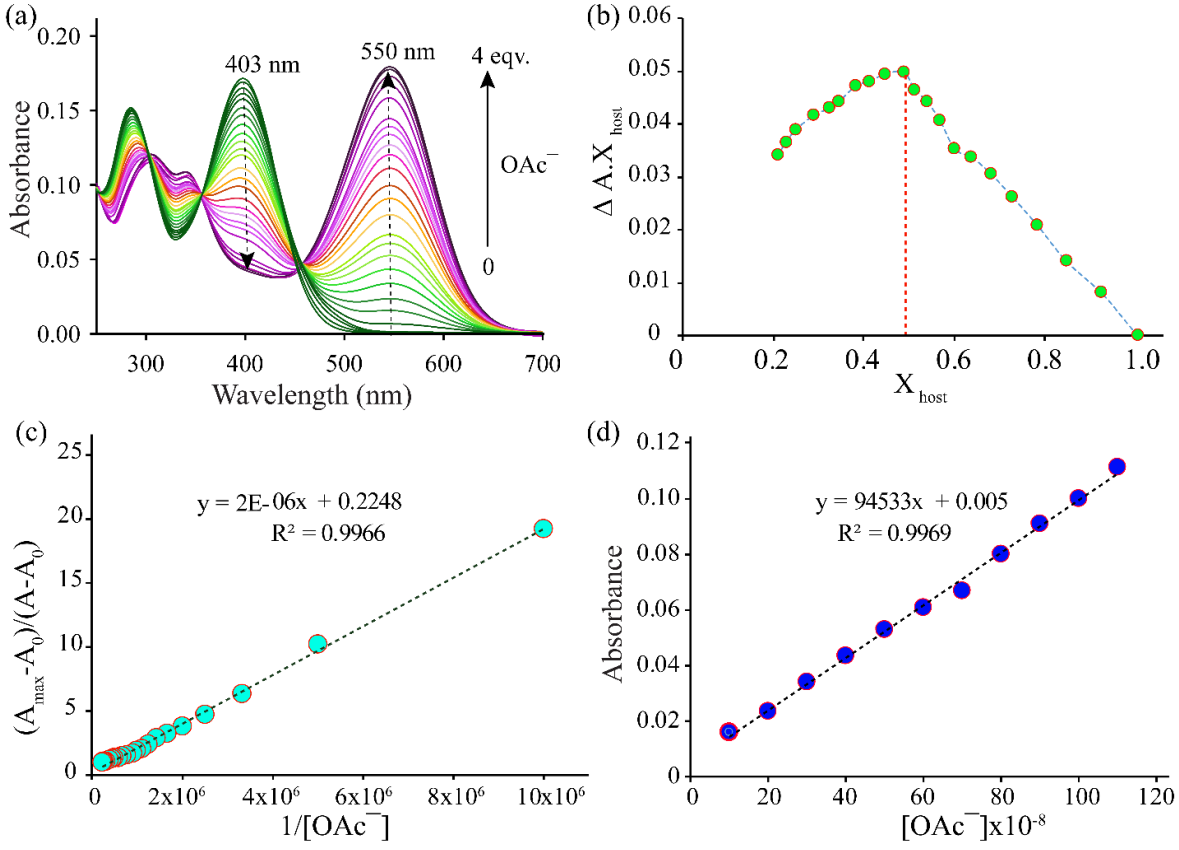

Figure A5.4 (a) UV–vis titration spectra of the probe **L**4 upon incremental addition of OAc^- ion (0–4 equiv.) in CH_3CN. (b) Job's plot for determining the stoichiometry of the probe **L**4 and OAc^- ion and (c) The corresponding Benesi−Hildebrand plot for binding constant determination. (d) Absorbance intensity at 550 nm versus OAc^- ion concentrations for lowest detection limits (LOD) calculation.

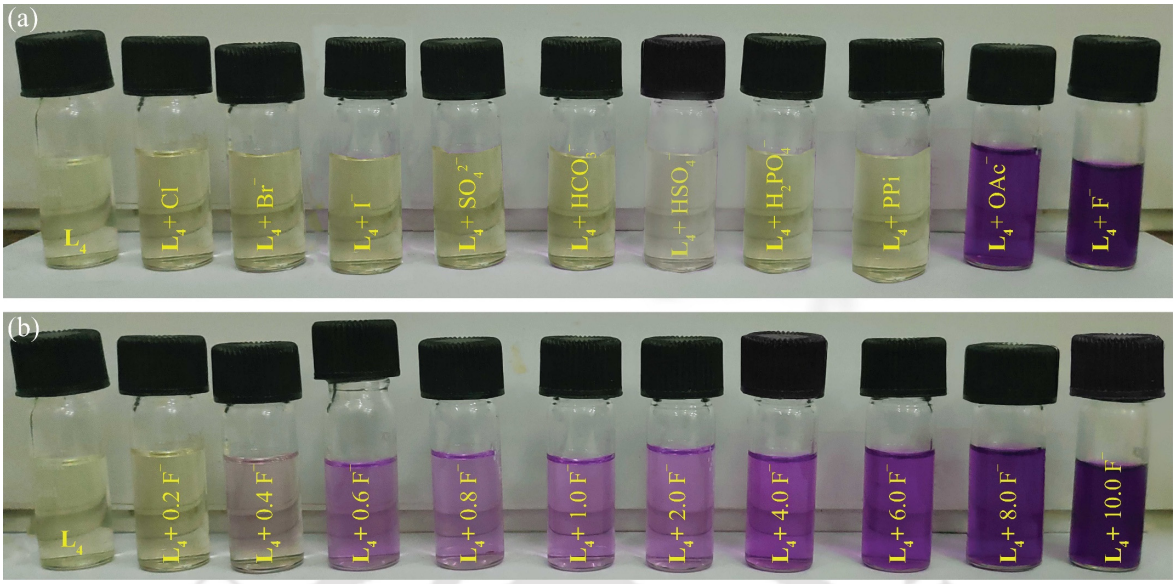

Figure A5.5 (a) Naked eye sensing of F^- and OAc^- using probe **L4** in acetonitrile (b) Colorimetric change of **L4** solution with the addition of fluoride ion till 10 equiv.

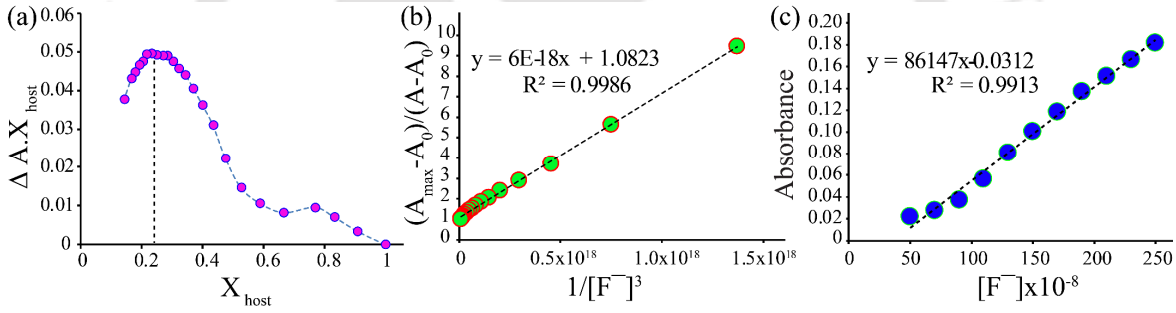

Figure A5.6 (a) Job's plot for determining the stoichiometry of the probe **L5** and F^- ion and (b) The corresponding Benesi−Hildebrand plot for binding constant determination. (c) Absorbance intensity at 450 nm versus F^- ion concentrations for lowest detection limits (LOD) calculation.

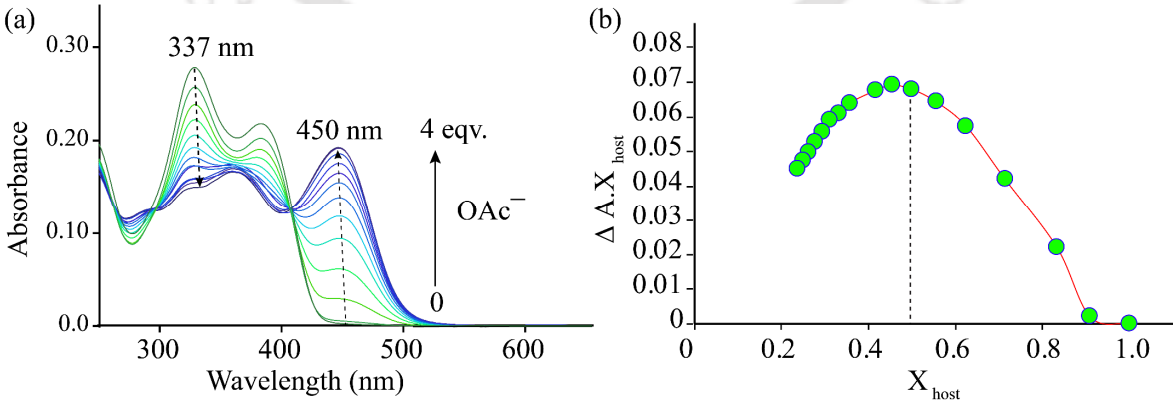

Figure A5.7 (a) UV-Vis absorption change of **L5** with increasing concentration of OAc^-. (b) The corresponding Job's plot and (c) Benesi−Hildebrand plot for binding constant determination.

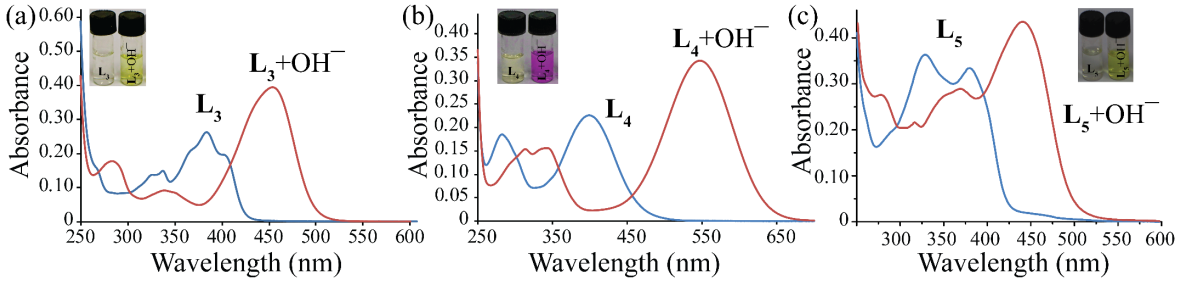

Figure A5.8 Comparative absorption spectra of hydroxide addition to the chemosenors (a) L_3, (b) L_4, and (c) L_5 in acetonitrile. Inset: Visible colour change upon addition of the hydroxide anions to the probe solutions.

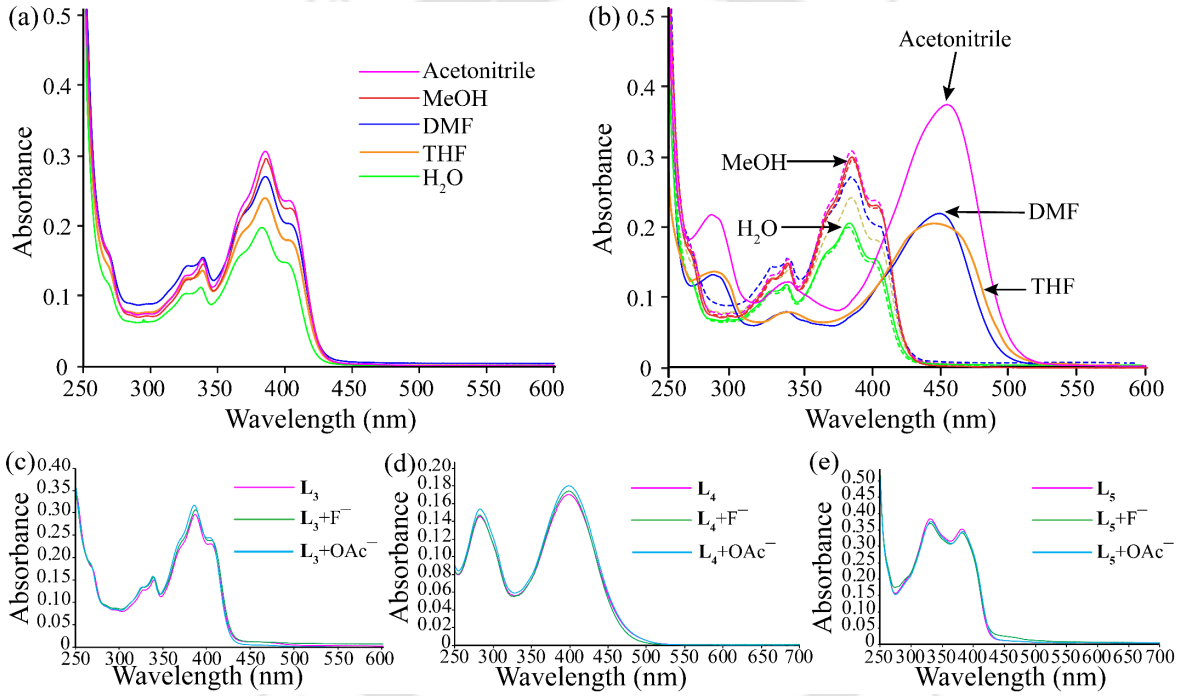

Figure A5.9 (a) Absorption spectra of L_3 (10 mM) in different solvents. (b) Corresponding change in the absorption specta of L_3 in different solvent in presence of fluoride anion (50 mM) (Dotted line represents the original absorption spectra in absence of the anion). (c) Change in absorption spectra of L_3 in acetonitrile: H_2O=4:1solution (10 mM) with fluoride and acetate anion (50 mM). (d) Change in absorption spectra of L_4 in acetonitrile: H_2O=4:1solution (10 mM) with fluoride and acetate anion (50 mM). (e) Change in absorption spectra of L_5 in acetonitrile: H_2O=4:1solution (10 mM) with fluoride and acetate anion (50 mM).

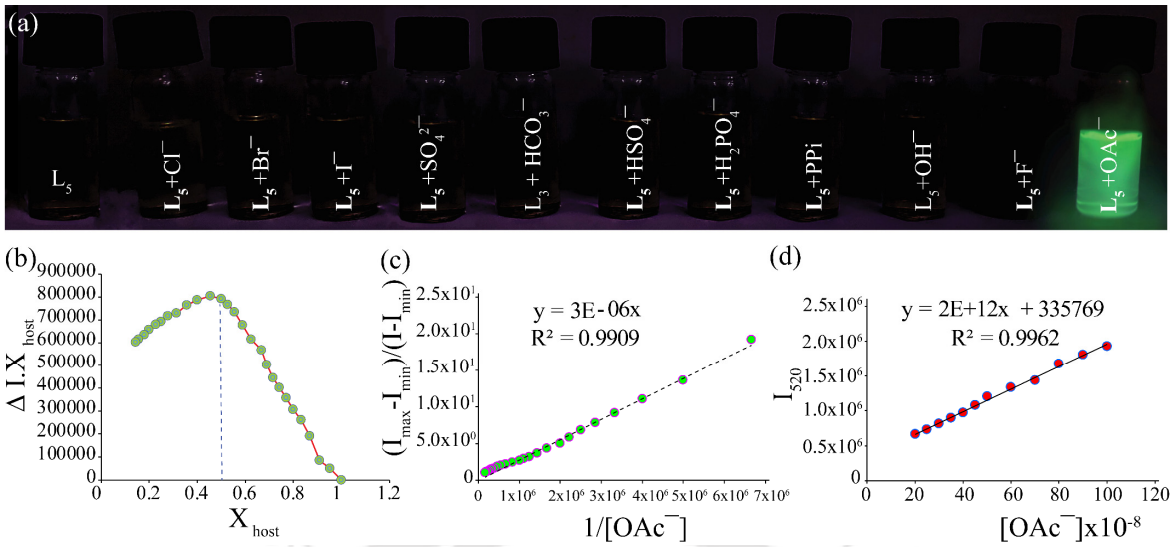

Figure A5.10 (a)Visual changes in fluorescence of **L5** under UV light (λ_{ex} = 365 nm) in Acetonitrile. (b) Job's plot for determining the stoichiometry of the probe **L5** and OAc^- ion and (c) The corresponding Benesi–Hildebrand plot for binding constant determination. (d) Fluorescence intensity at 520 nm versus OAc^- ion concentrations for lowest detection limits (LOD) calculation.

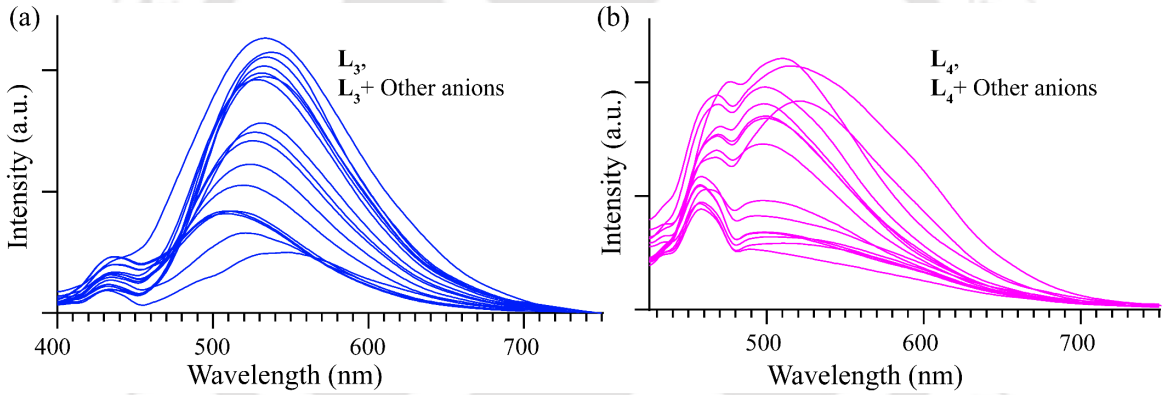

Figure A5.11 Fluorescence emission changes of (a) **L3** and (b) **L4** with various anions.

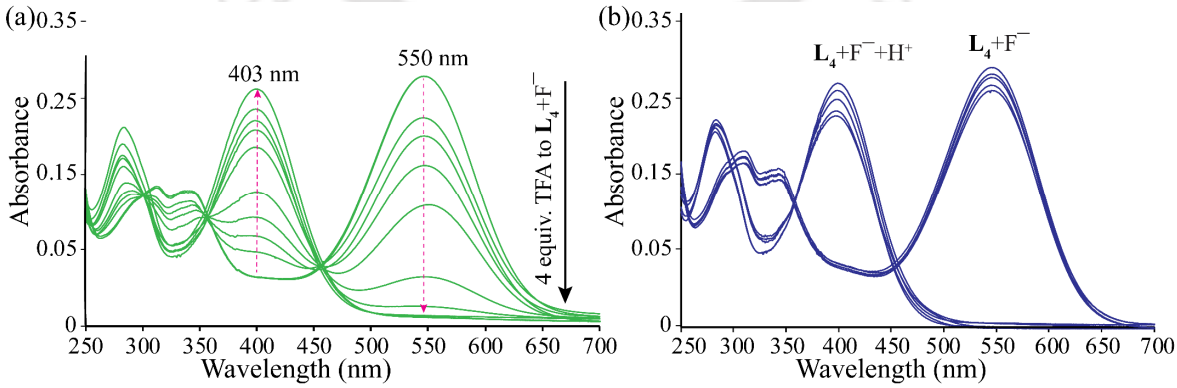

Figure **A5.12** (a) Titration of **L4**-F^- complex with Trifluoroacetic acid. (b) Reversibility test of the probe **L4**; Bathochromatic shift of 147 nm with the addition of fluoride ions (F^-) and reversed back to the original upon addition of TFA (upto 5 cycles).

Table A5.1 The comparison of our chemosensors with Schiff base based F^- and/or acetate sensors available in recent literatures.

Sl No.	References	LOD for fluoride	LOD for acetate	Solvent system	Remarks
1	Our chemosensors	3.35×10^{-8} M by **L_4**	2.907×10^{-8} M by **L_5**	Acetonitrile	**L_4** Colorimetric fluoride sensor, **L_5** Turn on Fluorescent Acetate sensor
2	G. G. G. Kumar, M. P. Kesavan, G. Sivaraman, J. Rajesh, *Sensors and Actuators B*, 2018, **255**, 3194-3206.	0.30 µM	NA	PBS buffer	Colorimetric and NIR fluoride sensor
3	D. Sharma, A. Kuba, R. Thomas, S. K. A. Kumar, A. Kuwar, H. -J. Choi, and S. K. Sahoo, *Spectrochimica Acta Part A: Molecular and Biomolecular Spectroscopy,* 2016, **157**, 110–115.	NA	7.37×10^{-6} M	DMSO: H_2O (95:5)	Acetate selective fluorescent turn-on sensor
4	Q. Lin, X. Liu, T.-B. Wei, Y.-M. Zhang, *Sensors and Actuators B*, 2014, **190**, 459–463.	NA	4.0×10^{-7} M	DMSO	Acetate selective fluorescent turn-on sensor
5	C.-B. Bai, J. Zhang, R. Qiao, S.-Y. Mu, M. Meng, B. Wei, C. Wang, C.-Q. Qu, and Y.-T. Ji, *SN Applied Sciences*, 2020, **2**, 567.	NA	4.6×10^{-9} M	HEPES Buffer: acetonitrile (2:8)	Acetate selective fluorescent turn-on sensor
6	G. R. Youa, G. Ji. Park, S. A. Lee, Y. W. Choi, Y. S. Kim, J. J. Lee, and C. Kim, *Sensors and Actuators B*, 2014, **202** 645–655.	NA	140.0×10^{-6} M	DMSO/bis–tris buffer (8:2)	Colorimetric acetate sensor
7	S. Goswami, S. Maity, A. C. Maity, A. K. Das, B. Pakhira, K. Khanra, N. Bhattacharyya, and S. Sarkar, *RSC Adv.*, 2015, **5**, 5735-5740.	12.7 µM	NA	Acetonitrile	Fluoride selective fluorescent turn-on sensor
8	S. Ghosha, A. Gangulya, A. Bhattacharyya, M. A. Alam, and N. Guchhait, *RSC Adv.*, 2016, **6**, 67693-67700.	1.3µM	NA	Acetonitrile	Colorimetric fluoride sensor

In summary, this thesis reports the efforts and outcomes in designing, improvising certain benzimidazole and benzothiazole functionalized receptors and their binding propensity towards biologically and environmentally relevant anions in solution phase as well as solid state.

Introduction of novel non-symmetric tripodal receptors has enabled us to explore the anion recognition chemistry with new directions in receptor designing and the recognition events through efficacious anion binding in both solid as well as solution phase, which the typical tripodal receptors have been missing. As discussed in Chapter 3, the introduction of amide linked nitrophenyl moiety as the third arm to the symmetric benzimidazole arms has made **L_1** suitable for selective recognition of octahedral SiF_6^{2-} and tetrahedral SO_4^{2-}/HSO_4^- anions in solid state. Moreover, the acidic benzimidazole −NH and amide −NH are sufficient to interact with fluoride in acetonitrile with visible colorimetric changes. These photophysical properties have been improved in Chapter 4 as **L_2**, another novel non-symmetric tripodal acts as a "turn-on*"* ratiometric fluorescent sensor for fluoride ion with a limit of detection 4.63×10^{-8} M in the solution phase. In solid state, **L_2** can selectively bind sulfate ion. By tuning the functionalities of the third arm, our design of non- symmetrical tripodal receptors has successfully recognized anions in both the solution phase as well solid state, which is otherwise a stimulating task to endeavour. Paper strips of the chemosensor **L_1** and **L_2** can also be used for the quick detection of fluoride ions.

As selective anion binding in both solid and solution phase has been demonstrated with the help of the non-symmetric tripodals, we have accentuated our impetus to attain better selectivity and sensitivity in the solution phase. The benzothiazole based Schiff base receptors **L_3**, **L_4** and **L_5** can selectively sense fluoride and acetate ions in acetonitrile solution via absorption spectroscopy. Selectivity of acetate ion has been shown to achieve via differential fluorescence response of **L_5** in acetonitrile solution based on complementarity with the binding sites where the lowest detection limit is found to be 2.907×10^{-8} M. Boolean type logic gates at the molecular level based on the reversible behaviour of the probes have also been fabricated.

Concisely, this thesis portrays a sequential plethora of systematic development in the field of chemosensing as well as solid state study. Starting with the synthesis of a novel non-symmetric tripodal and its anion binding study in both solid state and solution (Chapter 3), we have continued our study with another non-symmetric tripodal analogue in emission spectroscopy based solution study assisted by its solid state anion recognition (Chapter 4) to conclude with series of three simple Schiff bases as selective and sensitive anion sensors in solution phase only (Chapter 5). Keeping in mind the added benefits of non-symmetrical tripodals, recognition and binding of

anions could be engaged in specific applications such as removal and extraction toxic anions and salts from water, drug delivery, transmembrane anion transport, salt solubilization, extraction, catalysis, stabilizing the anionic reactive intermediates inside the molecular assembly, etc. The non-symmetric third arm can be modified deliberately with richer fluorophore or chromophore to have better photophysical properties. These can even be adjusted with appropriate anion binding sites to encapsulate anions of varied dimensionality. Our works on distinctions of anions with analogous chemical properties viz. F^- in presence of OAc^- or vice versa have been achieved by tuning smart designs of receptors, which in turn, would help in distinguishing such anions in a physiological medium as well.

The chemistry of anion receptors and chemosensors has gained an innumerable response from the supramolecular research fraternity in the recent past. After the Nobel Prize in supramolecular chemistry in 1987 to Charles J. Pedersen, Jean-Marie Lehn and Donald J. Cram, the design and application of fluorescent molecular devices increased exponentially. Since then different approaches have been taken to couple the binding sites and signalling units in efficacious design framework so that selective and sensitive recognition of different anionic species could take place. A precise molecular recognition event between a chemosensor and anionic guest can be utilized in numerous applications in analytical chemistry, supramolecular science, biochemistry, physical chemistry, medicinal chemistry, toxicology, forensic sciences. It paves way for the modern nanochemistry too. For these applications to accomplish their potential, the fundamental work lies in the tuning and modification of the receptor molecules. Making the chemosensors easily soluble in aqueous media and detection of analytes in biological media with vivid spectral response at longer wavelength are the prospects that these receptors bear. Although the results included in this thesis are extremely useful from a fundamental viewpoint, there are other challenging aspects in supramolecular chemistry that need to be addressed from an application point of view. Research in these areas with a focus on technological and biomedical applications, based upon the remarkable anion sensing appears to be forthcoming.

NILOTPAL BORAH

Date of Birth: 11-12-1988

Place of Birth: Kamalabari, Majuli, Assam.

Nationality: Indian

Email: b.nilotpal@iitg.ac.in, nilotpal.borah.1588@gmail.com

Father's name: Chandra Kanta Borah

Occupation: Service (Retired)

Mother's name: Late Binu Bhuyan

Religion: Hinduism

Nationality: Indian

Languages known: Assamese, English, Hindi.

Blood group: O +ve

Permanent Address:

C/O: Chandra Kanta Borah,

Doria Gaon, P.O.: Kamalabari,

Dist: Majuli, Assam, India

PIN: 785106

Present Address:

C/O: Chandra Kanta Borah,

Nandanpur, Near Earl Grey Hotel,

Ajanta Byepass, Kotoky Pukhuri, Dist: Jorhat, Assam

PIN: 785006

Academic Summary

2013-present: Ph.D. student at Indian Institute of Technology Guwahati, India.
Thesis title: "**Recognition of anionic guests with benzimidazole and benzothiazole functionalized acyclic hosts: solution phase and solid state studies" (Thesis submitted)**

2010-2012: Master of Science in Chemistry (CGPA 8.78) from Gauhati University, Guwahati, Assam, India.

2007-2010: Graduation (Chemistry) (70.4%) from B. Borooah College, Guwahati, Assam, India.

2004-2006: 12th (Science), AHSEC (72.6%) from J.B. College, Jorhat.

2007: 10th, SEBA (77.83%) from Majuli A. H. High School, Majuli.

Honours and awards

- Qualified National Eligibility Test (NET) for Lectureship, 2017.
- Qualified Graduate Aptitude Test in Engineering (GATE), 2013, 2015, 2016, 2018, 2019.

Research Interests

- Combined Solid state and solution phase studies of biologically and environmentally relevant anions in a non-symmetric tripodal framework.
- Design and synthesis of colorimetric and fluorescent probes.
- Colorimetric and Fluorescence sensing of biologically important ions and molecules.

Expertise

- Spectroscopic techniques (UV, Fluorescence, FT-IR), Optical and fluorescence microscopy, Single crystal x-ray diffraction, Powder XRD, NMR spectroscopy, mass spectrometry.

Publications

Book Chapters:

1. Progressive Endeavour of Molecular Recognition: Sensing of ions to neutral guests, ISBN: 978-93-89940-80-0, Topic: Small molecule fluorescent chemosensors for recognition of neutral molecules.

Journals/ Research Papers:

1. N. Borah, A. Gogoi and G. Das, Competitive anion binding aptitude of benzimidazole and amide functionality of a non-symmetrical receptor in solid state and solution phase, *Supramol. Chem.*, 2016, **28**, 275–283.
2. N. Borah, B. Nayak, A. Gogoi and G. Das, A benzimidazole-based non-symmetrical tripodal receptor for the ratiometric fluorescence sensing of fluoride ions and solid state recognition of sulfate ions, *New J. Chem.*, 2019, **43**, 16497–16505.
3. N. Borah, S. De, A. Gogoi and G. Das, A series of benzothiazole based Schiff bases for

colorimetric sensing of fluoride and acetate ions: acetate induced turn-on fluorescence for selectivity, *New J. Chem.*, 2020, **44**, 18703–18713.

Conference attended

- Poster presented in Frontiers in Chemical Science 2016, Indian Institute of Technology, Guwahati.
- Poster presented in Modern Trends Inorganic Chemistry (XVII) 2019, Indian Institute of Technology Guwahati, Guwahati.
- Poster presented in Science for Sustainable Development (SSD-2020) and won the Best Poster Presentation award, Department of Chemistry, B. Borooah College, Guwahati.